SYNTHESIS AND NMR SPECTROSCOPY OF *N,N'*-BIS(2-THIOETHANOYL)-2,3-DIAMINOPROPANOIC ACID DERIVED CARRIER CHELANTS FOR TECHNETIUM RADIOIMAGING

By

RABINDRANATH BANSEE MAHARAJH, B.Sc.

A Thesis
Submitted to the School of Graduate Studies
in Partial Fulfilment of the Requirements
for the Degree
Doctor of Philosophy

McMaster University

SYNTHESIS OF CARRIER CHELANTS FOR TECHNETIUM RADIOIMAGING

DOCTOR OF PHILOSOPHY (1993) McMaster University

(Chemistry) Hamilton, Ontario

TITLE: Synthesis and NMR Spectroscopy of *N,N'*-bis(2-thioethanoyl)-2,3-diaminopropanoic Acid Derived Carrier Chelants For Technetium Radioimaging

AUTHOR: Rabindranath Bansee Maharajh, B.Sc. (McMaster University)

SUPERVISOR: Professor R. A. Bell

NUMBER OF PAGES: xix, 244

Abstract

Because of its availability and favorable disintegration characteristics, there has been interest in recent years to bind technetium-99m (^{99m}Tc) to carrier molecules for use as tissue-specific diagnostic radiopharmaceuticals. In contribution to this effort, this thesis describes some investigations into the synthesis and NMR spectroscopy of novel bifunctional chelants for ^{99m}Tc radioimaging. Using bifunctional chelate strategies, a series of diamide disulfur (DADS) ligand conjugates of biologically active, carrier compounds were prepared for development into prospective myocardial and gastroenterological imaging agents. Carrier molecules of the intended myocardial agents included cardioactive compounds, such as C_{11} and C_{16} long chain fatty acids and the cardenolide aglycone digitoxigenin. DADS ligand derivatives of cholic acid, taurine and β-cyclodextrin were also synthesized in an effort to determine their potential utility as gastroenterological technetium imaging agents. The conjugation of ligands to steroidal molecules represents a new approach towards the production of ^{99m}Tc-based radiopharmaceuticals.

The 10-membered heterocycle, *N,N'*-[dimethyl-(2,2'-dithiobisethanoyl)] ethylenediamine (**40**), was prepared to aid in the interepretation of the complex NMR spectral characteristics observed in many of the DADS ligands. It exists in solution as a mixture of two *Z,Z* and one *Z,E* disulfide and amide ring conformers and has been characterized by NOE, ^{1}H-^{1}H, ^{1}H-^{13}C shift correlated NMR and molecular modelling studies. Among the *Z,Z* ring conformers, Z,Z_1 and Z,Z_2, the former predominates and interconverts with the latter isomer by rotation about the S-S bond with an apparent

activation energy of 14.5 ± 1.3 kcal/mol. Coalescence of N-CH_3 signals occurred at about 127 °C at 500 MHz, which corresponded to an approximate barrier to amide rotation of 19.3 kcal/mol. Aromatic solvent induced shifts (ASIS) in C_6D_6 have corroborated molecular mechanics and NOE predictions of amide stereochemistry. The structure of the *Z,E* stereoisomer of **40** has been determined by single crystal X-ray diffraction at 296 K. A large geminal N-CH_2 inequivalence (> 2 ppm in $CDCl_3$) was seen in the *Z,Z* conformers. Based on empirical calculations of chemical shifts, roughly one-half of the observed splitting was rationalized in terms of nearly equal contributions from magnetic anisotropy and electric field shielding mechanisms of the amide carbonyl groups. An implication of these results is the possibility of using α-C*H* (and eventually -*C*H) shifts to probe the local conformational space in structured proteins and other complex amides.

Acknowledgements

This thesis would be incomplete without acknowledging the valuable assistance of several people. I wish to thank my research supervisor, Professor R.A. Bell, for sharing his expert knowledge and guidance throughout the course of this work. His flexibility gave me the intellectual freedom to pursue and implement many ideas.

Special thanks are due to Dr. D.W. Hughes for his guidance at the NMR console and for many enlightening discussions relating to the NMR phenomenon. I am also indebted to Dr. A.D. Bain for his sage advice and review of the dimethyl disulfide (**40**) manuscript. I am grateful to Dr. J.F. Britten for the X-ray analysis of **40** and Drs. T. Hemscheidt, J.D. Laposa, L. Li, D.B. MacLean, B.E. McCarry, M.J. McGlinchey and R. Smith for very helpful discussions relating to this research. Technical contributions were generously made by B.G. Sayer and G. Timmins. Thanks are also necessary to the members of my thesis committee, Drs. G. Coates, P. Harrison and C.J.L. Lock and to my external examiner, Dr. J.W. Lown, for their interest and input.

And to my fellow inmates and friends with whom I shared ABB 465 - Fred, Chuck, Heinz-Pete, Todd and John - thanks for the good times and laughs. May you all discover the secret of transmuting Pb into Au!

I would like to express my last words of thanks to my wife, Deepika, who patiently endured the many nights and weekends that were spent on the NMR spectrometer and writing this thesis. Your continued confidence and support helped me to laugh at my problems and spurred me to try that much harder.

Finally, I am very grateful to McMaster University for financial assistance.

To my beloved parents whose unfailing support and sacrifices have made this work possible

Table of Contents

List of Abbreviations and Symbols

AN	acetonitrile
Ar	aryl
bp	boiling point
br	broad (spectral)
°C	degrees Celsius
CAD	coronary artery disease
CDI	carbonyldiimidazole
CI-MS	chemical ionization mass spectrometry (spectrum)
CO_2-DADS	diamide disulfur carboxylate; specifically, *N,N'*-bis (2-thioethanoyl)-2,3-diaminopropanoic acid
COSY	correlated spectroscopy (in NMR)
$\Delta\delta_{OBS}$	observed chemical shift difference between geminal protons
δ	chemical shift in parts per million downfield from tetramethylsilane
d	day(s); doublet (spectral)
DCC	1,3-dicyclohexylcarbodiimide
DCI-MS	desorption chemical ionization mass spectrometry (spectrum)
DCU	1,3-dicyclohexylurea
ddH_2O	doubly-distilled, deionized water
dec.	decomposed (in melting point determination)
DEI-MS	desorption electron ionization mass spectrometry (spectrum)
dH_2O	distilled water
DIARS	*o*-phenylenebis(dimethylarsine)
DMAP	4-dimethylaminopyridine
DME	dimethoxyethane
DMF	*N,N*-dimethylformamide
DMPE	dimethylphosphinoethane
DMSO	dimethylsulfoxide
DNMR	dynamic nuclear magnetic resonance
DTNB	5,5'-dithiobis-(2-nitrobenzoic acid)
DTPA	diethylenetriaminepentaacetic acid
EDC	1-(3-dimethylaminopropyl)-3- ethylcarbodiimide hydrochloride
EDCU	1-(3-dimethylaminopropyl)-3-ethylurea (salt or free base)
EDTA	ethylenediamine tetraacetic acid
EI	electron impact (in mass spectrometry)
Et	ethyl
EtOAc	ethyl acetate
FAB-MS	fast atom bombardment mass spectroscopy (spectrum)
FID	free induction decay (in NMR)
g	gram(s)
$G^{\neq}$	Gibbs free energy of activation
h	hour(s)
HEDP	sodium (or calcium) 1-hydroxyethyl-1,1-diphosphonate
HIDA	hepatobiliary iminodiacetate(s)

HRMS	high resolution mass spectrometry (spectrum)
Hz	hertz
i-Pr	isopropyl
IR	infrared (spectroscopy)
^{n}J	nuclear spin-spin coupling constant through *n* bonds (in Hz)
J-Mod	*J*-modulated ^{13}C NMR experiment (aka. spin-sort)
k	rate constant
L	liter(s)
lit.	literature
μ	micro
m	multiplet (spectral), meter(s), milli
M	moles per liter, molecular ion (in mass spectrometry)
Me	methyl
MHz	megahertz
min	minute(s)
mm Hg	millimeters of mercury
mM	millimoles per liter
mol	mole(s)
mp	melting point
MS	mass spectroscopy
m/z	mass to charge ratio (in mass spectrometry)
ν_{MAX}	frequency absorbance/transmission (in IR spectrometry)
NEt_3	triethylamine
NHS	*N*-hydroxysuccinimide
NMR	nuclear magnetic resonance
Nu	nucleophile
Pd/C	palladium supported on carbon
pH	$-\log_{10}[H^+_3O]$; measure of acidity
Ph	phenyl
ppm	parts per million
q	quartet (spectral)
R_f	retention factor (in adsorption chromatography)
RI	relative intensity
RMS	root mean squared
rt	room temperature
s	singlet
SAR	structure-activity relationship(s)
t	triplet
$t_{1/2}$	half-life (of a radionuclide)
TFA	trifluoroacetic acid
THF	tetrahydrofuran
TLC	thin layer chromatography
TMS	tetramethylsilane
Tr	trityl (triphenylmethyl)
Ts	tosyl (*p*-toluenesulfonyl)
UV	ultraviolet
v/v	volume per volume
w	weak (in IR spectroscopy)
w/v	weight per volume

List of Figures

List of Tables

When asked how his mind operates, Steven Hawking, acclaimed the world's greatest living scientist, responded:

"I work on intuition, thinking that an idea ought to be right. Then I try to prove it."

"The stream of knowledge is heading toward a nonmechanical reality; the universe begins to look more like a great thought than like a great machine."

Sir James Jean, The Mysterious Universe.

CHAPTER I

INTRODUCTION

In the practice of diagnostic nuclear medicine, a radiopharmaceutical, generally a gamma-ray emitting one, is administered *in vivo* so that the radioisotope becomes localized in a specific organ or region of the body. The successful targeting of diagnostic radionuclides to diseased tissues and tumors provides not only a tool for the diagnosis of cancer and heart or brain ailments, but also demonstrates the feasibility for therapy where ligand systems can be applied to therapeutic nuclides. For diagnosis, technetium-99m (Tc-99m or ^{99m}Tc) is at present the most commonly used radionuclide for well-documented reasons (see Section 1.2).

1.1 Anatomical *vs* Functional Imaging

The importance of radiopharmaceuticals in diagnostic medicine hinges on the fact that the physiological function of an organ, as well as its structure, can be visualized. The availability of this information complements other imaging modalities and has resulted in a better understanding of disease and improved practices in medicine.

Over the years, scintigraphy, ultrasound, computed tomography (CT) and magnetic resonance imaging (MRI) have been used as primary imaging modalities. Because CT and MRI generally provide far superior anatomical detail of tissues, the role of scintigraphy has gravitated more towards the study of organ *function* using

radioimaging agents. Thus, the general trend in nuclear medicine has been towards more quantitation of function as an integral part of organ imaging. The functional ability of any organ is a prime indicator of its state of health and is clearly important information for the diagnosis and treatment of systemic abnormalities. To illustrate, the introduction of ^{99m}Tc-labeled iminodiacetate (IDA) analogues (see Figure 3.1) in 1976 has had a major impact on the diagnostic workup of hepatobiliary diseases because of their dual capacity to provide morphologic and physiologic information simultaneously. Specific diagnosis of various hepatobiliary diseases are made by combining morphologic alterations seen on scintigraphy with the physiologic parameters measured quantitatively.[1]

1.2 Physical Properties of ^{99m}Tc

Technetium has made a major impact in the diagnosis of human diseases, with over six million diagnostic imaging procedures carried out with ^{99m}Tc compounds annually in the United States.[2] In 1960, Richards suggested that ^{99m}Tc, a metastable radionuclide of technetium, possessed decay properties that were ideally-suited for diagnostic imaging.[3] Summarized schematically in Figure 1.1, these properties include:

1) A short half-life of 6.0 hours, which dramatically reduces the radiation risk to patients in comparison to most conventional radionuclides, while maintaining excellent statistical counting conditions.
2) A 140 keV γ-ray energy, which is optimal for detection by scintillation cameras and is poorly absorbed by body tissues. Moreover, there is no particulate radiation.[4]
3) A relatively stable daughter nuclide, which minimizes long-term hazard from particulate radiation. The parent nuclide, ^{99}Mo, is also relatively stable ($t_{1/2}$ =

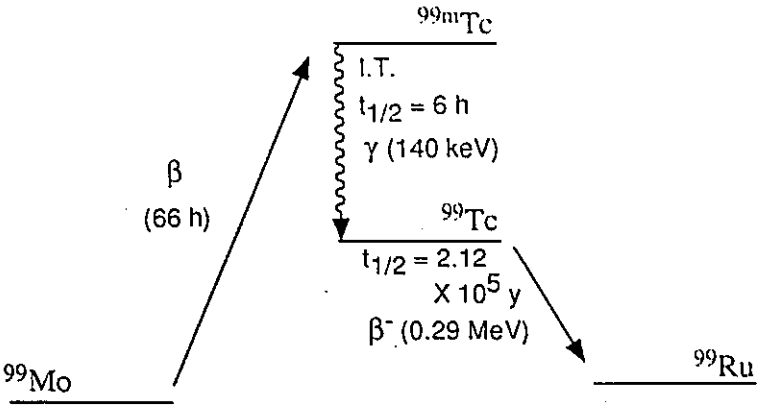

Figure 1.1: The preparation and nuclear decay properties of ^{99m}Tc. Adapted from ref. 4.

67 hours) and has led to the development of a generator which had made ^{99m}Tc available on demand at any hospital. The generator consists of ^{99}Mo adsorbed on an alumina column from which ^{99m}Tc, in the form of pertechnetate ($^{99m}TcO_4^-$), could be eluted with a saline solution.

4) The ability of technetium to accept a relatively wide range of donor groups, which allows for the preparation of a large series of different ^{99m}Tc-labeled radiopharmaceuticals for use in the varied diagnostic problems encountered in routine clinical practice.[5]

Moreover, these attributes allow the routine administration of doses of 30 mCi which allow high photon-flux levels, facilitating lesion detection by single-photon-emission computerized tomography (SPECT).

A typical labeling procedure consists of mixing $^{99m}TcO_4^-$, obtained from the ^{99}Mo generator, with a reducing agent in the presence of the desired ligand. Various reducing agents include stannous ion, ferric chloride plus ascorbic acid, ferrous ion and sodium borohydride and nonmetallic reducers such as hydrogen iodide, concentrated

HCl or hydrazine.[6] The concentration of the labeled material which is sufficient to produce suitable images is usually at the nanomolar level and therefore has very little or no physiological effect.

1.3 Design of ^{99m}Tc Radiopharmaceuticals

Although ^{99m}Tc can be used directly as a radioimaging agent, the vast majority of technetium radiopharmaceuticals are chelates of technetium in lower oxidation states. These radiopharmaceutical complexes can be categorized into three general groups (see Table 1.1).[7] In the first group, *technetium-tagged radiopharmaceuticals*, ^{99m}Tc functions exclusively as a radiolabel for large substances, such as proteins, colloids and cells. The binding of the radionuclide to such large systems does not significantly perturb the intrinsic biodistribution of the tagged substance; ^{99m}Tc simply serves as a convenient label to permit the external monitoring of the biological distribution of the tagged compound. In this tagging procedure, the technetium label is bound by donor groups intrinsic to the macromolecule. These Tc-labeled systems generally are not stable chelates or chemically well-defined and are not amenable to detailed investigation by the techniques of inorganic chemistry.

One particularly promising area under active investigation is the use of ^{99m}Tc-labeled monoclonal antibodies as agents for the detection of localized disease, such as tumours.[8]

Technetium-essential radiopharmaceuticals - the second class of radiopharmaceuticals - comprises those compounds whose biological distribution is primarily determined by the intrinsic physicochemical properties of the Tc complex and the metal (hence its specific epithet). Because of the small size of the chelating moiety, the biodistribution of the chelate is usually significantly different from the

Technetium-tagged Radiopharmaceticals	Technetium-essential Radiopharmaceticals
1. Particles and colloids: Tc-macroaggregated albumin, Tc-albumin microspheres, Tc-ferric hydroxide aggregates, Tc-sulfur colloid,Tc-antimony colloid, Tc-phytate 2. Proteins: Monoclonal antibodies, albumins, fibrinogen, urokinase 3. Cells: Erythrocytes, leucocytes, lymphocytes, platelets 4. Small molecules: Bone agents, e.g., polyphosphates, pyrophosphates, diphosphonates, iminodiphosphonates	1. Heart-imaging agents: Tc-$(CNR)_6^+$, Tc-DIARS, Tc-DMPE 2. Infarct-avid agents: Tc-pyrophosphate, Tc-glucoheptonate, Tc-tetracycline, and Tc-HEDP 3. Hepatobiliary agents: Tc-HIDA (and related analogues), Tc-pyridoxylidine-glutamate, Tc-isomercaptobutyric acid, Tc-dihydrothioctic acid 4. Kidney function agents: Tc-DADS-CO_2, Tc-DADS, Tc-DTPA, Tc-EDTA, Tc-MIDA, Tc-citrate 5. Kidney structure agents: Tc-gluconate, Tc-glucoheptonate, Tc-mannitol, Tc-dimercaptosuccinic acid, Tc-insulin, Tc-Fe-ascorbate

Table 1.1 ^{99m}Tc-radiopharmaceuticals.

ligand molecule. Although many useful (Tc-essential) radiopharmaceuticals have been found, often serendipitiously, the alteration in distribution of the parent molecule has limited the predictive ability in radiopharmaceutical design.[7]

1.3.1 Bifunctional Radiopharmaceuticals

The third category of Tc radiophamaceuticals - sometimes considered as a subclass of technetium-tagged radiochemicals - includes Tc complexes of "bifunctional ligands". A bifunctional ligand is a ligand system capable of forming a covalent bond with an appropriate (biologically active) substrate, while retaining the ability to bind a metal, such as ^{99m}Tc . When the bifunctional ligand forms a metal complex with Tc, it

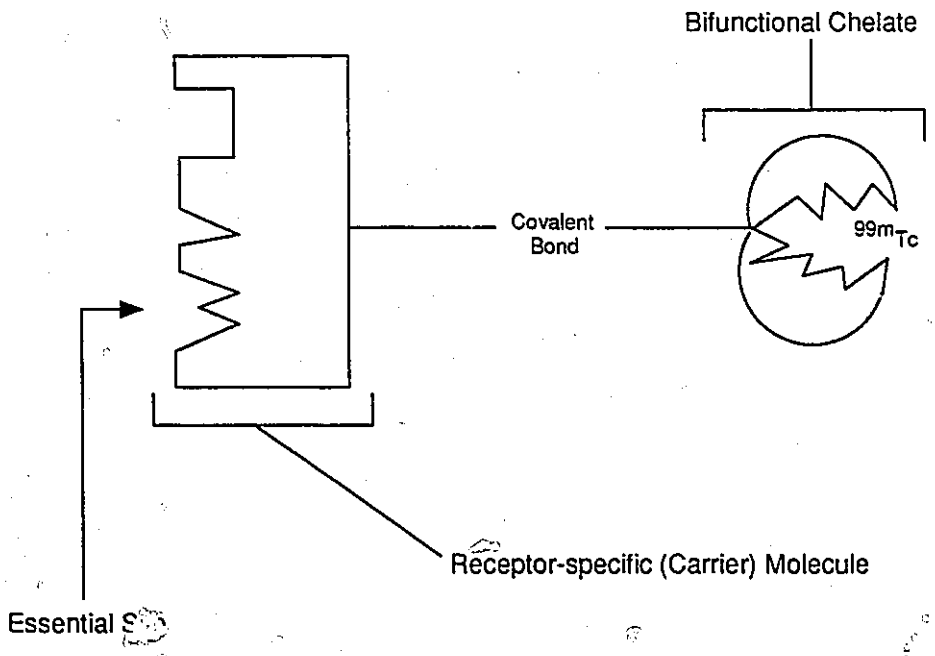

Figure 1.2: Schematic illustration of a receptor-specific, biologically active molecule labeled with ^{99m}Tc by the bifunctional approach.

is then referred to as a *bifunctional* (technetium) *chelate* (see Figure 1.2). This method

of labeling molecules is called the *bifunctional approach* and leads to the formation of *bifunctional radiopharmaceuticals*.[7]

In Tc radiochemistry, this dual-function nature of the bifunctional chelate permits the radiolabeling of an appropriate, tissue-specific biological compound (or "carrier") with the formation of *well-defined* chemical bonds to *both* the biomolecule and radionuclide. The ability of the bifunctional ligand to form these stable bonds is an important property for prospective radiopharmaceuticals because non-specific binding of the radioisotope is minimized, leading to optimal image sensitivity and discrimination. The chelate complex, for this reason, must be able to resist acid or cation-promoted dissociation in the low pH conditions of the stomach and liver, and the high cation concentrations in serum, *e.g.*, $[Ca^{2+}] = 1.25$ mM, $[Zn^{2+}] = 10^{-5}$ M.[9]

Generally, the carrier molecule belongs to one of two categories: 1) drugs which elicit some type of pharmacological response in the target organ (*e.g.*, antiarrhythmic drugs for increasing the force of myocardial contraction in heart therapy or hypoglycemic agents which stimulate insulin release); and 2) metabolic substrates (*e.g.*, long chain fatty acids which are used as an energy source in metabolizing heart muscle). Many biochemicals have well established physiological pathways and a rational prediction of their biodistribution can be stated.[7]

One major problem in bifunctional radiopharmaceutical design is that the conjugation of the ligand (or the Tc-99m chelate) to the biological molecule must not significantly alter its inherent biodistribution, if concentration of the radiolabeled conjugate in targeted tissues is to be successful. As will be discussed in Section 1.3.2, successful localization can be accomplished if the label is attached to a modifiable site[7] on the carrier molecule. However, the actual radiometal labeling procedure introduces a rather large, charged "foreign" group into the carrier in comparison to, for example,

radiohalogenation with fluorine or iodine. Because of the size and charge of the labeling group, it is important to determine whether the biological properties of the labeled molecule are significantly altered by the foreign substituent. This question must be addressed for each labeled radiopharmaceutical by *in vivo* monitoring of its pharmacologic properties and rate of metabolism in comparison to the clinically-accepted standard or the C-14 (or H-3) derivative.[10] While the bifunctional approach has been shown to be useful for some radionuclides, applications to ^{99m}Tc have met only limited success.[11]

1.3.2 Receptor-Binding Radiotracers

Many drugs and biologically active compounds induce physiological effects in the body when given in relatively low doses. These effects are a result of highly specific tissue localization mechanisms. The primary event in the biological action of many peptides, steroid hormones and drugs is thought to be the specific binding to a particular chemical site on the cell's plasma membrane or in the cytosol. These cellular sites - that are responsible for initiating a specific biological response from the binding of a guest molecule - are called *receptors* and are generally proteineous in composition.[12] Guest substrates may be bound by cellular receptors to participate in metabolism (*e.g.*, glucose in the brain or long chain fatty acids in myocardium) or to take part in a specific ligand-substrate interaction (*e.g.*, enzyme catalysis).[12] The recognition of an antibody by an antigen is yet another illustration of this receptor-mediated binding interaction.

Nuclear medicine could benefit greatly from the high pharmacological activity and molecular specificity of the receptor-binding mechanism, if this potential could be harnessed to build more effective radiopharmaceuticals. Perhaps the most

critical feature of an agent designed for heart, brain or pancreas imaging could be its ability to localize exclusively in these organs, thereby enabling favorable image contrast against the background. In principle, tissue targeting can be achieved if the radiolabel is judiciously attached to a carrier compound. Receptor-binding would then allow the radioactivity to concentrate in the appropriate tissues. The site of attachment of the radioactive tag to the carrier, however, is crucial for tissue specificity, as determined from structure-activity relationships (SAR).

That part of the drug or biomolecule - which is important for receptor recognition and/or binding - is called the "essential" site (see Figure 1.3).[7] Attachment

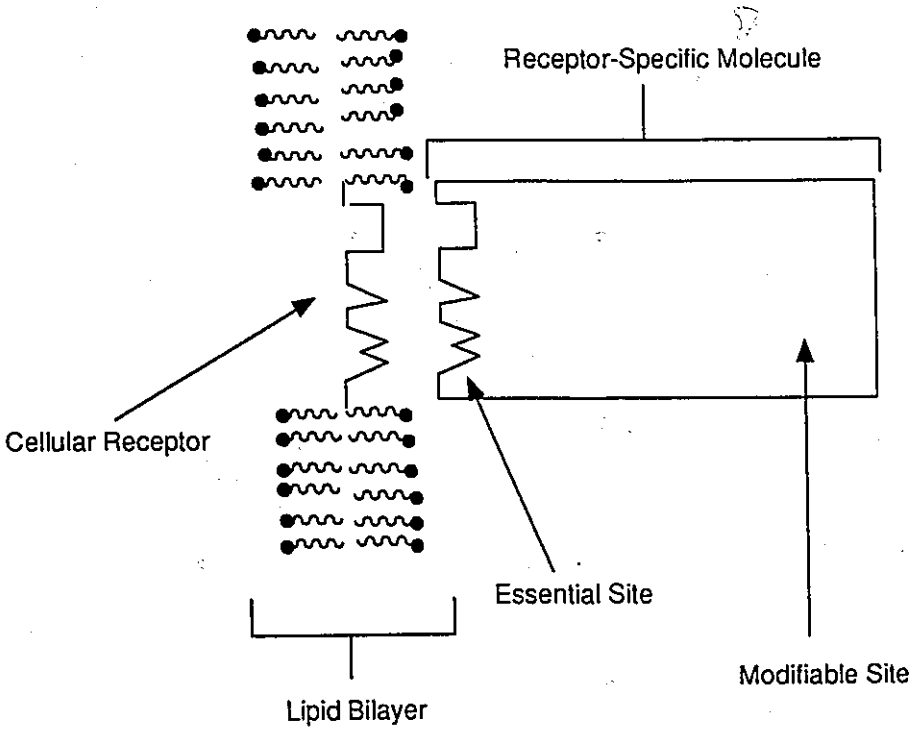

Figure 1.3: Schematic illustration of the binding of a receptor-specific molecule to its cellular receptor.

of the technetium chelate in this region of the molecule will invariably reduce or, more likely, eliminate binding affinity. Conversely, the biomolecule may possess another site

at which structural modification will not significantly alter receptor recognition and binding ability. Consequently, for the development of prospective, site-specific bifunctional radiopharmaceuticals, it is important to conjugate the ^{99m}Tc complex at this "modifiable" region of the biologically active molecule.

The concept of receptor-specific design - which is based on a prior knowledge of the structural requirements of a target receptor protein - is both simple and rational and may constitute the newest, most economical approach to clinically successful radiopharmaceuticals.[13] Stemming from SAR studies of the pharmacological behavior in animals of a series of close structural analogs, or from *in vitro* binding studies, reasonably accurate stereochemical models are available for the opiate receptor, the estrogen receptor and the dopaminergic receptor, to name a few. The exploitation of receptor properties for the development of imaging agents has been reviewed.[12,13]

In addition to receptor-binding effects, localization of radiotracers in target tissues is also a function of physical (*e.g.*, lipid solubility or molecular size) or chemical mechanisms (*e.g.*, phagocytosis, particle entrapment, simple and exchange diffusion, space/pool imaging and plasma protein binding).[6,14] Heindel has reviewed the development of numerous successful radiopharmaceuticals prepared by applications of receptor-binding mechanisms and has summarized the traditional physical partitioning mechanisms as well.[15]

1.4 Steroids as Receptor-Binding Carriers for Bifunctional ^{99m}Tc Chelates

Previous work has shown that alkylating agents employed in cancer therapy can be successfully delivered to hormone binding receptors in tumors by conjugating the alkylating agent to steroid compounds.[16,17,18] Workers in this field correctly

assumed that the lipophilic nature of the steroid molecule - combined with its lock-and-key specificity in receptor recognition and binding - could penetrate membrane barriers and transport the oncolytic agent to targeted tissues.

Steroidal hormone receptors present in target tissues and receptor-positive tumors formed the basis for the development of ^{18}F-labeled steroid radiotracers as *in vivo* positron emission tomography (PET) imaging agents. The utility of ^{18}F-labeled estrogens for imaging the estrogen receptor-positive breast tumors have been demonstrated.[19] Hence, it should be likewise possible to develop analogous ^{99m}Tc-labeled steroids to image other bodily tissues, since many tissues contain steroidal receptors. Moreover, the substitution of ^{99m}Tc, with its excellent imaging characteristics and ready availability, for ^{18}F in these compounds would remove the synthetic and practical limitations set by the latter nuclide's short physical half-life of 111 minutes.

1.5 Objectives of this Thesis

Most approaches taken in the development of Tc-based, radiopharmaceutical imaging agents have been confined to either the tagging of macromolecules or cells, according to "technetium-tagged" methodology, or relatively simple molecules (*e.g.*, ligands), *via* "technetium-essential" strategies. However, the tagging of *intermediate-sized* molecules with Tc-99m via *bifunctional methodology* has not been extensively reported, despite several, significant advantages of such a combined approach:

1) the potential for the specific targeting of judiciously-derivatized, receptor-binding radiopharmaceuticals to tissues traditionally considered to be difficult to image (*e.g.*, the non-excretory organs).

2) the ready availability and optimal radioimaging properties of ^{99m}Tc.
3) the formation of stable, well-defined bonds to both the radiolabel and carrier molecule. This results in higher tissue to background contrast levels and superior images.
4) the potential for radiopharmaceutical design through a more structured and logical approach (in comparison to Tc-essential methods).
5) an accessibility to a relatively inexpensive pool of physiologically active carrier compounds, such as drugs, oligopeptides and metabolic substrates. Other more complex carriers (such as antibodies) are limited by higher cost and development times.

Using bifunctional methodology, the conjugation of a ^{99m}Tc chelate with relatively small carrier compounds of known tissue specificity (at non-essential, receptor-binding sites) may result in radiopharmaceuticals of marked localization potentials. Steroids, as a unique class of highly-active yet relatively compact biological molecules, seem especially suited for ^{99m}Tc tagging since steroid target organs - such as the heart, adrenal, mammary, prostate glands, and, to a lesser extent, organs of the hepatobiliary system - are not easily studied by conventional radiographic or nuclear medicine procedures. To date, however, no published effort has been made to harness the tissue-specific, receptor-binding mechanism of steroidal carriers for the production of ^{99m}Tc-based bifunctional radiopharmaceuticals, despite some reported successes of Tc bifunctional radiopharmaceuticals.[20,21]

A method for diagnosing areas of myocardial ischemia and infarction would be a major achievement in medicine.[22] Thus, a major objective of our program was to conjugate a suitable technetium bifunctional ligand (see Chapter 2) to inotropic digitoxigenin and long chain fatty acids (see Chapter 3) for subsequent development as

^{99m}Tc-based myocardial imaging agents. Ligand derivatives of taurine, β-cyclodextrin and cholic acid were also prepared for development as potential ulcer and gastrointestinal radioimaging agents (see Chapter 4). With the possible exception of the taurine bifunctional conjugate (**36**), all ligand-carrier conjugates were designed to evaluate organ function through receptor-binding and/or physical localization mechanisms. As these ligand compounds often display dauntingly complex NMR spectral profiles, a major portion of this work was devoted to an analysis and discussion of the underlying physical and chemical properties of the diamide disulfide heterocycle (see Chapters 5 and 6).

CHAPTER 2

SYNTHESIS OF THE DADS-CO_2 BIFUNCTIONAL LIGAND

2.1 DADS-CO_2 as a Bifunctional Ligand for Technetium

Fritzberg *et al.* have successfully applied Davison's diamide disulfur (DADS) ligand system to ^{99m}Tc labeling of antibody fragments in cancer therapy.[23,24] Unlike other non-specific metal chelants (*e.g.*, EDTA and DTPA), the DADS ligand was designed specifically to coordinate technetium.[25] As a result, this N_2S_2 ligand system forms highly stable,[24] tetradentate complexes with technetium (*i.e.*, ^{99m}Tc-N_2S_2, see Figure 2.1, **5a**) in the +5 oxidation state. Studies on a variety of

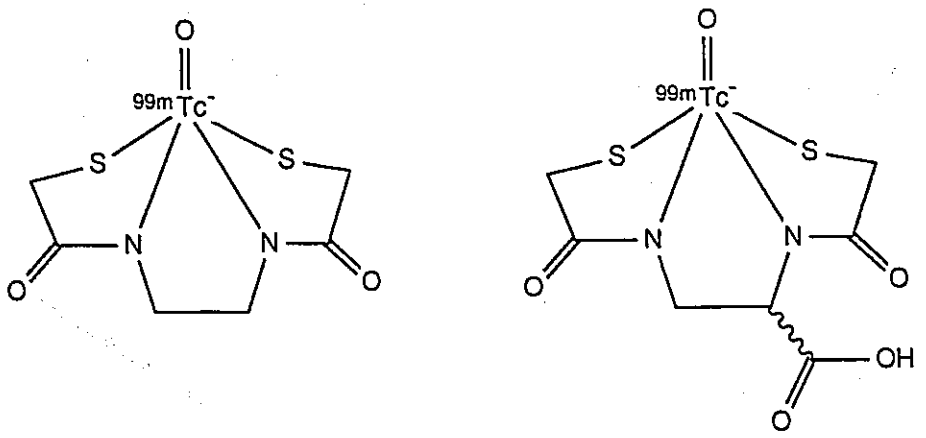

5a **5b**

Figure 2.1: ^{99m}Tc complexes of DADS (5a) and DADS-CO_2 (5b).

compounds incorporating the DADS donor group showed that high yields of ^{99m}Tc complexes of predicted structure were obtained.[26,27,28] Other potential metal-binding

groups, such as the carboxyl group in DADS-CO_2 complex (see Figure 2.1, **5b**), do not participate in binding.[29]

The above characteristics of the ^{99m}Tc-DADS-CO_2 complex epitomize the salient properties of the ideal bifunctional chelate. Moreover, the DADS ligand system is highly amendable to structural modification[30] using standard synthetic techniques and commercially-available reagents, and as such, represents an attractive chelant to systematically evaluate structure-activity requirements for the preparation of site-specific radioimaging agents. Consequently, the bifunctional DADS-CO_2 ligand was chosen for the development of Tc-based radiopharmaceuticals in this research.

A possible drawback of the DADS ligand system, however, may be traced to an insufficient lipid solubility to permit diffusion of the bifunctional radiopharmaceutical through lipoidal barriers.[12] In many cases, the target binding site is intracellular and the Tc-99m agent must be lipophilic enough to penetrate the capillary wall and the target cell's lipid bilayer membrane. The polar diamide functions and (negatively) charged nature of the Tc-DADS complex, may render the radiopharmaceutical too hydrophilic for successful localization to cellular binding sites. As earlier stated, experimental testing is the only unequivocal way to determine the success of tissue targeting. However, the issue of adequate chelate lipophilicity is only expected to be important in the development of the proposed imaging agents for myocardium or other non-excretory organs. Those suggested for gastrointestinal or hepatobiliary imaging would necessarily require a hydrophilic character to achieve a similar localization as seen in their polar parent compounds.

If empirical findings show the DADS-CO_2 ligand to be too hydrophilic for development as a myocardial imaging agent (as can be inferred from prominent hepatobiliary excretion[31]), it can be modified to the mercaptoamine (BAT) complexing

system of Kung *et al.*,[32] whose technetium chelates have been found to have sufficient lipid solubility to diffuse through the blood-brain barrier.

2.2 Synthetic Strategies toward the Development of ^{99m}Tc-DADS-CO_2 Bifunctional Radiopharmaceuticals (5c)

A retrosynthetic analysis for the synthesis of a general ^{99m}Tc-DADS-CO_2 bifunctional radiopharmacetical (**5c**) is presented in Figure 2.2. In general, the synthetic approach taken in the construction of intermediates was based on amide- or ester-forming condensation reactions. The target radiotracer can be realised from the *S*-protected derivative **5e**, following deprotection and subsequent chelation of Tc-99m. Condensation of a *S*-protected DADS carboxylic acid (**3a**) and the appropriate carrier molecule, with the formation of an ester or amide conjugative link, should then afford the conjugate **5e**. The most straightforward approach towards the synthesis of the DADS-CO_2 bifunctional ligand **3a** would be to couple two equivalents of a suitably *S*-protected thioglycolic acid (2-mercaptoacetic acid) with one equivalent of 2,3-diaminopropanoic acid. The synthesis of the ligand system was subsequently investigated from these commercially-available starting materials.

The synthetic sequence is important to the overall yield of the proposed radiopharmaceutical **5c**. For example, the convergent procedure of conjugating ligand **3a** and a carrier molecule minimizes the number of synthetic transformations which involves the potentially expensive and reactive carrier. A linear synthesis - where a part of, or the entire ligand framework, is sequentially built onto a carrier template (for example, see ref. 32) - would not be cost or time effective and may not be suitable where the carrier molecule possesses reactive or sensitive functional groups. In addition, a convergent strategy is highly amenable to the speedy assembly of

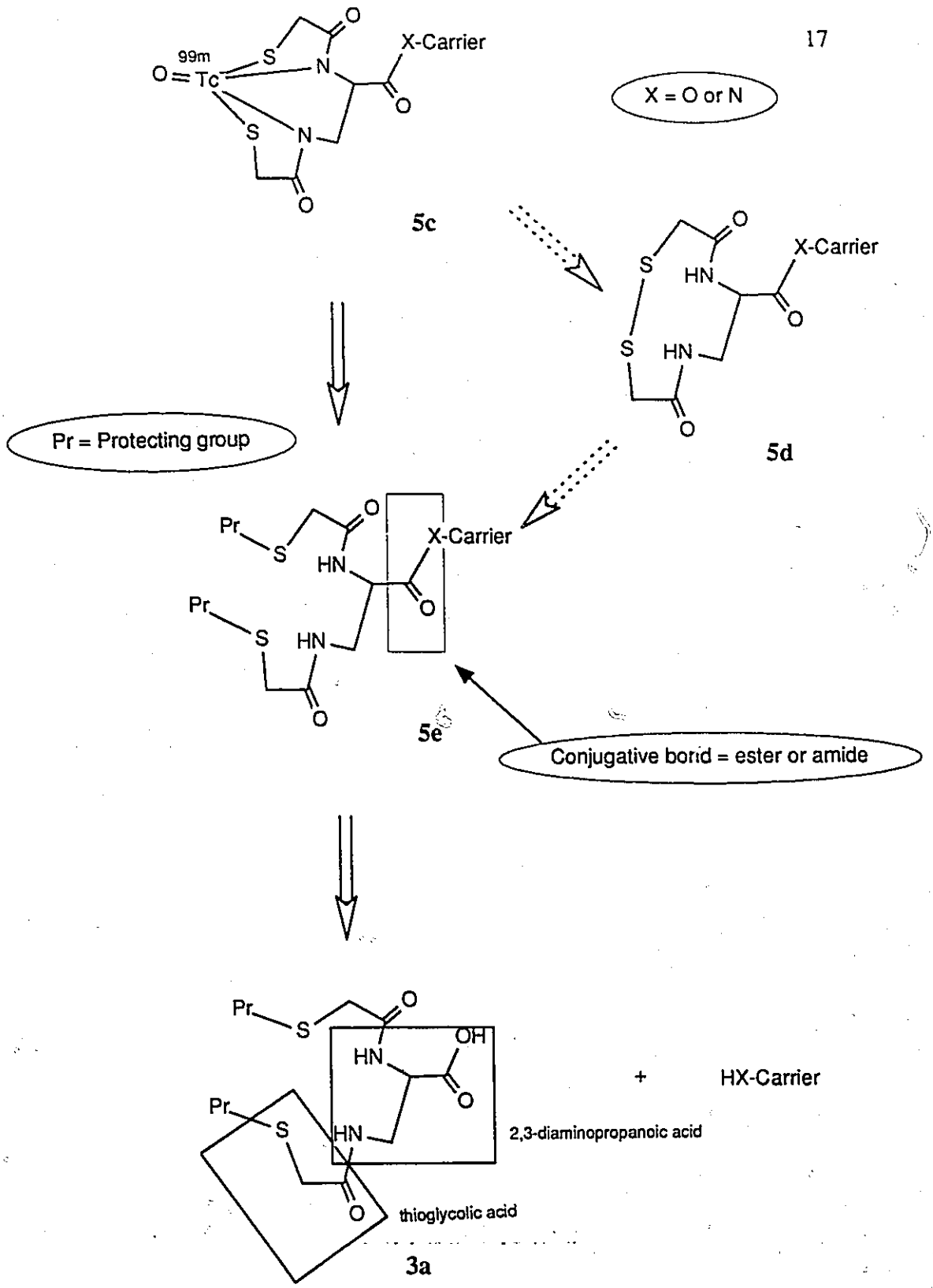

Figure 2.2: Retrosynthetic analysis for the synthesis of a ^{99m}Tc-DADS-CO_2 bifunctional radiopharmaceutical (5c).

prospective tissue-specific radioimaging agents: upon selection of a suitable carrier, a synthesis of **5c** can be completed within three steps (*i.e.*, conjugation, deprotection and chelation). The chelation of Tc-99m as the final step ensures that the radiopharmaceutical preparation of **5c** is maximally "carrier-free"; this minimizes the saturation of target tissue sites by technetium conjugates incorporating the ineffective ^{99}Tc radionuclide. This approach contrasts with other bifunctional strategies where conjugation to the carrier takes place after ligand complexation with ^{99m}Tc.[24]

Protection of the thiol group in thioglycolic acid and its derivatives was deemed necessary since the free functionality would interfere with the planned carboxyl activations in subsequent amide or ester-forming reactions. The choice of the *S*-protecting group and the method for its cleavage was crucial for the efficiency of the proposed synthesis. Thiol groups are normally protected as aryl thioethers, hemithioacetals or thioesters[33]; however, deprotection frequently requires harsh conditions that can lead to decomposition when sensitive functional groups are present. Moreover, the sulfur products of these acidic or basic deprotection schemes can also engage in side reactions, including acid-catalysed *N*- to *S*-acyl transfer initiated by SH attack to neighbouring amide groups and disulfide polymerization *via* thiolate coupling.[32,34] In the former case for example, decomposition of C_{11} substituted DADS fatty acid amide conjugates has been noted in our lab during *S*-detritylation using the CF_3COOH/Et_3SiH method.[35] This is suspected to proceed *via* nucleophilic attack of the unmasked SH group to the protonated C=O function at the C_{11} amide, resulting in a six-membered thiolactone and the corresponding 11-amino fatty acid (based on analogy to ref. 36). Thus, the high reactivity of unprotected sulfur atoms - compounded with harsh deprotection methods - make this synthetic strategy less desirable for the development of radioimaging precursors.

As the carrier-ligand conjugate **5e** must endure the conditions leading to *S*-deprotection (see Figure 1.5), we wished to develop a deprotection procedure for sulfur which was exceedingly mild in its operation, compatible with the widest range of carrier and ligand substrates, yet afforded relatively stable sulfur derivatives. We noted that iodine had been used in the removal of trityl groups from sulfur with facile, *in situ* oxidation to disulfides.[37] Moreover, disulfides are stable, readily prepared and easy to cleave with mild reductants (for example, Sn(II)) to form the dithiol required for coordination with ^{99m}Tc and, as such, represent attractive precursors to Tc chelants. That is to say, reduction of the primary disulfide group and pertechnetate ion by stannous salts and subsequent complexation to afford **5c** can be achieved simultaneously in a one-pot chelation step. This convenient labeling process also attractively lends the disulfide form of ligand conjugate **5e** (**5d**) to "instant kit" formulation. The synthesis was therefore undertaken through the "protected" disulfide conjugate **5d**, using trityl as the sulfur protecting agent and iodine as its deprotectant.

Radiolabeling and *in vivo* testing of the carrier-ligand conjugates (*i.e.*, compounds **19**, **21**, **23**, **27**, **34**, **36** and **38**) prepared in this study will be accomplished in co-operation with the Department of Nuclear Medicine at the McMaster University Medical Center.

2.3 Synthesis and Characterization of *N,N'*-bis[2-(triphenylmethyl)thioethanoyl] -2,3-diamino propanoic acid (3)

The *S*-protected DADS-CO_2 bifunctional ligand **3** was prepared according to the synthetic pathway outlined in Scheme 2.1. Tritylation of the SH function of thioglycolic acid using triphenylmethanol and boron trifluoride etherate as a Lewis acid catalyst[35] readily afforded the protected acid **1**. The carboxyl group was subsequently

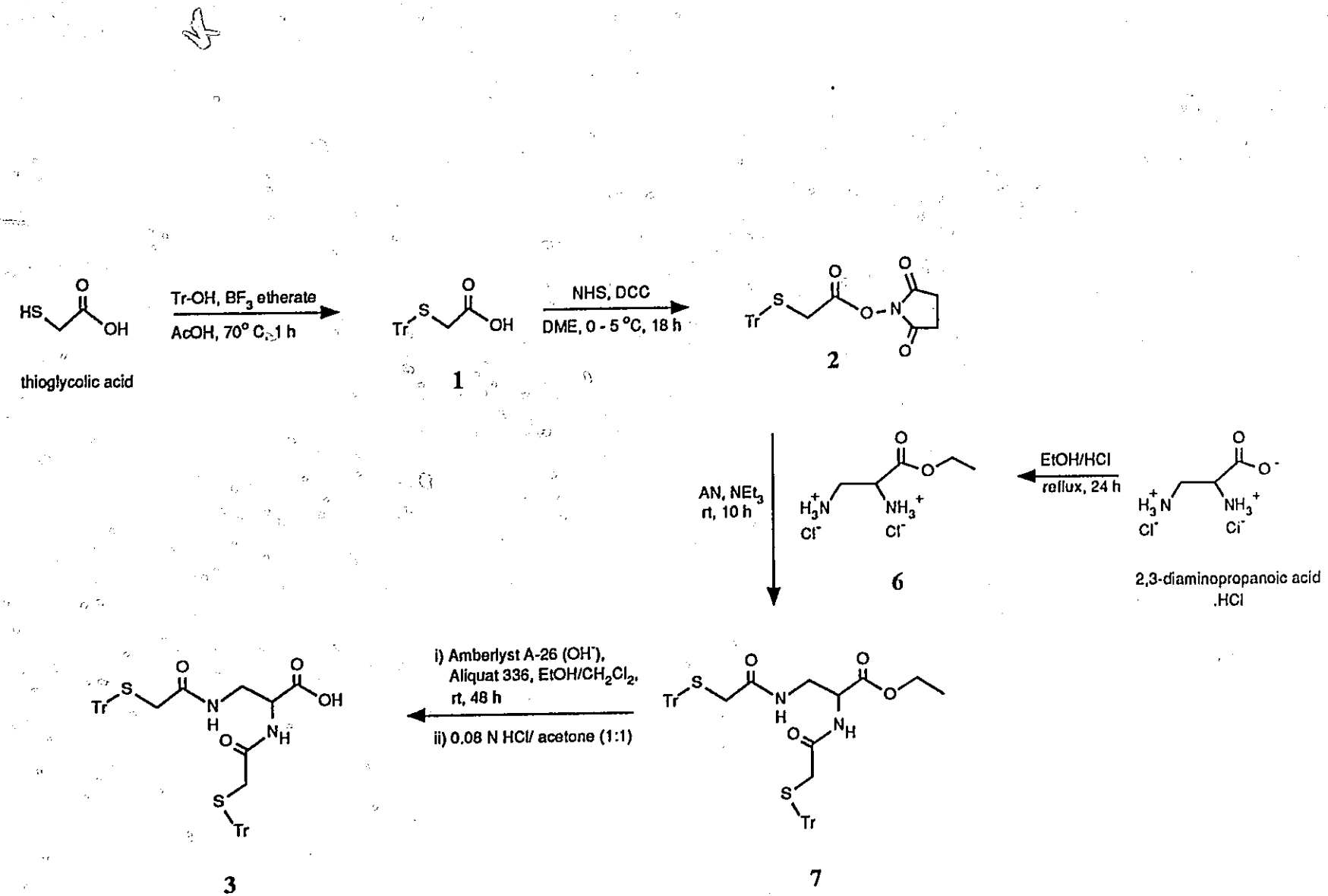
thioglycolic acid
Tr-OH, BF3 etherate
AcOH, 70° C, 1 h
1
NHS, DCC
DME, 0 - 5 °C, 18 h
2
EtOH/HCl
reflux, 24 h
2,3-diaminopropanoic acid .HCl
AN, NEt3
rt, 10 h
6
i) Amberlyst A-26 (OH-), Aliquat 336, EtOH/CH2Cl2, rt, 48 h
ii) 0.08 N HCl/ acetone (1:1)
7
3

Scheme 2.1

activated with *N*-hydroxysuccinimide (NHS) and 1,3-dicyclohexylcarbodiimide (DCC)[38] to give the succinimidoyl ester **2**. The physical and spectroscopic properties of intermediates **1** and **2** were entirely consistent with *S*-protection and carbonyl activation (see Sections 7.6.1 and 7.6.2).

Concurrently, ethyl 2,3-diaminopropanoate dihydrochloride (**6**) was prepared from the commercially-available, parent acid monohydrochloride in refluxing ethanolic HCl under standard Fischer esterification conditions. Ester formation was confirmed by the detection of a new ninhydrin positive spot at R_f 0.27 (70% *n*-PrOH, 28% dH_2O; 2% HCOOH), as well as a prominent ester carbonyl stretching absorption at 1745 cm^{-1} in its IR spectrum. In addition, an interesting confirmation of the COOEt group was revealed by the 200 MHz ^1H NMR spectrum of **6**, where two quartets were noted at δ ~4.23 and separated by 0.008 ppm. This separation increased at 500 MHz, suggesting that the observed multiplicity was a result of the almost-perfect superimposition of the two different signals and not a coupling effect. An absorption in the range δ 4.1 - 4.3 was highly diagnostic of a methylene group at the α-hydroxyl position of an ethyl ester fragment, while the field-dependency of the quartet shift separation indicated that these CH_2 protons were diastereotopic. The observed O-C*H*$_2$CH$_3$ diastereotopicity was presumably a result of the group's proximity to the C-1 stereocenter (see Section 5.2).[39] Moreover, the ^{13}C NMR spectrum of **6** revealed signals at δ 13.75 and δ 62.65, corresponding to the methylene and methyl carbon resonances of the $COOCH_2CH_3$ moiety.

Treatment of two equivalents of the *N*-hydroxysuccinimidoyl ester **2** with the diamino ester **6** in acetonitrile resulted in the acylation of both nitrogens and the formation of the diamide adduct **7**. As evidence for diamide formation, ^1H and ^{13}C NMR spectra showed characteristic amide resonances at 6.26 and 6.82 ppm and 168.48

and 168.69 ppm, respectively. In addition, IR spectroscopy indicated strong peaks in the 1520-1660 cm^{-1} region, which was characteristic of Amide I and II C=O absorptions. Alternatively, compound **7** was synthesized *via* DCC-mediated coupling of acid **1** and the diamino ester **6**. Although the isolated product from this reaction showed significant contamination by dicyclohexylurea (DCU), higher yields of the diamide acid **3** was obtained by the DCC coupling method, providing that crude **7** was used directly without purification in ion-exchange mediated ester hydrolysis.

The ethyl ester **7** was hydrolyzed to the free acid **3** in 92% yield *via* catalytic assistance from a macroreticular anion-exchange resin in the hydroxide form and a tetraalkylammonium phase transfer reagent. Spectroscopic examination of the residue, obtained from acidic elution of the resin, indicated a structure that was consistent with the diamide acid **3**. ^1H NMR spectroscopy of **3** in deuterated dimethylsulfoxide (DMSO-d_6) revealed a doublet and triplet at δ 7.61 and 7.75, corresponding to the C_6O-N*H* and C_4O-N*H* amide groups, respectively. Moreover, one S-CH_2 group appeared as an AB quartet (^2J = -13.9 Hz) at δ 2.79, while the other pair gave a singlet at δ 2.75 (see Section 5.1 for further details). ^{13}C NMR spectra corroborated the ^1H NMR findings, showing two signals in the carbonyl amide region (δ 169.28 and δ 170.24). The magnetic non-equivalence of the S-CH_2 groups was also apparent from the closely-separated pair of signals at δ 35.66 and δ 35.84. Positive fast atom bombardment mass spectroscopy (FAB-MS) confirmed a M+1 ion at *m/z* 737.

2.3.1 Anion-Exchange Chromatography as a Novel Hydrolysis and Purification Method

The macroreticular anion-exchange method of hydrolysis also doubled as an effective purification scheme for the removal of non-anionic impurities, particularly the

troublesome DCU by-product of previous DCC-mediated coupling reactions (see Figure 2.3). These contaminants and the phase-transfer catalyst were easily removed by washing the carboxylate resin with two column volumes of ethanol and acetone. Elution of the free acid from the resin with a weakly acidic solution of aqueous HCl in acetone furnished **3** in high yield after work-up.

Curiously, the activity of the hydroxide form of the ion-exchange resin was found to decrease with time when stored in ethanol. Most notably, a distinctive amine odour was also detected in old preparations, which often required a preliminary "airing" period in a fume-hood after opening the resin storage container. This perplexing observation was rationalized in terms of a first order decompostion of the resin as indicated in Scheme 2.2.

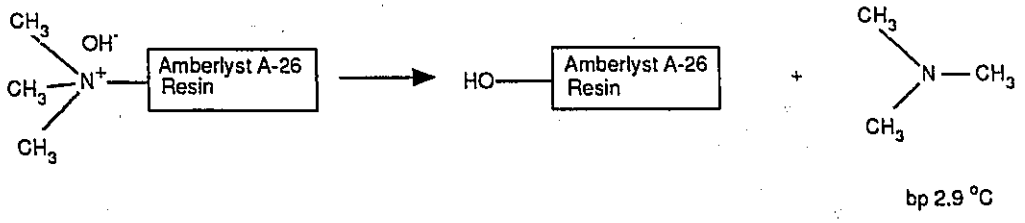

Scheme 2.2

This suggested decomposition of the resin was based on similar reactions involving trimethylalkylammonium salts and hydroxide ion.[40] Note that the volatile trimethylamine by-product can serve to account for the amine smell of old resin preparations. Consequently, with these observations in mind, prewashed resin in the chloride form was converted to the hydroxide form *just prior* to use in ester hydrolysis.

2.3.2 Difficulties Encountered in the Synthesis of 3

Initial strategies toward the synthesis of the diamide **3** were aimed at coupling the protected acid **1** directly with the unesterified diamino acid *via* the

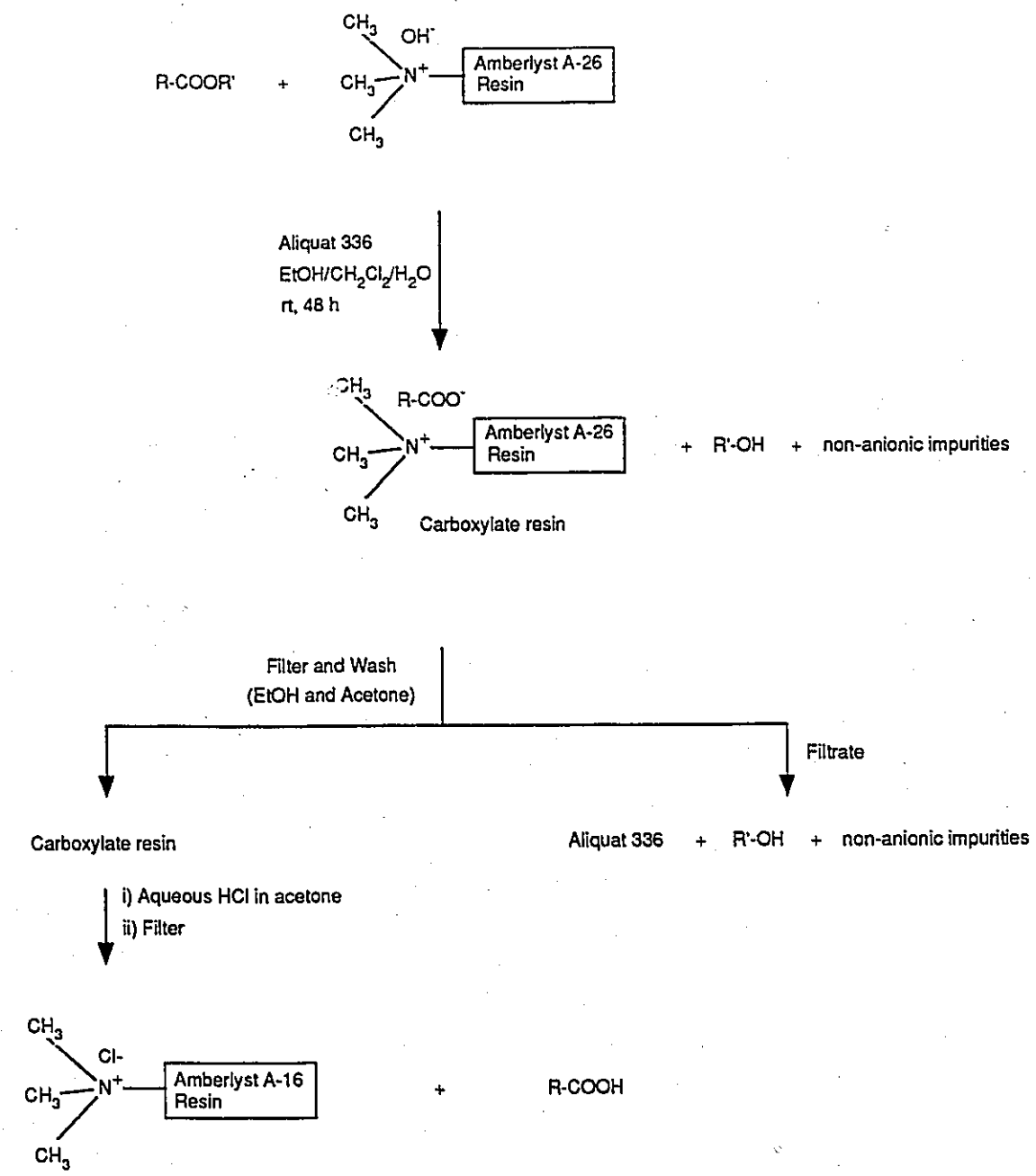

Figure 2.3: Hydrolysis of ester R-COOR' and purification of the resulting acid R-COOH from non-anionic impurities. Aliquat 336 = tricaprylylmethylammonium chloride.

carbonyldiimidazole (CDI)[41,42] and NHS activation of **1**.[35] Although this synthetic plan had the appeal of avoiding cumbersome esterification and hydrolysis steps (as in Scheme 2.1), numerous attempts in this area failed to afford good yields of the diamide. The poor yields were believed to have resulted from the solvolysis of acid-activated intermediates of **1** by the protic solvent components that were required to ensure dissolution of the highly-polar 2,3-diaminopropanoic acid reactant. Protic solvents were necessary components of the reaction mixture since the diamino acid defied solubility in neat aprotic matrices and it was found to be taken up only in water-$NaHCO_3$ or methanol-NEt_3 mixtures.

Clearly, an aprotic solvent is preferred to a protic one in order to avoid solvolysis of the reactive acyl intermediates generated for subsequent amide formation. It was anticipated, however, that the 10^6-fold greater nucleophilicity of the amine relative to water[43] would ensure faster aminolysis rates and acceptible yields of the desired amide, particularly if a slight excess of CDI reagent was used. Thus, several CDI-mediated condensations were attempted in protic solvent mixtures, typically by adding a mildy-basic, aqueous solution of the amino acid to a solution of the activated imidazolide (**1a**, Scheme 3.6) in aprotic solvents such as tetrahydrofuran (THF), dimethoxyethane (DME), acetonitrile (AN) and DMSO. Analysis of the reaction mixtures disclosed the incomplete formation of the diamide (**3**), with reactants comprising the major components. The recovery of starting material from these protic solvent systems hinted that the rate of hydrolysis of the acyl imidazolide intermediate was comparable to that for aminolysis. Clearly, the high moisture-sensitivity of the reactive acyl imidazolide **1a** precluded its utility as an efficient coupling reagent in aqueous environments.

The search for an activated acid intermediate of **1** that was sufficiently inert

to solvolysis in the protic environment led to the preparation of the *N*-hydroxysuccinimidoyl ester of **1** (2)[35] and its subsequent coupling to 2,3-diaminopropanoic acid in dimethylformamide (DMF)-water mixtures. Although improved yields of **3** were noted relative to the CDI method, regrettably, 20-30% of the activated ester hydrolysis product, **1**, was detected by TLC. This low amide yield arose from the incomplete solubility of the amino acid nucleophile and/or the activated ester in the final reaction mixture. For example, it was possible that the diamino acid formed polar aggregates in the binary solvent, which reduced the effective concentration of the diamine in solution and, ultimately, product yield. Subsequent trials, therefore, involved the substitution of $NaHCO_3$-water with NEt_3-methanol solvent mixtures to ensure homogeneity and a reduction in the solvolysis rate of the activated ester. Although TLC indicated the formation of **3** [R_f 0.22, 10% MeOH in methylene chloride (CH_2Cl_2)] and the disappearance of the succinimidoyl ester **2** (R_f 0.92), an estimated 30% of the reaction mixture was contaminated by the methyl ester adduct, Tr-S-CH_2-COOMe.

Coupling of 2,3-diaminopropionic acid .1HCl and **1** was also attempted using the water soluble EDC [1-(3-dimethylaminopropyl)-3-ethylcarbodiimide .1HCl] coupling reagent.[44,45] In this reaction, a solution of the amino acid in distilled water (dH_2O) and triethylamine (NEt_3) was added to a stirred solution of **1** and EDC in DME after a 10-minute activation period. Turbidity was induced upon slow addition of the amino acid solution. TLC of the reaction mixture after 18 hours revealed starting materials as the major products.

The poor yield of **3**, possibly due to the lack of a suitable aprotic solvent for the diamine and activated ester reagents, prompted the development of ester derivatives of 2,3-diaminopropanoic acid to enhance its lipophilicity in these solvents.

Accordingly, methyl and ethyl esters were prepared and they were found to dissolve in DME and AN, enabling amide coupling to take place in either of these low-boiling, aprotic solvents in the complete absence of water or methanol. As expected, solvolysis products of the activated ester were not observed. Owing to its greater solubility in aprotic solvents, the ethyl ester **6** was employed for the synthesis of **3**, as depicted in Scheme 2.1.

2.4 Proposed Mechanism of *S*-Detritylation and Oxidative Cyclization

S-Detritylation of protected ligand precursors employing 1.1 equivalents of I_2 - or 2.1 equivalents in the case of the *S*-trityl cyclodextrin conjugate **37** (see Section 4.4.4) - occurred quantitatively with concommitant cyclization to the intramolecular disulfide. Though the mechanism of this curious two-step, one-pot reaction has not been reported to our knowledge, it most likely progresses *via* a sulfenyl iodide intermediate,[46,47] with the reaction's driving force hinging on the high resonance stability of the departing trityl cation in the transition state. Two possible pathways for this detritylation-cyclization process are presented in Figure 2.4, with iodine or hydrogen iodide concentrations determining the direction of the reaction paths.

During the initial stages of deprotection when the concentration of iodine is high and that of HI low, Pathway A is favored. In this scheme, the first elementary step involves a donor-acceptor interaction between two iodine molecules and trityl sulfide sulfur atoms, leading to the formation of a 1:1 charge transfer (CT) complex. Experiments have shown that aliphatic sulfides and iodine form strong complexes in solution and in the gas phase. Tideswell and McCullough[48] have measured the equilibrium constant for complexation, $K_{complexation}$, at 20 °C in CCl_4 to be 71 $L.mol^{-1}$ for dimethylsulfide and iodine. In a separate study, Tsubomura and Lang[49] have

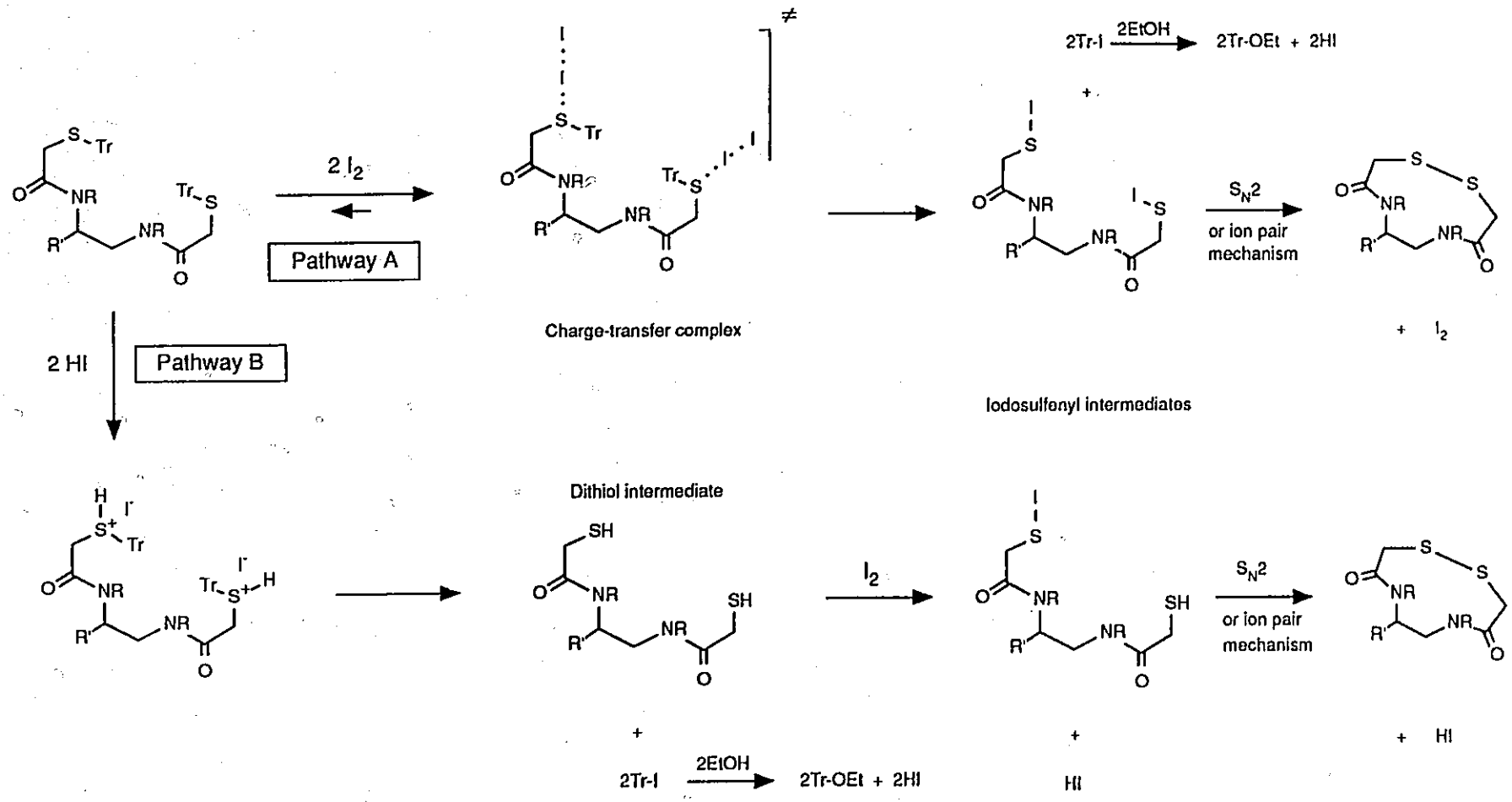

Figure 2.4 : Proposed pathways for the deprotection and oxidation of *S*-trityl ligands with I_2. R = H or CH_3 ; R' = H or CO-NH(O)-Carrier.

reported $K^{20°C}_{complexation}$ = 210 L.mol^{-1} for the diethylsulfide-I_2 CT complex. As the differences in these values apparently reflect the electron releasing abilities of the *S*-alkyl groups and the induced, effective charge on the S atom, a large estimate of $K^{20°C}_{complexation}$ can be inferred for the CH_2-S-Tr substructure of protected ligand intermediates. The essence of this comparison is to note that complexation between iodine and the *S*-protected ligands is highly favored and that *both* sulfur atoms are likely to complex with iodine molecules and form CT adducts during the early stages of the reaction.

Unlike disubstituted aliphatic sulfide-I_2 complexes (which do not undergo further reaction), the Tr-S··I_2 activated complex readily loses trityl iodide and stabilizes to a diiodosulfenyl intermediate. The driving force for this reaction is presumably linked to the high resonance stability of trityl cation in the transition state. The existence of sulfenyl iodides is well-established[46,47,50] and they are the accepted intermediates in the oxidation of organic divalent sulfur by iodine.[50]

The conversion of the diiodosulfenyl intermediate to the intramolecular disulfide may proceed through the formation of pentacovalent sulfur intermediate (I), initiated by intramolecular attack of the second S-I function in a S_N2 fashion.

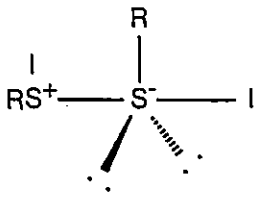

I

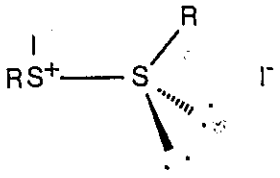

II

However, as Ciuffarin and Guaraldi have noted in their work on nucleophilic substitution reactions involving sulfenyl halides and *n*-butylamine, sulfur-sulfur coupling through an ion-pair intermediate (II) cannot be ruled out.[51] Finally, iodide

combines with iodonium ion to form neutral iodine which can be recycled into Pathway A (or B) to continue the deprotection sequence. Thus, for every two iodine molecules consumed per protected ligand molecule, one molecule is regenerated.

As the reaction proceeds as depicted by Pathway A, the concentration of I_2 drops and that of HI increases through ethanolysis of trityl iodide. In this concentration regime, HI molecules begin to compete with I_2 for basic sulfide sites on the protected ligand *via* Pathway B. If the concentration of I_2 is sufficiently low, then protonation of both sulfur atoms by HI can occur to afford a dihydroiodide salt intermediate. This *S*-protonated species may plausibly be stabilized through heterolytic cleavage of the *S*-trityl bond with the formation of trityl iodide and a dithiol. Subsequently, a SH function of the dithiol can displace iodide from an iodine molecule to generate a thiol-sulfenyl iodide. As in Pathway A, cyclization can occur through displacement of I^- by SH attack - by either a S_N2 or ion-pair mechanism - to form the 10-membered disulfide heterocycle and HI.

2.5 Oxidation of the Iodosulfenyl Intermediate of 7 by O_2

Test reactions aimed at deprotecting and oxidizing the *S*-trityl ether **7** under standard reaction conditions led to the observation of small quantities of M+16 and M+32 ions in the mass spectrum of the products. It would seem that the iodosulfenyl and/or thiol intermediates are sensitive to overoxidation by dissolved oxygen, leading to the formation of thiosulfinates and higher oxidized analogues.[52] To overcome this side reaction, any reaction mixture containing **7** was degassed for 30 minutes at 15 mm Hg, both before and after the addition of I_2 crystals. This procedure virtually eliminated all product contamination by higher oxidation products. Apart from MS analysis, no attempt was made to characterize or isolate the oxidized products of **7**.

CHAPTER 3

SYNTHESIS OF MYOCARDIAL IMAGING AGENTS

3.1 General Introduction

Myocardial perfusion radioimaging with thallium-201 (^{201}Tl or thallous ion) has become a routine part of the clinical evaluation of patients with coronary artery disease (CAD). While the initial distribution of ^{201}Tl reflects local blood flow (*i.e.*, perfusion), it is not the ideal radiotracer. Rapid serial evaluation of perfusion is not possible because of its long physical half-life (73 hours) and slow myocardial clearance. Its long $t_{1/2}$ also prevents the use of high injected activities. Image quality is marginal because of its low energy (X-ray) emission which leads to tissue attentuation. Furthermore, it is expensive and its myocardial distribution reflects flow for only a short time after stress because of redistribution.[53] These drawbacks can be avoided through a Tc-99m based myocardial imaging agent, since Tc-99m is widely regarded as the optimal emitter for diagnostic imaging applications. Owing to its excellent physical decay properties and its ready availability from ^{99}Mo-^{99m}Tc generators (see Section 1.2), ^{99m}Tc is the radioisotope of choice for myocardial imaging. Strauss and Pitt[54] have hypothesized that, in relation to ^{201}Tl, a ^{99m}Tc agent would offer a two-fold increase in resolution and allow a four-fold increase in the dose that could be administered. Thus, the development of a routine myocardial perfusion agent based on Tc-99m is an important - albeit to date elusive - goal of cardiovascular nuclear medicine.[55]

Several new ^{99m}Tc complexes for regional myocardial perfusion imaging have been reported.[56-63] These agents are prospective replacements for ^{201}Tl as the major radiopharmaceutical for routine nuclear medicine application. The ^{99m}Tc isonitrile cations (see Figure 3.1), initially developed by Jones and Davison, have reached the final stage of clinical trial and possibly represent the best candidates for the replacement of ^{201}Tl imaging.[56] The first agent in this series, TBI (^{99m}Tc-*t*-butylisonitrile), showed pronounced uptake and retention reflecting regional perfusion. However, its initial lung uptake and subsequent high liver retention clearly indicates the need for further improvement.[57] A new generation of isonitriles, TMIBI (^{99m}Tc-2-methoxyisobutylisonitrile) and TCPI (^{99m}Tc-2-carboxypropylisonitrile), showed improved liver and lung washout but with the same myocardial uptake and prolonged retention as TBI.[58-60] TMIBI or "Sestamibi" was chosen for further development and is currently in the advanced stages of clinical trials. Boronic acid adducts of technetium dioximes (BATO) have also been reported.[61] Initial clinical study has indicated that they may be useful as myocardial perfusion tracers.[62] Another group of ^{99m}Tc-(arene)$_2^+$ compounds, which are "sandwich" complexes, was reported[63] and initial studies in animal models showed very high myocardial uptake and prolonged retention.[64] Among all of these potential ^{99m}Tc imaging agents for the heart, TMIBI and CDO-MeB (a neutrally-charged BATO derivative, see Figure 3.2) have been extensively tested in humans and are well on their way to commmercialization under the trade names Cardiolite® (NEN-Dupont, N. Billerica, MA) and Cardiotec® (Squibb, New Brunswick, NJ), respectively.[65]

3.2 Pharmacology of Some Cationic Imaging Agents

The idea of investigating ^{201}Tl and cationic ^{99m}Tc isonitriles to localize in

R	Name	Abbreviation
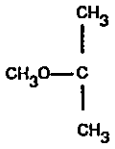	Tc-hexakis-methoxy isobutyl isonitrile	TMIBI (Tc-sestamibi)
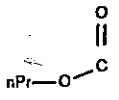	Tc-hexakis-carboxy propyl isonitrile	TCPI
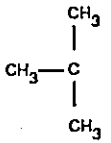	Tc-hexakis-tertiary butyl isonitrile	TBI

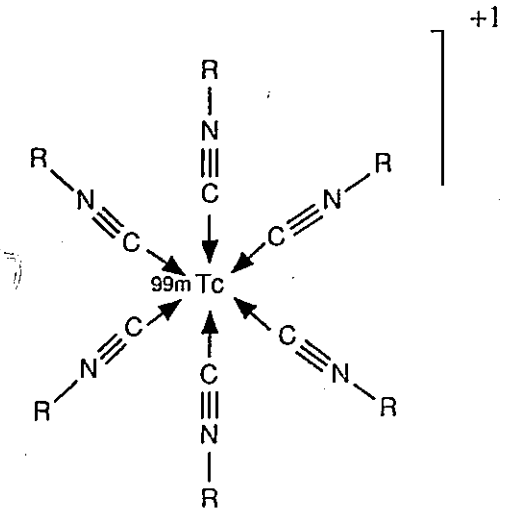

Figure 3.1 : Cationic ^{99m}Tc isonitriles.

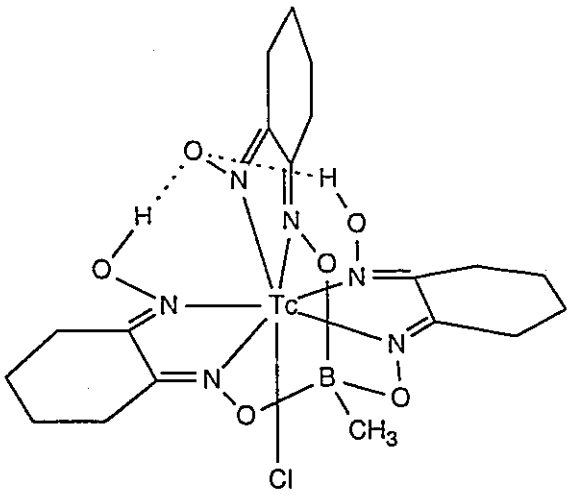

Figure 3.2: Chemical structure of ^{99m}Tc-cyclohexane-dione dioxime-methyl boronic acid (^{99m}Tc-CDO-MeB).

the heart in proportion to myocardial blood flow used as the operating principle the observation that many cations have an affinity for the heart.[66] However, studies involving isolated myocytes to explore uptake mechanisms showed that the extraction of thallous ion occurs through the Na^+,K^+-ATPase pump, while that of TCPI and TMIBI resulted through an unknown means. Further tests showed that the uptake of the isonitriles could not be reduced by ouabin inhibition of Na^+,K^+-ATPase; they were mainly associated with the cell membrane. Though these two agents go to the myocardium and remain there for a considerable period of time, the distribution of ^{201}Tl constantly changes as it moves toward equilibrium, whereas that of TMIBI is reported to be essentially fixed.[65] Nevertheless, with the actual mechanism for myocardial uptake aside, it is abundantly clear from animal and human imaging studies that thallous ion, the ^{99m}Tc isonitriles and the neutral BATO complexes behave as probes for myocardial *perfusion.*

The concept of heart imaging using "perfusion" agents is based on

measurements of *vessel blood flow,* which is not necessarily equivalent to tissue perfusion or blood flow through myocardial tissue.[65] Ideally, a measure of the *metabolic* state of the tissue is required, as this information would furnish *directly* the functional ability of the heart, as in ischemia. However, at present, no ^{99m}Tc myocardial agents have been developed as probes of cardiac metabolism. The objective of this research, in part, is to fill this medical need through the development of prospective, ^{99m}Tc-based imaging agents to assess myocardial function *via* metabolic uptake mechanisms.

3.3 ^{99m}Tc Fatty acid-based Agents for Myocardial Imaging

3.3.1 Introduction

Nonesterified, long chain fatty acids (C_{14}-C_{18}) serve as an important fuel for normal functioning heart muscle.[67] Evans and associates[68] proposed that regions of the myocardium with impared metabolism or diminished arterial blood flow might be imageable through the use of radioiodinated oleic acid. Bilheimer *et al.* have reported that injection of [^{11}C]oleic acid into dogs inflicted with acute myocardial infarction induced localization of the radioactivity in the peripheral and border zones of the lesion.[69] Reduced uptake of γ-emitting, radiolabeled fatty acids in ischemic or infarcted myocardium was later demonstrated with [^{131}I]oleic acid,[70,71,72] 16-[^{123}I]iodo-9-hexadecenoic acid,[73] 17-[^{123}I]iodoheptadecanoic acid[74] and 1-[^{11}C]palmitic acid.[75]

In patients with CAD, ischemic regions may be clearly recognized in myocardial scintigrams as photo-deficient areas because of the lack of tracer accumulation. A decrease in coronary perfusion is accompanied by a marked diminution of myocardial fatty acid uptake. This decreased uptake is not solely an

expression of decreased delivery of fatty acid due to a decreased blood flow: in ischemic myocardium, there is also evidence to suggest that the extraction rate of the fatty acid is reduced. These effects combine to enhance the effect of reduced perfusion. Thus, in contrast to the situation with glucose, where a decrease of delivery is partially offset by an increase of the extraction rate, myocardial fatty acid uptake has to be regarded as a very sensitive index of myocardial ischemia.[76] These findings demonstrate the potential of radiolabeled fatty acids as metabolic probes of myocardium, specifically as agents for the detection of infarcted or ischemic areas.

However, the promising radioimaging ability of the above iodinated fatty acids are offset by a number of limitations. The *in vivo* stability of radioiodinating compounds is limited because of dehalogenating enzymes which increase blood activity levels by the release of radioiodide.[67,77] Moreover, ^{131}I has poor physical decay properties for imaging with a γ-scintillation camera, while ^{123}I is expensive and not readily available. The short, 20-minute half-life and positron emission (yielding a penetrating γ radiation of 511 keV) of the ^{11}C radioisotope restricts ^{11}C-labeled imaging agents to medical institutions having cyclotrons and positron cameras.[67]

The development of a ^{99m}Tc-based fatty acid imaging agent - which, like its radioiodinated counterparts, accumulates in proportion to local metabolic activity in impaired myocardium - would be an important complement to existing myocardial perfusion agents. Some researchers have succeeded in developing ^{99m}Tc-labeled fatty acids, only to be halted by modest myocardial localization. Livini *et al.* labeled mercapto derivatives of palmitic acid with ^{99m}Tc.[69] A similar approach was attempted by Loberg and co-workers,[78] who labeled undecanoic acid derivatives using iminodiacetate (IDA) as the chelating group. In both cases, the myocardial uptakes of these radiochelates were lower than that for [^{3}H]palmitic acid. This difference was

thought to be due to the formation of high molecular weight, 2:1 fatty acid-technetium complexes and/or the lower lipophilicity of the ^{99m}Tc-labeled compounds.[6,67,69,78]

The development of a fatty acid tracer which contains the tetradentate DADS chelating system should result in a 1:1 fatty acid-technetium complex with a higher myocardial localization ability. Moreover, the DADS ligand is structurally amenable to modification and, therefore, represents an attractive chelant system to probe systematically for the optimal lipophilic requirements to achieve good heart localization. Thus, some long chain fatty acids were subsequently modified to accomodate the DADS-CO_2 bifunctional ligand.

3.3.2 Synthesis and Characterization of Fatty Acid Ligands

A C_{11} fatty acid DADS ligand (**27**) was prepared as outlined in Scheme 3.1. The amine methyl ester hydrochloride **24** was prepared from commercially-available 11-aminoundecanoic acid in 98% yield under conditions of typical Fischer esterification. Proton and ^{13}C NMR confirmed COO*C*H_3 resonances at 3.55 and 51.06 ppm, respectively. IR analysis also revealed a strong, presumably H-bonded, carbonyl absorption at 1720 cm^{-1}. This fatty ester amine was subsequently coupled with acid **3** using DCC activation to furnish the amide **25** in 93% yield. Amide formation was verified by NMR and IR analyses. The H-11 multiplet had shifted from 2.68 ppm in **24** to 3.08 ppm in the product, while the appearance of a triplet at 6.64 ppm was indicative of the newly-formed amide proton at $C_{1'}$. The corresponding carbon signals were noted in the ^{13}C NMR spectrum: a paramagnetic shift of the C_{11} resonance to 39.66 ppm and the appearance of the $C_{1'}$ signal in the carbonyl region. Absorbances due to the aromatic groups in **25** could also be noted in NMR and IR spectra. Deprotection and oxidative cyclization to the intramolecular disulfide **26** proceeded in 37% yield.

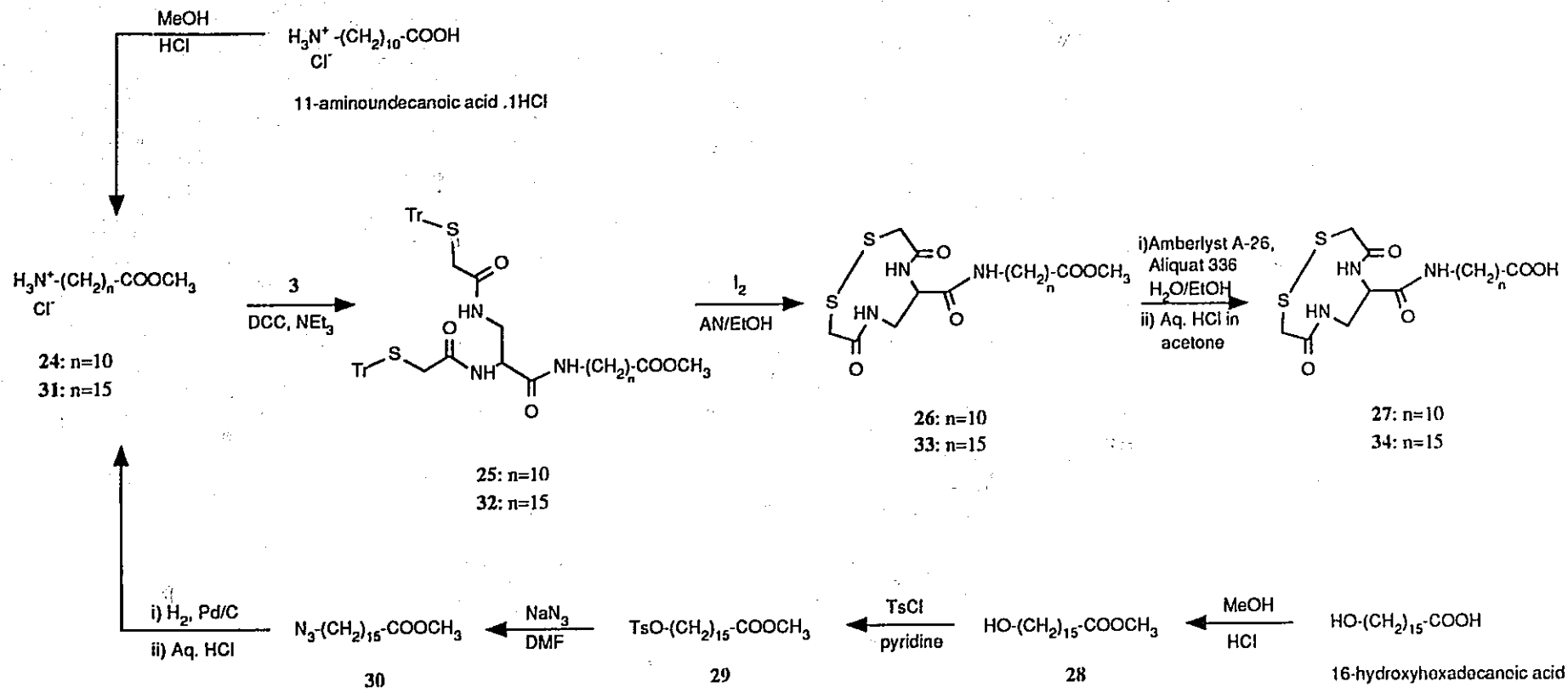
MeOH
HCl
H_3N^+-$(CH_2)_{10}$-COOH
Cl^-
11-aminoundecanoic acid .1HCl
H_3N^+-$(CH_2)_n$-$COOCH_3$
Cl^-
24: n=10
31: n=15
3
DCC, NEt_3
25: n=10
32: n=15
I_2
AN/EtOH
26: n=10
33: n=15
i)Amberlyst A-26, Aliquat 336
H_2O/EtOH
ii) Aq. HCl in acetone
27: n=10
34: n=15
i) H_2, Pd/C
ii) Aq. HCl
N_3-$(CH_2)_{15}$-$COOCH_3$
30
NaN_3
DMF
TsO-$(CH_2)_{15}$-$COOCH_3$
29
TsCl
pyridine
HO-$(CH_2)_{15}$-$COOCH_3$
28
MeOH
HCl
HO-$(CH_2)_{15}$-COOH
16-hydroxyhexadecanoic acid

Scheme 3.1

Cyclization was inferred from the marked broadness of the proton and carbon signals of the ligand in its NMR spectra. This phenomenon was rationalized in terms of slow chemical exchange resulting from ring isomerization and is a characteristic NMR property in these diamide disulfur cycles (see Section 5.3) using $CDCl_3$ as a solvent. The absence of trityl absorbances from NMR and IR spectra provided additional evidence for successful deprotection. When characterization of **26** was not necessary, as in post-trial syntheses, the disulfide conjugate and impurities were co-isolated by extraction and this crude mixture was used directly for the following hydrolysis. This procedure avoided an excessive loss of the ambiphilic fatty ester disulfide **26** through purification and improved the overall yield of **27**.

Ester hydrolysis of **26** to afford the free acid **27** was mediated by a macroreticular anion-exchange resin in the OH^- form (see Section 2.3). This novel hydrolytic procedure also doubled as an effective method for the purification of the polar fatty acid product from Tr-OH, Tr-OEt, DCU and other non-anionic impurities generated in previous steps. IR, ^1H and ^{13}C NMR analyses of the resin-isolated solid indicated the absence of the methyl ester function at 1740 cm^{-1}, δ 3.6 and δ 51.42, respectively. Moreover, the complexity of the ligand resonances in DMSO-d_6 (see Section 5.3) suggested that the cyclic ligand structure of **27** was intact and not affected by hydrolysis.

The synthesis of the C_{16} fatty acid DADS ligand **34** is outlined in Scheme 3.1. This synthesis was similar to that for the C_{11} fatty acid ligand **27**, with a notable exception: the C_{16} hydroxyl group of the 16-hydroxypalmitic acid starting material must be transformed into the NH_2 function to enable amide conjugation with acid **3**. Ligand-fatty acid conjugation *via* a C_{16} ester link was considered (to avoid a multistep $OH \rightarrow NH_2$ transformation) but the selective ester hydrolysis of the terminal $COOCH_3$

function in the presence of an internal conjugative ester bond was reasoned to be too difficult. The most straightforward route to the C_{16} amino fatty acid from the OH-substituted derivative would involve tosylation of the hydroxyl group, displacement of the resultant *O*-tosylate by azide ion and subsequent reduction to furnish the amine. This approach was adopted to carry out the OH $\rightarrow$ NH_2 manipulation.

Commercially-available 16-hydroxypalmitic acid was converted to its methyl ester **28** in 96% yield under relatively dilute (3.3 mM) Fischer esterification conditions. TLC using a 10% MeOH in CH_2Cl_2 mobile phase showed the appearance of a higher-running component at R_f 0.64 and the disappearance of the free acid at R_f 0.39. Spectroscopic analysis of the product was also consistent with the formation of **28**, particularly ^1H and ^{13}C NMR, which showed the new $COOCH_3$ resonances at δ 3.66 and δ 51.40, respectively. Higher concentrations of the hydroxy fatty acid in methanolic HCl afforded significant amounts of the intermolecular ester, $OH\text{-}(CH_2)_{15}\text{-}COO\text{-}(CH_2)_{15}COOCH_3$. This product was characterized by TLC, where it eluted at R_f 0.73 (10% MeOH in CH_2Cl_2), and ^1H NMR, where it showed a characteristic $COOCH_2$ triplet at 4.1 ppm. Its formation was also favored *via* transesterification during work-up, if prior removal of dissolved HCl gas from the methanolic reaction mixture was not performed on a rotary evaporator at *ca.* 0 °C.

The reaction of tosyl chloride and hydroxy-ester **28** in pyridine to afford tosylate **29** was complicated by the unexpected formation of by-products. TLC of the reaction mixture using a 15% EtOAc in hexanes mobile phase revealed three new components: R_f 0.0, 0.28 and 0.54, with the former two spots possessing a UV chromophore. Purification of the worked-up sample by column chromatography and subsequent NMR and IR spectroscopy of each constituent suggested that the UV

active, R_f 0.28 component was the desired tosylate **29**. A downfield shift of the H-16 triplet from δ 3.60 in the hydroxy ester **28** to δ 3.99 in the new component was observed, which was consistent with the substitution of the hydroxyl function with the strongly electron withdrawing tosylate group. In contrast, for the UV inactive component at R_f 0.54, the H-16 protons had moved slightly upfield to 3.50 ppm. In conjunction with its chromatographic properties and the absence of tosyl resonances in the ^{1}H NMR spectrum, this unknown was most likely the 16-bis ether **29c**, formed from the S_N2 displacement of the tosylate **29** by alcohol **28** (see Figure 3.3). ^{1}H NMR spectroscopy of the UV-absorbing material at R_f 0.0 revealed a spectral profile which was remarkably similar to those for quaternerized aliphatic pyridinium salts (such as cetylpyridinium chloride monohydrate[79]) sharing characteristic N^+-CH_2 resonances at *ca.* 4.8 ppm. Consequently, this component was characterized as the fatty ester-pyridinium adduct **29b**. A comparison of H-16 proton integrals for an unpurified sample from the tosylation reaction indicated that the desired tosylate **29** was produced in about 67% yield, while the by-product bis ether **29c** and pyridinium salt **29b** were formed in 14% and 19%, respectively.

Recognizing the identities of these by-products and that they arose from competing, bimolecular side reactions suggested that the order of reagent addition and concentrations may be useful in optimizing the yield of tosylate. For example, the slow addition of alcohol **28** to a concentrated (1 M) solution of tosyl chloride in pyridine - but ensuring a relatively dilute concentration in alcohol - should favor the reaction kinetics for 16-*O*-tosylation while minimizing formation of the bimolecular bis ether. In addition, immediate quenching upon completion of reaction should also minimize the amount of solvolysis product **29b**. Regrettably, a few, judiciously-quenched trial reactions - incorporating a constant 1 M concentration of tosyl chloride but a variable

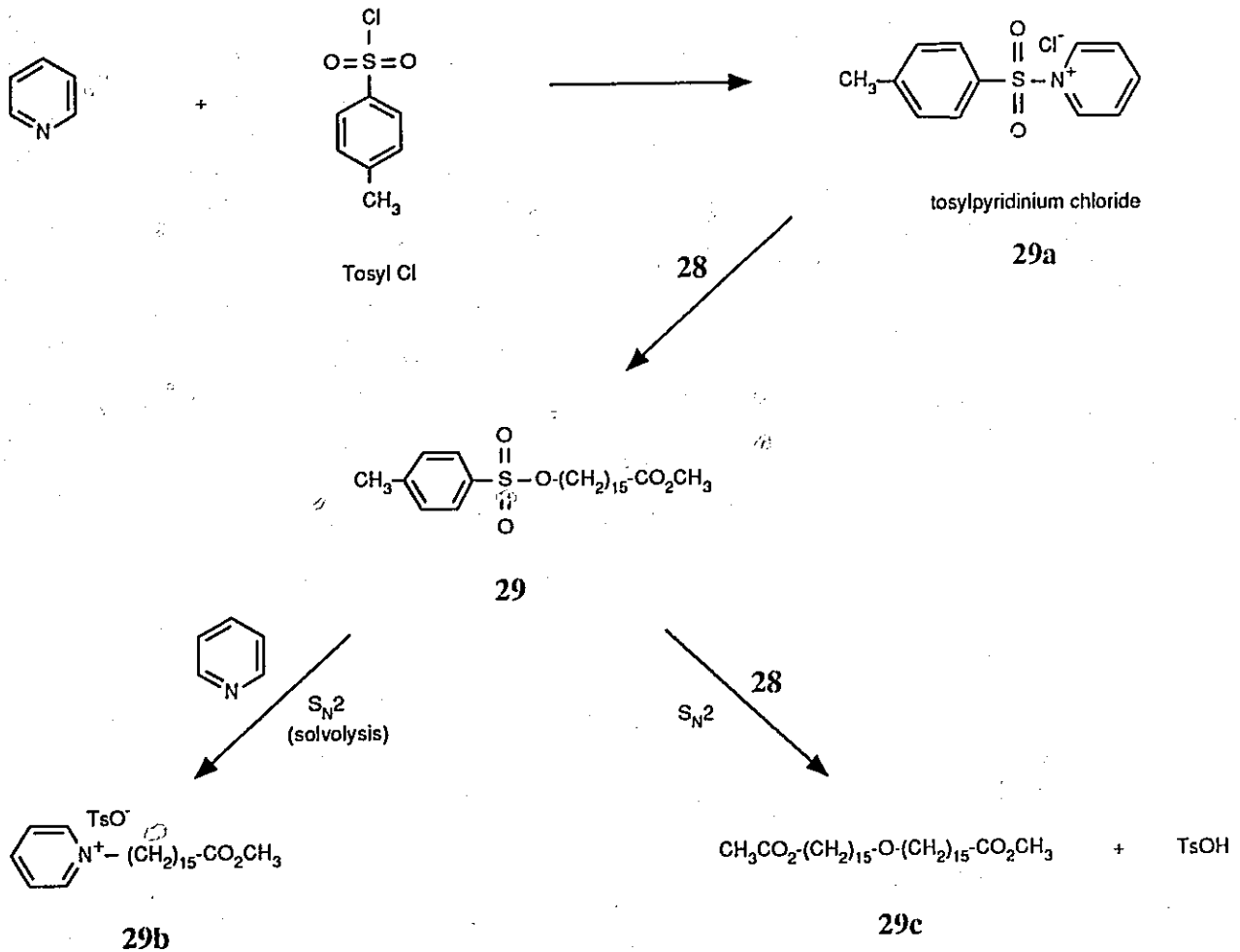

Figure 3.3: Suggested pathway for the formation of tosylate 29, pyridinium fatty ester salt 29b and 16-bis ether 29c.

one in the alcohol **28** - indicated no significant reduction of either the ether or alkylpyridinium contaminants.

The displacement of tosylate in **29** by azide ion in DMF readily afforded the low melting, 16-azido ester **30** in 98% yield. A prominent N_3 IR stretch at 2090 cm^{-1} and the ^1H NMR H-16 triplet at 3.24 ppm assisted in the characterization of this compound.

The azide **30** was subsequently reduced to the primary amine and isolated as its hydrochloride salt **31** by two reduction methods: catalytic hydrogenation (with H_2 gas as the hydrogen source) and catalytic transfer hydrogenation[80] (with ammonium formate as the hydrogen source). The former, classical reductive method gave a higher yield than the latter, presumably because of the simpler work-up. Evidence of the amine functionality was noted by a ninhydrin positive spot at R_f 0.30 (20% MeOH in $CHCl_3$), as well as in ^1H and ^{13}C NMR spectra where the H-16 and C_{16} resonances appeared at 2.72 and 40.03 ppm, respectively. Moreover, the positive FAB-MS spectrum showed an intense ion at *m/z* 286, corresponding to the M+1-HCl structure.

The isolation of amine **31** as its hydrochloride salt avoided the formation of polymeric amides which is possible with the free base (**31b**, Scheme 3.2).[81]

Conjugation of the amine fatty ester **31** and the ligand acid **3** using DCC as the condensing agent afforded the amide **32** in 76% yield. ^1H NMR showed a downfield shift of the H-16 triplet from δ 2.72 in **31** to δ 3.16 in the amide product and the appearance of the C_1 amide proton triplet at δ 6.82. Deprotection and oxidative cyclization to the disulfide cycle **33** occurred in 43% yield. Characterization of this compound was similar to that given for **26**, with the exception of a M+1 peak at *m/z* 518 in the positive NH_3 DCI spectrum.

Methyl ester hydrolysis of **33** to the free acid **34** was accomplished *via* the

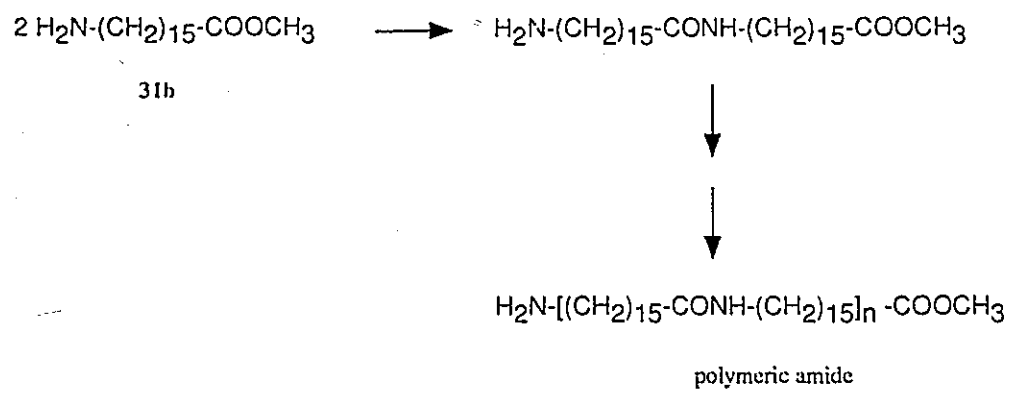

Scheme 3.2

macrorecticular anion-exchange method (Section 2.3) and the product acid was characterized in a similar manner as described for **26**.

3.3.3 Requirement for Carboxyl Protection in Fatty Acids

Initial strategies aimed at the synthesis of fatty acid-ligand conjugate **25** entailed the direct *N*-acylation of 11-aminoundecanoic acid with acid **3**. This direct amide coupling method is synthetically attractive in that it avoids the cumbersome protection and deprotection of the carboxylic acid function in the manner illustrated in Scheme 3.1. Thus, in a trial reaction, a slightly-basic solution of 11-aminoundecanoic acid .1HCl was slowly added to a solution of acid **1** and DCC after a 10-minute activation period. TLC of the reaction mixture indicated a mixture of at least five new components, the major one being unreacted acid **1**. Although no attempt was made to isolate and characterize these constituents, secondary reactions involving the carboxylate anion of the fatty acid was strongly suspected, given that quantitative yields of amide **25** were obtained when the COOH function of the aminoundecyl nucleophile was protected as its methyl ester (see Section 7.6.28). Therefore, the

presence of these unknown components may be inferred from side reactions involving the following intermediates of 11-aminoundecanoic acid:

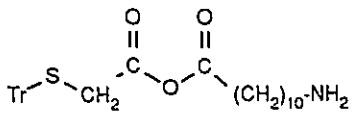

24a

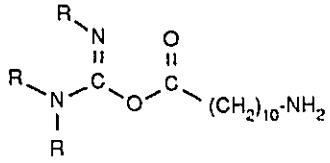

24b $R = C_6H_{11}$

Regardless of the mechanistic outcome however, the formation of by-products most likely resulted from reactions of the free carboxylate group of the 11-aminoundecanoic acid nucleophile with DCC. Therefore, protection of the COOH function of the amino acid was carried out as the corresponding methyl ester. An advantage of an ester protecting group was the facility for the purification of the target disulfide acid **27** from "sticky", ambiphilic impurities (*e.g.*, Tr-OEt, Tr-OH and DCU), using the established hydrolysis-separation procedure of the macroreticular anion-exchange resin (see Scheme 2.3).

3.4 A ^{99m}Tc Digitoxigenin-based Agent for Myocardial Imaging

3.4.1 Introduction

Cardenolides, otherwise known as cardiac glycosides, are found in several families of plants - most notably the genus *Digitalis* - and comprise an outstanding class of drugs. Digitalis, a preparation made by the extraction of dried seeds and leaves of the common foxglove (*Digitalis purpurea*), is used extensively in heart therapy to cure cardiac failure and to slow the ventricular rate in atrial fibrillation and flutter. The most important pharmacodynamic property of Digitalis, however, is the ability to increase the force of myocardial contraction.[82]

The active components of *Digitalis* extract are the glycosides of

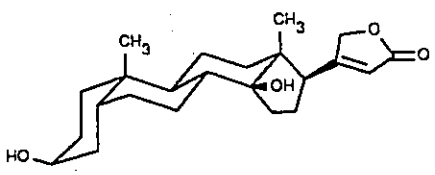

digitoxigenin

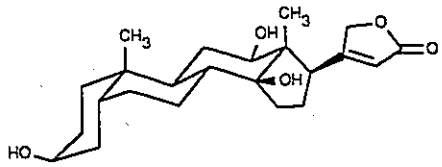

digoxigenin

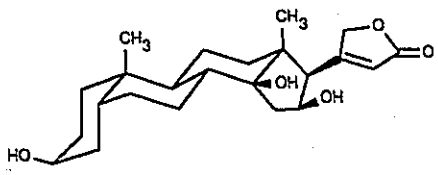

gitoxigenin

Figure 3.4: Perspective formulae of the aglycone components of Digitalis glycosides.

digitoxigenin, digoxigenin and gitoxigenin (see Figure 3.4). Qualitatively, the physiological activity of these cardiac glycosides resides in the steroidal or aglycone component (see Figure 3.4), rather than in the carbohydrate residue. Among the most widely studied aglycones is digitoxigenin [3β, 14β-dihydroxy-5β-card-20(22)-enolide], which is obtained by acid hydrolysis of the glycoside, digitoxin. Digitoxigenin may be considered to possess the minimimum structural requirements for cardiotonic activity. Its structure is unique among other classes of steroids, in that *both* the A/B and C/D ring fusions are *cis*. This geometry places the β or "upward" hydroxyl group at C_3 in the axial orientation. The C_{14} OH group has, likewise, the β configuration. A change in

configuration at C_5 creates a *trans* A/B fusion and results in a sharp diminution in cardiotonic activity. Epimerization at C_3 (to 3-epidigitoxigenin), loss of the C_{14} hydroxyl group, or saturation of the C_{17} unsaturated lactone group also leads to a loss in activity.[83]

3.4.2 Na^+, K^+-ATPase as the Digitalis Receptor

Though the mechanistic basis of the inotropic effects of cardiotonic steroids is still uncertain, there is considerable evidence to support the theory that these effects result from the inhibition of myocardial Na^+, K^+-ATPase.[84,85] This enzyme is an integral component of the pumping mechanism which transports Na^+ and K^+ ions across cell membranes against the natural electrochemical gradient. One important body of evidence which correlates myocardial Na^+, K^+-ATPase with the active transport of Na^+ and K^+ and with the effects of cardiac glycosides on heart muscle contractility is the analysis of structure-activity relationships (SAR): a persistent connection exists between cardiotonic activity and the inhibition of both Na^+, K^+-ATPase and the active transport of Na^+ and K^+ ions by cardiac glycosides.[85] Irrespective of the role of Na^+, K^+-ATPase in the mediation of effects on myocardial contractility, the enzyme contains a receptor for Digitalis and allied compounds.

The idea for the development of a myocardial, ^{99m}Tc-based radioimaging agent was spawned from the high binding affinity of cardiac glycosides to Na^+, K^+-ATPase. Although this enzyme is widely distributed *in vivo*, digitalis glycosides have been shown in distribution studies to concentrate specifically in cardiac tissue at levels 15 to 30 times those in the plasma and over double the quantities found in skeletal muscle.[86] The marked difference in the distribution between the heart and other areas suggests a special binding affinity of cardiotonic steroids to *myocardial* Na^+,

K^+-ATPase, implying a unique form - and/or *modus operandi* - of the enzyme in cardiac muscle. Nevertheless, the covalent attachment of the bifunctional DADS ^{99m}Tc chelate at a modifiable site of a cardiotonic steroid (see Figure 1.3) should furnish a promising receptor-binding radiopharmaceutical specific for the heart. The cardenolide aglycone, digitoxigenin, was selected as the biological carrier because of its commercial availability and established binding affinity for Na^+, K^+-ATPase, as judged through its potent inotropic activity.[87] Moreover, from SAR studies, derivatization at the 3β hydroxyl position does not appreciably diminish cardiotonic properties[88,89] and this site thus can be regarded as a "modifiable" site for conjugation with the DADS-CO_2 chelate.

3.4.3 Side Reactions of Digitoxigenin

The most straight-forward synthetic strategy toward the development of a digitoxigenin-based DADS ligand would be to directly conjugate the ligand acid **3** to the C_3 hydroxyl group of digitoxigenin *via* an ester linkage, followed by *S*-deprotection. The successful implementation of this strategy, however, requires an understanding of the limitations imposed by the sensitive character of the aglycone. For example, the C_{14} hydroxyl group is easily dehydrated in acidic environments to form unsaturated products (Scheme 3.3). Moreover, under basic conditions, an internal rearrangement between the *cis* C_{14} hydroxyl and lactone groups can occur, leading to the formation of an "isogenin" (Scheme 3.4).[83] The reaction is irreversible and the original α,β-unsaturated lactone system cannot be regenerated. Thus, the potential for these undesirable transformations underscores the necessity for mild and neutral chemical manipulations involving derivatives of digitoxigenin.

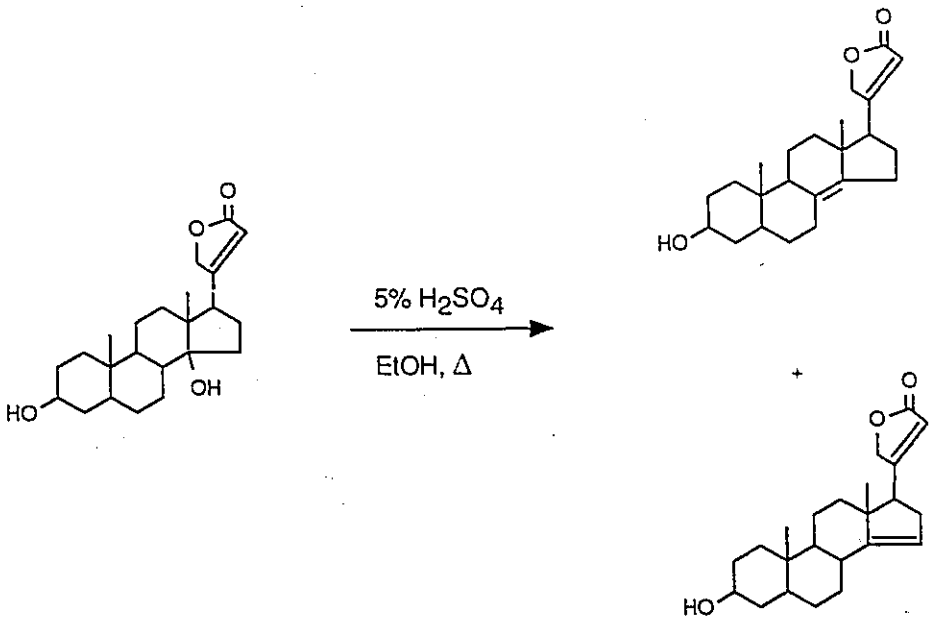

Scheme 3.3

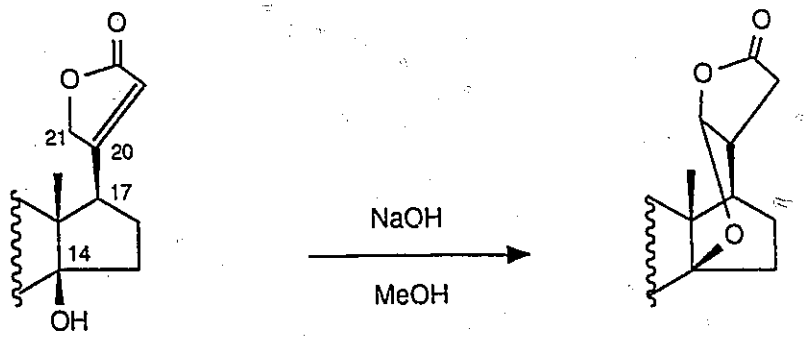

Digitoxigenin

Isodigitoxigenin

Scheme 3.4

3.4.4 Cholesterol as a Test Compound for Digitoxigenin

The development of a mild but efficient procedure for esterifying the α-branched ligand-acid **3** to the cardiac aglycone was accurately perceived as

non-trivial: the reacting groups are somewhat hindered, particularly the axial 3β-OH of digitoxigenin (see Figure 3.4). Anticipating the high cost and the potential toxicity that would accompany repetitive usage of digitoxigenin in trial experiments, the synthesis was tested using cholesterol. Cholesterol is inexpensive, non-toxic and somewhat similar to digitoxigenin in structure, except for the difference in the configuration of the C_3 OH group (in the sterol, the OH is equatorial). As such, cholesterol is a reasonable steroidal model to develop the chemisty for coupling and subsequent deprotection steps. After having "fine-tuned" the reaction conditions using the model compound, the synthesis was repeated using digitoxigenin as the carrier. Indeed, this synthetic detour may conveniently result in an effective cholesterol-based ^{99m}Tc radiopharmacetical. For example, ^{131}I-labeled iodocholesterol has been shown to be a valuable radioimaging agent for adrenal tumors.[6]

3.4.4.1 Cholesterol-ligand Conjugation *via* CDI

With this exploratory strategy in focus, ester coupling was initially attempted through the CDI method (Scheme 3.5). Many variations of imidazolide activation of

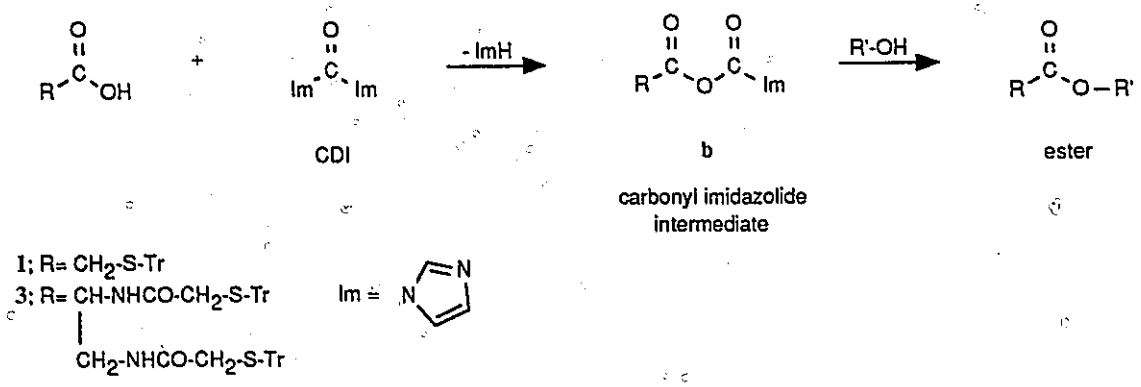

Scheme 3.5

the carboxyl function of **3** were performed, of which none proved to be successful (*e.g.*, see **11**, Section 7.6.13). A 0.3 fold excess of CDI was used to ensure complete activation of **3**, since the purity of the commercially-available reagent is variable due to its extreme sensitivity to water. Moreover, the presence of residual water in the reaction set-up would result in some loss of CDI by hydrolysis. Poor yields of the desired acylated products may be attributed to the considerably faster reaction rate of excess CDI with cholesterol than with the acyl imidazolide **3b**.[42] This undesirable side reaction between the alcohol and coupling reagent leads to an imidazole-*N*-carboxylic ester (**c**) and subsequently either the steroidal dicarbonate (**e**) or, quite likely, the monoalkylcarbonate (**d**, see Scheme 3.6). Morton *et al.* have shown that the yield of the imidazole-*N*-carboxylic ester may be as high as 90% and that of the desired acyl imidazolide (**3b**) only 10%, if 1.5 equivalents of CDI was used for acid activation.[42] TLC of the final reaction mixture supported this possibility, as many nonpolar components with R_f values greater than that of cholesterol (R_f 0.21 in CH_2Cl_2) were detected. The acylation reaction must therefore be performed in the absence of excess CDI. The method of selectively destroying excess CDI in the presence of the activated imidazolide by incubation with Sephadex LH-20[42] was attempted but preliminary results proved to be discouraging. At this point, the decision to employ a different, less water-sensitive coupling reagent was made.

3.4.4.2 Cholesterol-ligand Conjugation *via* DCC/DMAP

Ester coupling of acid **3** to cholesterol was also attempted using the DCC/DMAP system,[90,91] but without encouraging results (see **11**, Section 7.6.14). TLC of the reaction mixture after one week revealed unreacted cholesterol (R_f 0.21, CH_2Cl_2), an unknown aromatic material (R_f 0.09, CH_2Cl_2) and a minute amount of **3**.

^1H NMR spectroscopy of the CH_2Cl_2 extracts of the reaction mixture indicated cholesterol to be the major (non-DCU) component (> 60%). A second, UV-absorbing material (~30%) - having the characteristic spectral profile of **14** (see Section 3.4.5.3) - was also determined. The absence of signals in the 4.5-5.2 ppm range (where the C_3 methine proton of cholesteryl esters typically resonate) suggested that the desired cholesterol-ligand ester **11** was not formed.

3.4.5 Evaluation of Coupling Efficiency through Standard Reactions

The results of NMR and TLC indicated that the coupling chemistry for ligand-steroid conjugation was clearly unsatisfactory. The most apparent rationale that can account for these observations would include "steric retardation" and/or an ineffectiveness in the DCC/DMAP activation system. The former effect is related to large steric interactions possible in the transition state stemming from reacting the hindered, secondary hydroxyl group of cholesterol with the α-branched acid **3**. Moreover, solvent effects may also have had a role on the poor ester yield: in the non-polar CH_2Cl_2 solvent, cholesterol may exist as reverse micelles with their hydrophobic carbon framework oriented toward the solvent matrix while the polar hydroxyl groups are shielded in the interior of a hydrophilic cavity.

Consequently, a number of standard reactions were devised to test: (a) the effectiveness of the DCC/DMAP activating system to promote coupling and; (b) to determine the viability of esterification about the sterically hindered environments of the reacting carboxyl and hydroxyl functionalities of **3** and cholesterol.

3.4.5.1 Synthesis and Characterization of **15**

Employing typical coupling conditions with DCC/DMAP reagents,

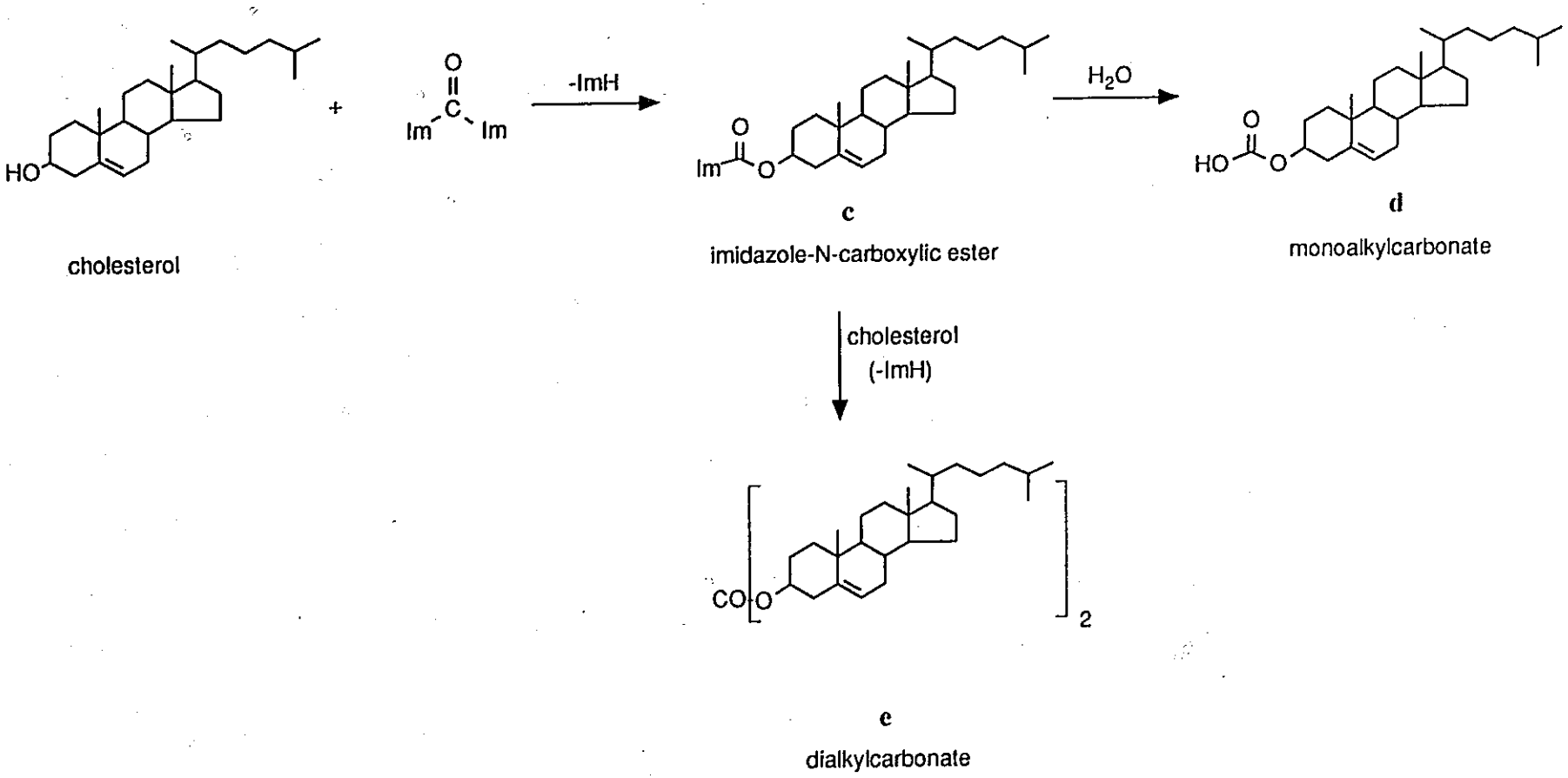

cholesterol

Scheme 3.6

cholesterol was successfully condensed with hindered diphenyl acetic acid within four hours to afford the ester **15** in 89% yield. ^{1}H NMR spectroscopy revealed a downfield shift of the broad multiplet of C_3 methine resonance from 3.49 ppm in cholesterol to 4.69 ppm in the suspected ester. Chemical ionization mass spectroscopy (CI-MS) were also consistent with the formation of **15**, showing a M+18 ion at *m/z* 598. This experiment demonstrated the high coupling efficiency of the DCC/DMAP system and that cholesterol can be quantitatively acylated with hindered acids.

3.4.5.2 Synthesis and Characterization of 12

To probe the steric forces at work in the hindered carboxylic acid **3**, the two following reactions were attempted. Cyclohexylamine was allowed to react with **3** in absence of the DMAP catalyst. TLC revealed the complete consumption of the acid at R_f 0.22 (10% MeOH in CH_2Cl_2) and the appearance of a new component at R_f 0.32 (2% MeOH in CH_2Cl_2). ^{1}H NMR spectroscopy confirmed the product to be the desired cyclohexyl amide **12**, through the assignment of the characteristic resonances at 3.56 and 6.69 ppm to the CONH-C*H*-$(CH_2)_5$ and CON*H*-C_6H_{11} protons. As for **15**, the formation of the hindered amide **12** in high yield reinforced the coupling effectiveness of the DCC reagent.

3.4.5.3 Synthesis and Characterization of 13 and 14: Evidence for Rearrangement of the *O*-Acyl Urea of 3

The next test reaction attempted to esterify **3** with cyclohexanol, an alcohol which closely mimicks the hindered environment of the C_3 hydroxyl group of cholesterol. TLC and NMR spectroscopy of the reaction product supported the formation of two new, UV active components. Using a mobile phase of 2% MeOH in CH_2Cl_2, the major (~50%) component eluted at R_f 0.67, while the minor (~30%) one

occurred at R_f 0.75. In the proton NMR spectrum, certain key resonances suggested the presence of the required cyclohexyl ester **13**: a quartet at 4.17 ppm implied that the asymmetric C_2 methine proton was adjacent to an ester function (compare with 4.15 and 4.20 ppm of esters **7** and **10**), while the broad (*ca.* 40 Hz) multiplet at 4.78 ppm was characteristic of an axial C*H*-$(CH_2)_5$ resonance alpha to a O-C=O group (compare with methine resonances of 5.00, 4.75 and 4.81 ppm of the respective isopropyl, *sec*-butyl and cyclohexyl acetates[92]). Proton integration revealed a second set of key resonances which were assigned to a second component in slightly higher composition. This compound was proposed to be the *N*-acyl urea analog of the acid **3** (**14**). The formation of *N*-acyl urea derivatives has been previously noted in DCC-mediated reactions[90] and is generally believed to result from the rearrangement of the activated *O*-acyl urea **3c** (see Figure 3.5).

As depicted in Figure 3.5, two synthetic outcomes are possible from the reactive acyl agent **3d**: cyclohexanol can undergo nucleophilic attack at the polarized carbonyl carbon with rate constant $k_{\text{nucleophilic attack}}$, to form the desired cyclohexyl ester **13**; or alternatively, the imino nitrogen of the DCU amidate anion can also react at the carbonyl carbon of **3d**, *via* an (assumed) intramolecular process with rate constant $k_{\text{rearrangement}}$, to give the unreactive *N*-acyl urea **14**. To test the rearrangement proposal, the acid **3** was allowed to react with DCC and DMAP in a control experiment under standard esterification conditions for 4 days, *but in the absence of an alcohol nucleophile* (see Section 7.6.17). TLC indicated the complete disappearance of **3** and the appearance of the R_f 0.67 component observed in the synthesis of **11** and **13**. The ^{1}H NMR spectrum of the isolated product was consistent with the *N*-acyl urea derivative of **3** (**14**) because of the following assignments: the quartet at the characteristic chemical shift of 4.33 can be attributed to the asymmetric H-2 protons

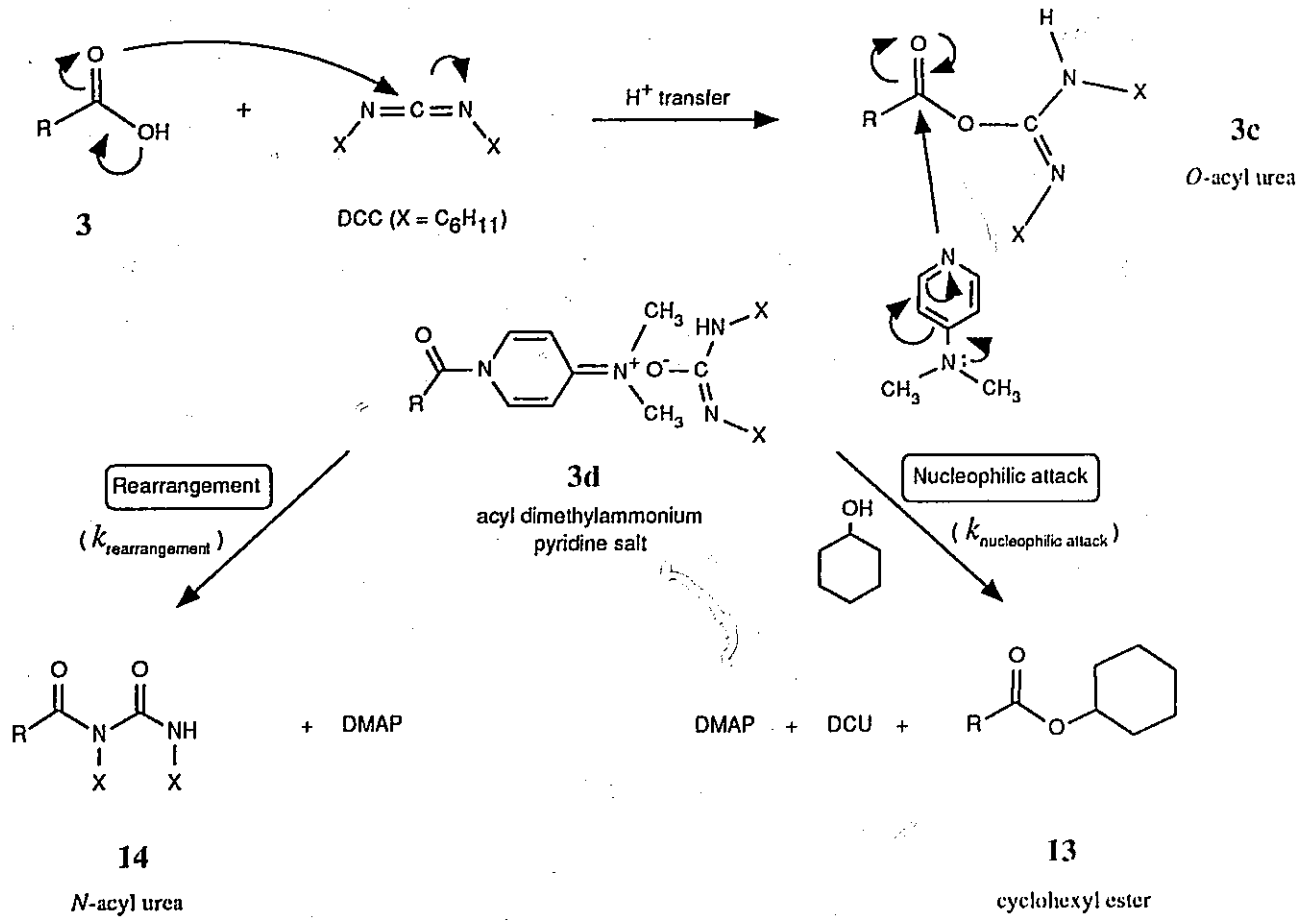

Figure 3.5: Suggested pathway for the formation of cyclohexyl ester **13** and *N*-acyl urea **14** .

proximate to an amide function, while resonances at δ 5.88, 6.10 and 7.00 are ascribed to the amide protons associated with C_2, C_4 and C_6, respectively.

The formation of **14** underscores the background complication of rearrangement when attempting to couple hindered alcohols and acids of type **3** *via* DCC/DMAP methods. In relatively nucleophilic and unencumbered systems, $k_{\text{nucleophilic attack}}$ is much greater than $k_{\text{rearrangement}}$ and the desired amide or ester becomes the major product as seen, for example, in the synthesis of the cyclohexyl amide **12** and the diphenyl acetate **15**. However, in certain systems, a combination of large steric and poor nucleophilicity factors can decrease the rate of nucleophilic attack to a level where rearrangement can compete. This latter point was demonstrated through the conversion of **3** to the rearranged product **14**. These factors, therefore, are proposed to explain the poor product yields observed for the esterification of cholesterol and cyclohexanol to acid **3**.

Since ester formation is a bimolecular process, then halving the reaction volume should increase its rate four-fold. However, experiments where acid and alcohol concentrations were increased showed little or no enhancement in the yield of the cholestryl ester **11** in relation to *N*-acyl urea **14**, as judged by TLC. Moreover, the solubility of the reactants in a suitable aprotic solvent became limiting at these low reaction volumes.

3.4.6 Modification of 3 to Incorporate a Spacer Chain

Given the failure of the normally effective DCC/DMAP and CDI coupling methods, it is unlikely that another activating system could be applied successfully toward the synthesis of 3-*O* substituted steroidal esters of acid **3**. The problem is evidently related to the high steric conjestion about reacting groups and not a

shortcoming of the coupling agents or reaction conditions. With this focus, the synthesis towards these esters was modified to accommodate an unbranched spacer chain which will ultimately link the technetium ligand to the steroidal carrier. A glycyl synthon would suit this purpose, as it can connect acid **3** to the C_3 hydroxyl group of cholesterol (and ultimately digitoxigenin) through amide and ester bonds, respectively. More importantly, however, minimal branching at the α-carbon should ensure quantitative esterification yields because of the reduced crowding adjacent to its carboxyl group.

The choice of the glycyl synthon was based on commercial availability, cost and the ability to be readily incorporated into the existing synthetic method. Methyl glycinate hydrochloride seemed to satisfy all these constraints. The most prudent strategy would involve condensing the amino ester with acid **3** *via* amide coupling using DCC activation, hydrolysis of the resultant methyl ester adduct **16** and subsequent esterification of the glycyl acid **17** to the C_3 hydroxyl group of cholesterol through DCC/DMAP-mediated acylation to generate the *S*-protected ligand-steroid conjugate **18** (see Schemes 3.7 and 3.8). Detritylation of **18** and cyclization to the disulfide ligand **19** should readily occur using iodine. A strategic advantage of modifying the ligand acid **3** with the glycyl spacer first and then conjugating the adduct to the steroid - as opposed to the reverse direction - is the benefit of exposing the chemically-sensitive and costly biological carrier to fewer synthetic manipulations. Therefore, the synthesis of a spacer adduct of **3** was undertaken using methyl glycinate .1HCl.

3.4.6.1 Synthesis and Characterization of the Glycylamide of **3** (**17**)

Acid **3** and $Cl^-H_3N^+$-CH_2-COOMe were quantitatively converted to the amide derivative **16** by DCC activation in an acetonitrile-chloroform solvent mixture

(Scheme 3.7). Amide formation was confirmed by a number of methods, most notably by ^{1}H NMR where the glycyl α-CH_2 resonance has shifted from δ 3.80 (DMSO-d_6)[93] in the amino ester reactant to δ 3.92 in the amide product. Moreover, these methylene protons, like those at C_3 and at the O-CH_2 position in ester **7** (Section 5.2), have become diastereotopic, adding an interesting dimension to support amide formation. Geminal non-equivalence - which was revealed by their ABX resonance pattern - is a result of the proximity of the CH_2 spin system in the glycine residue to the stereocenter at C_1.[39] In the following transformation, hydrolysis of **16** in 0.1 N NaOH in aqueous ethanol afforded the free acid **17** in 91% yield after an acidic work-up. ^{1}H and ^{13}C NMR spectra showed the absence of the methyl ester function at δ 3.70 and δ 54.75, respectively, confirming hydrolysis.

3.4.7 Synthesis and Characterization of Cholesteryl-ligand Conjugate **19**

The key transformation in this linear synthesis was the conjugation of the glycyl acid **17** to the C_3 position of cholesterol (Scheme 3.8). Using DCC/DMAP as the activating agent for the carboxyl group, a new, UV-active spot was detected on TLC after the addition of the sterol. This component was isolated and purified from unreacted cholesterol and other aromatic impurities to afford a white solid in 54% yield. TLC and IR spectroscopy of the product indicated a R_f value higher than that for cholesterol (*cf.* R_f 0.81 and 0.64, respectively; 10% MeOH in CH_2Cl_2) and a prominent carbonyl absorption at 1740 cm^{-1}. However, the assignment of key shifts in ^{1}H and ^{13}C spectra provided unequivocal evidence that the product was the steroid conjugate **18**. The downfield shift of the H-3 multiplet, from δ 3.49 in cholesterol to δ 4.62 in the product, suggests it is adjacent to an electron withdrawing group such as an ester. The C_3 resonance in ^{13}C NMR also shows a similar shift from δ 71.9 to δ 75.4, again

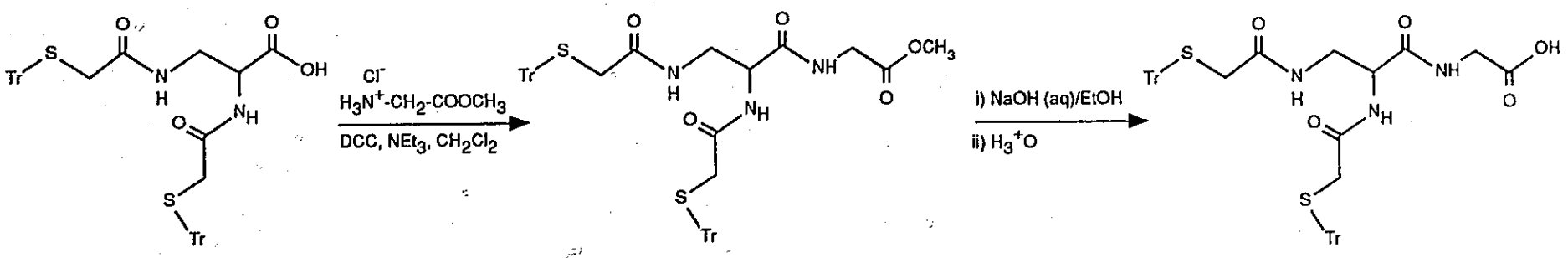

3 **16** **17**

Scheme 3.7

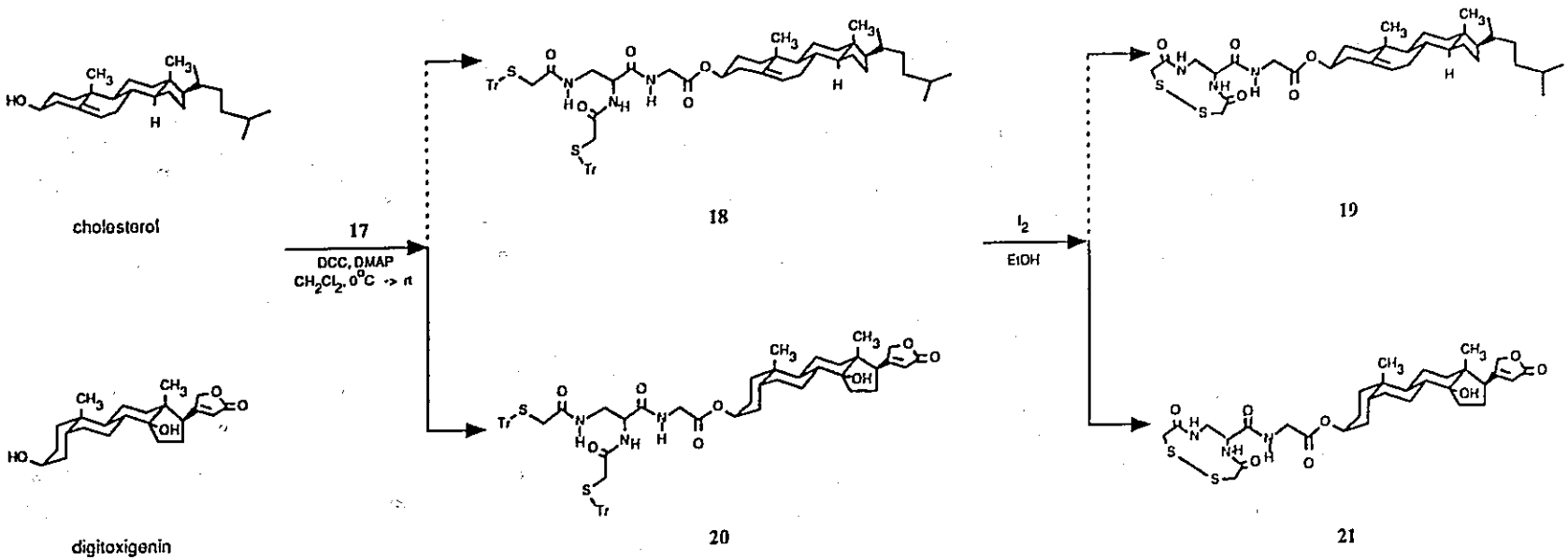
cholesterol
17
DCC, DMAP
CH_2Cl_2, 0°C -> rt
18
I_2
EtOH
19
digitoxigenin
20
21

Scheme 3.8

supporting ester formation.

The successful synthesis of the glycyl-linked cholesteryl ligand **18** confirmed the existence of large steric effects that disfavored direct esterification of acid **3** and the sterol and the requirement for an unbranched spacer to connect the two domains. However, as only 54% of conjugate **19** was isolated, the method was inefficient: TLC of the reaction mixture revealed the presence of unconsumed cholesterol and a UV-absorbing (*i.e.*, aromatic) impurity at R_f 0.55 (10% MeOH in CH_2Cl_2) of combined relative intensity of *ca.* 30%. The latter component was also noted in greater amounts in the synthesis of the digitoxigenin glycyl ligand conjugate **20** (*vide infra*). Although no attempt was made to isolate and characterize this compound, its TLC polarity characteristics and UV-absorbing properties suggested that it may have been the *N*-acyl urea derivative of acid **17**. If this is the case, then rearrangement of the *O*-acyl urea intermediate of **17** was still relatively significant within the time frame for nucleophilic attack by alcohol, particularly during the latter stages of the reaction when the concentration of nucleophile was low. Trial reactions employing the polar DMSO solvent instead of CH_2Cl_2 were successful in eliminating the *N*-acyl urea component at R_f 0.55 with the complete consumption of acid **17**. Acetonitrile and DMSO/CH_2Cl_2 (2:1 v/v) were also investigated, but neither solvent system succeeded in preventing the formation of the R_f 0.55 component. Neat DMSO, it would seem, was the ideal solvent for the coupling reaction, offering the most efficient conversion of reactants to the ester product **18**. However - given the poor solubility of cholesterol in small volumes of DMSO and the difficulty in removing this high-boiling, ambiphilic solvent during work-up - it was felt that the slightly better coupling efficiency in DMSO could be compromised by a simpler work-up using methylene chloride as the reaction solvent. Therefore, the coupling of cholesterol and **17** was carried out in CH_2Cl_2. The greater

esterification efficiency in these solvents can be rationalized in terms of the degree of solvent separation of the ion pair **3d** (see Figure 3.5). In the polar DMSO solvent, the amidate and acyl pyridinium ions are more densely solvated and separated than in the non-polar CH_2Cl_2 solvent. This results in a "looser" ion pair association of intermediate **3d**, which may lead to a reduction in the rate of the rearrangement reaction because of an *increased* separation between the reacting ionic entities. In addition, DMSO may favor the formation of "normal" micelles, wherein the reacting C_3 hydroxyl group would be more exposed to the polar solvent matrix for coupling with the acylating reagent **3d**. In contrast, employing the non-polar CH_2Cl_2 as the reaction solvent may reduce the rate of nucleophilic attack because the polar OH function would be shielded by the hydrophobic exterior of the steroidal hydrocarbon framework in a reverse micelle scenario.

The final transformation in this model synthesis was the deprotection of the conjugate **18** and intramolecular cyclization to the disulfide **19**. The addition of 1.1 equivalents of iodine to a degassed, 5 mM solution of **18** in absolute ethanol resulted in the quantitative disappearance of the starting material at R_f 0.81 and the appearance of a new component at R_f 0.51 (10% MeOH in CH_2Cl_2). This material was isolated in 32% yield following purification and characterized spectroscopically to be the disulfide **19**. All protons and most ^{13}C resonances associated with the ligand appendage appeared as broad signals: this is a characteristic property of the 10-membered disulfide heterocycle in $CDCl_3$ indicating slow conformational exchange (see Section 5.3). The absence of the trityl protecting group from IR and NMR spectra confirmed quantitative *S*-deprotection.

A concern in employing iodine as a deprotectant for the *S*-tritylated cholestryl conjugate **18** was the undesired iodination of the C_5-C_6 olefinic bond of the

steroid. However, no unusual shifts were noted for this unsaturated system in the NMR spectra. For example, the ^{13}C resonances of C_5 and C_6 are virtually invariant after the deprotection-oxidation of **18** (at δ 139.3 and δ 122.9, respectively). Presumably, the rate of C_5=C_6 dihalogenation is much slower than that of complexation with the S-Tr groups, which resulted in no detectable quantities of the diiodonated product.

3.4.8 Synthesis and Characterization of Digitoxigenin-ligand Conjugate **21**

Given that the groundwork chemistry for steroid-ligand conjugation and deprotection had been successfully developed using the cholesterol model, the synthesis was repeated with digitoxigenin (Scheme 3.8). The ligand acid **17** was conjugated at the 3-OH group of the cardiac aglycone using similar conditions as worked out for cholesterol, yielding the conjugate **20** in 59% yield. Spectroscopic data were consistent with the formation of the required 3-*O* ester conjugate: the H-3 proton of the steroid had shifted downfield to 5.12 ppm, while the ^{13}C NMR spectrum showed a new C_3 resonance at 71.90, shifted from 66.81 ppm in digitoxigenin. The IR spectrum indicated a strong ester carbonyl stretching at 1740 cm^{-1}, in addition to aromatic C=C and C-H absorbances at 3050, 1485, 1440, 735 and 690 cm^{-1}. The tertiary $^{13}C_{14}$ resonance appeared uneffected in both the free and conjugated steroid, confirming the absence of acylation of the C_{14} hydroxyl group. Detritylation of **20** using I_2 as the deprotectant readily afforded the disulfide **21** in 24% yield. As for the cholestryl disulfide **19** and other cyclic ligands analyzed in $CDCl_3$-based solvents, deprotection and cyclization was inferred from the broadness of the ligand proton and ^{13}C resonances and by the absence of aromatic signals in the ^1H and ^{13}C NMR spectra. Positive FAB-MS also indicated the presence of a M+1 ion at *m/z* 664. Moreover, ^1H and ^{13}C NMR shifts suggested that the sensitive α,β-unsaturated lactone at C_{17} had not lost its integrity during the previous transformations.

CHAPTER 4

SYNTHESIS OF GASTROENTEROLOGICAL IMAGING AGENTS

4.1 General Introduction

The last 22 years have seen the development of many compounds labeled with ^{99m}Tc for use primarily as hepatobiliary imaging agents. A summary of these agents in chronological order are: toluidine blue, penicillamine, tetracycline, dihydrothioctic acid, mercaptoisobutyric acid, pyridoxy derivatives such as pyridoxylideneglutamate, pyridoxylidinephenylanaline and other pyridoxylideneanimates, carboxyl-hydroxyquinoline, substituted acetanilide iminodiacetates (IDA ligands), ethylenediamine-*N,N'*-diacetates and orthoiodohippurate analogues. Among this extensive list of hepato(H)-biliary radiopharmaceuticals, the IDAs (or HIDA compounds) have been the most extensively used for basic and clinical research (see Figure 4.1). The clinical utility of IDA cholescintigraphy has been demonstrated for a number of disorders, including intrahepatic and extrahepatic biliary duct obstruction, Caroli's disease, acute cholecystitis, post-traumatic or post-operative bile leak, organic and functional derangements of the biliary-enteric junction and the possible evalution of hepatocellular carcinoma metastases.[94]

Despite a respectable list of clinical precedence and impressive diagnostic functions, HIDA derivatives cannot be considered ideal agents for cholescintigraphy. Cardioactive effects and hepatobiliary transport sensitivity rank prominently among

well-documented disadvantages.[94] A review of recent literature indicates that, while imaging procedures have successfully overcome many of the diagnostic challenges posed by the hepatobiliary organs, progress in other relevant areas of the gastroenterological system is lacking. New or improved imaging agents are continually being sought to fill a specific diagnostic application, particularly for the evaluation of organ function in diseased states. Consequently, a major aim in this segment of research was to develop novel gastroenterological agents that may be suitable for these applications. It is hoped that encouraging results in the initial testing of the proposed agents will stimulate the discovery and development of new classes of ^{99m}Tc-based gastroenterological radiopharmaceuticals.

4.2 A ^{99m}Tc Cholic Acid-based Agent for Enterohepatic Imaging

4.2.1 Introduction

Bile is a mixture of mono-, di- and tri-hydroxy steroidal acids, which in man are predominantly conjugated with glycine. Conjugated bile acids are produced in the liver, collected in the biliary passages, stored and concentrated in the gall bladder and intermittently discharged into the common bile duct. In the duodenum, bile helps to neutralize the gastric chyme and to emulsify dietary lipids. Their emulsifying action enables intestinal mucosa to absorb fat-soluble nutrients, such as cholesterol and lipophilic vitamins. In the distal ileum, bile acids are reabsorbed and are then returned to the liver through the portal system to complete the enterohepatic circulation.[95]

In general, pathways of gastrointestinal absorption are more specific than those of excretion. Although many substances are rapidly excreted by the liver into the bile following intravenous administration - *e.g.*, ^{99m}Tc HIDA agents or ^{131}I-labeled sodium rose bengal - few compounds, however, are reabsorbed and fewer still are

X	Y	Name	Abbreviation
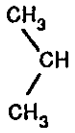	H	N-(2,6-diisopropyl) IDA	DISIDA
CH_3-CH_2	H	N-(2,6-diethyl) IDA	DIDA
H	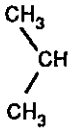	N-(p-isopropyl) IDA	PIPIDA
H	C_4H_9	N-(p-n-butyl) IDA	BIDA

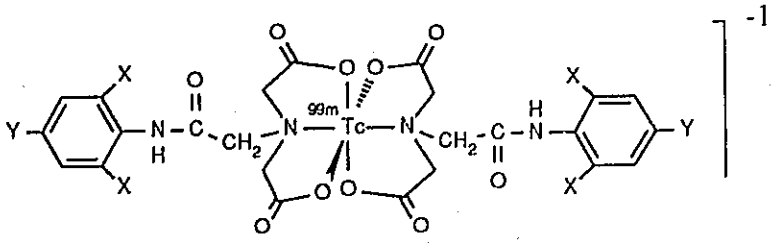

Figure 4.1: ^{99m}Tc-HIDA analogs.

reabsorbed and re-excreted unchanged. This is presumably a consequence of the high molecular specificity built into the active, ionic absorption and transport process of the intestinal wall.[96] Although there are many radioactive tracers suitable for studying the excretory function of the liver and extrahepatic biliary ducts (*e.g.*, see Section 4.1), all of these can be improved upon in some capacity and few - if none at all - are suitable for studying the complete *enterohepatic circulation* (the gut, liver and biliary tree).[96]

A number of researchers have indicated that a ^{99m}Tc cholic acid agent could be useful as a hepatobiliary radiopharmaceutical, with the additional advantage of providing a scintigraphic method for assessing ileal absorptive function. Hofmann has emphasized the need for a tracer which behaves like a bile acid and could be employed to investigate enterohepatic circulation, especially ileal reabsorption.[97] Galli and Maini have also pointed out the potential utility of ^{99m}Tc-labeled bile acids as novel hepatobiliary radiopharmaceuticals.[94] There are a number of reasons to support these unique claims: the hepatocellular transport mechanisms for bile acids differ in part from those of other anions (and presumably [^{99m}Tc-HIDA]$^{-1}$ complexes)[98,99] and their liver extraction coefficient is the highest among all the substances tested to date.[100] In addition, one of the earliest manifestations of hepatocellular dysfunction is a reduction in bile acid transport capacity, which makes these steroidal acids a very sensitive indicator of liver cell function.[101]

To our knowledge, however, the only investigative study in this area involved cholic acid derivatives tagged with selenium-75 at various positions on the C_{17} side chain.[96] These bile acid analogs have demonstrated very similar hepatobiliary excretion and gut absorption properties when compared with that of [24-^{14}C]cholic acid. Unfortunately, the nuclear properties of ^{75}Se are not optimal for imaging[94]: this deficiency may have prevented the selenium-tagged cholic acid compounds from

seeing widespread clinical usage. Thus, if the substitution of ^{99m}Tc - with its excellent diagnostic imaging characteristics (see Section 1.2) - for ^{75}Se in these cholic acid analogs is made, then a practical and novel agent which is suitable for detecting small-bowel disease may result. On this basis, a major aim of this study was to prepare a ^{99m}Tc-tagged, bifunctional derivative of cholic acid for subsequent development as an enterohepatic radiopharmaceutical.

Based on the ^{75}Se-tagged cholic acid study, the C_{17} side chain would appear to be a modifiable area suitable for the attachment of the ^{99m}Tc-DADS-CO_2 chelate, with receptor recognition and binding being primarily determined by the hydroxy-steroid skeleton. Moreover, the fact that cholic acid is mainly found *in vivo* as its equally-active glycine or taurine conjugate also supports the design strategy that amide derivatization of the C_{24} carboxylic acid function should not significantly alter ileal absorption.

4.2.2. Synthesis and Characterization of Cholic Acid Conjugate 23

The cholic acid DADS-CO_2 conjugate **23** was prepared as outlined in Scheme 4.1. Acid **3** was conjugated to 3-cholamidopropylamine[102] *via* DCC activation

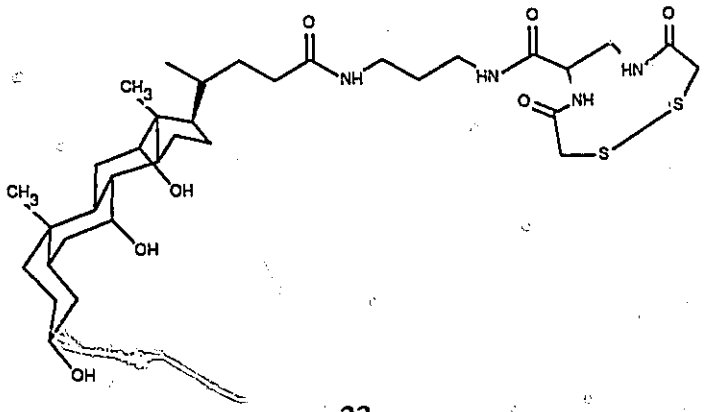

23

and gave amide **22** in 98% yield. Characterization of **22** by ^{13}C NMR spectroscopy

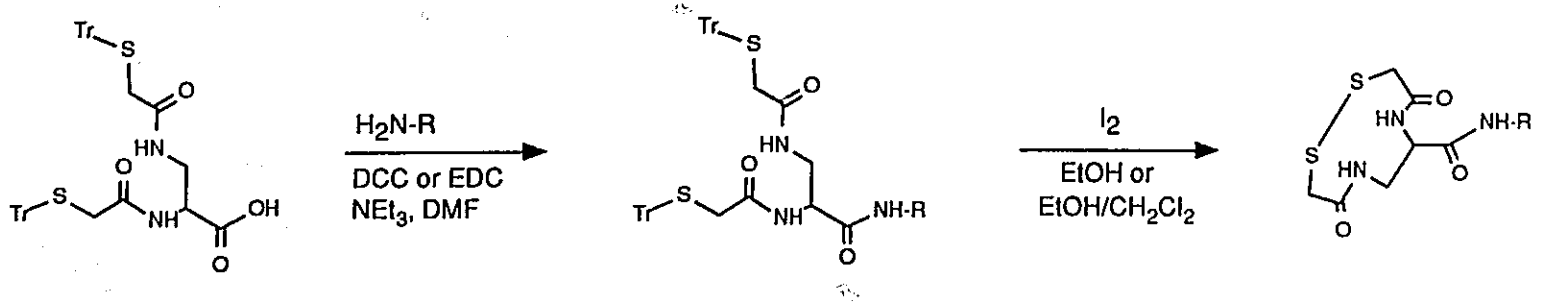

3

22: R = CAPA
35: R = TAUR
37: R = β-CD

23: R = CAPA
36: R = TAUR
38: R = β-CD, HI salt

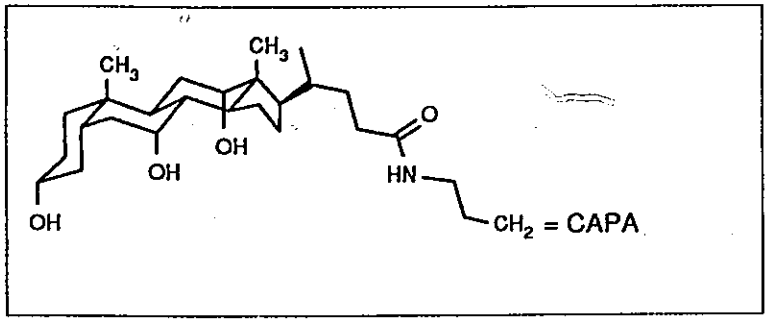

Na O_3S-CH_2-CH_2 = TAUR

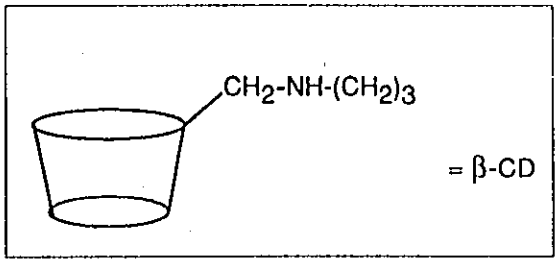

Scheme 4.1

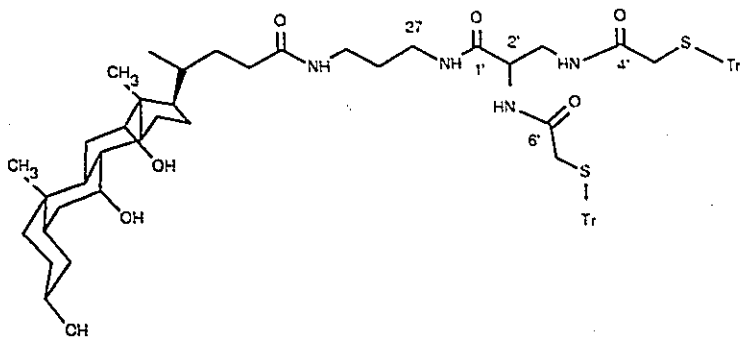

22

revealed the appearance of three new carbonyl resonances corresponding to $C_{1'}$, $C_{4'}$ and $C_{6'}$ of the ligand moiety. These observations - in addition to the newly-created $C_{1'}$ONH proton resonance at 7.86 ppm - were consistent with the proposed acylation of the C_{27} amino group. The tetraamide **22** was subsequently deprotected and converted to disulfide **23** in 45% yield, following the established procedure using iodine as the deprotectant-oxidant. Positive FAB-MS of **23** showed a M+1 ion, while IR and NMR spectra indicated the absence of trityl absorbances. As in other DMSO-d_6 solvated ligand cycles, intramolecular cyclization was inferred from the complex nature of the $C_{2'}$-H ^{1}H and ^{13}C resonances (see Section 5.3).

4.3 A ^{99m}Tc Taurine-based Agent for Gastric Ulcer Imaging

4.3.1 Introduction

In the opinion of many surgeons, an imaging agent which can localize in ulcerated tissues of the gastrointestinal tract would be even more valuable than a hepatobiliary tumor-localizing radiopharmaceutical. The failure to detect and localize occult abdominal abscesses is regarded as a major surgical problem.[6] The development of such an imaging agent, therefore, would clearly be a boon to nuclear medical

practitioners.

4.3.2 Sucralfate: A Sulfated Sugar with Ulcer Localizating Abilities

Among the pharmacological properties of sulfated oligosaccharides is their peculiar ability to localize in ulcerative areas of epithelia and to protect these regions from digestive enzymes to promote healing.[103] Sucralfate (Carafate®, see Figure 4.2),

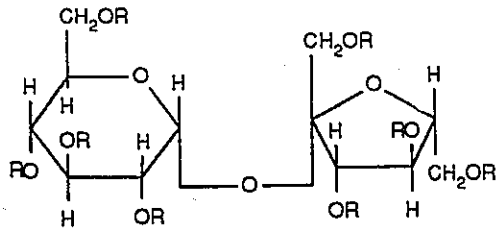

Figure 4.2: Structural formula of sucralfate.

a basic aluminium salt of sucrose octasulfate, has been used for over two decades as an effective therapeutic in the treatment of both duodenal and gastric ulcers.[104] The *in vivo* antiulcer activity of sucralfate has been attributed to its binding with serum proteins exudated by the ulcerous lesion. The resulting protein-sulfate complex is resistant to hydrolysis by harmful agents such as pepsin and gastric acid and it binds selectively to the ulcer site to establish a local protective barrier.[105] The binding interaction is especially strong: in man, the gel remains adherent to ulcerated epithelium for over 6 hours.[104] Results of a pH-dependent study[106] show that this specific binding is electrostatic in nature, with the negatively-charged sulfate groups in sucralfate combining with positively-charged sites on the protein at gastric acidity levels (pH < 4).

The successful localization of ^{99m}Tc-labeled derivatives of sucralfate and sucrose sulfate in ulcerated epithelia[103] suggests the possibility of directing technetium-tagged complexes of other sulfated compounds to these areas for ulcer imaging. Based on the electrostatic nature of the sucralfate binding mechanism, the anionic sulfate group - which remains fully ionized at gastric acidity - is essential for target tissue accumulation. Therefore, in the design of a prospective ulcer-avid radiopharmaceutical, carrier candidates must incorporate a strongly acidic group, such as a sulfonic acid or sulfate function. The amino sulfonic acid taurine satisfies this condition. We proposed that a ^{99m}Tc-DADS taurine agent may prove to have clinical significance in the evaluation of gastrointestinal ulcer diseases and other related dysfunctions that are associated with the loss of mucosal integrity. Therefore, efforts have been directed toward the preparation of a taurine derivative equipped with a DADS-CO_2 chelant.

4.3.3 Synthesis and Characterization of Taurine Conjugate **36**

The taurine DADS ligand conjugate **36** was synthesized as shown in Scheme 4.1. Taurine was coupled to acid **3** *via* 1-(3-dimethylaminopropyl)-3-ethylcarbodiimide

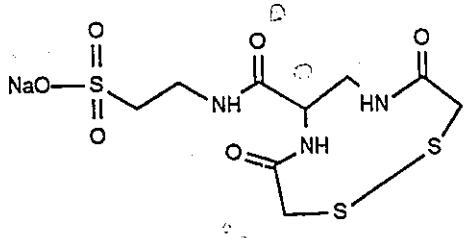

36

.HCl (EDC) activation to afford the amide conjugate **35** in 96% yield. The extreme

hydrophilic character of the conjugate presented a formidable challenge for its separation from other polar substances, such as DMF solvent, EDCU, NaCl and excess taurine. After bulk removal of DMF under high vacuum, the residue was suspended in hot ethanol and filtered to remove unreacted taurine. The sodium salt **35** was subsequently precipitated from a dilute aqueous solution of the concentrated ethanolic filtrate by salting with NaCl. The aqueous solution was acidified just prior to salt

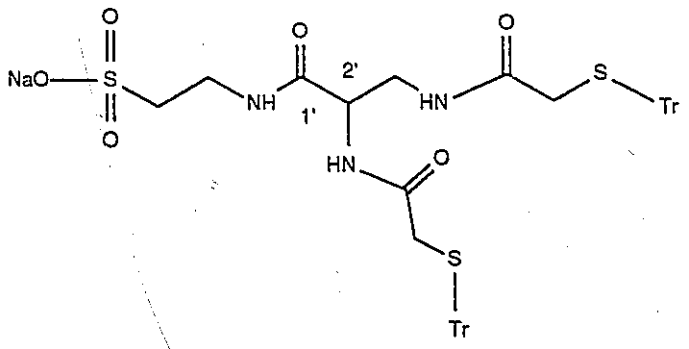

35

addition to enhance the solubility of the EDCU contaminant in solution through the formation of its hydrochloride salt. The collected residue was suspended in hot ethanol and filtered to remove residual amounts of NaCl. TLC of the solid obtained after the evaporation of ethanol showed excellent homogeneity. Negative FAB-MS revealed an intense peak at *m/z* 842, corresponding to a loss of Na^+ from the molecular ion. Amide formation was also evident in ^1H and ^{13}C NMR spectra through the appearance of the C_1'ON*H* signal at 7.90 ppm and a third amide signal in the ^{13}C carbonyl region. Iodine-effected detritylation of **35** led to the formation of the disulfide **36** in 33% yield. The marked broadness and complexity of the proton and carbon signals of the product and the absence of trityl resonances suggested successful deprotection and intramolecular disulfide formation.

4.4 A ^{99m}Tc Cyclodextrin-based Agent for Lower Bowel Imaging

4.4.1 Introduction

The mucosa of the gastrointestinal tract can be visualized as a semi-permeable membrane which allows passage of water and nutrients but excludes other compounds. Molecules of various sizes are known to cross this barrier by active and passive mechanisms. Molecular size appears to determine the mechanism of transport: small or intermediate-sized compounds can cross the plasma membrane of the microvilli, whereas macromolecules are gradually taken up by endocytosis at the base of the microvilli. In addition, the ends of the villi - where extrusion of mature cells occurs - may present a variable breach in the epithelial barrier and represent yet another gateway for molecular entry. Macromolecules are also known to be taken up by M-cells overlying lymphoid collections.[107]

However, the permeability of healthy intestinal mucosa towards molecules of different molecular size changes when it becomes inflamed or infected.[108] It seems that in patients afflicted with Crohn's disease or celiac disease, infected intestinal membranes become *more pervious* to larger molecules than smaller ones. Thus, the differential permeability of probe molecules through the intestinal wall can be used as a marker for the evaluation of intestinal wall function. Since a better understanding of intestinal permeability (or function) of large molecules might generate further insight into the pathogenesis and therapy of some gastrointestinal and systemic diseases, studies in this area are highly desirable.

4.4.2 *In Vivo* Measurement of Intestinal Permeation *via* ^{99m}Tc Imaging

Intestinal permeation has been measured in man and animals using a variety of probe molecules. Typically, the probe is administered orally and the amount of the

compound excreted in urine is measured with respect to time. Assuming negligible metabolism of the probe, intestinal permeation of the test substance is taken as directly proportional to its urinary excretion. Finally, the probe substance is quantified in the urine by either extraction and derivatization procedures, or by scintigraphy in the case of a radioactive probe.[107] However, these methods of analysis suffer from the disadvantages of being tedious and time consuming procedures, not the least being the need to collect and process urine. A more appealing strategy for the analysis of the test substance might be to employ a ^{99m}Tc-labeled probe, where the potential for diagnostic imaging and quantitative analysis is possible *directly in the* in vivo *environment* without the need for technically demanding, post-excretory, analytical assays. Consequently, the specific diagnosis of dysfunctions and diseases of the intestinal wall can be determined through the combination of morphologic and quantitative physiologic changes as outlined in reference 1.

4.4.3 β-Cyclodextrin as a Carrier Molecule for a ^{99m}Tc-labeled Intestinal Probe

Clinical measurements of permeation pathways have been carried out using probes in the 100-500 dalton range (*e.g.*, lactulose, mannitol, L-rhamnose, ^{51}Cr-EDTA and polyethylene glycol (PEG 400)) or on larger molecules with molecular weights greater than 10,000 daltons (*e.g.*, polyvinylpyrrolidine and albumin).[107] However, intermediate-sized molecules have not been studied thus far. A number of conditions must be fufilled for a compound to find acceptance as a permeability probe. The molecule should be non-toxic and have well characterized properties - such as, hydrodynamic dimensions, molecular weight, charge and polarity.

The unusual shape and size of cyclodextrins[109,110] (see Figure 4.3 for an illustration of β-cyclodextrin) makes them unique probe candidates with respect to the

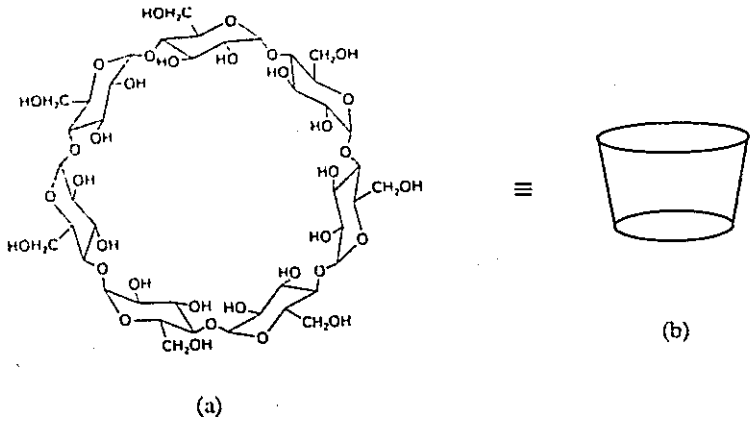

Figure 4.3: Structural formula (a) and a schematic illustration (b) of β-cyclodextrin.

above criteria. These torodial-shaped molecules have a molecular weight of about 1300 daltons and are uncharged in aqueous solution at physiological pH. Cyclodextrins are hydrophilic but also display marked lipophilic properties similar to PEG 400 and should therefore pass across the bowel wall as observed for these ethylene glycol polymers[107] and other sugars and alcohols.

The objective of this section of research was to synthetically modify a β-cyclodextrin amine derivative to incorporate a DADS-CO_2 chelant for the technetium-99m nuclide. Such a compound offers the possibility of a simple, novel and aesthetically acceptable method of investigating bowel permeability and certain gastrointestinal diseases.

4.4.4 Synthesis and Characterization of Cyclodextrin Conjugate **38**

The β-cyclodextrin DADS-CO_2 bifunctional ligand **38** was synthesized in

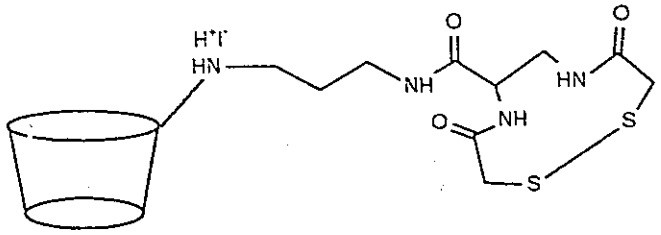

38

16% overall yield as shown in Scheme 4.1. Conjugation of the cyclodextrin diaminopropane **37a** (a gift from Dr. Alfredo Capretta) with the *S*-trityl ligand **3** *via*

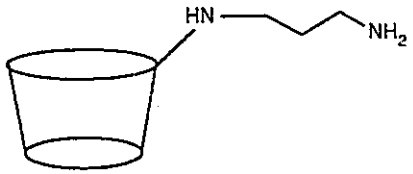

37a

EDC activation in DMF gave the amide adduct **37** in 53% yield. Analysis of the ^{1}H

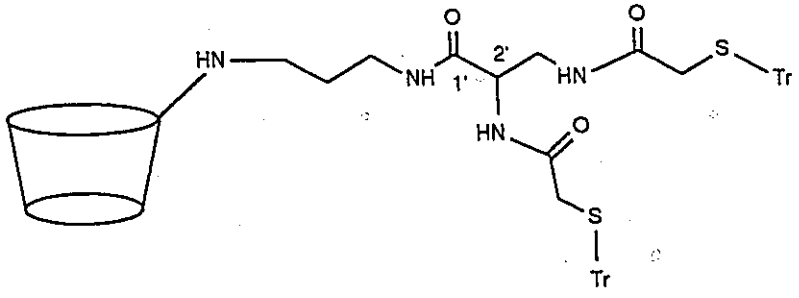

37

NMR spectrum revealed a shift to lower field of the C_2-*H* signal relative to acid **3** (δ 4.02 in **37** from δ 3.89 in **3**), while the ^{13}C NMR spectrum showed the appearance of a

third resonance in the amide region between 167.33 and 167.71 ppm, corresponding to the newly-formed C_1-O-NH bond. The IR spectrum also revealed the absence of a prominent C=O carboxylic acid stretching frequency in the range 1725-1740 cm^{-1}, providing further confirmation of amide coupling.

Initial attempts to detritylate the β-cyclodextrin ligand conjugate **37** under standard deprotection conditions (employing 1.1 equivalents of I_2) resulted in the recovery of *ca.* 35% of **37** after work-up. This unexpected result can be attributed to the formation of a 1:1 guest-host complex between iodine and the cyclodextrin. In support of this postulate, a crystal structure of the iodine complex of α-cyclodextrin has been reported, clearly showing one molecule of I_2 encapsulated by the six-membered carbohydrate ring.[111] The cyclodextrin molecule is known to possess a hydrocarbon-like interior, which can dissolve relatively non-polar compounds (like I_2) in much the same manner as hydrocarbon solvents.[112] Therefore, based on these observations and the well-known affinity of iodine for starch, it is reasonable to propose the existence of a reversible guest-host complex between I_2 and β-cyclodextrin. This 1:1 bound complex can serve to rationalize the high recovery of unprotected conjugate **37**, which was noted when 1.1 equivalents of I_2 was used for deprotection. Consequently, deprotection of **37** was repeated using 2.1 equivalents of I_2 and, by maintaining high dilution conditions to preclude intermolecular disulfide formation, *in situ* intramolecular oxidative cyclization readily afforded the monomeric disulfide **38** in 31% yield. Positive FAB-MS indicated a M+1 peak at *m/z* 1423 and ^1H and ^{13}C NMR spectra confirmed the absence of the trityl group. Cyclization was also inferred from the marked signal complexity of all ^{13}C resonances pertaining to the complexing system (see Section 5.3).

CHAPTER 5

NMR SPECTROSCOPY OF THE DADS LIGAND. PART 1

5.1 General Introduction

NMR spectra of open chain or cyclic derivatives of the N_2S_2 ligand were often markedly complex, inviting interpretations based on product decomposition (*e.g.*, disulfide polymerization) and/or contamination by reaction by-products. The objective of this segment of research was to determine the underlying physical and chemical properties of the DADS system which gave rise to their perplexing NMR spectral profiles.

5.2 Magnetic Non-Equivalence at the C_5 and C_7 Environments in Tritylated Intermediates

Examination of the geminal S-CH_2 protons resonances of ester 7 (*ca.* 3.0-3.1 ppm) revealed the superimposition of an AB quartet ($\Delta\delta_{OBS}$ = 0.05 ppm, ^2J = -15.6 Hz) on a singlet (see Figure 5.1). This effect, which was also noted for many other *S*-tritylated ligand intermediates, implied that one geminal pair of α-thiotrityl methylene protons was magnetically non-equivalent relative to the other at the 500 MHz field strength. The observed selective S-C*H*$_2$ non-equivalence could result from: a) the induction of stereochemical non-equivalence - upon the closer C_7 methylene protons - by the C_1 stereocenter[39,113]; b) chirality-independent, differential shielding by the amide carbonyl anisotropy[113]; or c) restricted rotation, resulting from amide partial

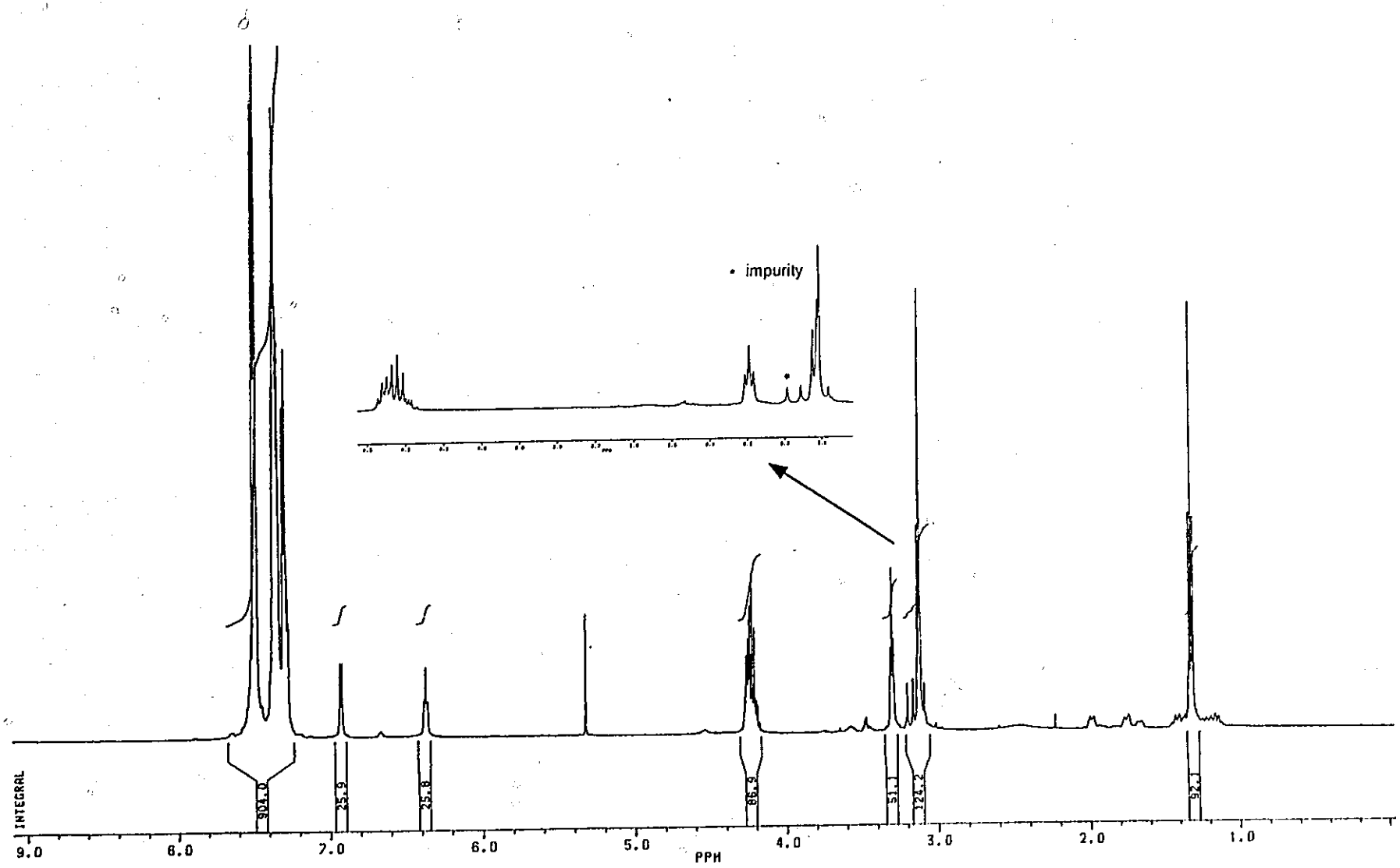

Figure 5.1: 500 MHz ^{1}H NMR spectrum of **7** in $CDCl_3$ at 303 K. Inset: expansion between 3.0 and 4.3 ppm.

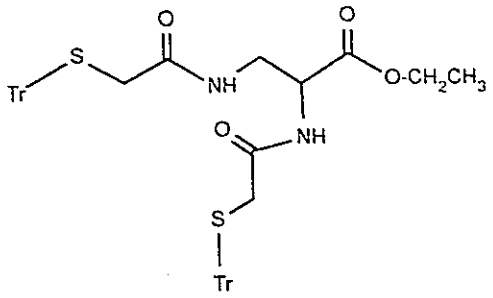

7

double bond character, amide hydrogen bonding to oxygen and/or sulfur, or π-π interactions. If c) is operative, then heating the sample should overcome these relatively small rotational barriers and equilibrate proton environments. Warming **7** to 122.6 °C at 200 MHz did not result in observable change of the S-CH_2 proton resonances relative to the room temperature spectrum: an empirical indication that the previously-stated intramolecular bonding interactions were not the source of the observed non-equivalence. Moreover, given the high field ^1H and ^{13}C magnetic equivalence of *both* pairs of the S-CH_2 groups in the ethylene diamide **41**, the

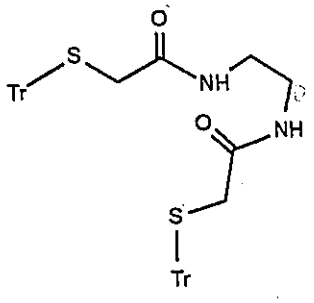

41

arguments for differential shielding based on amide carbonyl and prochiral[39] mechanisms seemed improbable. Therefore, the origins of the observed S-CH_2

chemical shift difference in tritylated intermediates such as 7 was most likely due to chirality-induced non-equivalence. In principle, the presence of the C_1 chiral center confers magnetic non-equivalance upon *all* methylene protons, including those at C_7; however, their non-equivalence cannot be observed at 500 MHz.

A small (0.3 ppm) difference was also noted between C_5 and C_7 shifts in ^{13}C NMR spectra of most *S*-tritylated DADS-CO_2 ligands at 126 MHz. Since C_5 and C_7 are not "diastereotopic", their magnetic non-equivalence cannot be rationalized by analogy of the diastereotopic shielding argument used for their attached protons. This differential carbon shift presumably resulted because of the inductive influence of the COOH substituent at C_2: C_7 resonates at lower field than C_5 due to its closer proximity to the electron withdrawing carboxyl group.

5.3 Analysis of Ethyl *N,N'*-(2,2'-dithioacetyl)-2,3-diaminopropanoate (**8**) in DMSO-d_6 and $CDCl_3$

Compound **8** was synthesized and judged to be a pure sample as evidenced by HRMS, IR, TLC and melting point determinations (see Section 7.6.10). In the high

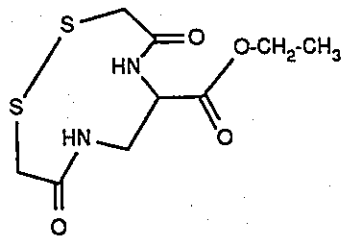

8

resolution mass spectrum, an excellent correlation was found between calculated and observed mass units for the molecular formula $C_9H_{14}N_4O_4S_2$, with a difference of only

0.0008 mu. IR spectroscopy also disclosed key absorbances which were consistent with ester (1735 cm^{-1}) and amide (1640 and 1550 cm^{-1}) groups. TLC indicated a single component at R_f 0.78 (80% *n*-PrOH, 18% H_2O, 2% HCOOH). Moreover, the white solid melted over a two-degree range, suggesting excellent purity.

However, like the acid **5** (see Section 7.6.6), ^1H and ^{13}C NMR spectra of **8** in DMSO-d_6 were dauntingly complex, indicative of a mixture of compounds (see Figures 5.2 and 5.3; Table 7.2). Examination of the C_2-H methine resonances in ^1H and ^{13}C spectra (*ca.* 3.8-4.9 and 52.1-53.0 ppm, respectively) suggested the presence of at least four different chemical species, while in the carbonyl region, as many as nine separate, ^{13}C signals were noted. The NMR data seemed to imply that the disulfide was impure - a conclusion which contradicted the results of the above mentioned characterization methods. The possibility that polymeric disulfides were present was not supported by MS.

Since the prochirality of the ring CH_2 groups or the presence of the chiral center at C_1 cannot fully account for the complexity of the ^1H NMR spectrum in DMSO-d_6, the possibility of slowly exchanging, ring conformers was investigated. Ball and stick models indicated that the 10-membered disulfide heterocycle is large enough to accomodate the rotation of the entire amide group through the ring, provided that the substituent of the N atom was a simple hydrogen atom (as in **8**). To test this hypothesis, the C_1 unsubstituted, *N*-methyl disulfide (**40**) was prepared. In this model compound, ring interchange would require the passage of the N-CH_3 group through the middle of the ring - a sterically unfavorable process. The ^1H and ^{13}C spectra (see Figures 6.1 and 6.2) proved to be complex, suggesting ring interchange by rotation of a complete amide unit through the ring was an unlikely mechanism for rationalizing the NMR spectra of **8** in DMSO-d_6.

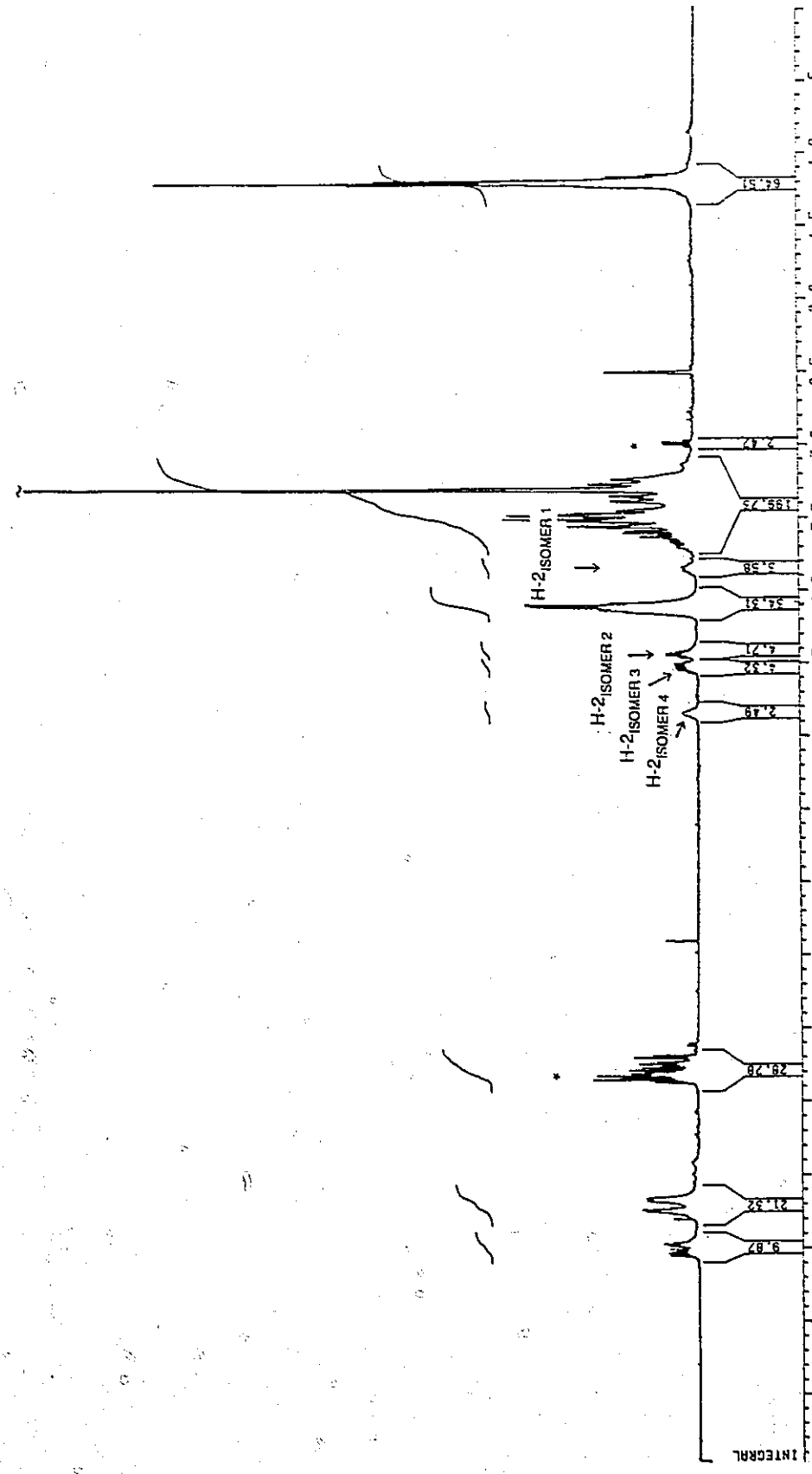

Figure 5.2: 500 MHz ^{1}H NMR spectrum of **8** in DMSO-d_6 at 303 K.

* Tr-OCH_2CH_3 (impurity)

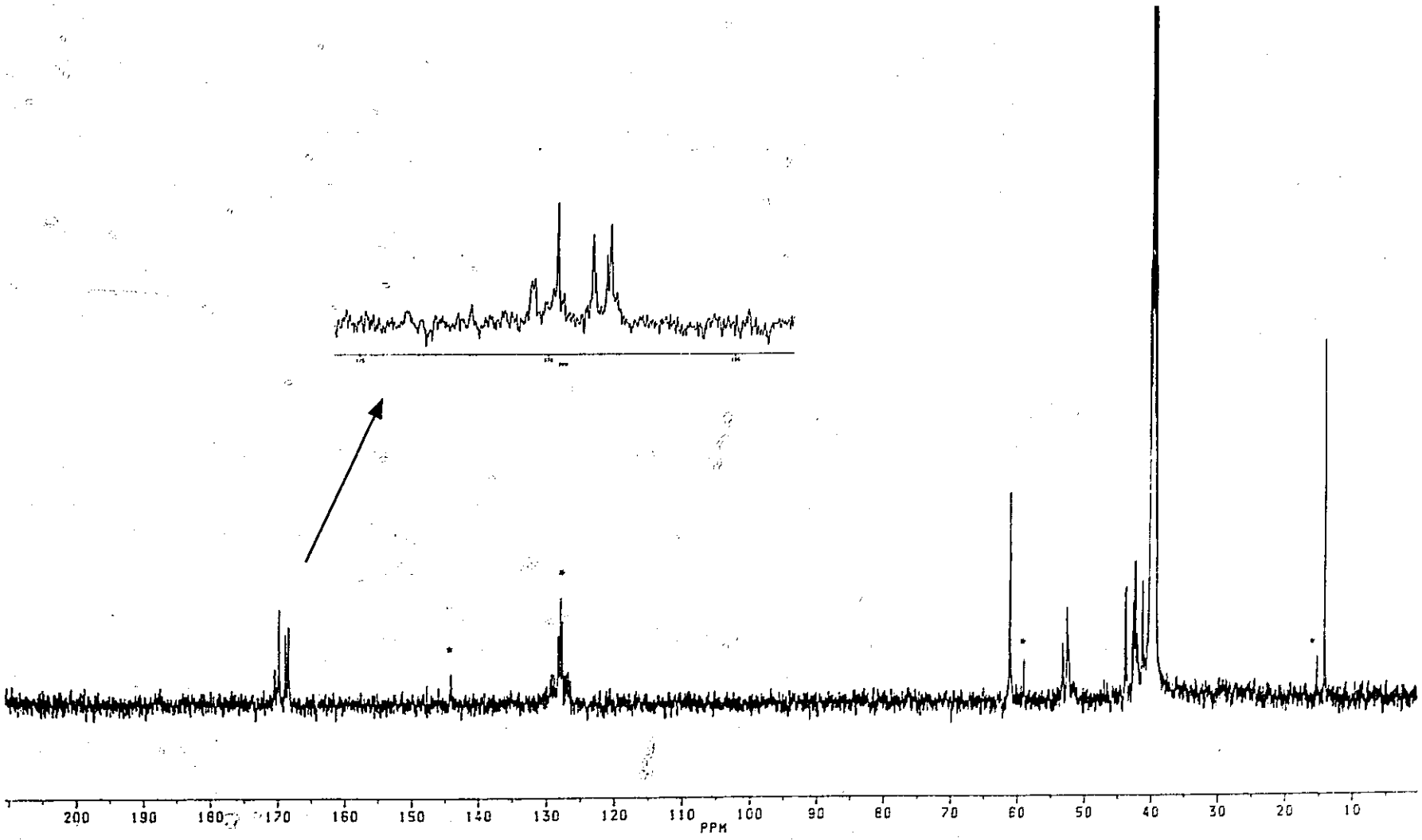

Figure 5.3: 126 MHz ^{13}C NMR spectrum of **8** in DMSO-d_6 at 303 K.

Another proposal was investigated: restricted rotation about amide and disulfide linkages have been reported[92,114] to be slow on the NMR time scale, resulting in an equilibrium mixture of discrete geometric isomers at room temperature, where each isomer possesses a unique NMR spectrum. Although the rate of rotational isomerization is temperature-dependent, warming the DMSO-d_6 solvated disulfide ester **8** to 120 °C (see Figure 5.4) did not induce an appreciable change in its ^{1}H NMR spectrum at 250 MHz, unlike that for the dimethyl disulfide **40** (see Figure 6.3). The variable temperature data did not necessarily refute the possibily of restricted rotation; however, they did suggest that, if such a phenomenon was operative, the barriers to isomerization were too high to observe appreciable change at 120 °C (*vide infra*). High barriers to conformational isomerization are possible in strongly polar solvents, such as DMSO-d_6, as they can form hydrogen bonds with the amide protons of **8** to confer high conformational stability on conformers (*vide infra*). With the *N*-dialkyl analog **40**, hydrogen bonding is not possible as for **8**, so conformational exchange can be observed at temperatures below the instrumentally-imposed ceiling temperature of *ca.* 120 °C (see Section 6.1).

Given the aforementioned proposal of solvent stabilization, the effect of non-polar deuterated solvents was investigated, with the ^{1}H and ^{13}C spectra in $CDCl_3$ presented as Figures 5.5 and 5.6. Compared with the DMSO-d_6 sample, spectral features have been markedly simplified to permit an unambiguous assignment of all spin systems (see Table 7.2). The findings of the $CDCl_3$ experiment served to strongly confirm the suspected origins of spectral multiplicity in the DMSO-d_6 spectrum of **8**: in DMSO-d_6, hydrogen bonding and dipole-dipole interactions between the solvent and protic amide functions of **8** resulted in the stabilization of the room temperature, ground-state ring conformers *relative to the transition state for isomerization* (see

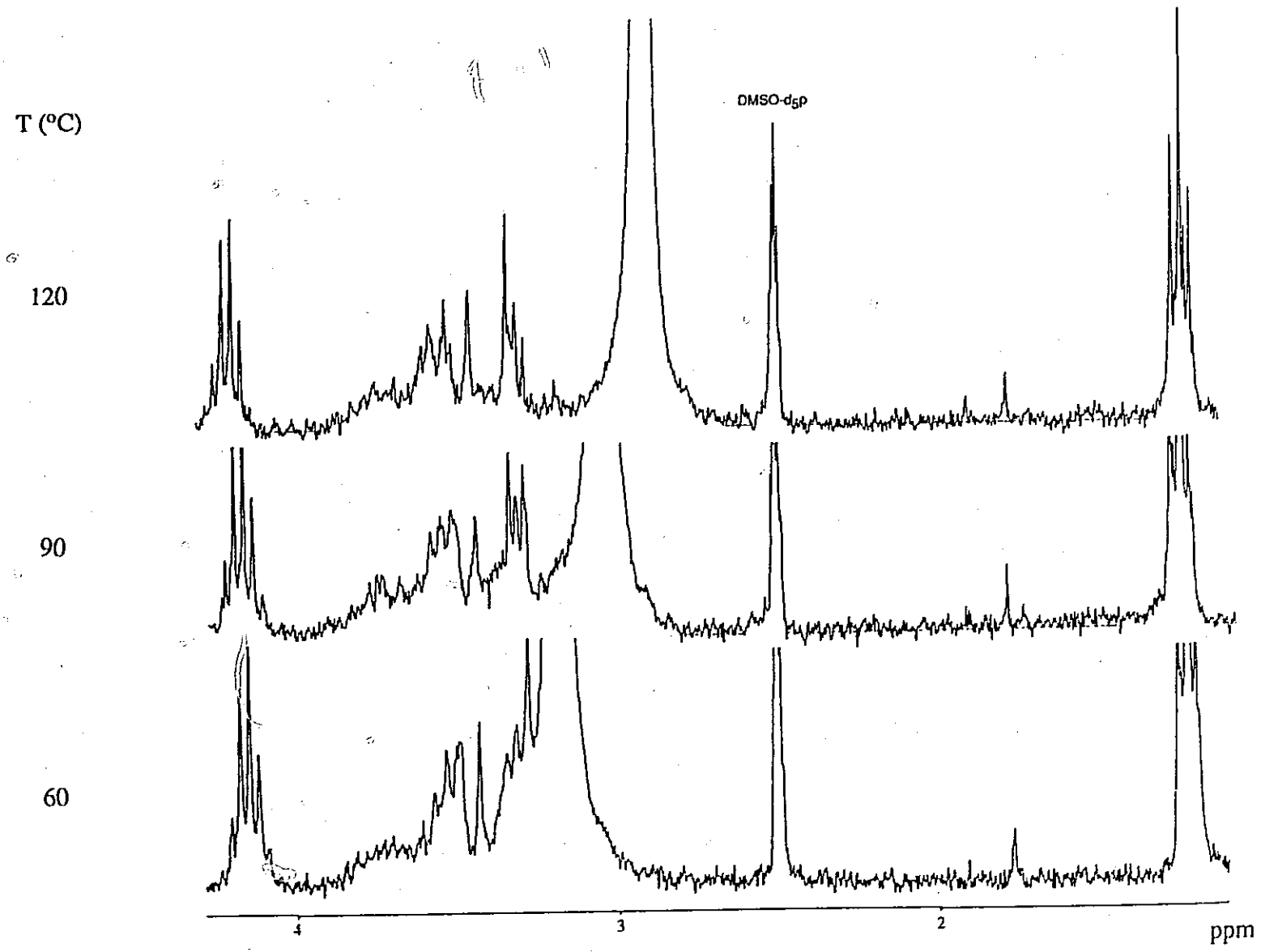

Figure 5.4: 500 MHz ^{1}H NMR variable temperature spectra of **8** in DMSO-d_6.

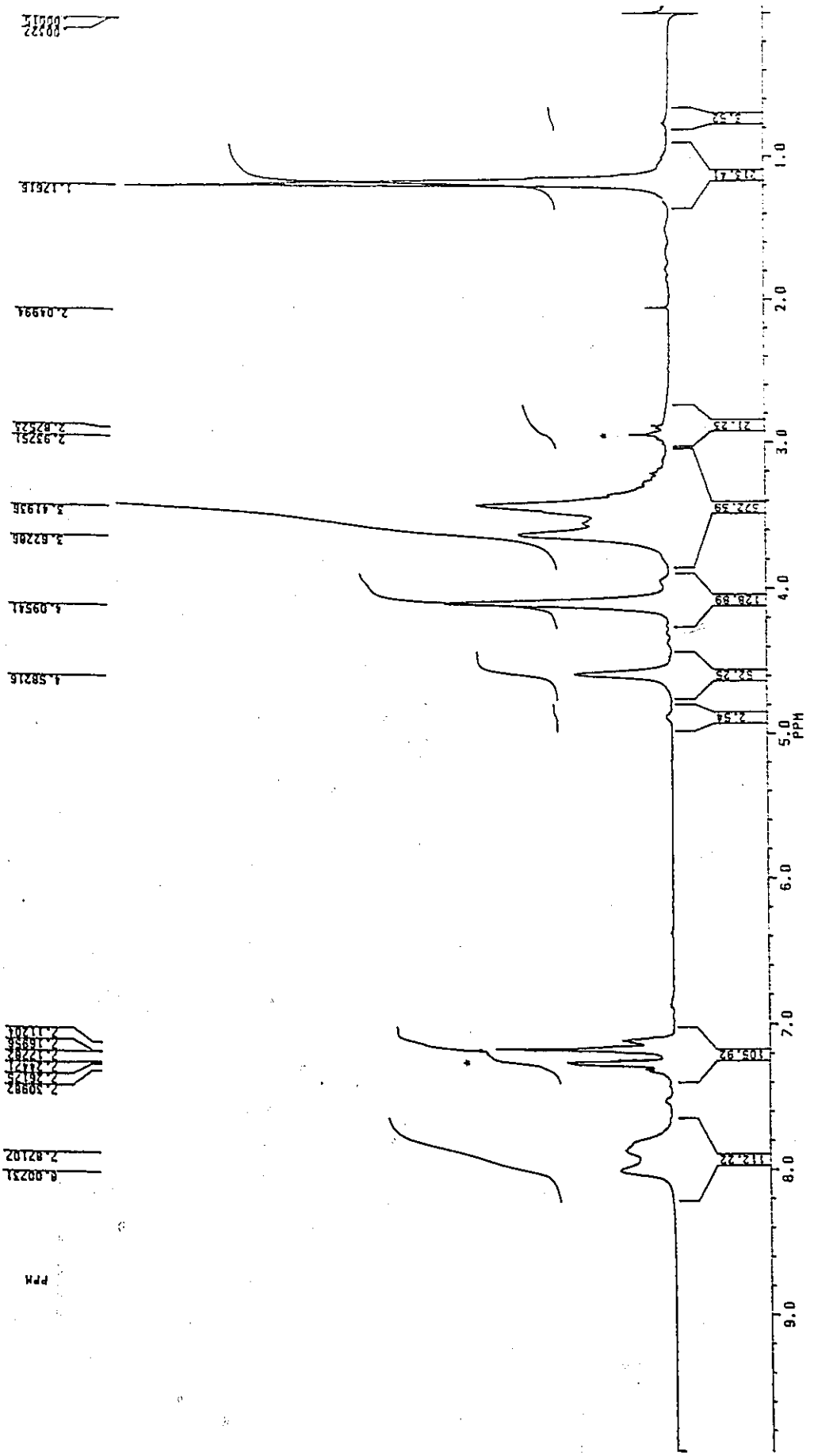

Figure 5.5: 500 MHz ^{1}H NMR spectrum of **8** in $CDCl_3$ at 303 K.

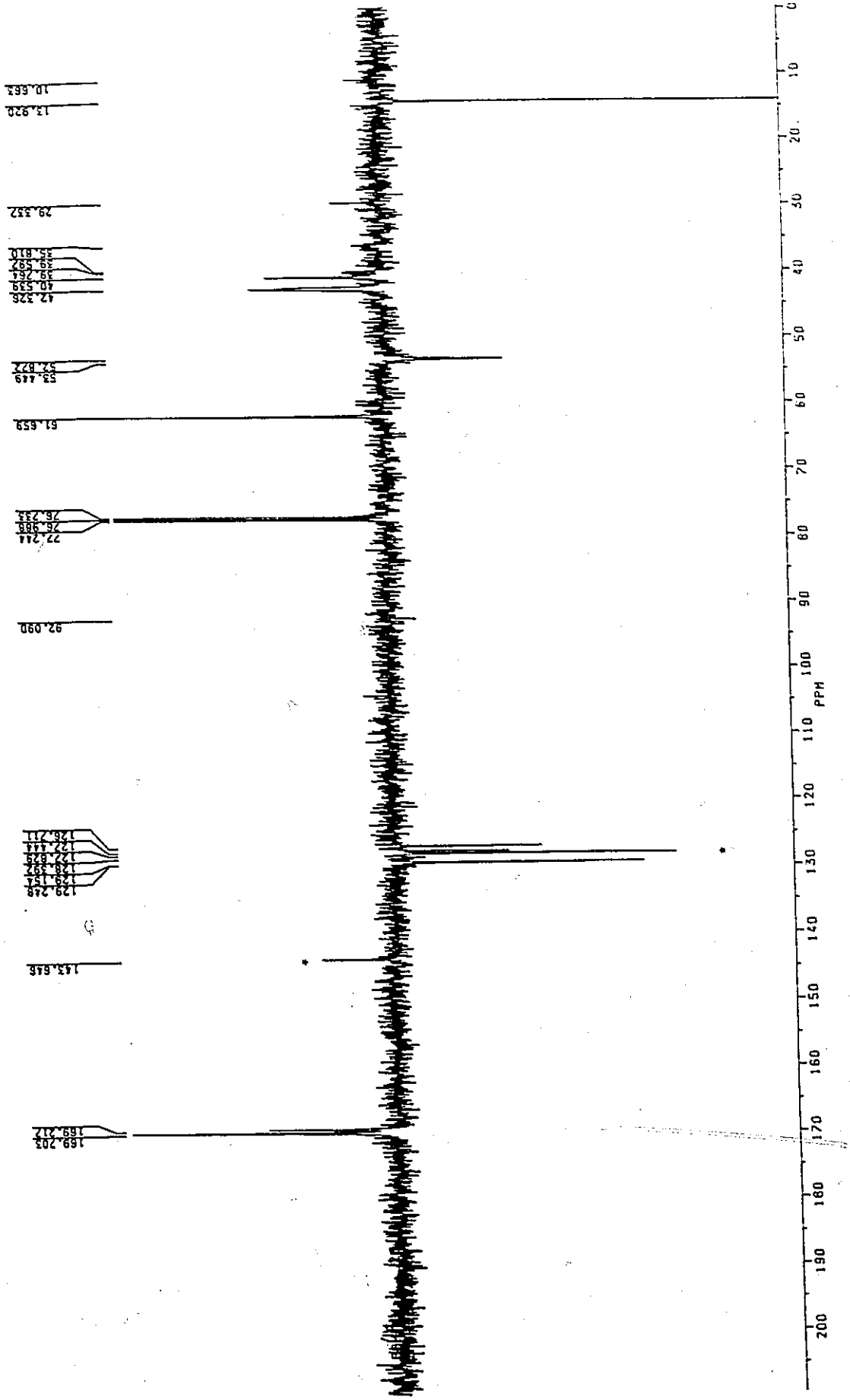

Figure 5.6: 126 MHz *J*-modulated ^{13}C NMR spectrum of **8** in $CDCl_3$ at 303 K.

Figure 5.7). This "freezing out" of ring conformers into deep potential energy wells -

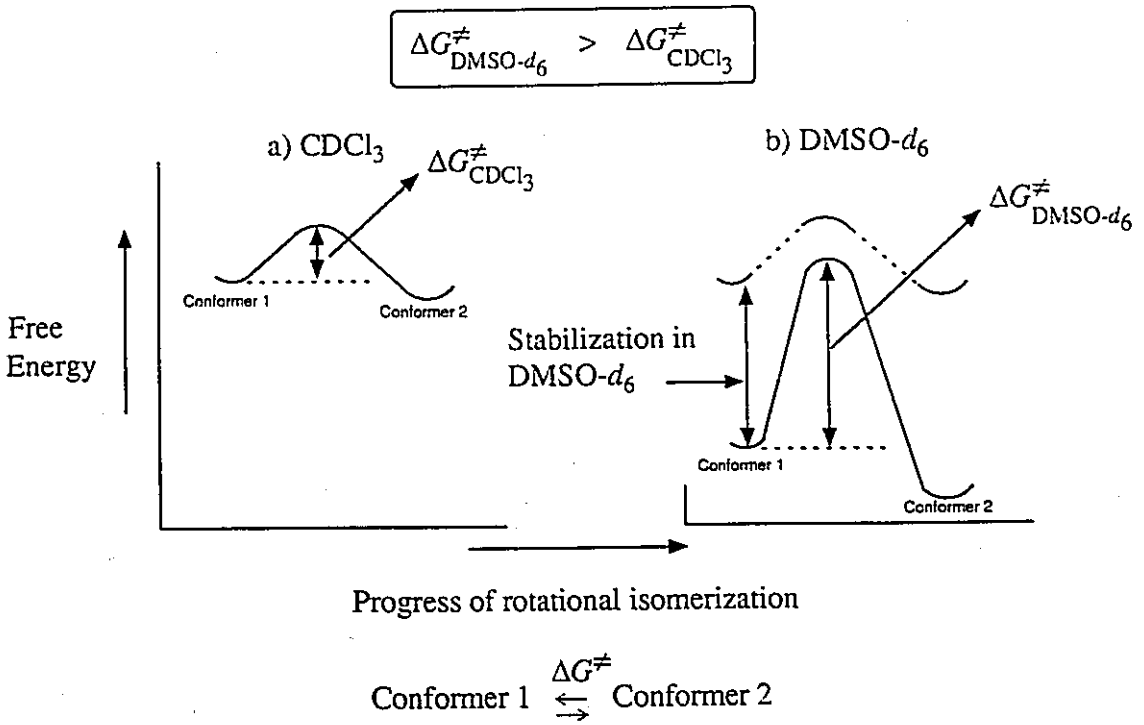

Figure 5.7: Effect of solvent [(a) $CDCl_3$ *vs* (b) DMSO-d_6] on the free energy change of activation, $\Delta G^{\neq}$, for an isomerization process involving bond rotation in **8**. Intermolecular solute-solvent bonds in DMSO-d_6 stabilize ground state ring conformations relative to the transition state for rotation, thereby increasing $\Delta G^{\neq}$.

which are separated by high barriers to interconversion (as measured by $\Delta G^{\neq}$) - effectively reduces the rate of ring conformational interconversion. As a result, the signals in the DMSO-d_6 spectrum of **8** became sharp relative to that of the $CDCl_3$ sample, with the absorptions from each of the many ring conformers overlapping to give the observed spectral multiplicity. The barriers to isomerization in DMSO-d_6 must be quite high (*i.e.*, $\Delta G^{\neq} > 20$ kcal/mol) in order to rationalize the negligible effect of high temperature (120 °C) on the ^{1}H NMR spectrum of **8**. Differential ring conformer stabilization in non-polar $CDCl_3$ was not nearly as pronounced as for DMSO-d_6

because of the inability of the former solvent to form strong hydrogen bonds with **8**. This allowed ring isomers to rapidly interconvert over lower rotational barriers (see Figure 5.7 a) and manifested themselves as broader resonances in the $CDCl_3$ spectrum. This solvent effect was also observed in the ^{13}C NMR spectrum of $CDCl_3$ and DMSO-d_6 solvated samples of the *N*-monoalkylated disulfide **42** (see Section 7.6.46) and possibly holds broader application in *N*-monoalkylated lactams, where the ring exerts a critical combination of rigidity and flexibility to allow the stabilization of the amide (and/or disulfide) group through solvation with polar solvents. Evidence of conformational isomerism was not noted in NMR spectra of the open chain precursors **7** and **41**, indicating that a ring structure is required for the observation of solvent effects described earlier.

Four, approximately equally-populated, ring isomers, which were identified by their C_2-H resonances (labeled as $H\text{-}2_{ISOMER\ 1}$, $H\text{-}2_{ISOMER\ 2}$ *etc*, see Figure 5.2) were detected in the DMSO-d_6, ^1H NMR spectrum of **8**. The ^1H-^1H COSY experiment (see Figure 5.8) confirmed that these methine signals belonged to separate spin-systems with connectivities to the C_3-H protons in the 3.3-3.5 ppm range, thereby constituting different conformations. Ring isomers 1 and 4 (ISOMER 1 and ISOMER 4) had rather broad C_2-*H* resonances (small T_2) and did not show up as diagonal elements, presumably because of the rapid decay of their magnetization from the XY plane of the detector.

The C_2-*H* region of the $CDCl_3$ spectrum of **8** (see Figure 5.5) revealed residual amounts of what appeared to be the DMSO-d_6 observed isomers (at δ ~4.0 and δ ~4.9). This observation spurred the following experiment: a solution of **8** in $CDCl_3$ was cooled to -40.4 °C to decrease the rate of conformational exchange and to determine if the broad proton resonances of the room temperature spectrum could be

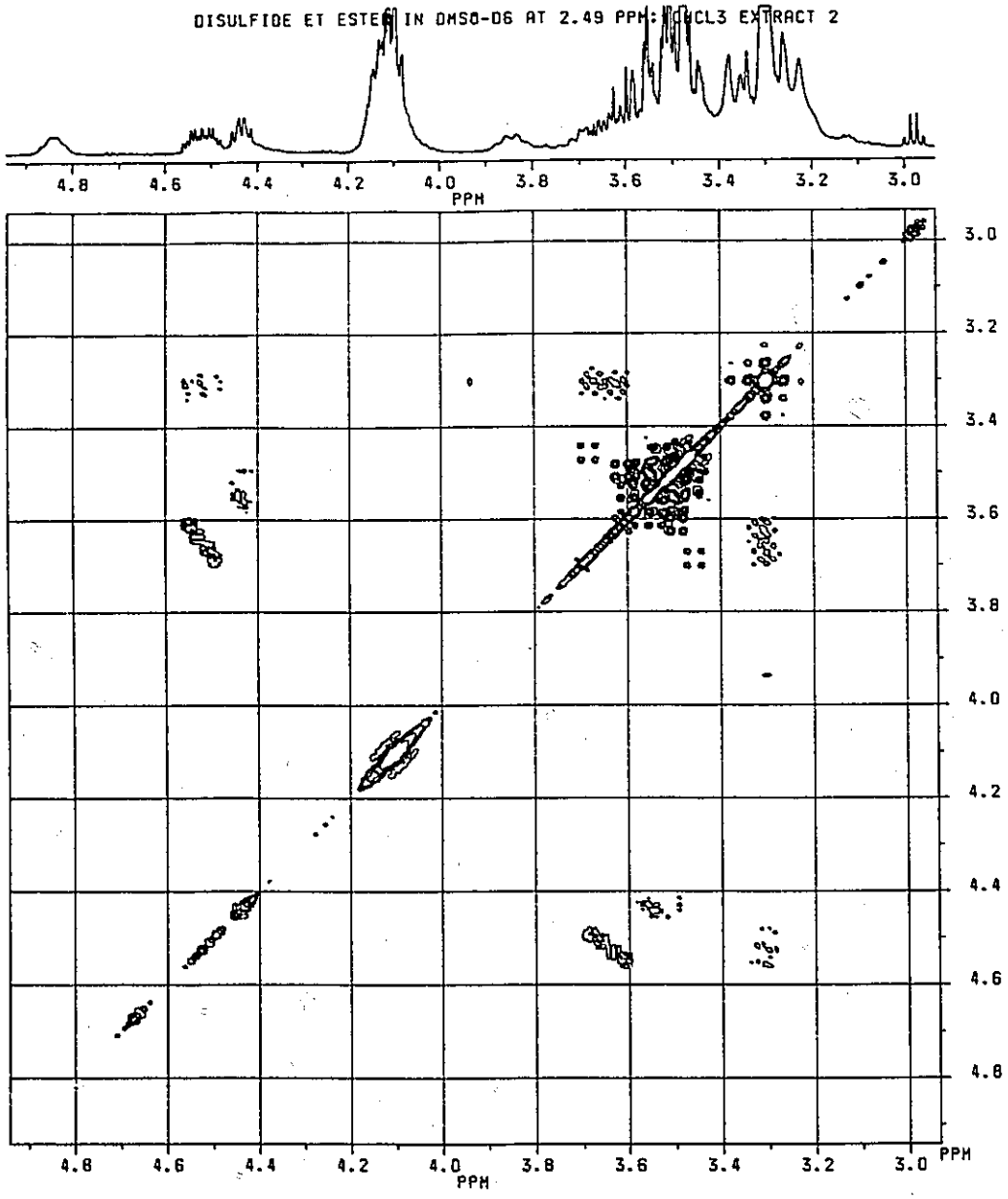

Figure 5.8: 500 MHz ^{1}H NMR COSY-45 spectrum of **8** in DMSO-d_6 at 303 K.

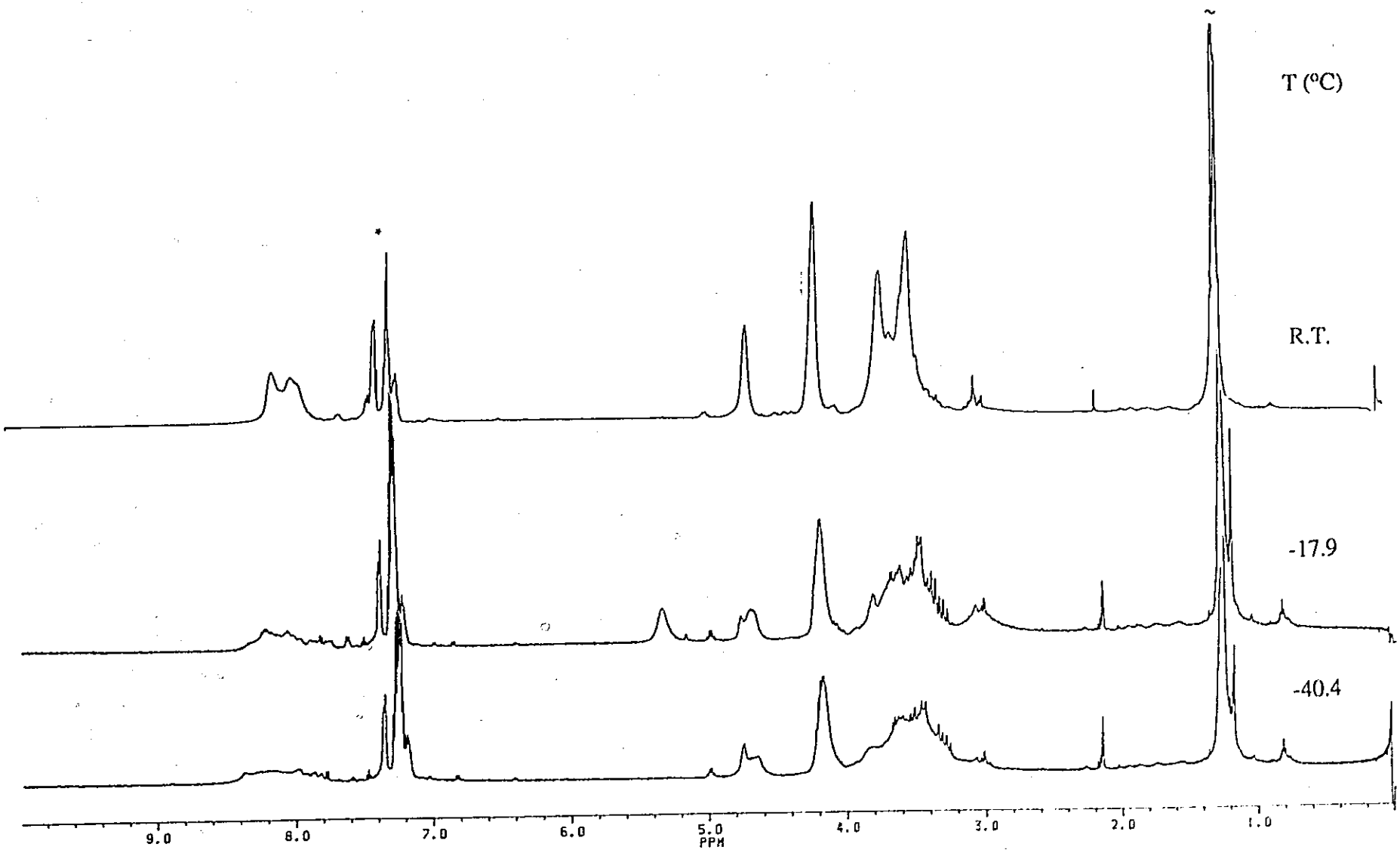

Figure 5.9: 500 MHz ^{1}H NMR variable temperature spectra of **8** in $CDCl_3$.

sharpened at a low temperature to generate the DMSO-d_6 isomers. Figure 5.9 illustrates the beginnings of sharpening and separation of all proton signals as the sample is cooled from room temperature to -40.4 °C. The addition of 5 mg of $Ca(ClO_4)_2$ also induced peak sharpening, presumably by locking some or all of the interconverting isomers into a rigid calcium chelate (see Figure 5.10).[115]

5.4 Conformational Analysis of *N,N'*-{dimethylbis[2-(triphenylmethyl)thioethanoyl]} ethylenediamine **39** in $CDCl_3$

Compound **39** proved to be an interesting NMR spectroscopic example of a chemically exchanging system having conformational preferences around the C-N amide bond. A superficial analysis of the room temperature ^1H and ^{13}C NMR spectra in

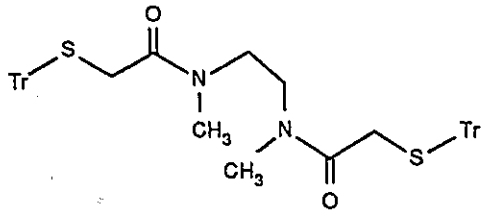

39

DMSO-d_6 (see Figures 5.11 and 5.12), revealed a rather complex resonance profile considering the molecule's symmetrical, non-cyclical structure and isolated spin systems. The NMR results appeared even more puzzling given that spectra taken in $CDCl_3$ were practically identical to the DMSO-d_6 ones, which eliminated the possibility for the dramatic solvent effects described for **8** (see Section 5.3).

The most plausible explanation to rationalize the multitude of NMR signals is restricted rotation about the two amide groups; a process which is sufficiently slow at

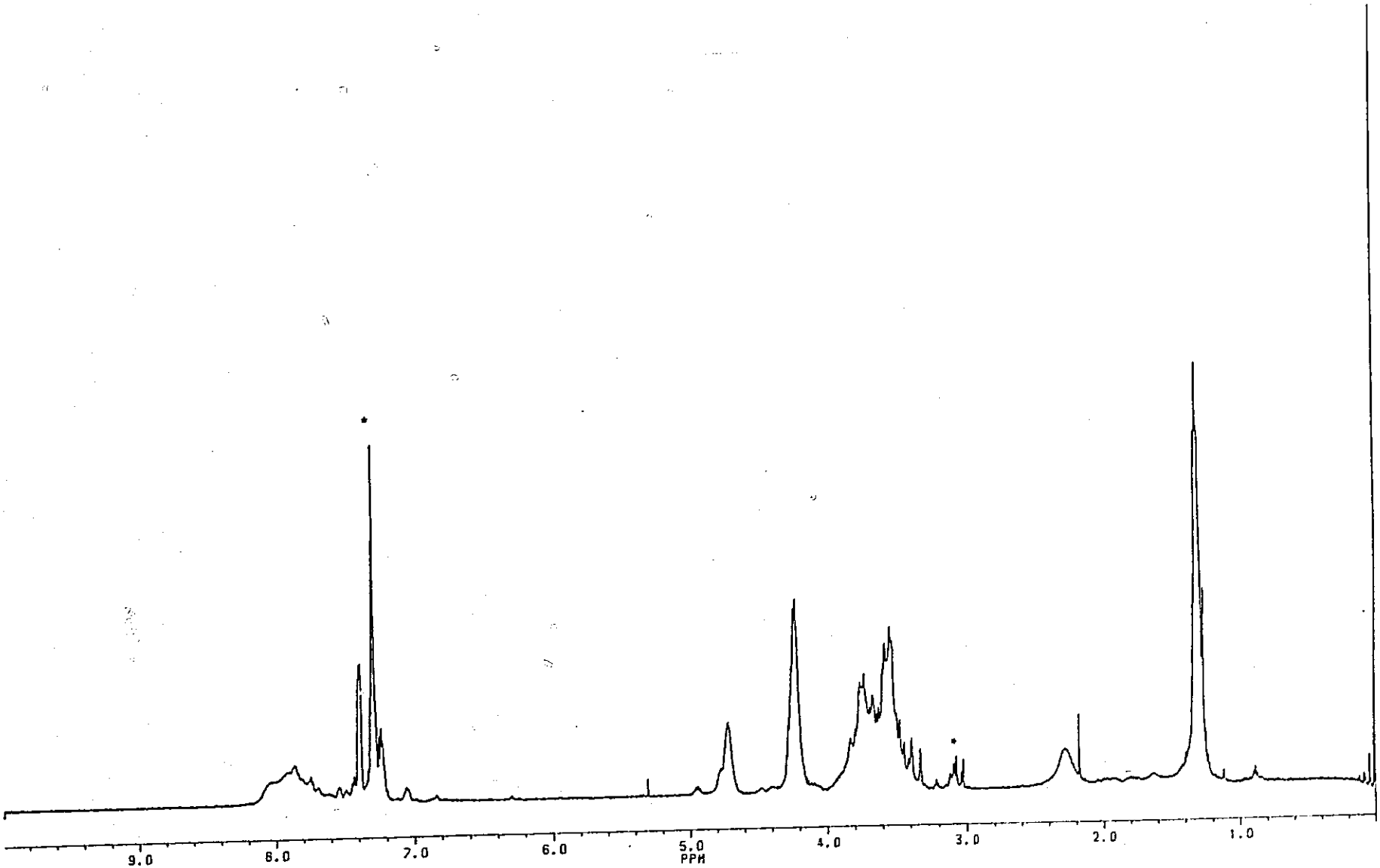

Figure 5.10: 500 MHz ^{1}H NMR spectrum of **8** with 5 mg of $Ca(ClO_4)_2$ at 303 K.

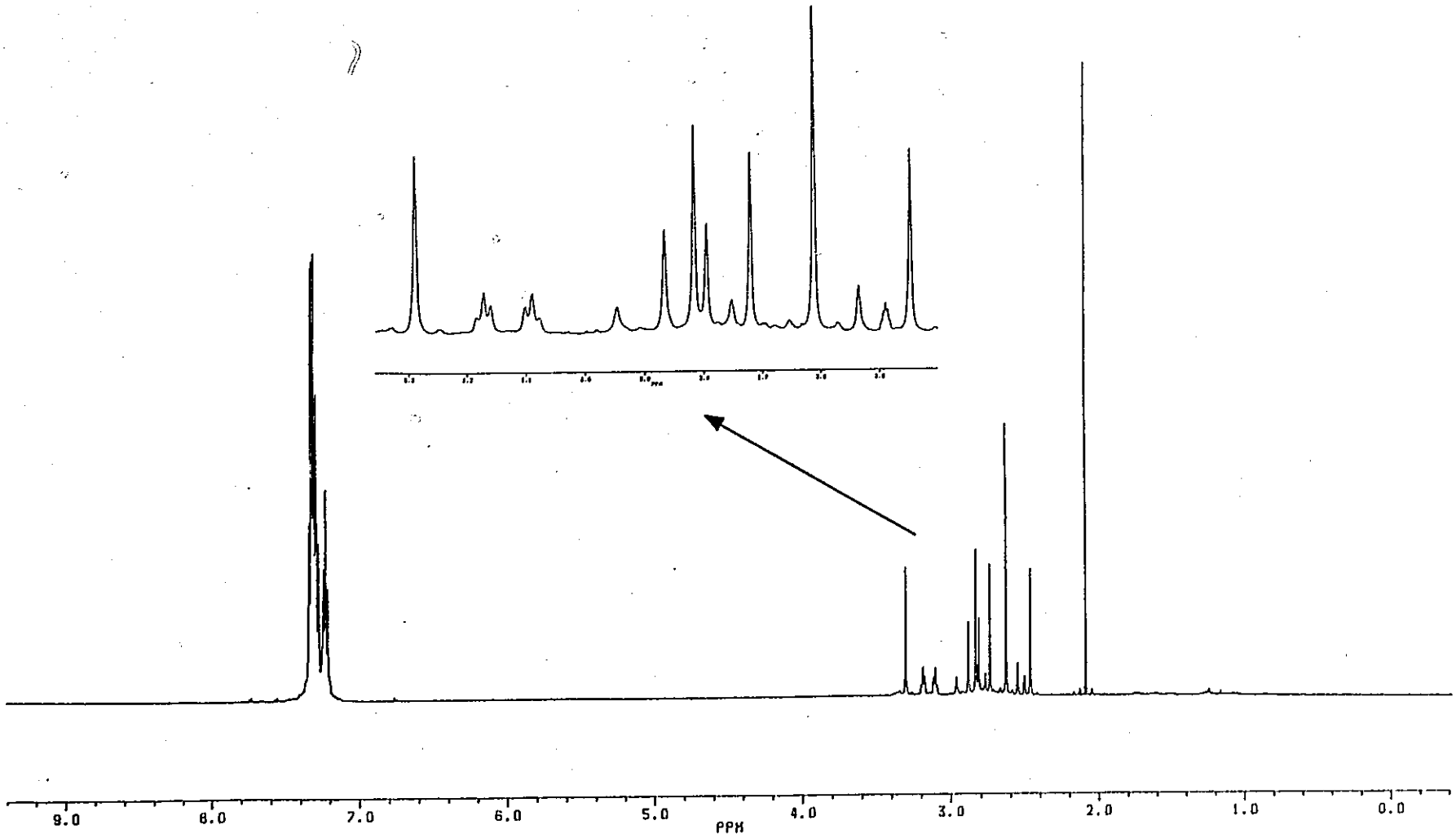

Figure 5.11: 500 MHz ^{1}H NMR spectrum of **39** in DMSO-d_6 at 303 K.

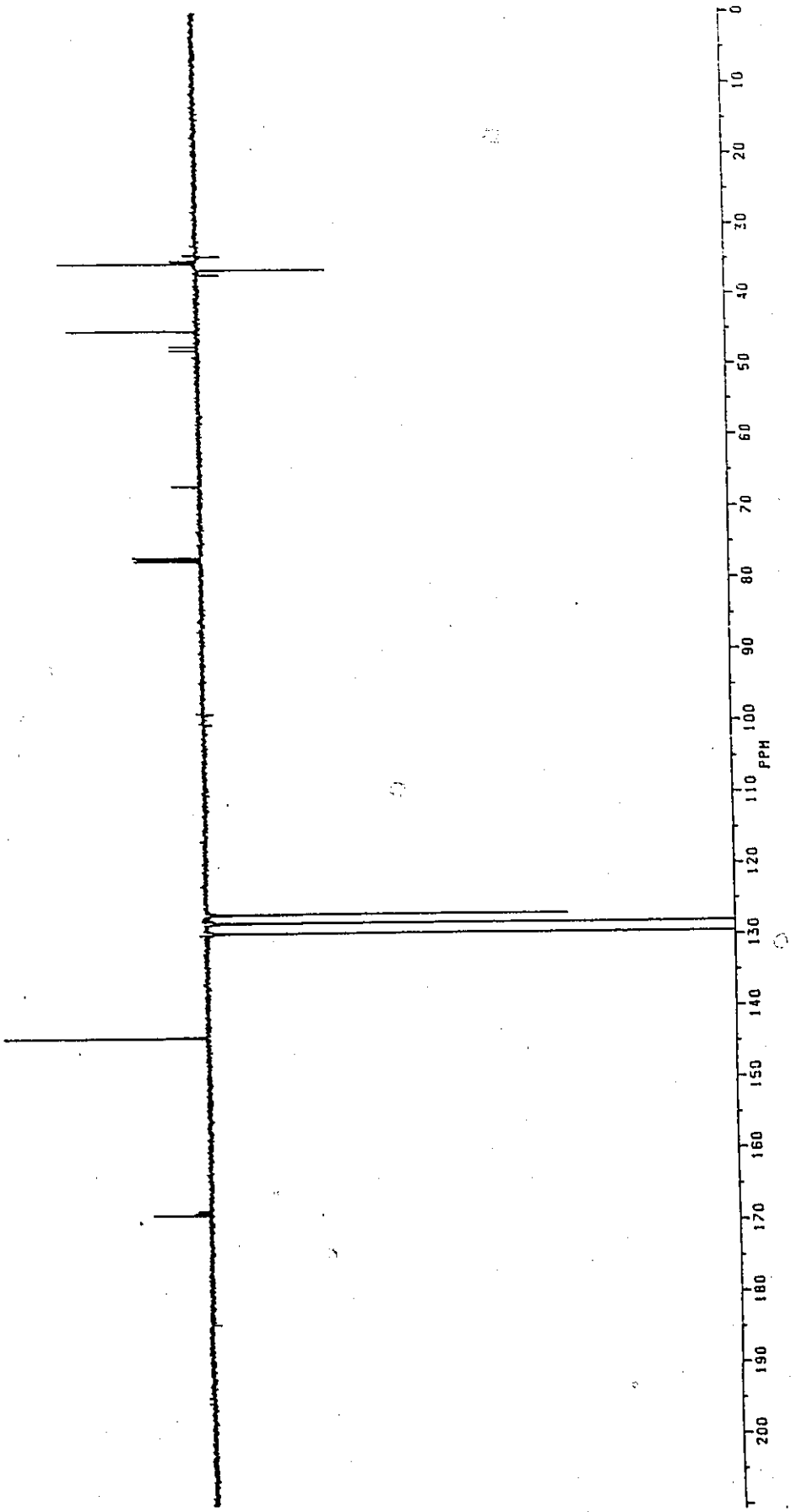

Figure 5.12: 126 MHz ^{13}C NMR spectrum of **39** in $CDCl_3$ at 303 K.

room temperature on the NMR time scale to allow the observation of distinct stereochemical environments for the alkyl substituents. Restricted amide rotation is attributed to partial double bond character derived from the following delocalized electronic structure:

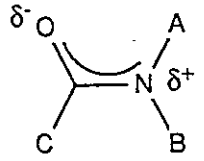

As a result, the environment of substituents A, B and C are not averaged and, depending on their chemical shifts, these groups can usually be observed as separate signals in the NMR spectrum.[92]

Elevated temperature ^{1}H NMR studies of **39** showed the temperature dependent coalescence of all aliphatic resonances into the three signals predicted for the symmetrical, averaged compound (see Figure 5.13). Based on peak integration of the averaged, 122.5 °C spectrum and following peak transitions from the room temperature to the high temperature limit, three separate sets of proton resonances - attributable to three geometric isomers - could be identified.

To verify this chemical rate process as restricted amide rotation, the free energy change of activation, $\Delta G^{\neq}$, was estimated to a first order approximation using a modified form of the Eyring formulation[116] (Equation 5.1):

$$\Delta G^{\neq} = RT_c\,[22.96 + \ln(T_c/\Delta\nu)] \qquad [5.1]$$

where T_c is the coalescence temperature (K), R is the universal gas constant and $\Delta\nu$ is the frequency separation (Hz) between two uncoupled, exchanging nuclei of equal resonance intensity. T_c was estimated from Figure 5.13 to be about 87 °C at 250 MHz, which afforded $\Delta G^{\neq} \approx$ 15.1 kcal/mol. This value was consistent with typical rotational

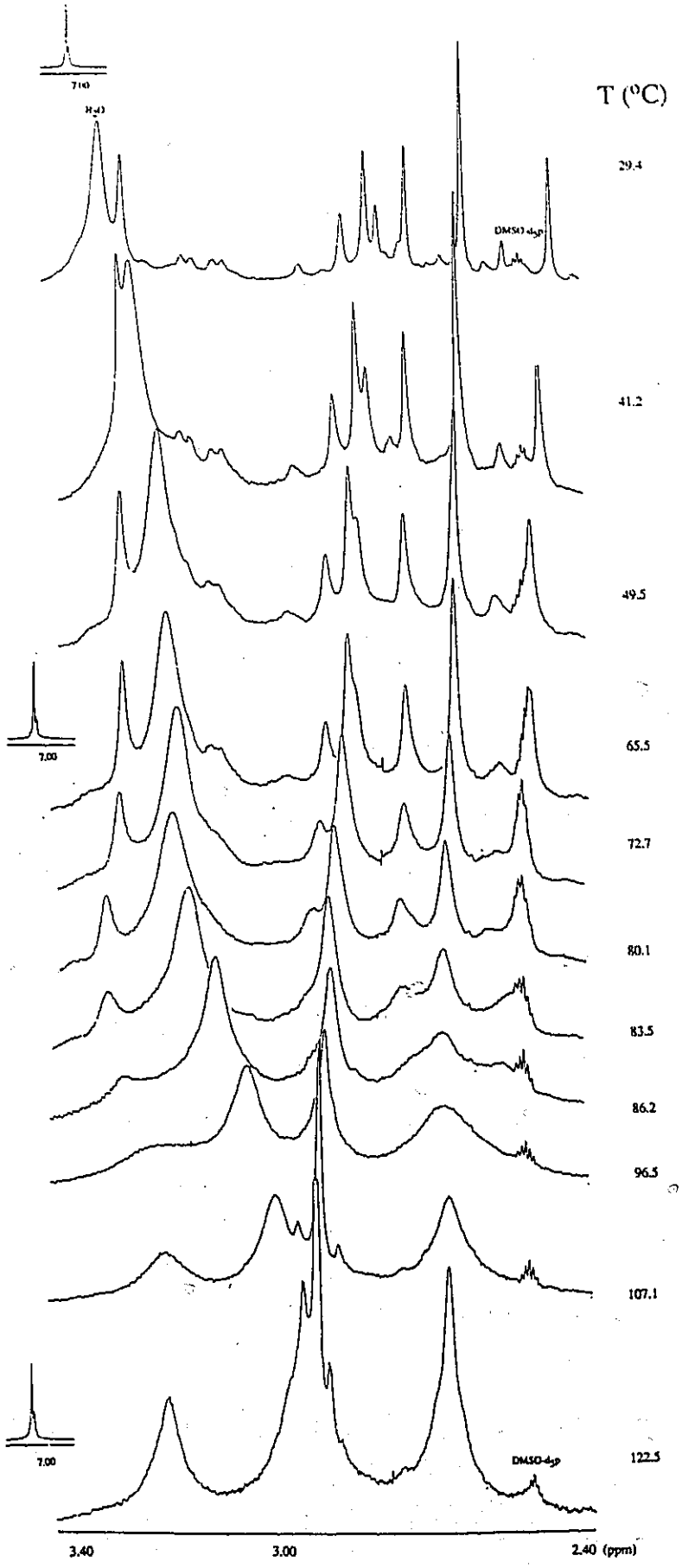

Figure 5.13: 200 MHz ^{1}H NMR variable temperature spectra of **39** in DMSO-d_6.

barriers reported for substituted *N,N'*-dimethylamides (*e.g.*, dimethylacetamide, $\Delta G^{\neq}_{298.2}$= 17.4 kcal/mol; dimethylpropanamide, $\Delta G^{\neq}_{298.2}$= 16.7 kcal/mol).[117] Thus, the fluxional process responsible for the complexity of the room temperature spectrum of **39** was most likely a result of restricted rotation about the amide groups. Other possible explanations might have included conformational preferences at the N-C_α bond[92] and/or π-π bond interactions[118] between trityl groups; however, these effects are quite likely to be less than 10 kcal/mol in this compound.

Having linked the multi-signal, room temperature spectrum of **39** to rotational isomerism about the amide groups, a total analysis of the ^{1}H NMR spectrum was developed. Figure 5.14 illustrates the possible amide rotamers of **39** that can co-exist at room temperature. It is known that population distribution among amide

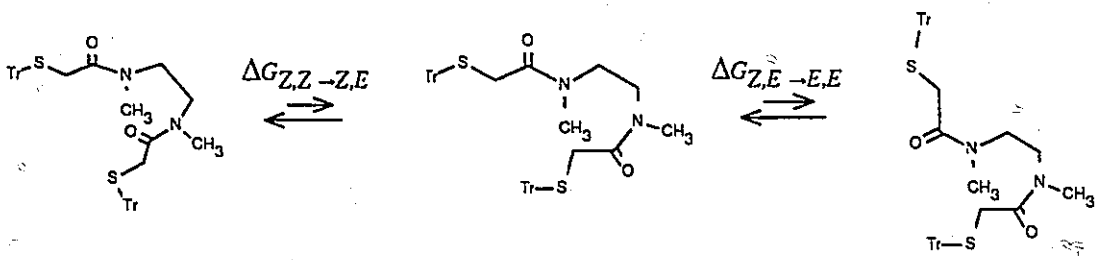

Figure 5.14: Amide isomerization of **39** in $CDCl_3$.

stereoisomers in symmetrically substituted *N,N'*-dialkylamides can be rationalized in terms of steric competition. In general, the *trans* isomer is energetically favored, except in small ring lactams where the conformation must be *cis* (see Figure 5.15 for a key to nomenclature of amide geometry).[92] Therefore, the following stability trend was expected for amide rotamers of **39**: *Z,Z* > *Z,E* > *E,E*; where the *Z,E* isomer is

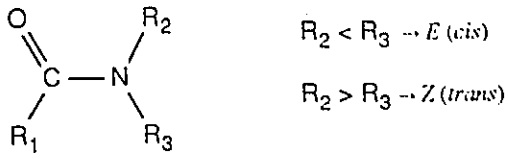

Figure 5.15: *E/Z* (*cis*/*trans*) nomenclature in amides. R symbolizes an alkyl group.

unsymmetric. Correlating peak integrals with the above stability trend, peak integration in the high temperature NMR experiment and symmetry arguments, the three geometric isomers were characterized in the ^{1}H and ^{13}C NMR spectra (see Tables 7.3 and 7.4, Section 7.6.43).

Configurations were also characterized and confirmed through the chemical shift of the *N*-CH_3 group.[114] In agreement with steric competition arguments, the diamide **39** was found to exist mainly in the *Z,Z* conformation in which the *N*-CH_3 resonances were always shifted downfield relative to the corresponding *N*-CH_3 signals of the *E,E* isomer. This observation was supported by the ^{1}H NMR resonances of *N,N*-dimethylacetamide where the *N*-CH_3 signal *trans* to the carbonyl oxygen resonates at ~0.1 ppm downfield from the *cis* signal in $CDCl_3$.[119] The same trend was observed to hold for the corresponding ^{13}C resonances.

The Boltzmann equation was employed to calculate the difference in free energy (ΔG) between the geometric isomers (Equation 5.2). Based on ratio intensities

$$\Delta G = -RT \ln (n_2 / n_1) \qquad [5.2]$$

of appropriate ^{13}C signals (see Table 7.4), the *Z,Z* conformer was energetically favored over the *Z,E* isomer by 0.55 kcal/mol ($\Delta G^{303}_{Z,Z \rightleftharpoons Z,E}$ = 0.55 kcal/mol) and the *Z,E* over the *E,E* by 0.88 kcal/mol ($\Delta G^{303}_{Z,E \rightleftharpoons E,E}$ = 0.88 kcal/mol).

CHAPTER 6

NMR SPECTROSCOPY OF THE DADS LIGAND, PART 2

6.1 General Introduction

The 10-membered heterocycle **40** was prepared to aid in the interpretation of the complex NMR spectral characteristics noted for the cyclic disulfides **5** and **8** in DMSO-d_6 (see Section 5.3). However, NMR spectroscopy of this compound proved to be complex in its own right, warranting further investigation.

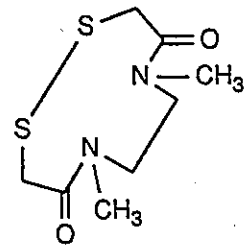

40

6.2 Conformational Analysis

6.2.1 ^{1}H and ^{13}C NMR Spectroscopy

The cyclic disulfide **40** ran as one spot when examined by thin layer chromatography and melted over a 1.0 °C range indicating good sample homogeneity. Infrared, Raman and mass spectra of the product were consistent with its proposed monomeric structure (see Section 7.6.44). The ^{1}H and ^{13}C NMR spectra (see Figures 6.1 and 6.2), however, showed dramatically complex resonance profiles despite the established chemical purity of the sample and its symmetry-related, spin isolated sets of

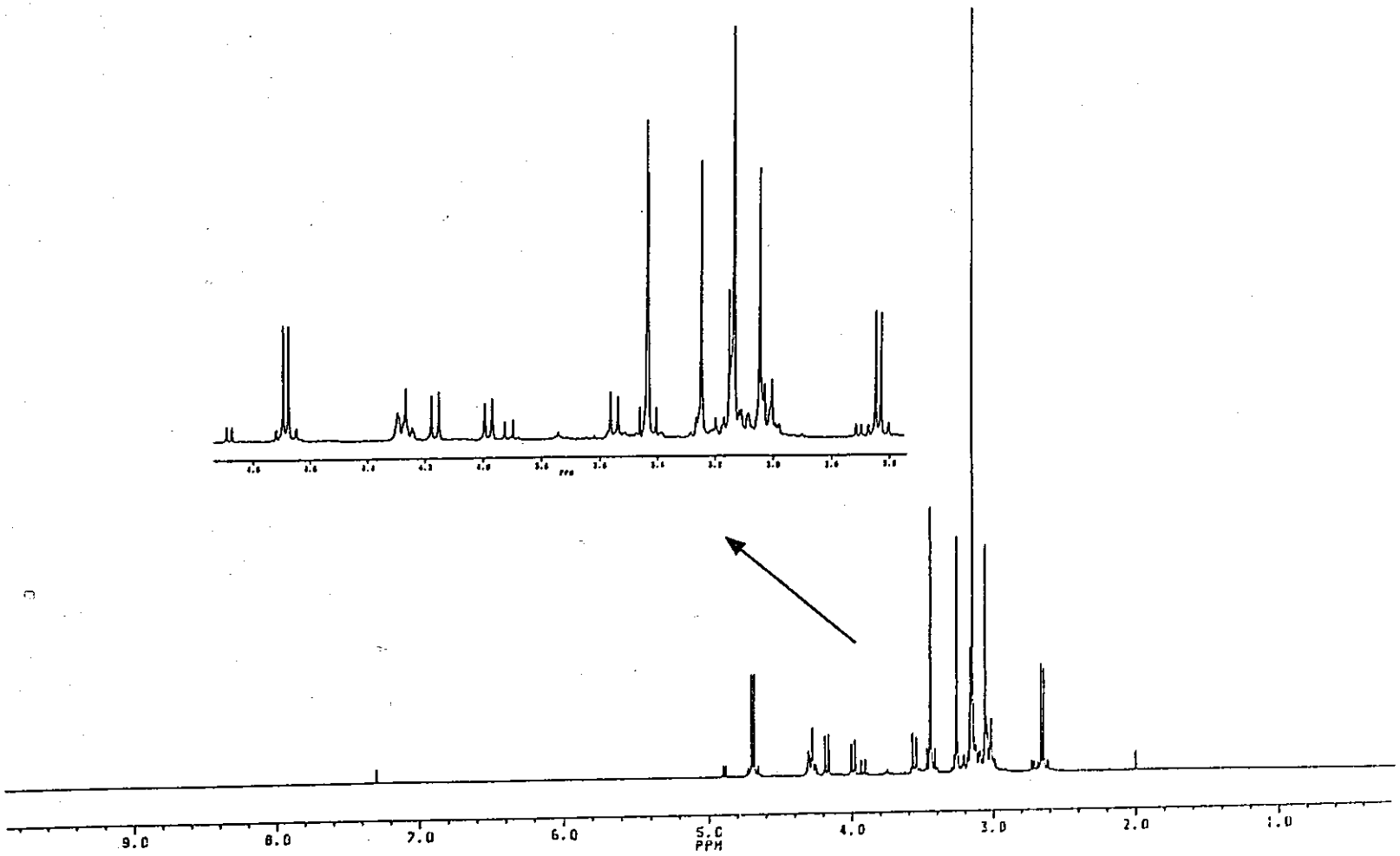

Figure 6.1: The 500 MHz ^{1}H NMR spectrum of **40** in $CDCl_3$ at 303 K. Inset: expansion between 2.5 and 5.0 ppm.

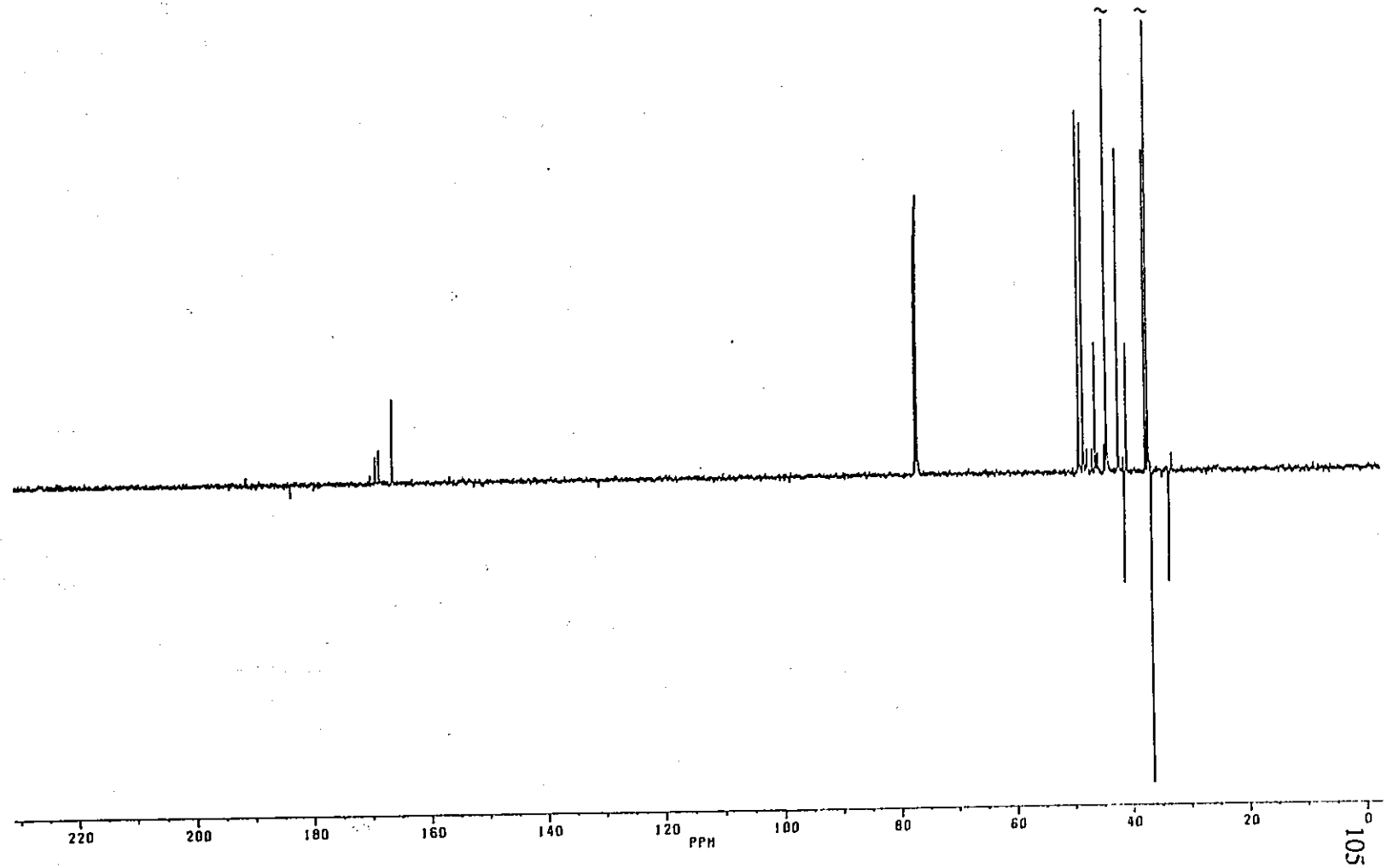

Figure 6.2: The 126 MHz *J*-modulated ^{13}C NMR spectrum of **40** in $CDCl_3$ at 303 K.

^{1}H and ^{13}C nuclei. That this multiplicity of lines arose from the presence of different ring conformers was suggested from the ^{13}C spectrum which showed 12 lines in the aliphatic region (δ 30-50) rather than the anticipated three. This increased number of lines was rationalized by noting that each amide group can exist in either *Z* (*trans*) or *E* (*cis*) stereochemistry due to restricted amide rotation (see Figure 5.15 for a key to *Z*/*E* nomenclature in amides): this enables the cyclic disulfide to adopt, in principle, three conformations with the amide groups *Z*,*Z*, *Z*,*E* and *E*,*E*.

6.2.2 ^{1}H DNMR Studies

Variable temperature ^{1}H NMR spectroscopy was employed to determine the presence of conformational isomers. Studies in the temperature range -61.5 °C to 30.0 °C in $CDCl_3$ indicated that the conformers were in slow exchange at room temperature and below, thereby conferring distinct stereochemical environments of the alkyl substituents. At higher temperatures in DMSO-d_6, interconversion rates increased, as evidenced from the gradual coalescence of all resonances (see Figure 6.3). However, it was not possible to observe the three signals expected in the regime of fast exchange at 500 MHz, as this would require heating the sample to an impractically-high level (*i.e.*, > 127.4 °C).

To verify this chemical rate process as restricted amide rotation, the free energy of activation, $\Delta G^{\neq}$, was estimated using Equation 5.1. T_c was estimated from Figure 6.3 to be about 127 °C at 500 MHz, based on the coalescence of the singlets at 2.42 and 2.71 ppm (later ascribed to the N-CH_3 resonances of the unsymmetrical *Z*,*E* conformer). This afforded $\Delta G^{\neq}_{127} \approx 19.3$ kcal/mol. The measured barrier is consistent with those typically reported for substituted *N*,*N*'-dimethylamides (*e.g.*, dimethylacetamide, $\Delta G^{\neq}_{25.2} = 17.4$ kcal/mol; dimethylpropanamide, $\Delta G^{\neq}_{25.2} = 16.7$

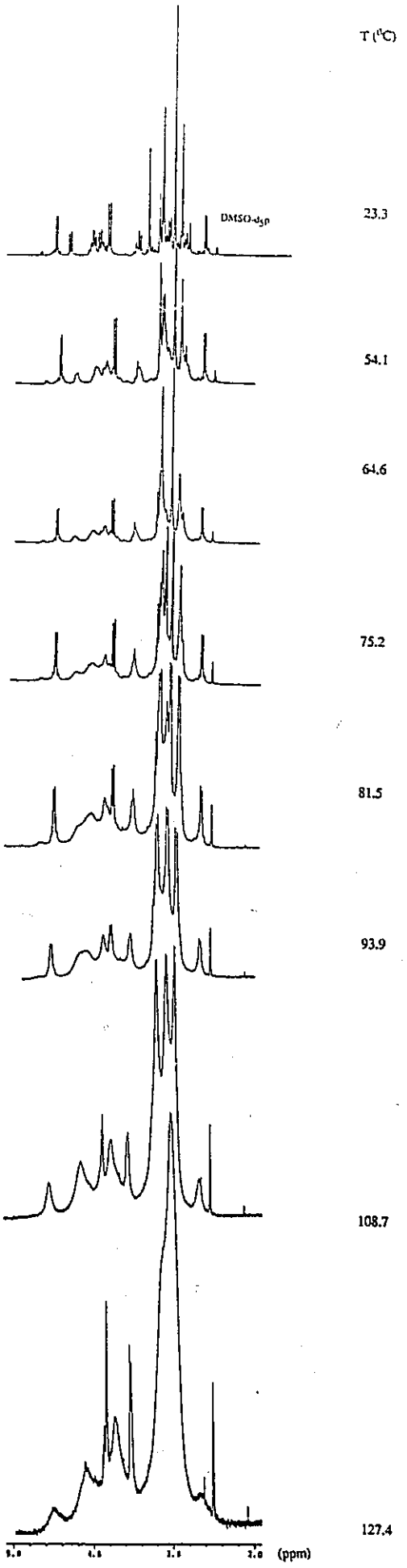

Figure 6.3: 500 MHz ^{1}H NMR variable temperature spectra of **40** in DMSO-d_6.

kcal/mol).[117] Restricted rotation associated with the S-S linkage and ring inversion presumably contributes to this composite $\Delta G^{\neq}$, thus magnifying it in relation to typical acyclic amide rotational barriers. Therefore, a fluxional process is responsible for the complexity of the room temperature NMR spectra of **40** and it is most likely a result of restricted rotation about the amide groups, which leads to the formation of discrete ring conformers. Other likely restricted rotation-based explanations would include conformational preferences at the disulfide linkage; however, this effect is not likely to be greater than 15 kcal/mol in cyclic systems (*e.g.*, see Section 6.3.2).[120,121]

A heteronuclear ^{1}H-^{13}C 2D NMR shift correlated experiment at room temperature identified the geminal pairs of diastereotopic protons for *three* geometric isomers and, with the aid of standard chemical shifts, permitted the location of their NCH_2CH_2N groupings. Two of these appeared as sets of A_2B_2 (or AA'BB') spin systems in the F_1 (^{1}H) domain, consistent with two symmetrical isomers, and the third as a more complex ABCD spin system for an unsymmetrical isomer (see Figure 6.4). Crossections in F_2 (^{13}C) revealed proton ^{2}J values of normal magnitudes (*ca.* -13 to -15 Hz, see Figure 6.5 and Table 7.5). The experiment also permitted the assignment of carbon signals associated with the three isomers. The ^{1}H-^{1}H connectivity patterns in each isomer were confirmed through a homonuclear 2D COSY-45 NMR experiment (see Figure 6.6).

The findings of the 2D and DNMR experiments, as well as patterns in signal multiplicity, suggested the presence of the three, interconvertible, conformational isomers of **40** at room temperature. These ring conformers have been attributed to two *Z,Z* and a *Z,E* amide configurations (see **43** and **44**, respectively). Among the *Z,Z* structures, the designation Z,Z_1 refers to the major ring conformer while Z,Z_2 indicates the minor one. These geometries have been shown to be consistent with the results of a

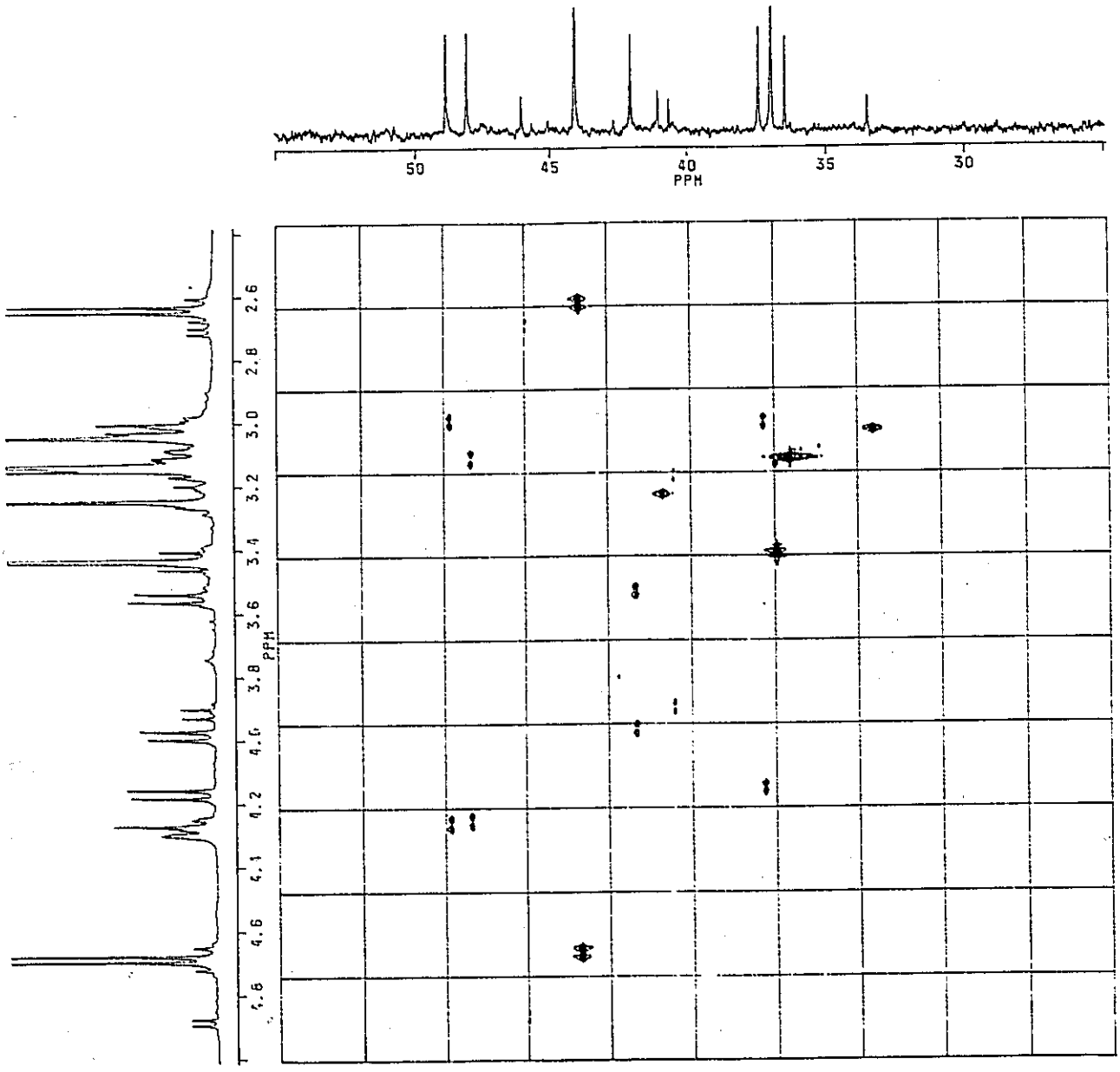

Figure 6.4: ^{1}H-^{13}C chemical shift correlated NMR spectrum of **40** in $CDCl_3$ at 303 K.

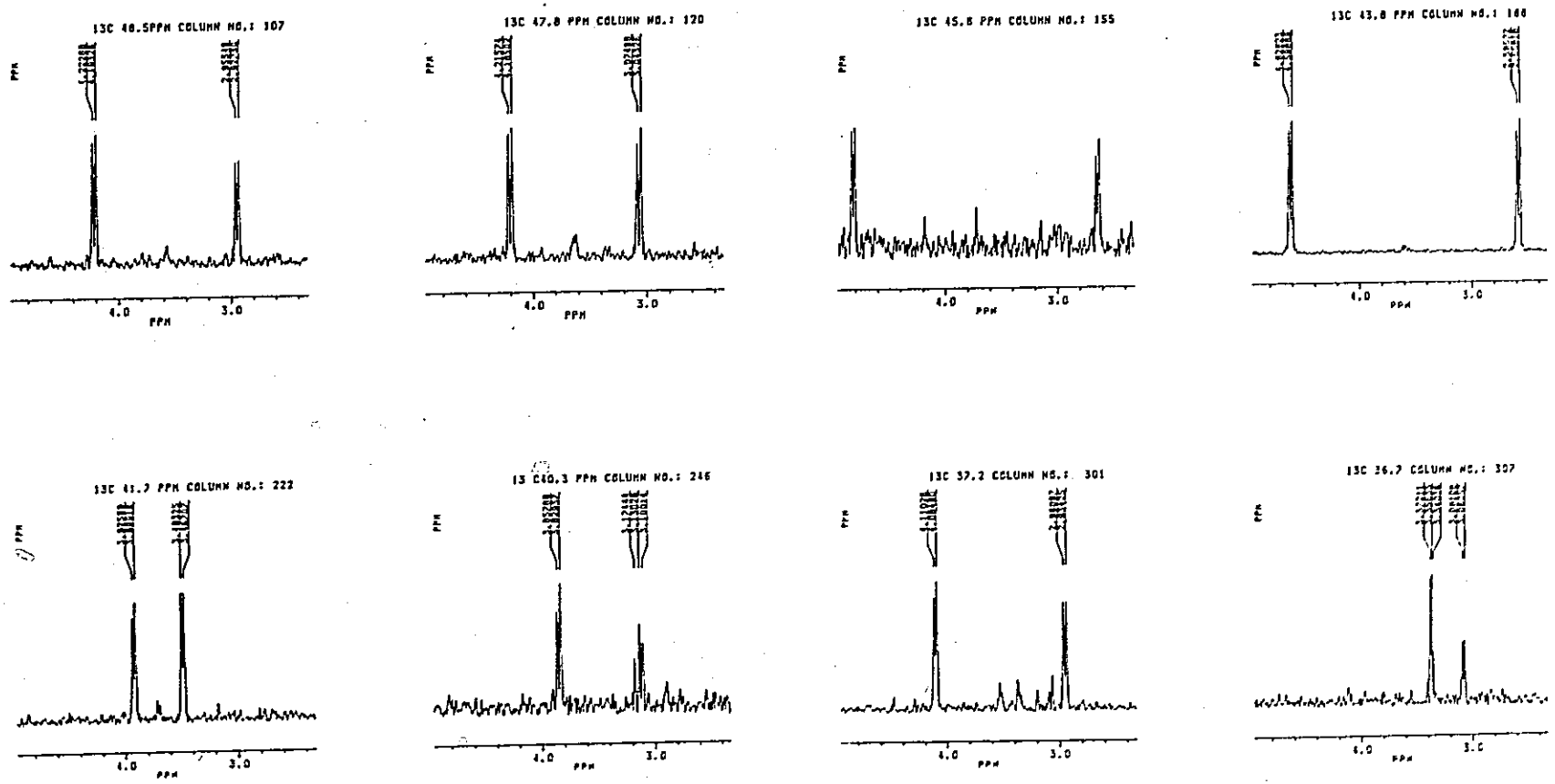

Figure 6.5: Crossections in F_2 from the ^{1}H-^{13}C chemical shift correlated NMR spectrum of **40** in $CDCl_3$ at 303 K.

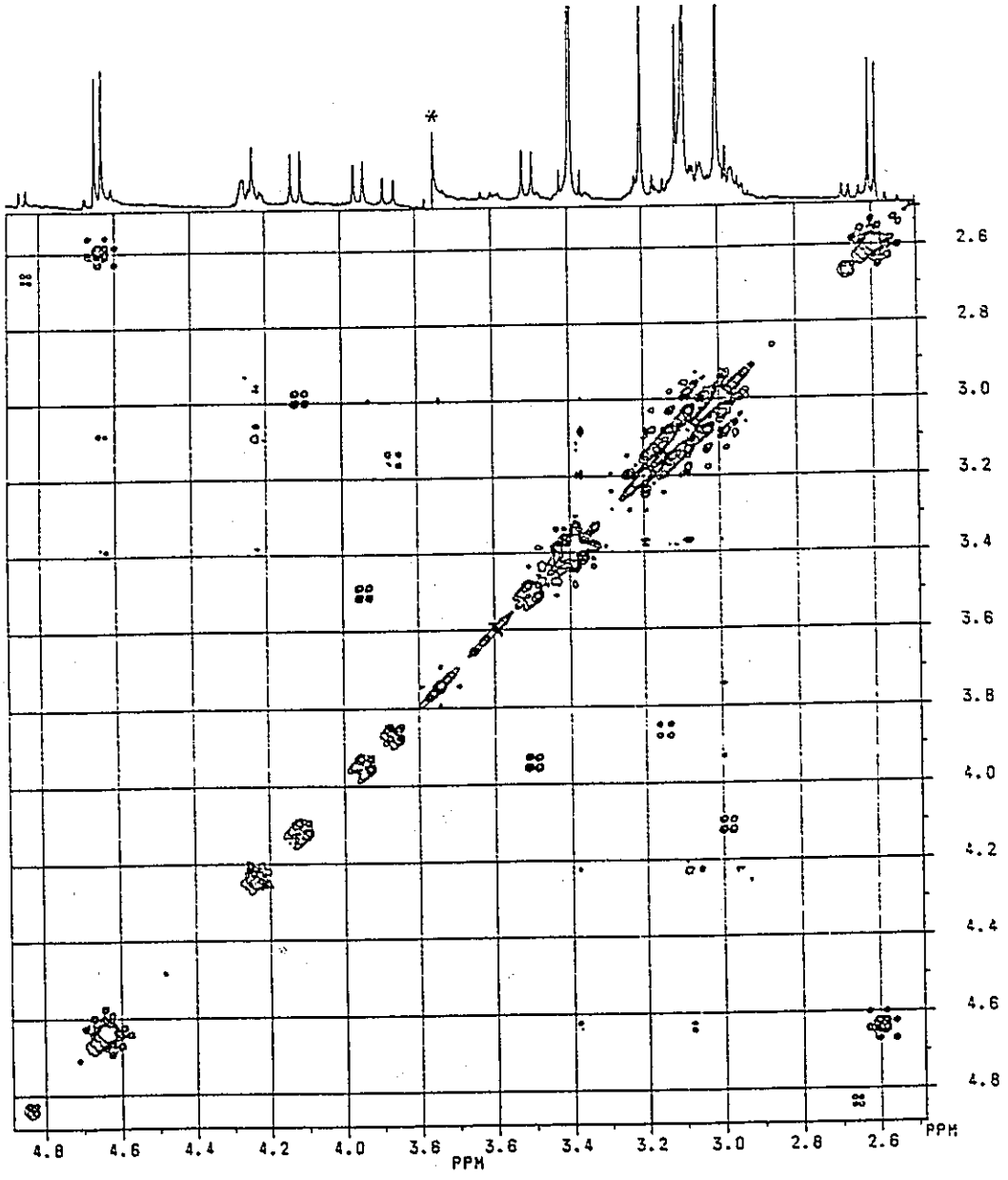

* Folded signal.

Figure 6.6: The 500 MHz ^{1}H-^{1}H NMR COSY-45 spectrum of **40** in $CDCl_3$ at 303 K.

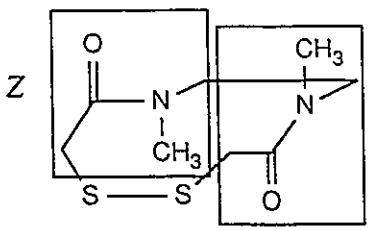

Z

43

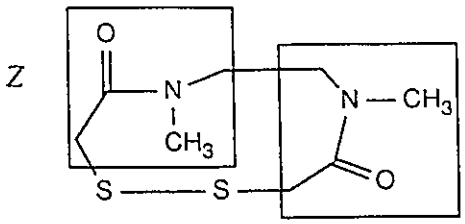

E

44

number of experimental approaches, including benzene dilution ^{1}H NMR shifts, nuclear Overhauser effect (NOE) experiments, single crystal X-ray diffraction studies, molecular modelling and proton shielding calculations (*vide infra*).

Proton integrals and ^{13}C resonance intensities (Tables 7.5 and 7.6) suggested the following stability trend among the conformers: $Z,Z_1 > Z,E > Z,Z_2$. This finding can be rationalized through the sterically-driven, conformational preferences governing *N,N'*-dialkylamides: in large-membered lactams, the *Z* or *trans* stereochemistry is energetically favored over *E* (*cis*).[122] Consequently, the *Z* configuration in **40** can be expected to be the predominant amide stereochemistry in solution. Based on the ratio of intensities of the N-CH_3 ^{13}C signals (Table 7.6) and, assuming a Boltzmann population distribution at 303 K, the Z,Z_1 ring conformer was favored over the *Z,E* by 0.61 kcal/mol and *Z,E* over the Z,Z_2 by 0.87 kcal/mol. Table 6.1 presents the corresponding percentage compositions in $CDCl_3$, as well as in DMSO-d_6 and C_6D_6 solvents. The results suggested that the isomeric composition of **40** appeared to be relatively independent of solvent.

The most noteworthy NMR feature of **40** is the large geminal shift differences ($\Delta\delta_{OBS}$) between the N-CH_2 protons of the *Z,Z* and, to a lesser extent, *Z,E* conformers. In $CDCl_3$, the largest $\Delta\delta_{OBS}$ was measured at 2.17 ppm for the minor Z,Z_2

Table 6.1: Calculated and observed population distributions for conformers Z,Z_1, Z,E and Z,Z_2 at 303 K.

Conformer	Calc. E_{Steric} (kcal/mol)	calculated Population Distribution[a]	Observed Population Distributions[a,b] $CDCl_3$	DMSO-d_6[c]	C_6D_6
Z,Z_1 (**40a**)	0	82%	53%	54%	54%
Z,E (**40c**)	2.03	3%	39%	29%	38%
Z,Z_2 (**40c**)	1.15	15%	8%	6%	8%

[a] According to the Boltzmann relationship:

$$n_2/n_1 = \exp(-\Delta G/RT) \qquad , T=303 \text{ K}$$

[b] Based on ^{1}H NMR integrals.

[c] Small amounts (< 12%) of additional conformers were detected and measured using ^{13}C NMR intensities.

isomer, while the Z,Z_1 and Z,E configurations recorded 2.05, 1.15 and 1.29 ppm, respectively (Table 7.5). The chemical shift differences were invariant with the concentration of **40** in $CDCl_3$, precluding any effects due to intermolecular association. These results suggested that the N-CH_2 (and S-CH_2) groups in the symmetrical Z,Z isomers are pairwise equivalent or enantiotopic and that the N-CH_2 protons have markedly different magnetic environments. Large geminal proton chemical shift differences have been observed in a few rigid, polyamide systems.[123-125] In cyclotetrasarcosyl, **45**, the isochronous pairs of the *N*-methylene protons are separated by about 2 ppm (in $CDCl_3$),[124] while one set of those for the tetrathiacyclododecane **46** have a chemical shift difference of 1.78 ppm (in $CDBr_3$).[125]

Invariably, such large (*i.e.*, > 1.5 ppm) *N*-carbonyl splittings appear to be associated with the sterically-favored Z amide stereochemistry, which places these protons in or close to the respective amide planes pointing toward the C=O groups.[126]

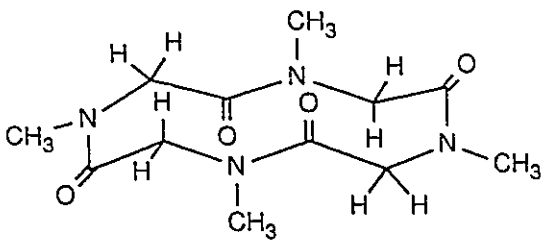

45

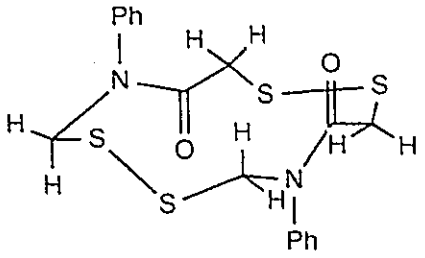

46

6.2.3 NOE Studies

To assist in the solution state conformational determination of **40**, NOE experiments were carried out in $CDCl_3$ at 303 K (500 MHz) on signals of the two major isomers. Representive difference NOE spectra for these isomers are shown in Figures 6.7 and 6.8. The inserts illustrate NOE interactions for a given geometric isomer, together with their interatomic distances as determined from MM2-calculated structures.

Unfortunately, adequate NOE determinations were not possible for the minor Z,Z_2 isomer, largely because of its low abundance and complications involving transfer of saturation. The latter phenomenon results from radiation transfer from the saturated resonance into other signals that are undergoing mutual chemical exchange,[127] namely the more populated Z,Z_1 and Z,E isomers. Saturation transfer effects were also observed for the Z,E and, to a lesser extent, the Z,Z_1 conformers; however, useful conformational information can still be obtained from these spectra if some caution is applied in spectral interpretation.

In the major isomer, irradiation of the AB S-CH_2 quartet at 3.43 ppm resulted in a large NOE of the *N*-methyl protons at 3.13 ppm [see Figure 6.7(a)], indicative of a pseudoaxial S-C*H* and N-CH_3 proximity about a *Z* amide configuration.

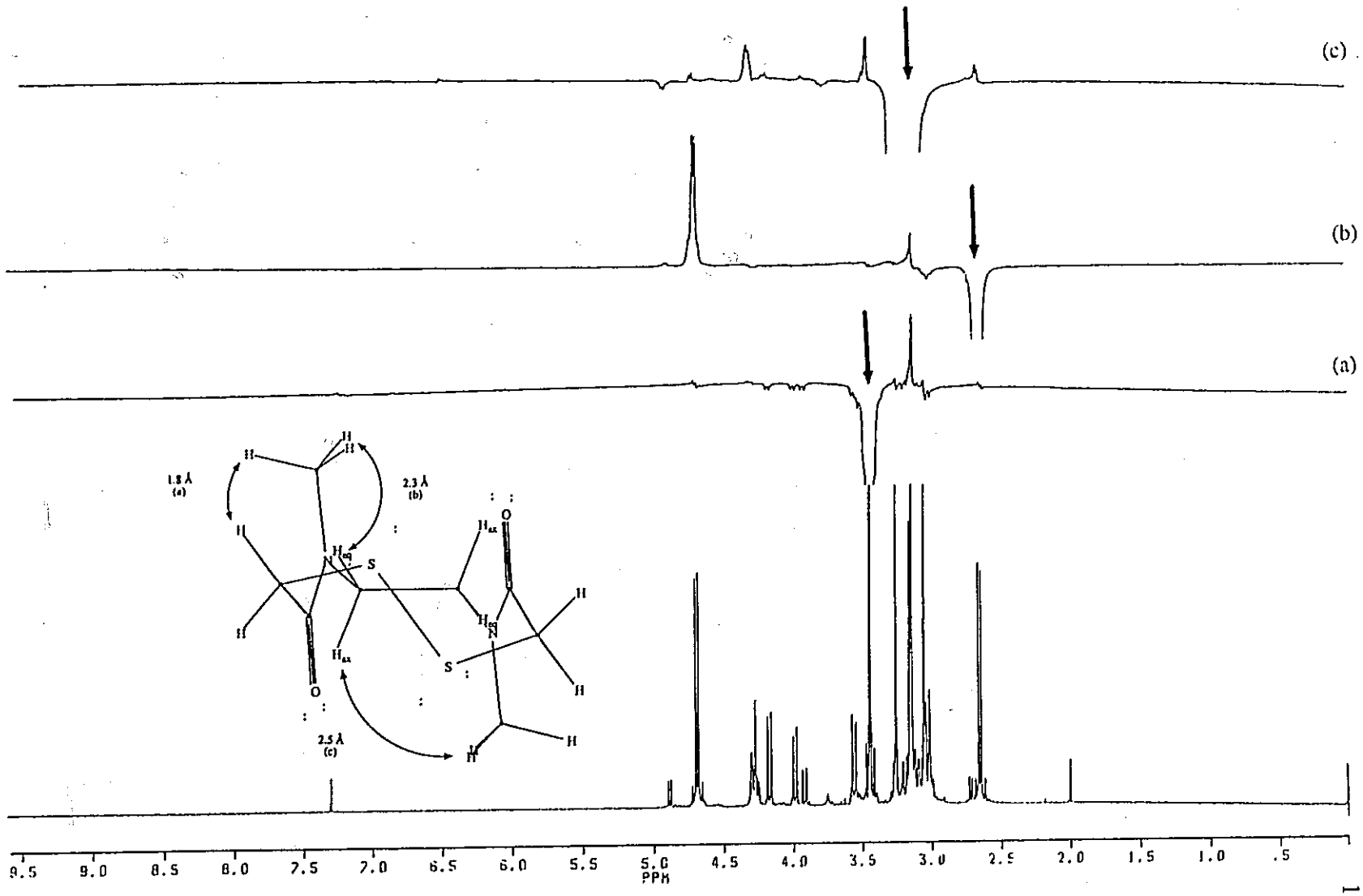

Figure 6.7: 500 MHz NOE difference spectra (a-c) of the Z,Z_1 stereoisomer of **40** in $CDCl_3$ at 303 K. The irradiated peak is indicated at the arrowed (⬇) frequency.

This enhancement was not expected for an *E* stereochemistry, as a larger distance would separate the appropriate protons. The observation of a NOE between the shielded N-CH_2 (2.64 ppm) and N-CH_3 [see Figure 6.7(b)] was consistent with a Z linkage, where the former protons occupy a *pseudoequatorial* position *syn* to the adjacent CH_3 group. Irradiation of the N-CH_3 resonance caused NOEs at, not only the expected positions of the shielded N-CH_2 and S-CH_2 protons, but also at the deshielded N-C*H* at 4.68 ppm [see Figure 6.7(c)]. The weaker enhancement of the deshielded N-C*H* (relative to the shielded protons) suggested a transannular proximity with its *opposite* N-CH_3 group - an interaction made possible through *psuedoaxial* configurations for both groups. Thus, a C_2 symmetric *Z,Z* conformation best matched the NOE observations noted for the major solution conformation of **40** (see **40a**, Figure 6.14).

In the non-symmetric isomer, irradiation of the S-C*H* signal at 3.55 ppm induced a strong enhancement of its geminal partner at 3.99 ppm as well as a weaker enhancement of the N-CH_2 protons at 4.27 ppm [see Figure 6.8(a)]. Based on the analysis of molecular models, the latter NOE was only possible between the pseudoaxial S-C*H* [H(3b)] and the pro-*R* N-C*H* [H(6b)] about the *E* amide group. The X-ray structure and molecular mechanics calculations (see Figures 6.11 and 6.14, **40c**) supported this result: with an interatomic separation of 1.97 Å, the electron clouds of these protons were overlapping by about 0.4 Å. The positive N-CH_3 enhancement at 3.24 ppm was most likely a result of saturation transfer to S-C*H* [H(10a)] at 4.16 ppm by which it is strongly relaxed [see Figure 6.8(c)]. Barring geminal enhancements, NOEs were not observed for the second *E* S-C*H* [H(3a)] signal at 3.99 ppm: this was consistent with a pseudoequatorial position [see Figure 6.8(b)].

Irradiation of the S-C*H* [H(10a)] resonance at 4.16 ppm [see Figure 6.8(c)]

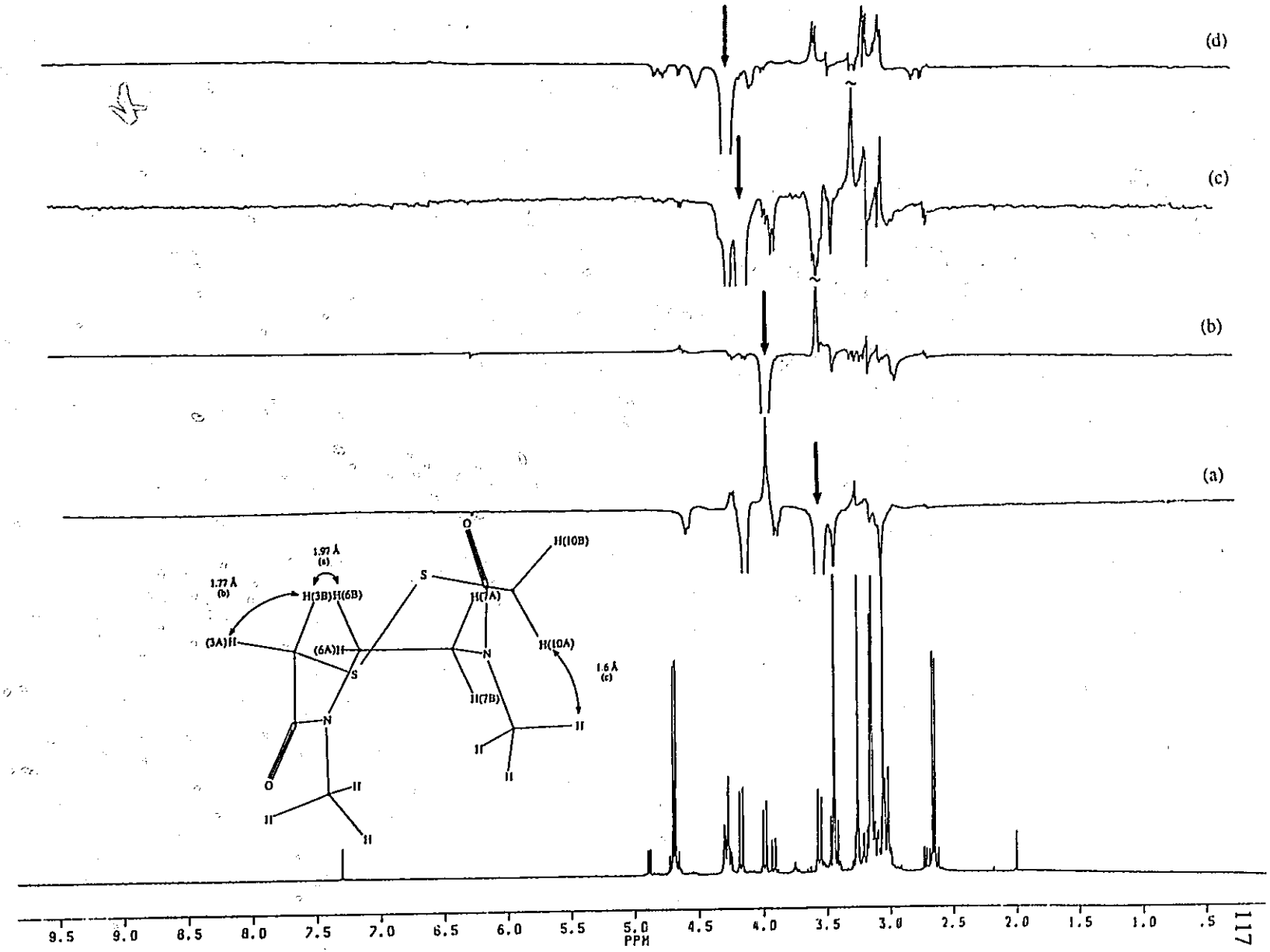

Figure 6.8: 500 MHz NOE difference spectra (a-d) of the *Z,E* stereoisomer of **40** in $CDCl_3$ at 303 K. The irradiated peak is indicated at the arrowed (↓) frequency.

induced strong enhancement of the downfield N-CH_3 protons at 3.24 ppm which was indicative of a dipseudoaxial disposition of protons about a *Z* amide bridge. Analysis of the *Z,E* computed model revealed that the point of closest approach of these protons was *ca.* 1.6 Å. Since this NOE was not consistent with an *E* amide stereochemistry, the enhancement supported the prediction[128] that the *downfield* N-CH_3 (and N-CH_3 by ^1H-^{13}C shift correlation, see Figure 6.4) belonged to the *Z* amide group in the *Z,E* conformer.

Irradiating the co-resonating, downfield N-CH_2 protons [H(6b) and H(7a)] at 4.27 ppm created moderate NOEs at 3.55, 3.10 and 3.01 ppm [see Figure 6.8(d)]. The 3.55 ppm enhancement arises from interaction of H(6b) with H(3b) [as in Figure 6.8(a)]. The latter two enhancements were most likely due to geminal interactions with the shielded *Z* and *E* N-CH_2 protons [H(7b) and H(6a), respectively]. Thus, a *Z,E* conformation best correlated with the NOE data obtained for the non-symmetric component of **40** (see **40c**, Figure 6.14).

6.2.4 Aromatic Solvent-Induced Shift (ASIS) Studies

The inability of NOE experiments to elucidate structural details for the minor Z,Z_2 component prompted an ASIS investigation to determine its solution state geometry. Studies on a variety of amides[129-132] have consistently shown that aromatic solvents shift the resonance peaks of the N-C_α protons *trans* to the carbonyl group *upfield* to a greater extent than those at the *cis* position. On this basis, these resonances can be assigned to a particular amide stereochemistry.

The accepted model[131] which rationalizes the ASIS effect in *N*-alkylamides is illustrated in Figure 6.9. The amide molecules associate in an electrostatic manner with the aromatic solvent molecules so as to place the nitrogen atom, with its fractional

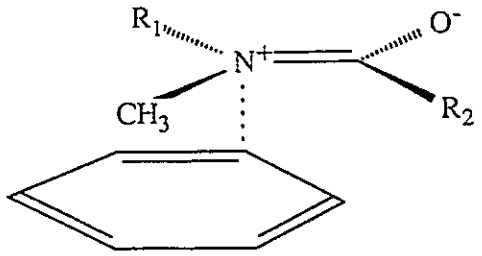

Figure 6.9: The aromatic solvent cluster model for interpreting the ASIS effect in 40.

positive charge, close to the region of high π-electron density in the aromatic ring and the negatively-charged carbonyl oxygen positioned far from the electron rich π-orbitals. In this coplanar arrangement of amide and benzene molecules, the *Z* methyl group would experience the large diamagnetic anisotropy at the center of the ring and would shift to higher field to a greater extent than the *E* methyl group. A study of the ^{1}H NMR spectrum of **40** (see Figure 6.10) in benzene-d_6 revealed that the N-CH_3 (and N-CH_2) resonances of both major (Z,Z_1) and minor (Z,Z_2) isomers exhibited very similar upfield aromatic solvent-induced shifts (0.56 and 0.61 ppm, respectively, relative to the $CDCl_3$ shifts). Since the major isomer was confirmed to have the *Z,Z* geometry, the benzene dilution experiments suggested that the minor isomer also possesses the *Z,Z* configuration. Their relatively large ASIS values were also consistent with a *Z* geometry.[133] Alternatively, an *E,E* stereochemistry in the minor isomer would have resulted in a smaller ASIS value and an increased separation between the N-CH_3 resonances of the major and minor isomers upon benzene-d_6 dilution. It is worth noting that the N-CH_2 splitting for the Z,Z_1 and Z,Z_2 ring conformers has increased to 2.58 and 2.69 ppm, respectively, in benzene-d_6.

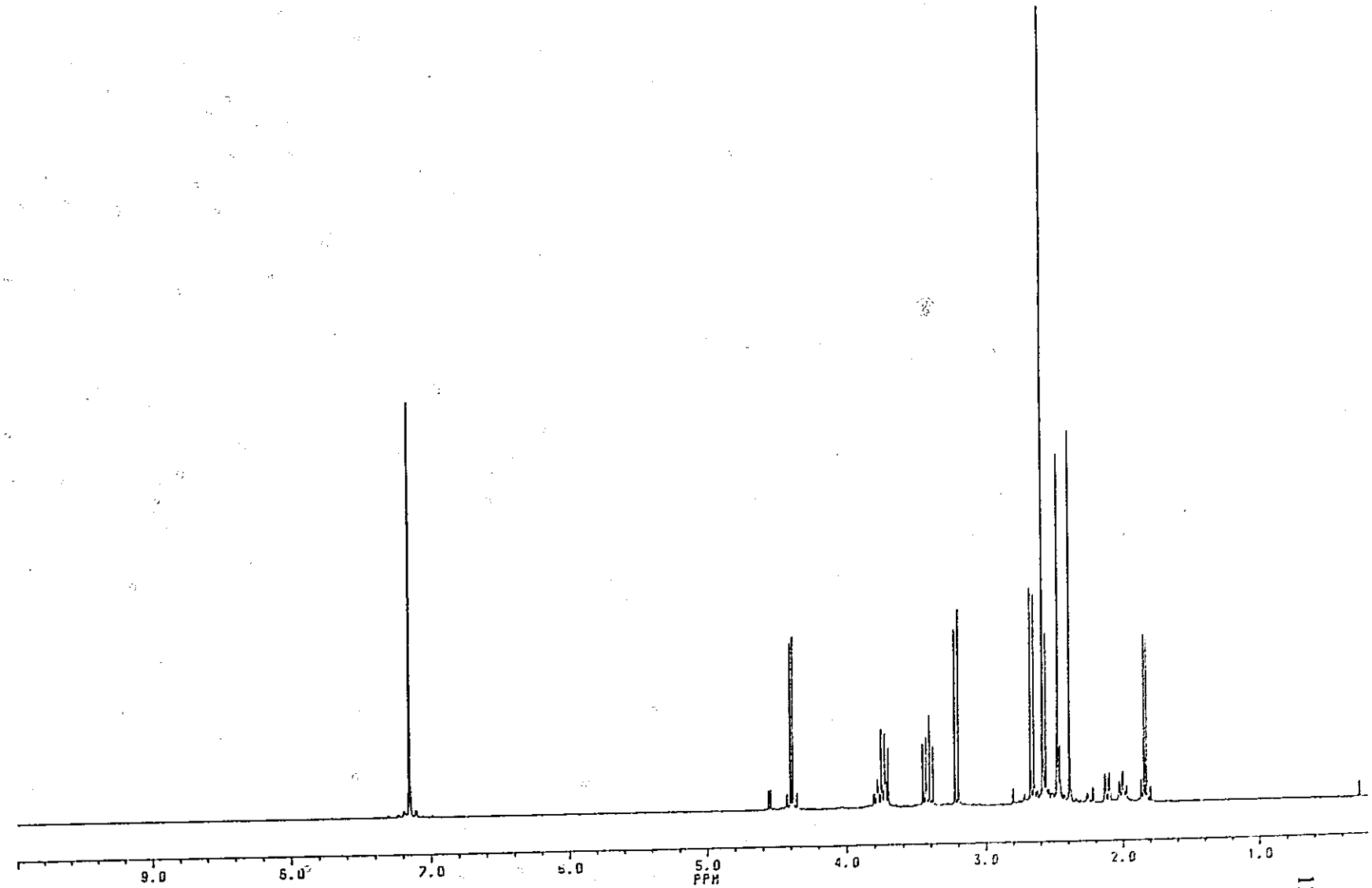

Figure 6.10: The 500 MHz ^{1}H NMR spectrum of **40** in C_6D_6 at 303 K.

6.2.5 Solid State Structure Studies

An X-ray diffraction study of **40** was undertaken in order to establish unambiguously the geometry which could give rise to the enormous NMR shift differences observed for the geminal methylene protons.

The geometry and numbering of the X-ray structure of **40** is shown in Figure 6.11; crystal data, atomic coordinates, bond lengths and bond angles are listed in Tables A.1 to A.6 in the Appendix. As the structure analysis revealed, the diamide **40** crystallized into the *Z,E* geometry. This was a surprizing result since NMR measurements had shown the Z,Z_1 isomer to be the dominant geometry in solution (Table 6.1). A survey of the bond angles and bond lengths in **40** indicated no unusual deviations from normal values. The disulfide and amide torsional angles (Table A.5) are very close to ground state values (*i.e.*, 90° and planarity, respectively) indicating low torsional strain in the *Z,E* ring.

A stereodiagram of the unit cell of the *Z,E* structure of **40** is shown in Figure 6.12. The unit cell contains two *Z,E* molecules which are related by a center of inversion. Molecules stack in columns with a high degree of packing efficiency given the unsymmetrical nature of the *Z,E* isomer. The most significant intermolecular contact is O(4)···C(8) which is 3.23 Å. Intramolecular non-bonding contacts were observed between O(9) and H(7a), and H(3b) and H(6b). These nuclei - separated by 2.346 Å and 2.007 Å, respectively - are within the sum of the accepted van der Waals radii for oxygen and hydrogen (1.4-1.6 and 1.2 Å, respectively).[134,135] These contacts may contribute, in part, to the rather large NMR shift differences observed for the geminal hydrogen nuclei of the *Z,E* conformation (see Table 7.5).

An understanding of the proton geometry about the *Z* and *E* amide groups - as provided by the crystal structure - allowed for an interpretation of the large $\Delta\delta_{OBS}$

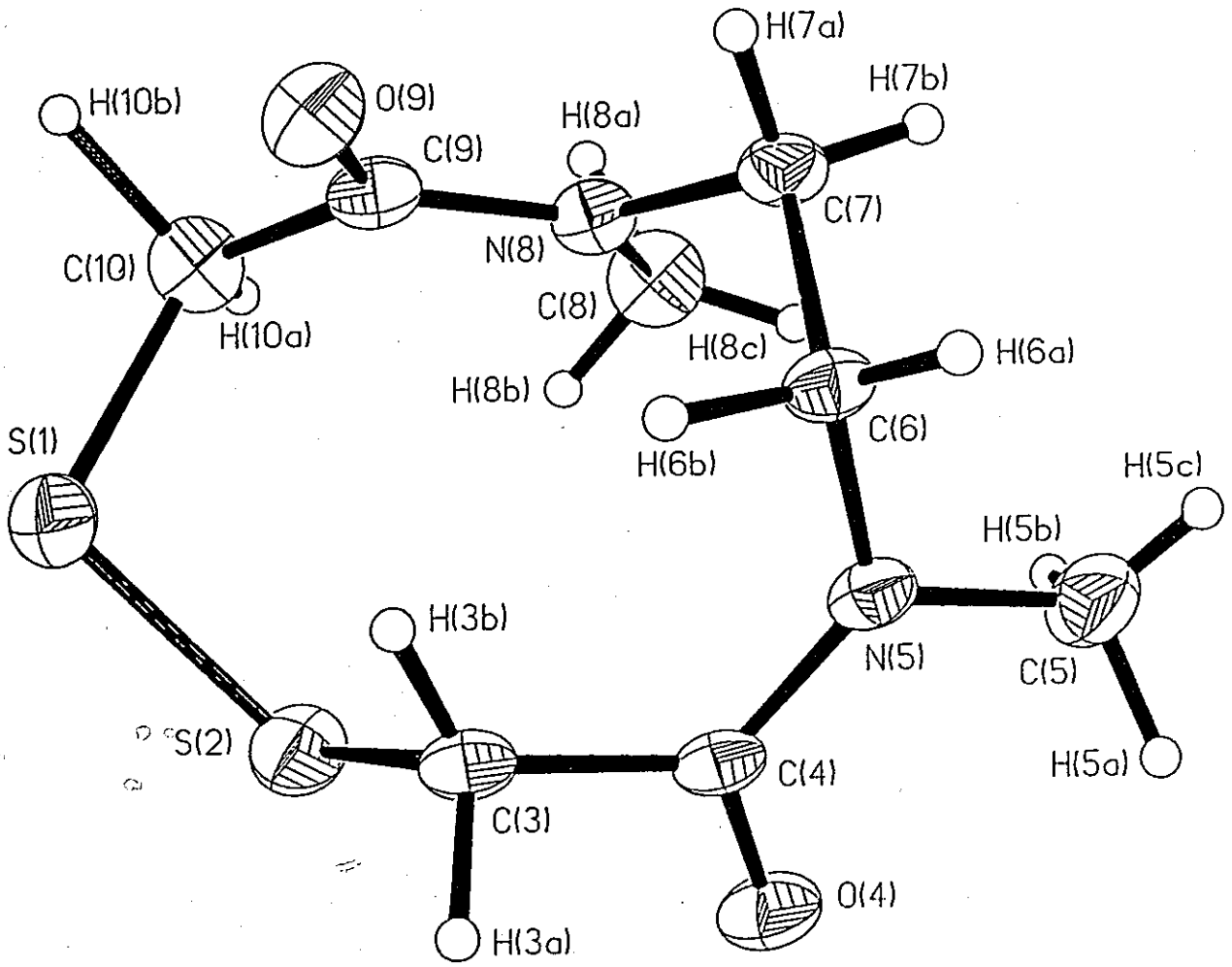

Figure 6.11: The crystal structure of the *Z,E* isomer of **40**. 30% probability thermal ellipsoids are shown for non-hydrogen atoms.

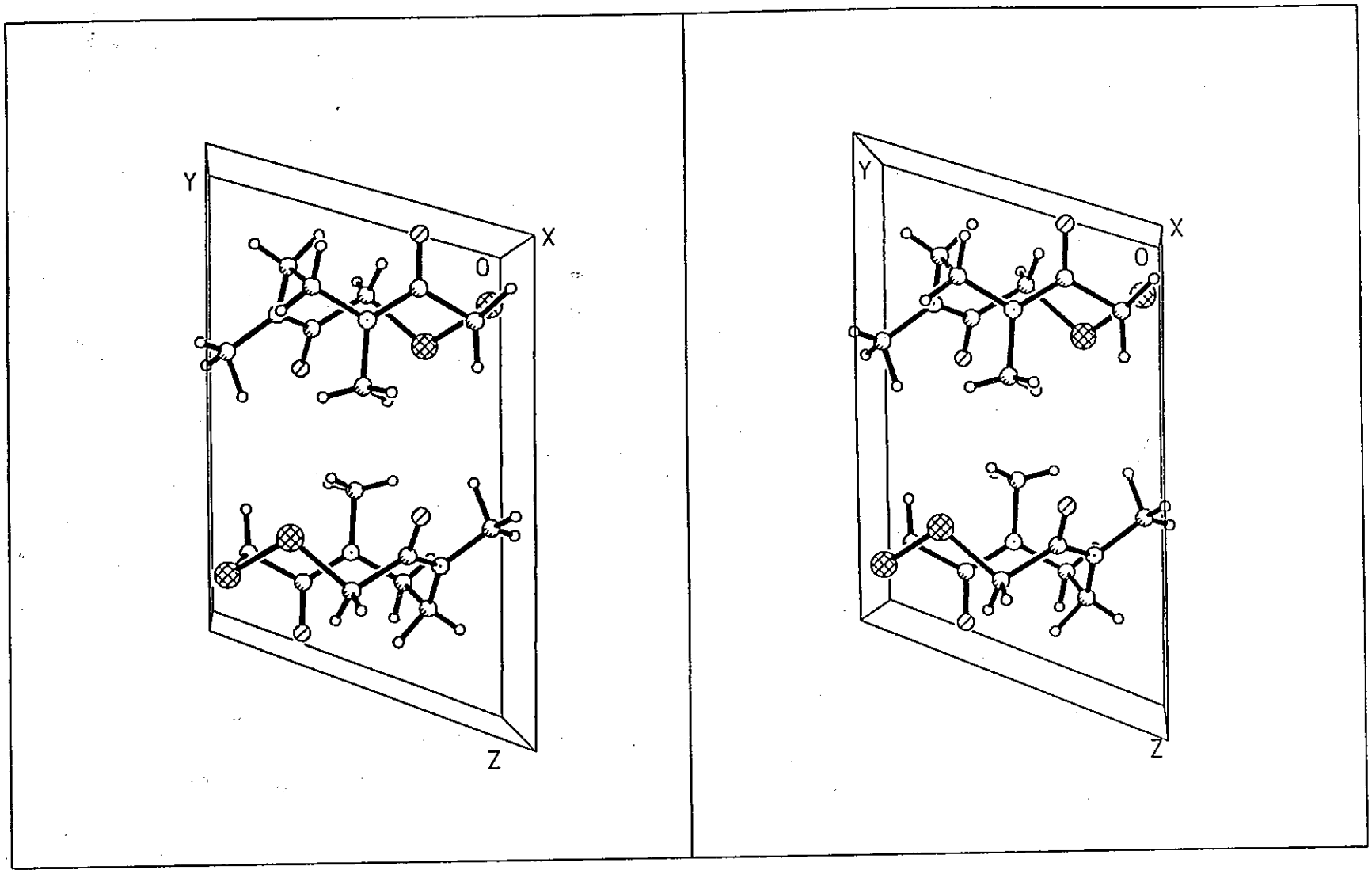

Figure 6.12: Stereodiagram of the unit cell of the *Z,E* structure of **40**.

noted for the geminal N-CH_2 protons (see Table 7.5). In addition, the excellent agreement between the NOE-derived conformational model of the *Z,E* isomer and the crystal structure established a link to proton shift assignments. For example, the magnitude of $\Delta\delta_{OBS}$ could be qualitatively explained by the positions of the geminal protons relative to their adjacent carbonyl group: in general, a proton will be more deshielded as it approaches the plane and/or midpoint of a carbonyl group.[126] In the *Z* amide system, H(7a) and H(7b) (see Figure 6.11) are 10.4° and 13.9° out of the amide plane defined by atoms O(9)-C(9)-N(8) and are located 2.359 and 3.359 Å respectively from the midpoint of the C=O bond. Therefore, H(7a) should resonate *downfield* from H(7b). Similarly, H(6b) and H(6a) of the *E* amide are 170.6° and 151.6° removed from the O(4)-C(4)-N(5) plane and are situated at a distance of 3.272 and 3.654 Å respectively from the midpoint of the carbonyl bond. Since H(6b) is "closer" to its adjacent amide group, it should appear at a lower shift than its geminal partner. It is interesting to note that the very similar deshielding influences on H(7a) and H(6b) appears to result from two different orientations of the protons - namely, *syn* and *anti* configurations, respectively - with respect to their adjacent C=O group. The above analysis of shielding trends was valuable in the assignment of proton chemical shifts in the *Z,Z* isomers (see Table 7.5).

If X-ray crystallographic data are used to assist in the structural elucidation of a molecule in solution, it is useful to present some evidence to support similarity between the molecular geometry in solution and in the solid state. This criterion was satisfactorily met through NOE determinations of the *Z,E* isomer. Support for a comparison of the solution and solid state geometries was primarily based on the characteristic NOE interactions between the H(6b)···H(3b) and the H(10b)···*Z* N-CH_3 protons, which were also noted in the crystal structure. Another method

involves a comparison of ^{13}C NMR spectra of the molecule in both states. To this end, the cross-polarization, magic angle spinning (CP-MAS) ^{13}C NMR spectrum of crystalline **40** was determined in the solid state at 25 MHz (see Figure 6.13). Unfortunately, excessive broadening of the ^{13}C resonances caused by dipolar coupling to ^{14}N nuclei, as well as signal overlap and sensitivity complications, prevented an unequivocal correlation of characteristic shifts between the solid state and solution state spectra in the 30-50 ppm range. Spectra recorded at a higher field and/or higher sample concentration would probably resolve this inadequacy.

An interesting outcome of the solid state experiment, however, was noted in the carbonyl region: two broad signals of unequal intensity (167.30 and 174.39 ppm) suggested the presence of at least two conformers in the crystal lattice. If the recrystallized sample of **40** consisted only of the *Z,E* geometric isomer, then only two, *equally-intense* resonances would be observed in this region. Based on chemical shift and intensity comparisons with the solution state ^{13}C spectrum (see Figure 6.2), the more intense signal at 167.30 ppm was ascribed to the Z,Z_1 structure, while the unresolved resonance at 174.39 ppm was indicative of the expected *Z,E* conformer. The observation of two solid state species could be explained by the co-crystallization of *Z,Z* and *Z,E* structures. The rather high barriers to amide isomerization could promote the crystallization of the *Z,Z* and *Z,E* amide ring conformers into separate lattice structures. For example, many acyclic monoamides have been reported to crystallize in either the *Z* or *E* geometry, with only one geometric rotamer in each unit cell.[136]

6.3 Computational Studies

The foregoing X-ray structure determination of the *Z,E* isomer provided a powerful link between ^{1}H NMR chemical shift and geometry. This information was

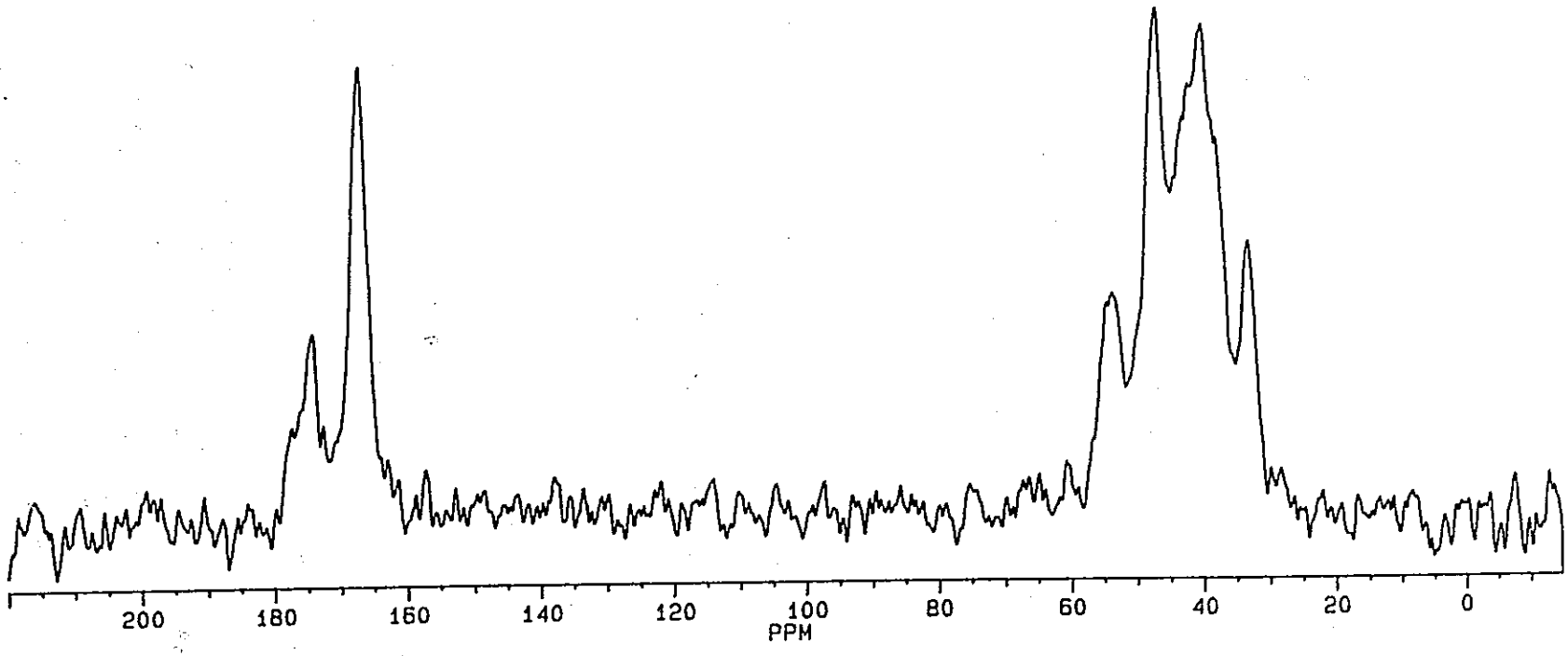

Figure 6.13: The 25 MHz CP-MAS ^{13}C spectrum of **40** at 303 K.

crucial not only for NMR shift assignments, but also for identifying different shielding mechanisms which have manifested themselves as unusually large $\Delta\delta_{OBS}$ values. Similarily, structural models of the *Z,Z* isomers were required to assist in NMR signal assignments and to provide an insight into the origins of their large N-CH_2 anisochronism. Consequently, a number of computational methods were investigated.

6.3.1 MMX Calculations

Molecular mechanics calculations were performed using PCMODEL to evaluate the conformational geometries and energies of the Z,Z_1 and Z,Z_2 structures. From over 90 unique starting geometries, a total of five conformers were found for **40** within 5 kcal/mol of the global minimum structure (see Table 6.2, Figure 6.14). Conformers **40a** (*Z,Z*), **40b** (*Z,Z*) and **40c** (*Z,E*) agreed well with the structural models inferred from NOE, thermodynamic, X-ray and NMR symmetry data. Based on this correlation, the observed conformers in the NMR spectra of **40** - Z,Z_1, Z,Z_2 and *Z,E* - were proposed to have similar structural characteristics as **40a**, **40b** and **40c**, respectively.

The X-ray determination of **40** confirmed one isomer to have the *Z,E* configuration (see Figure 6.11) which was presumed to be the source of the unsymmetrical set of NMR resonances. Among the set of *Z,E* isomers, **40c** provided the best correlation between calculated and experimental Boltzmann distributions (Table 6.1). Moreover, when **40c** was overlapped with the X-ray structure in PCMODEL, it was evident that they were similar (RMS deviation of atoms = 0.037 Å). To achieve a more realistic comparison, conformational changes that might be imposed on **40** by crystal lattice forces were removed from the X-ray structure by subjecting the molecule to the PCMODEL force field energy minimization program. The observed

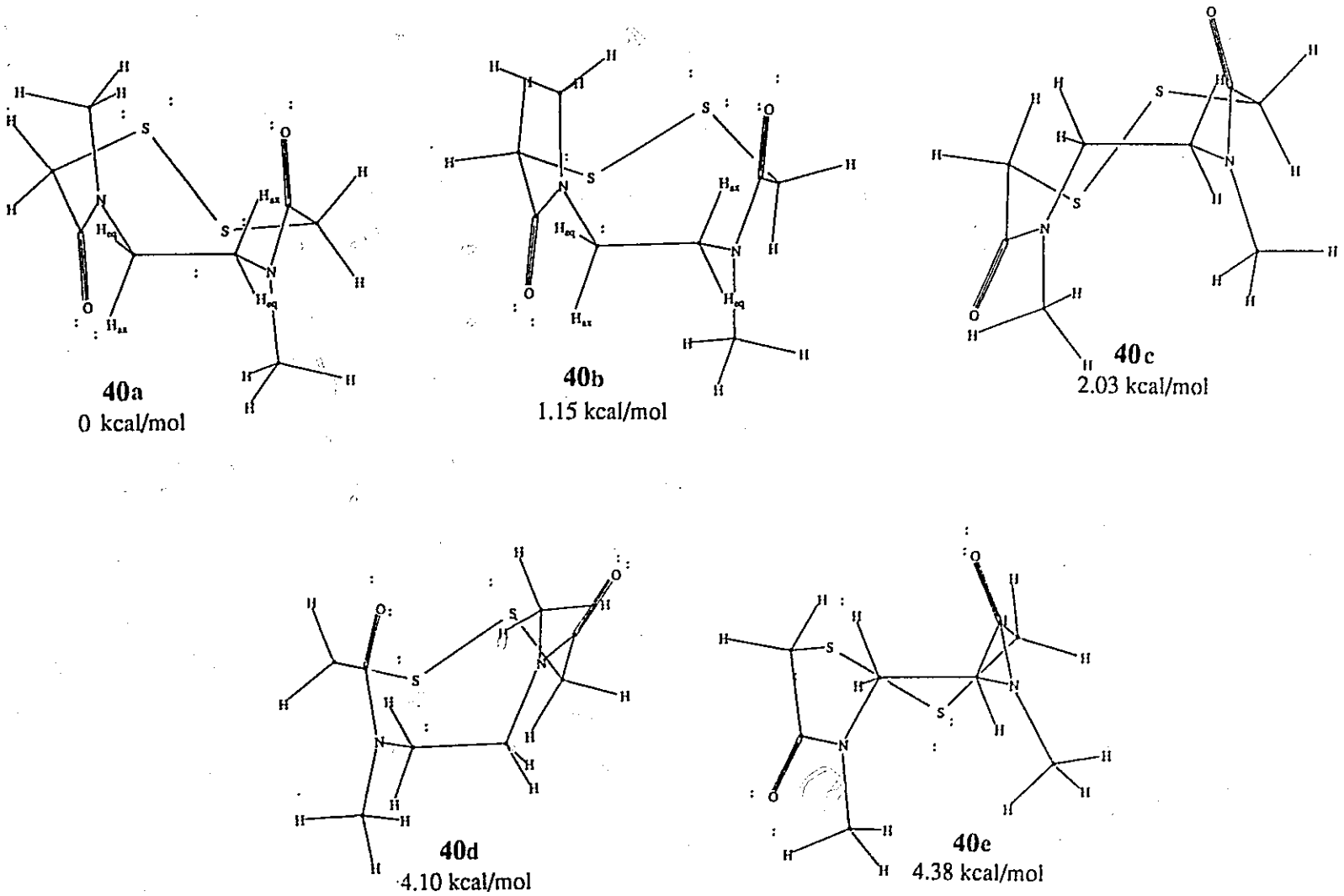

Figure 6.14: Stick plots of the five lowest, MMX energy conformers of **40** (**40a** - **40e**). The ethylene moiety is located at the front of each conformation and is aligned along the x-axis for all plots.

Table 6.2. Characterization data for the five lowest energy MMX conformers (40a - 40e) of 40.

Conformer	E_{Steric}[a] (kcal/mol)	Symmetry Group	Disulfide Chirality[b]	C-S-S-C Torsional Angle (Deg)	CH_3-N-C=O Torsional Angle (Deg)		$C-C_{sp2}$-N Bond Angle (Deg)		S-S Bond Length (Å)
					E	*Z*	*E*	*Z*	
40a (Z,Z)	0	C_2	R	-104.2	-	177.2	-	119.3	2.073
					-	177.2	-	119.3	
40b (Z,Z)	1.15	C_2	L	94.6	-	171.8	-	119.7	2.073
					-	172.4	-	119.6	
40c (Z,*E*)	2.03	-	L	86.9	1.8	173.1	121.5	120.0	2.070
40d (Z,*E*)	4.10	-	L	87.3	11.1	178.0	120.4	119.4	2.072
40e (Z,*E*)	4.38	-	R	-82.2	0.9	173.0	121.0	119.4	2.070
X-ray (Z,*E*)	-	-	L	85.9	2.9	175.1	120.5	119.2	2.035

[a] Relative steric energy.

[b] R=right-handed chirality; L=left-handed chirality.

change amounted to approximately 0.6 kcal/mol energy loss upon minimization. The resultant "minimized X-ray" structure was then superimposed on **40c** and **40d** to afford a virtually complete overlay with the former calculated structure (RMS deviation of atoms = 0.021 Å) but gave a poorer alignment with the latter (RMS deviation of atoms = 0.198 Å). Molecular mechanics had thus accurately predicted the solid state geometry of the *Z,E* conformer. This fact, coupled with the strong similarities between NOE and computed structural models, suggested that the MM2 force field was a reasonable probe for elucidating the solution state conformations of **40**. Conformer **40e** is the right-handed disulfide isomer of both **40c** (and the X-ray structure) and thus inadmissible.

Conformers **40a** and **40b** possess C_2 symmetry and a Z,Z configuration with both amide functions essentially coplanar and oriented in opposite directions. This *antiparallel* Z,Z arrangement has been reported for other *N*-substituted polyamide heterocycles, including cyclic amides **45** and **46**.[124,125] Steric and electronic factors may account for the configurational preference found in these systems. For example, in a parallel conformation, transannular methyl-methyl contacts and a large internal dipole moment (resulting from the sum of the moments from the parallel C=O groups) will undoubtedly be very destabilizing.

Molecular modelling data and mechanical models suggested isomers Z,Z_1 and Z,Z_2 are disulfide ring conformers. At room temperature, interconversion of these rotational isomers was sufficiently slow on the NMR time scale to allow detection by ^{13}C NMR spectroscopy (Table 7.6). Interconversion occurs presumably through the *cis* transition state by *ca.* 180° rotation about the asymmetric S-S bond (see Figure 6.15). A ^{13}C DNMR study was carried out with the objective of validating the molecular modelling results through the correlation of a measured barrier to interconversion to

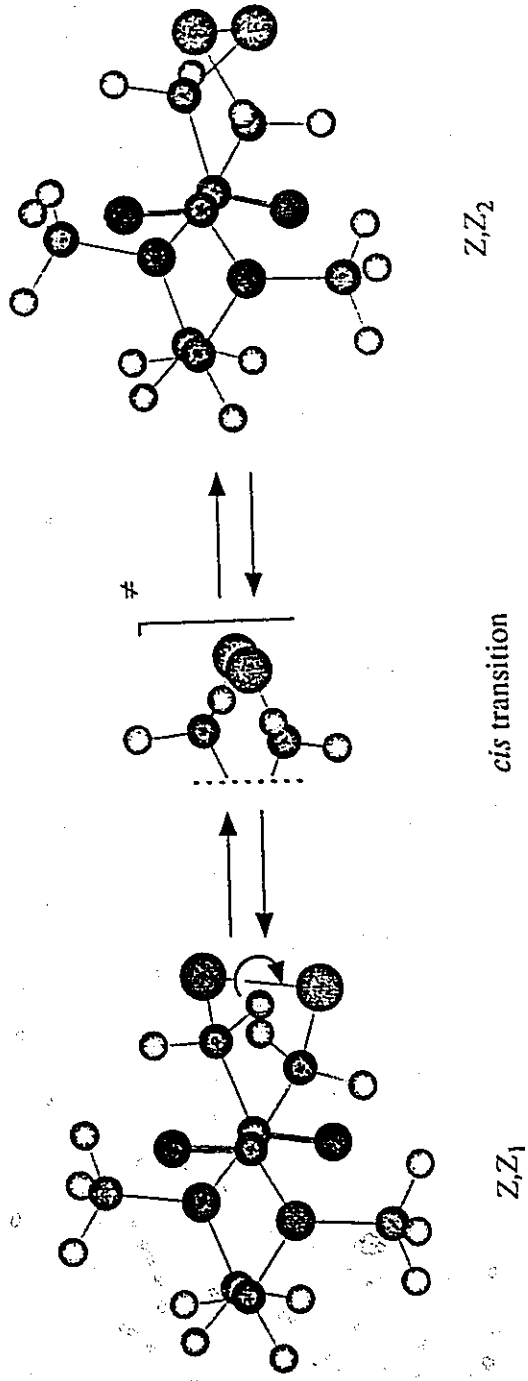

Figure 6.15: Ball and stick plots of the MMX-calculated diastereomers **40a** and **40b**, illustrating rotational isomerization about the S-S bond.

one for a disulfide rotation.

6.3.2 Measurement of the S-S Rotational Barrier for the $Z,Z_1 \rightleftharpoons Z,Z_2$ Equilibrium *via* ^{13}C DNMR Spectroscopy

The measurement of exchange rate constants as a function of temperature enables the calculation of activation parameters for an underlying chemical or physical process. For chemical systems undergoing conformational exchange, the energy barrier to interconversion has traditionally been measured by the free energy of activation, $\Delta G^{\neq}$, which may be calculated at a single temperature by means of the Arrhenius equation:

$$k = A \exp(-\Delta G^{\neq}/RT) \qquad [6.1]$$

One can also estimate the enthalpy of activation $\Delta H^{\neq}$ and entropy of activation $\Delta S^{\neq}$ from an Eyring plot of $\ln(k/T)$ vs $1/T$. However, most of the careful studies concerned with conformational processes in reasonably inert solvents indicate that $\Delta G^{\neq}$ values at different temperatures are equal[137] within the experimental error (± 0.2-0.5 kcal/mol), suggesting negligible $\Delta S^{\neq}$ values and $\Delta H^{\neq}$ almost coincident with $\Delta G^{\neq}$. Thus, in view of this result and the difficulty in obtaining accurate activation parameters,[138] the ensuing discussion will be confined to considerations of $\Delta G^{\neq}$ for rotation.

In order to acquire rate constants over a large as possible temperature range, the higher boiling DMSO-d_6 was used in place of $CDCl_3$ as a solvent for **40**. However, the ^{13}C NMR spectrum in DMSO-d_6 revealed small amounts of of additional isomers, the signals of which created an uncertainty in the assignment of the small Z,Z_2 N-CH_2 signal. Moreover, the chance of an inaccurate assignment was compounded by solvent shifts. Consequently, to account for these effects, a high field ^1H -^{13}C shift correlated

experiment was carried out and confirmed the chemical shifts of the Z,Z_2 isomer (see Figure 6.16).

Warming from 25.0 to 56.7 °C resulted in a temperature-dependent broadening and a subtle high-field migration of the Z,Z_2 N-C_α signal at 45.4 ppm (see Figure 6.17) - a phenomenon characteristic of a rate process. Rate constants, k, for this chemical exchange process were evaluated using the complete bandshape (CBS) method[139] (Figure 6.17). Based on the two-site exchange of the Z,Z_1 and Z,Z_2 N-CH_2 resonances (43.4 and 45.4 ppm, respectively) between 27.0 and 40.2 °C, the barrier to $Z,Z_1 \rightleftharpoons Z,Z_2$ interconversion ($\Delta G^{\neq}$) was measured to be 14.5 ± 1.3 kcal/mol (see Table 6.3, Figure 6.18). The height of this barrier lies close to the range reported for disulfide

Table 6.3: Calculated rate constants (from CBS analysis) and Arrhenius parameters for the $Z,Z_1 \rightleftharpoons Z,Z_2$ conformational equilibrium.

T (K)	k (s^{-1})	$1/T$ (K^{-1})	$\ln k$
298.5	0.6	0.00335	-0.5108
300.0	0.9	0.00333	-0.1054
302.0	1.0	0.00331	0
304.2	1.2	0.00329	0.1823
306.3	1.2	0.00326	0.1823
309.8	1.8	0.00323	0.5878
311.1	2.2	0.00321	0.7885
313.2	2.4	0.00319	0.8755
317.6	2.7	0.00315	0.9932
329.7	4.6	0.00303	1.5261

rotations in cyclic systems. For example, the barriers to inversion for 1,2-dithiane and 3,3,6,6-tetramethyl-1,2-dithiane have been reported to be 11.6 and 13.6 kcal/mol, respectively.[140,141]

The barrier of 14.5 kcal/mol was too low to be attributed to an amide

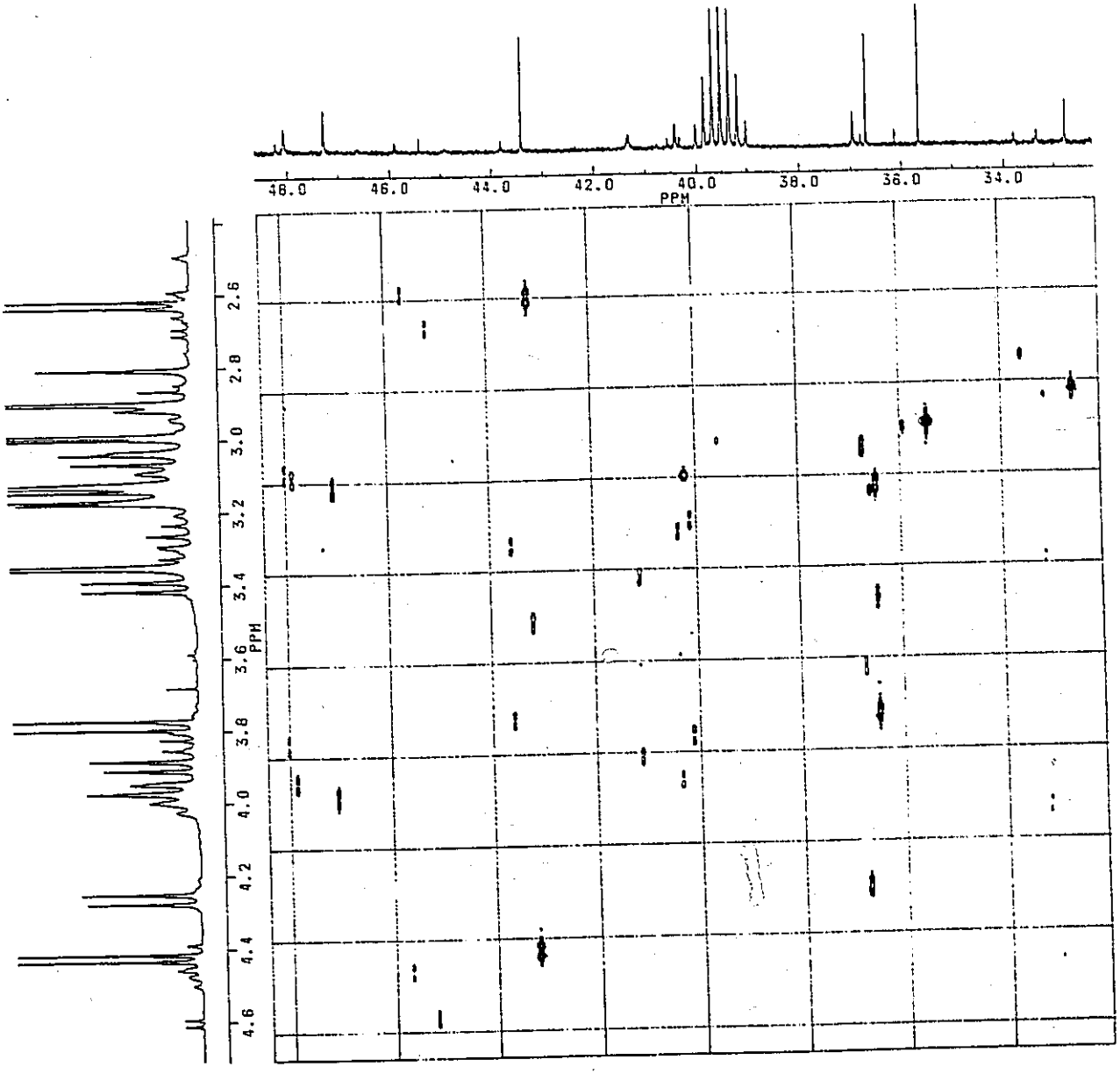

Figure 6.16: ^{1}H-^{13}C chemical shift correlated NMR spectra of **40** in DMSO-d_6 at 303 K.

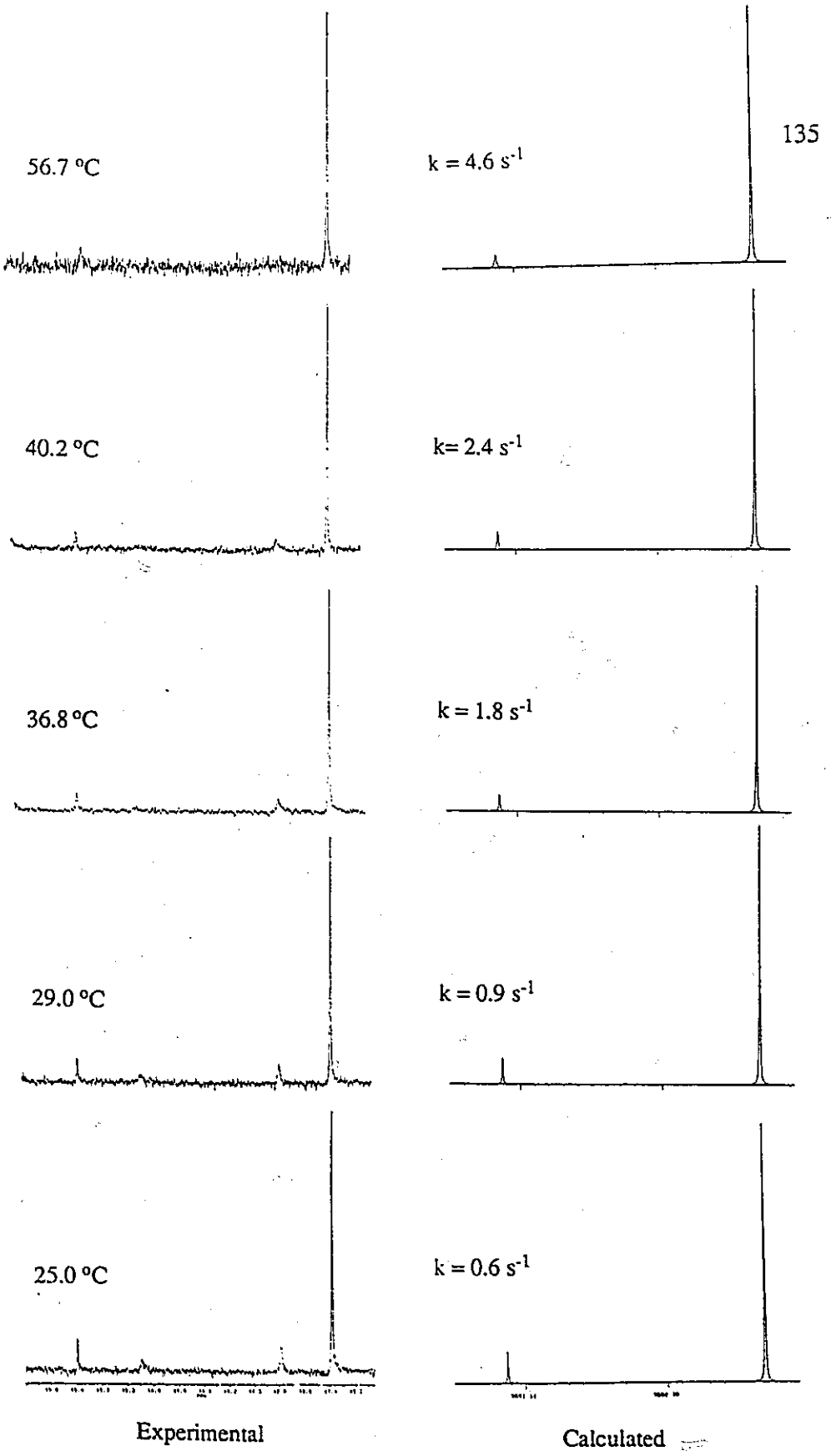

Figure 6.17: Variable temperature, 126 MHz ^{13}C NMR spectra of the Z,Z_1 and Z,Z_2 N-CH_2 signals of **40** in DMSO-d_6, with corresponding simulated spectra.

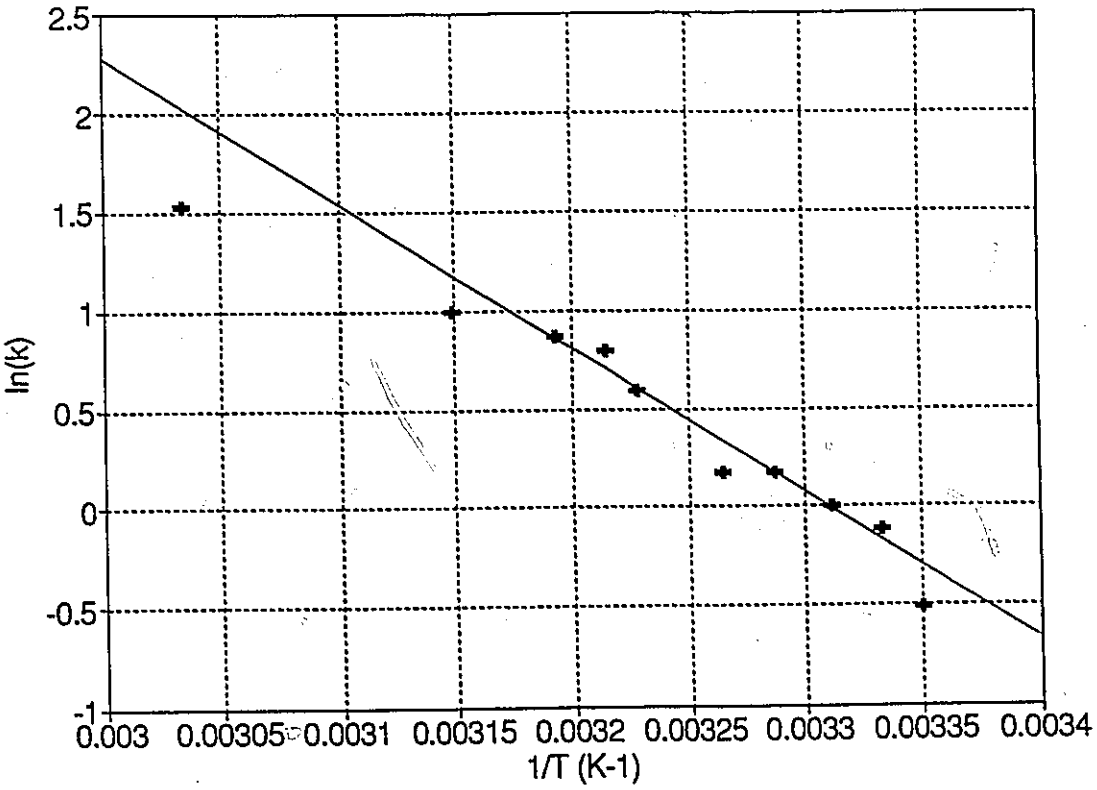

Figure 6.18: The Arrhenius plot of ln*k* *vs.* 1/*T* for the $Z,Z_1 \rightleftharpoons Z,Z_2$ conformational equilibrium.

rotation, particularly one occuring in a cyclic system (*cf.* the 19.3 kcal/mol barrier determined for amide rotation in the *Z,E* ring conformer, Section 6.2.2) and, although it was at the high end for reported disulfide rotations, it was reasonable to attribute the $Z,Z_1 \rightleftharpoons Z,Z_2$ chemical exchange process to a disulfide rotational mechanism as illustrated in Figure 6.15. A large component of the observed barrier is reflected in the energy profile of the acyclic disulfide bond, which has a maximum of *ca.* 8-10 kcal/mol at a CSSC dihedral angle of 0° (*i.e.*, for the *S-cis* transition state) and a minimum at 90° (see Figure 6.19).[142] The barrier is thought to arise principally from the mutual

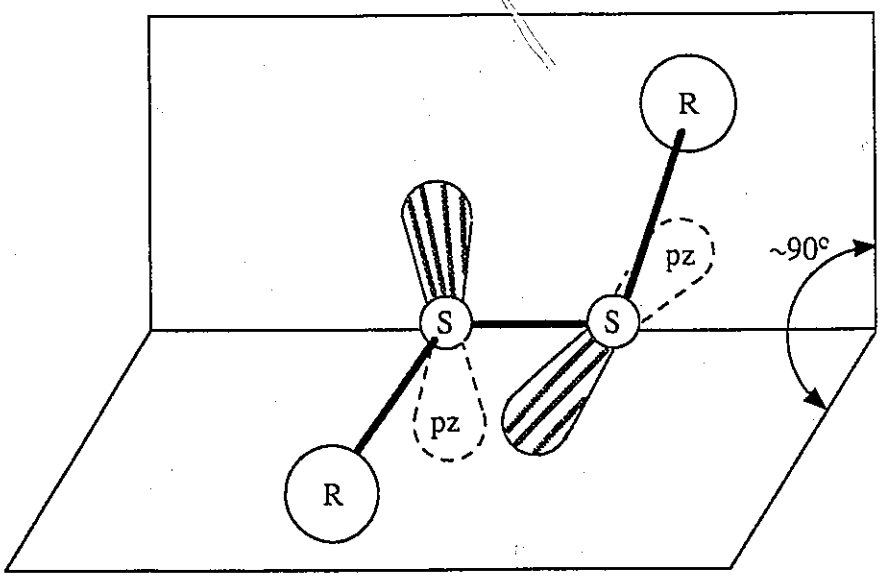

Figure 6.19: The lowest energy conformation of the RS-SR bond.

repulsion between the unshared pairs of 3*pz* nonbonded electrons on adjacent sulfur atoms.[143] In functionalized, cyclic disulfides such as **40** however, the presence of transannular electrostatic and steric interactions will increase the height of the disulfide rotational barrier. Moreover, the amide groups presumably confer additional rigidity to the ring and may also be a contributing factor to the relatively high barrier.

It is interesting to note that S-S rotation generated diastereomeric conformations and not enantiomers that are commonly observed in acyclic, unsymmetric disulfides.[144] The asymmetric nature of the ring introduces a second source of chirality, which, in combination with asymmetric disulfide rotation, confers a diastereomeric relation between the Z,Z_1 and Z,Z_2 stereoisomers.

Unlike the Z,Z_2 isomer, the S-CH_2 protons in the Z,Z_1 structure did not possess pseudoaxial geometry (see **40a**, Figure 6.14). Analysis of space-filling, mechanical models of the Z,Z_2 structure indicated that a psuedoaxial, S-CH_2 configuration brought one set of lone electron pairs on oppositely-related O and S atoms into close proximity. It appeared that the compromised, dipseudoequatorial geometry of the Z,Z_1 conformation defused this transannular interaction by directing the electrons away from each other. Moreover, a pseudoequatorial configuration of S-CH_2 protons was expected to be sterically preferable to a pseudoaxial one as 1,3-diaxial interactions with the methyl groups will destabilize the latter conformation. A combination of these electronic and steric effects may serve to explain the calculated and observed population distributions between the Z,Z_1 and Z,Z_2 ring conformers (Table 6.1).

The S-C*H*$_2$ chemical shifts also supported the calculated results which indicated the Z,Z_1 and Z,Z_2 conformations to be disulfide ring conformers. For example, the small chemical shift difference of 0.03 ppm between isochronous S-C*H* protons of the Z,Z_1 isomer (Table 7.5) is indicative of very similar magnetic environments. This observation was consistent with the dipseudoequatorial geometry of calculated structure **40a**. Alternatively, the larger 0.72 ppm difference noted for the corresponding protons of the Z,Z_2 structure correlated well with the magnetically dissimilar, pseudoaxial-pseudoequatorial environments predicted for the calculated **40b**

conformer.

MMX-conformational energies agreed moderately well with those of the observed populations (Table 6.1). Since molecular mechanics calculations mimic isolated molecules in their gaseous state, exact agreement between calculated and experimental populations is unattainable given the present level of computational sophistication. This situation arises from the inability to accurately incorporate solvent effects into the calculations. In addition, certain conformations may be differentially stabilized by solvation,[145] particularly in higher energy geometries. Consequently, the more energetic, gas-phase *Z,E* (**40c**) conformer may be stabilized to a greater extent than the lower energy Z,Z_2 structure, resulting in a thermodynamic reversal of solution state population levels. The effect may serve to rationalize the differences between calculated and experimental population distributions (Table 6.1), particularly for the *Z,E* structure.

In analogy to the chemical shift assignments made for protons of the *Z,E* crystal structure (see Section 6.2.5), the orientation of a MMX-calculated N-CH proton - in relation to its adjacent C=O group - will primarily determine its chemical shift. Consequently, for isomers **40a** and **40b** (see Figure 6.14), one isochronous N-C*H* pair occupied a pseudoaxial configuration (denoted as H_{ax}) which was essentially *cis* coplanar to the C=O group (*i.e.*, 9.2 and 1.4 degrees removed from the amide plane defined by the atoms O, C and N) and, therefore, should be the low-field protons at 4.68 and 4.88 ppm, respectively. An interesting confirmation of this pseudoaxial geometry was noted in the ^1H-^1H COSY spectrum (see Figure 6.6), where the 4.68 ppm signal was weakly correlated to the N-CH_3 resonance at 3.13 ppm. This was indicative of a stereospecific, four-bond coupling originating from the "W" configuration[146] which is often observed between axial protons alpha to C-18 or C-19 methyl groups in

steroids. Four-bond coupling to the methyl protons was not possible for the pseudoequatorial protons in this molecular configuration.

The second, isochronous set of geminal N-CH_{eq} protons in the Z,Z_1 and Z,Z_2 ring isomers occupied pseudoequatorial positions (denoted as H_{eq}) that were approximately 20.9 and 15.6 degrees out of the O=C-N amide plane. Their respective chemical shifts at 2.64 and 2.71 ppm implied that they were shielded in comparison to the rotationally-averaged, *Z,Z* N-CH_2 shift of 3.28 ppm for the open chain precursor **39** (Table 7.3). A comparison at a more quantitative level suggested that the H_{eq} protons were shielded by *ca.* 0.64 and 0.57 ppm, while the H_{ax} protons were deshielded by 1.40 and 1.60 ppm, respectively. Clearly, the shielding mechanisms - particularly the deshielding forces - at work in the conformational isomers of **40** were quite significant and worthy of further investigation.

6.4 Shielding Calculations

The objective of this section is to investigate the extent to which it is possible to identify the origins of and to quantify the large N-CH_2 nonequivalences observed in the Z,Z_1 and Z,Z_2 conformers, particularly in terms of the neighbouring group effect of the amide groups. Inductive and mesomeric (resonance) through-bond effects of the amide function were not expected to asymmetrically affect the N-CH_2 unit and assumed not to contribute to geminal nonequivalence (*i.e.*, $\Delta\delta_{DIA}$ (local) = 0). Consequently, the difference in the N-CH_2 shifts could be primarily attributed to through-space shielding mechanisms.

The observed chemical shift difference, $\Delta\delta_{OBS}$, between a geminal pair of N-CH_2 protons in the rigid heterocycle **40** can be evaluated from Equation 6.2.[147]

$$\Delta\delta_{OBS} = \Delta\delta_{MAG} + \Delta\delta_{EL} + \Delta\delta_{SOL} + \Delta\delta_{VDW} \qquad [6.2]$$

The terms $\Delta\delta_{MAG}$, $\Delta\delta_{EL}$, $\Delta\delta_{SOL}$ and $\Delta\delta_{VDW}$ refer to the *net* chemical shift between N-CH_2 protons ascribed to shielding contributions from magnetic anisotropy, electric field, solvent and van der Waals effects of all neighbouring groups in the molecule. The magnitude of these contributions to $\Delta\delta_{OBS}$ will now be examined in turn.

6.4.1 The Solvent Shift Contribution, $\Delta\delta_{SOL}$

The polar character of the amide group can contribute to $\Delta\delta_{OBS}$ through the polarization of the solvent *via* a reaction field. However, this shift contribution from the solvent ($\Delta\delta_{SOL}$) was demonstrated by Clayden and Williams to be unimportant in determining the methylene nonequivalence in cyclotetrasarcosyl, **45**.[148] A plot of the N-CH_2 chemical shift difference versus $(\epsilon - 1)/(\epsilon + 1)$, where ϵ is the solvent's dielectric constant, suggested that the splitting remained consistently large. The absence of exchangable protons and a concentration dependence for the magnitude of the N-CH_2 shift difference in **40** indicates that specific solvent-solute and/or solute-solute interactions are not likely shift factors either. Consequently, a $\Delta\delta_{SOL}$ component to the N-CH_2 nonequivalence in the conformationally similar *Z,Z* isomers of **40** is not expected to be significant and was neglected from the $\Delta\delta_{OBS}$ calculation.

6.4.2 The van der Waals Shift Contribution, $\Delta\delta_{VDW}$

Hydrogen atoms that are subject to intramolecular steric or van der Waals interactions with proximate nuclei often display shielding effects[149] that can be more marked than magnetic anisotropy shifts.[150] Qualitatively, the direction of shielding can be associated with the net nuclear charge on the resonant proton which, in turn,

depends on the predominance of either an attractive or repulsive interaction. For example, if the resonant proton feels an *attractive* van der Waals interaction with a proximate group, its effective nuclear charge will increase to result in an *upfield* shift (shielding) of the hydrogen nucleus. Conversely, in the *repulsive* van der Waals regime, electrostatic repulsion of interacting electron clouds will induce charge polarization in the H→C bond direction and produce a *downfield* shift (deshielding) of the resonant proton.[150] In general, intramolecular separations at or smaller than the sum of the van der Waals radii of the interacting groups usually result in repulsive van der Waals interactions, while attractive interactions will dominate at slightly larger interatomic distances. The attractive interaction is relatively weak compared to its stronger repulsive counterpart, making deshielding effects much larger than the shielding ones.[151] Instances of such deshieldings have been observed mostly in rigid systems, where one or more hydrogen atoms were forced too close to other groups because of rigid geometrical contraints.[149] For example, the magnitude of the δ_{VDW} shift and N-CH_2 nonequivalence in a series of hindered amides has been linearly correlated to the size and number of the interacting groups.[135]

In contrast to steric-based observations reported for **45**,[148] a $\Delta\delta_{VDW}$ contribution to $\Delta\delta_{OBS}$ cannot be ruled out since van der Waals contacts involving the downfield H_{ax} protons were detected in the calculated MMX (see Figure 6.20) and crystal structures of **40**. The degree of electron cloud overlap between H_{ax} and interacting groups can be taken as a rough measure of van der Waals compression and the resultant downfield shift that will be experienced by H_{ax}.[150] For example, a relatively large, downfield shift is predicted for the H_{ax} protons because of the combined overlap of its electron clouds with those from its adjacent carbonyl oxygen and opposite N-CH_3 protons. These through-space contacts can be seen in the CPK

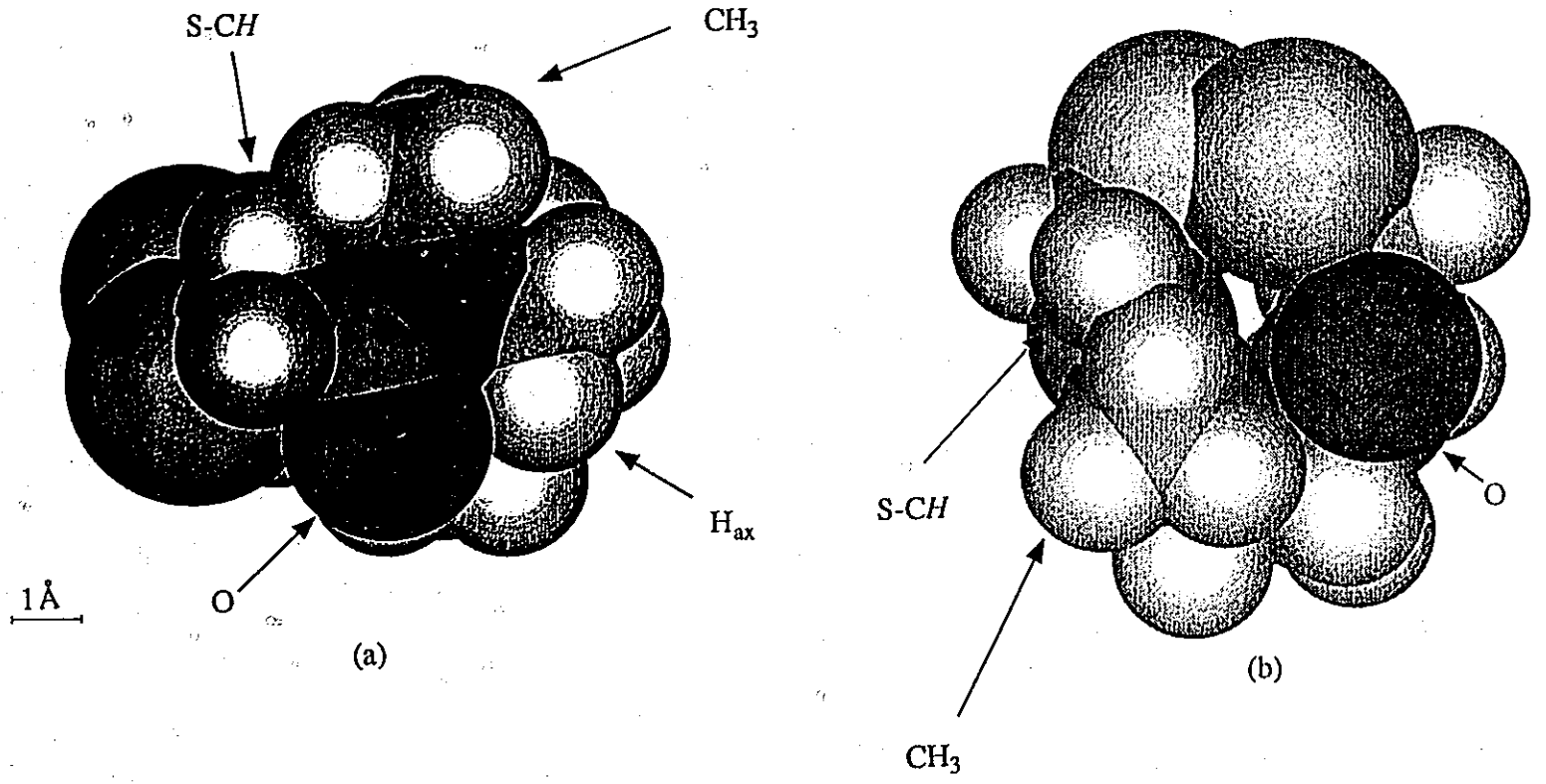

Figure 6.20: Space-filling models of **40b** from (a) side and (b) top perspectives. Note that the van der Waals compression of the S-CH pseudoaxial proton with the N-CH_3 protons, and the carbonyl oxygen with H_{ax}. The N-CH_3 group has been rotated by *ca.* 60° to illustrate steric compression.

space-filling representation of the Z,Z_2 conformer [see Figure 6.20(a)], where van der Waals radii (r_{VDW}) are used to illustrate an "effective size" for the electron cloud surrounding each atom. Calculations based on this scale model indicated that the oxygen (r_{VDW} = 1.5 Å)[152] and methyl (r_{VDW} = 2.0 Å) groups protrude into the electron cloud of the H_{ax} (r_{VDW} = 1.2 Å) protons by at least 0.2 and 0.1 Å respectively. The H_{eq} protons were not expected to be affected by a paramagnetic van der Waals shift mechanism given its sterically-unencumbered, psuedoequatorial geometry. However, small diamagnetic shifts were plausible *via* through-space, attractive van der Waals interactions and/or inductive, through-bond effects transmitted *via* the induced $H_{ax}\rightarrow C$ bond dipole (*vide supra*).

It is worthwhile to note in Figure 6.20(b) that the marked van der Waals compression between the pseudoaxial S-C*H* and proximate CH_3 groups in the Z,Z_2 conformer may be the dominant shielding mechanism responsible for the large geminal isochrony of the former protons (0.72 ppm). A similar interaction may also serve to rationalize the large geminal Z S-CH_2 splitting (1.13 ppm) in the *Z,E* isomer, where the electron clouds of H(10a) and H(8) (see Figure 6.11) overlapped by as much as 0.8 Å. Other through-space, steric interactions where paramagnetic van der Waals shifts could be significant include the proximate H(3b) and H(6b) protons of the *Z,E* conformer.

Unfortunately, in the absence of a general, predictive relationship equating both repulsive and attractive van der Waals interactions to chemical shifts, it was not within the scope of this account to calculate a $\Delta\delta_{VDW}$ contribution to $\Delta\delta_{OBS}$. Such determinations await the development of a satisfactory quantitative expression or computative method.

In light of the preceding $\Delta\delta_{SOL}$ and $\Delta\delta_{VDW}$ discussions, Equation 6.2 can be simplified to:

$$\Delta\delta_{CALC} = \Delta\delta_{MAG} + \Delta\delta_{EL} \qquad [6.3]$$

In order to carry out the $\Delta\delta_{CALC}$ measurements, the following simplifying assumptions were made: 1) the magnetic and electric dipoles of the amide groups were idealized as point dipoles located at the center of the C=O bonds; 2) the amide groups were approximated to carbonyl groups; 3) the magnitude of the N-CH_2 chemical shift difference was dependent primarily on the through-space shielding effects of the amide C=O bond. Assumptions 1) and 2) were necessary because of a lack of a reasonably simple and exact description of the magnetic susceptibility anisotropy and electric field of an amide group. The carbonyl approximation was validated by the diffraction study of **40**, which revealed the C=O amide bond lengths to be very close to C=O lengths in ketone systems (1.23 Å versus 1.22 Å, respectively).

The calculations were carried out using the susceptibility anisotropies and κ value derived by ApSimon and Beierbeck from least-squares analysis of methyl shifts in keto-androstanes in $CDCl_3$.[153] The constants $\Delta\chi$ and κ were based on induced magnetic and electric point dipoles located 0.60 Å from the carbonyl carbon atom halfway along the C=O bond. This position for the center of the point dipoles was selected since it is reported to afford the best correlation between calculated and observed chemical shifts.[147]

6.4.3 Magnetic Anisotropy and Electric Field Shift Contributions, $\Delta\delta_{MAG}$ and $\Delta\delta_{EL}$

The magnetic anisotropy shift perturbing a N-CH proton, δ_{MAG}, from the anisotropic amide dipole can be estimated from the modified form of McConnell's equation:[154]

$$\delta_{MAG} = 1/(3R^3)\ \{\Delta\chi_{xy}(1 - 3\cos^2\Theta_y) + \Delta\chi_{xz}(1 - 3\cos^2\Theta_z)\} \qquad [6.4]$$

where R is the distance between the midpoint of the C=O bond and the proton H under consideration; $\Delta\chi_{xy}$ and $\Delta\chi_{xz}$ are the magnetic susceptibilities between the y- and z-axes, respectively, and the axis in the C=O σ bond direction (*i.e.*, x-axis): Θ_y and Θ_z are the angles between R and the y- and z-axes, respectively [see Figure 6.21(a)].

The electric field shift of a N-CH proton resulting from the through-space influence of the amide dipole can be estimated from the modified form of Buckingham's equation:[155]

$$\delta_{EL} = \kappa E_{C\text{-}H} \qquad [6.5]$$

where κ is an experimentally-determined proportionality constant and $E_{C\text{-}H}$ is a geometrical factor given by Equation 6.6.

$$E_{C\text{-}H} = (3\cos\alpha\cos\beta - \cos\gamma)/R^3 \qquad [6.6]$$

R is the distance between the midpoint of the C=O bond and the proton H under consideration; α is the angle between C=O axis and R; β that between R and the C-H bond; and γ that between the C=O and the C-H vectors [see Figure 6.21(b)].[147,148]

The results of the magnetic anisotropy and electric field shift calculations for the Z,Z_1 and Z,Z_2 stereoisomers using the carbonyl approximation are presented in Tables 6.4 and 6.5, respectively.According to convention, positive δ values correspond to *paramagnetic* or *downfield* shifts, relative to the reference compound (TMS), whereas, negative values to *diamagnetic* or *upfield* shifts.

Carbonyl magnetic anisotropy and electric field shift mechanisms satisfactorily accounted for the large observed H_{ax} deshielding in conformers Z,Z_1 and

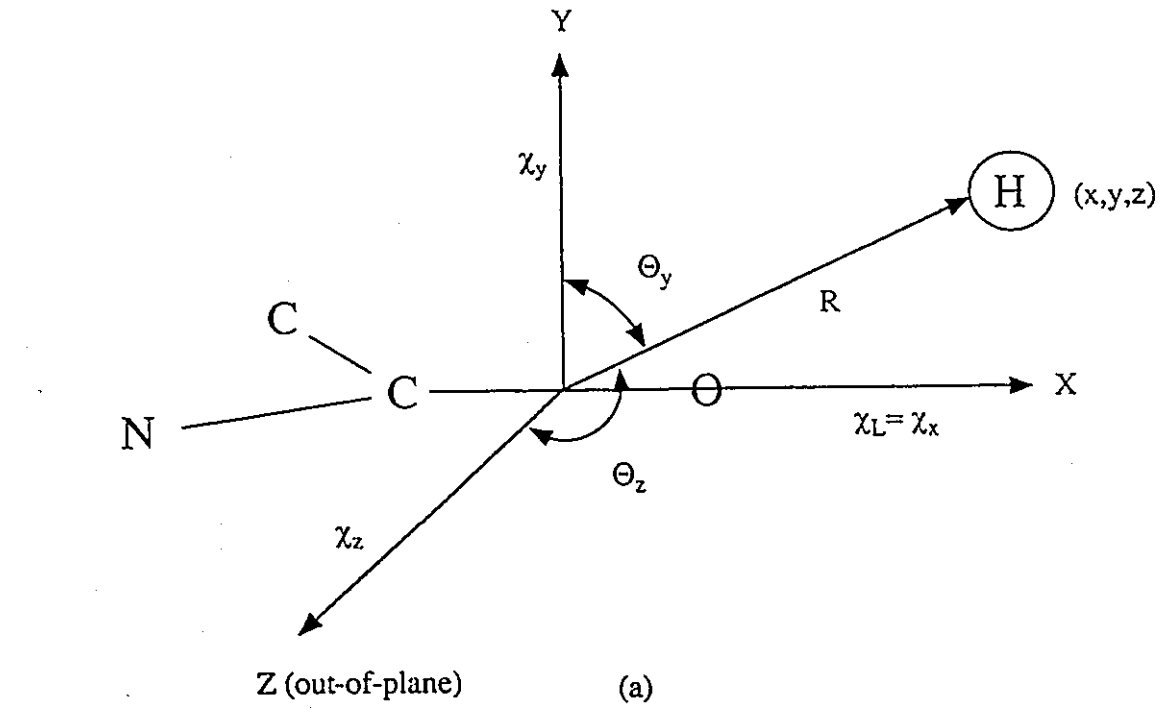

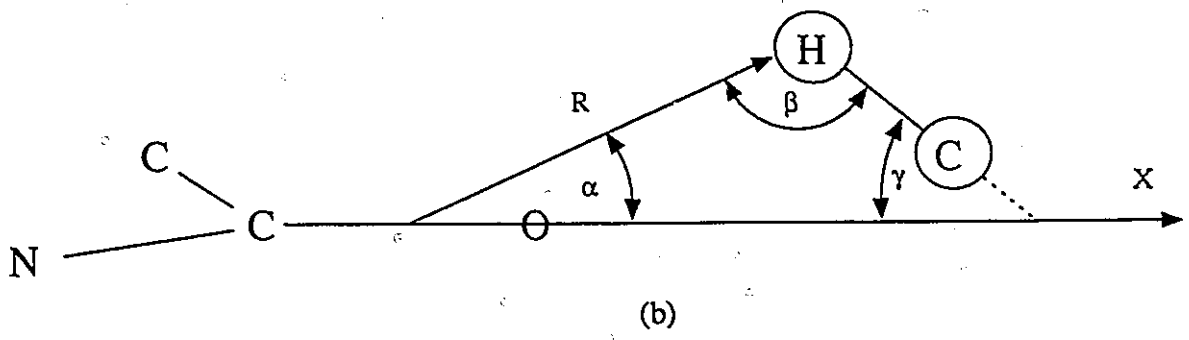

Figure 6.21: Coordinate systems for (a) the magnetic anisotropy shift and (b) the electric field shift determinations depicting anisotropic susceptibilities and geometrical parameters. The x-axis is taken as the axis of symmetry.

Table 6.4: Calculated magnetic anisotropy shifts for the N-CH_2 protons of 40a and 40b .[a]

		ADJACENT C=O				OPPOSITE C=O					
CONFORMER	N-CH Proton	Θ_y (Deg)	Θ_z (Deg)	R ($\times 10^{-8}$ cm)	δ_{MAG}^{ADJ} [b] (ppm)	Θ_y (Deg)	Θ_z (Deg)	R ($\times 10^{-8}$ cm)	δ_{MAG}^{OPP} [b] (ppm)	δ_{MAG} [c] (ppm)	$\Delta\delta_{MAG}$ [d] (ppm)
40a (Z,Z_1)	H_{eq}	158.8	97.0	3.47	0.28	140.6	129.3	4.15	0.14	0.42	0.62
	H_{ax}	168.5	97.4	2.47	0.97	129.0	133.0	4.07	0.07	1.04	
40b (Z,Z_2)	H_{eq}	160.4	97.3	3.43	0.31	137.2	132.7	4.22	0.12	0.42	0.57
	H_{ax}	161.6	105.2	2.43	0.95	129.0	129.2	4.19	0.04	1.00	

[a] Based on the carbonyl approximation with the dipole origin located at the midpoint of the C=O bond.

[b] $\Delta\chi_{xy} = -3.26 \times 10^{-29}$ cm^3/ molecule; $\Delta\chi_{xz} = -1.82 \times 10^{-29}$ cm^3/ molecule.[153]

[c] $\delta_{MAG} = \delta_{MAG}^{ADJ} + \delta_{MAG}^{OPP}$

[d] $\Delta\delta_{MAG} = \delta_{MAG}(H_{ax}) - \delta_{MAG}(H_{eq})$

Table 6.5: Calculated electric field shifts for the N-CH_2 protons of 40a and 40b .[a]

		ADJACENT C=O					OPPOSITE C=O						
CONFORMER	N-CH Proton	α (Deg)	β (Deg)	γ (Deg)	R ($\times 10^{-8}$ cm)	δ_{EL}^{ADJ} [b] (ppm)	α (Deg)	β (Deg)	γ (Deg)	R ($\times 10^{-8}$ cm)	δ_{EL}^{OPP} [b] (ppm)	δ_{EL} [c] (ppm)	$\Delta\delta_{EL}$ [d] (ppm)
40a (Z,Z_1)	H_{eq}	97.9	31.3	118.9	3.46	-0.03	84.4	40.2	55.1	4.15	0.05	0.02	0.48
	H_{ax}	66.5	82.4	24.8	2.47	0.53	108.9	42.2	153.8	4.07	-0.03	0.50	
40b (Z,Z_2)	H_{eq}	108.1	31.5	110.9	3.43	0.12	92.7	40.0	54.5	4.22	0.10	0.21	0.46
	H_{ax}	79.9	82.4	12.9	2.44	0.66	116.8	42.3	158.0	4.19	0.01	0.67	

[a] Based on the carbonyl approximation with dipole origin located at the midpoint of the C=O bond.

[b] $K = -10.6 \times 10^{-30}$ cm^3/molecule.[153]

[c] $\delta_{EL} = \delta_{EL}^{ADJ} + \delta_{EL}^{OPP}$

[d] $\Delta\delta_{EL} = \delta_{EL}(H_{ax}) - \delta_{EL}(H_{eq})$

Z,Z_2, but they did not seem to be the shielding source for the higher field H_{eq} protons. Based on an averaged Z,Z N-CH_2 shift of 3.28 ppm (see **39**, Table 7.3), C=O anisotropic and electric field shifts provided a paramagetic contribution totalling 1.10 and 1.03 ppm respectively to the 1.40 and 1.60 ppm shifts observed for Z,Z_1 and Z,Z_2. In contrast, the δ_{MAG} and δ_{EL} calculations did not indicate any diamagnetic contribution to the H_{eq} protons but, instead, suggested a slight low-field shift. The attractive van der Waals interaction described earlier may account for the missing diamagnetism that apparently influences the H_{eq} protons.

The calculated contributions of anisotropic and electric field shifts to geminal N-CH_2 nonequivalences were similar magnitude, in agreement with the findings of Zürcher and ApSimon *et al.*,[147,153] though the former mechanism was calculated to have about a 0.1 ppm greater contribution. An important generalization to emerge from these results is that magnetic anisotropy *and* electrostatic shielding mechanisms should be treated as being equally significant in discussions of deshielding effects in carbonyl systems. For amide systems in particular, the expected contribution of the electric field shift should be even greater than indicated by the calculated δ_{EL} (Table 6.5) values, since the shielding parameters used in these calculations were based on an approximation of the less polar, ketone carbonyl group.

Magnetic and electric field contributions to the calculated chemical shift difference ($\Delta\delta_{CALC}$) from both amide groups indicated that the shift was largely determined by the adjacent group, which is reasonable for a R^{-3} dependence.

When the combined effects of magnetic anisotropy and electric field shifts were considered, only about one-half of the observed Z,Z N-CH_2 splitting was accounted for. Perhaps the most obvious rationale for this chemical shift deficit can be argued from a combination of faulty parameter selection and approximations and a

failure to account for a potentially significant van der Waals shift contribution. At the level of empirical computation, the idea of a simple carbonyl approximating an amide system may be a gross oversimplification, given the amide's electron delocalization, and that a $C=N^+$ shift contribution from the dipolar resonance form of the amide group should be considered. In addition, for the present treatment, the C=O group was assumed to be the dominant shielding mechanism responsible for the large N-CH_2 shift difference. However, other conceivable shift effects (albeit much smaller) could also contribute to the N-CH_2 anisochrony. Through-space neighbouring group shifts are also possible for other groups, particularly C-C, C-H and S-S bonds. In analogy to sulfide[156] and amine[157] systems, lone pairs of electrons in the disulfide and amide groups may also exert shielding effects.

In addition, the separation of the N-CH_2 protons from the assumed dipole center of adjacent carbonyl groups ranges from about 2.4 Å for the *syn*, H_{ax} protons to about 3.5 Å for the *anti*, H_{eq} ones (Tables 6.4 and 6.5). At these relatively small distances, the validity of the dipole approximation in the magnetic anisotropy and electric field shielding calculations is uncertain. Didry and Guy[158] have reported errors in excess of 30% can result using the point dipole approximation at distances of 3 Å from the assumed center of an induced magnetic dipole and which become correspondingly greater at smaller distances. Therefore, caution must be applied (particularly for the shielding effects of the adjacent C=O on H_{ax}) in the application and interpretation of Equation 6.3 towards a quantitative evaluation of δ_{MAG} and δ_{EL}.

As an independent check against the accuracy of the calculated $\Delta\delta_{MAG}$ and $\Delta\delta_{EL}$ shifts given in Tables 6.4 and 6.5, visual and semi-quantitative determinations of the total shielding at all N-CH_2 protons were performed on the conventional models for the magnetic anisotropy and electric field shielding mechanisms of the carbonyl group

(see Figure 6.22).[159] The results of this qualitative comparison confirmed the direction (*i.e.*, sign) of shielding and approximate magnitude of the predicted shift contributions. In particular, a semi-quantitative determination for δ_{MAG} contributions were estimated from Pople's long-range shielding contour plots[160] while, for the δ_{EL} component, a visual inspection of all C-H orientations relative to the C=O electric field afforded a qualitative confirmation for the direction of shielding at the resonant proton.

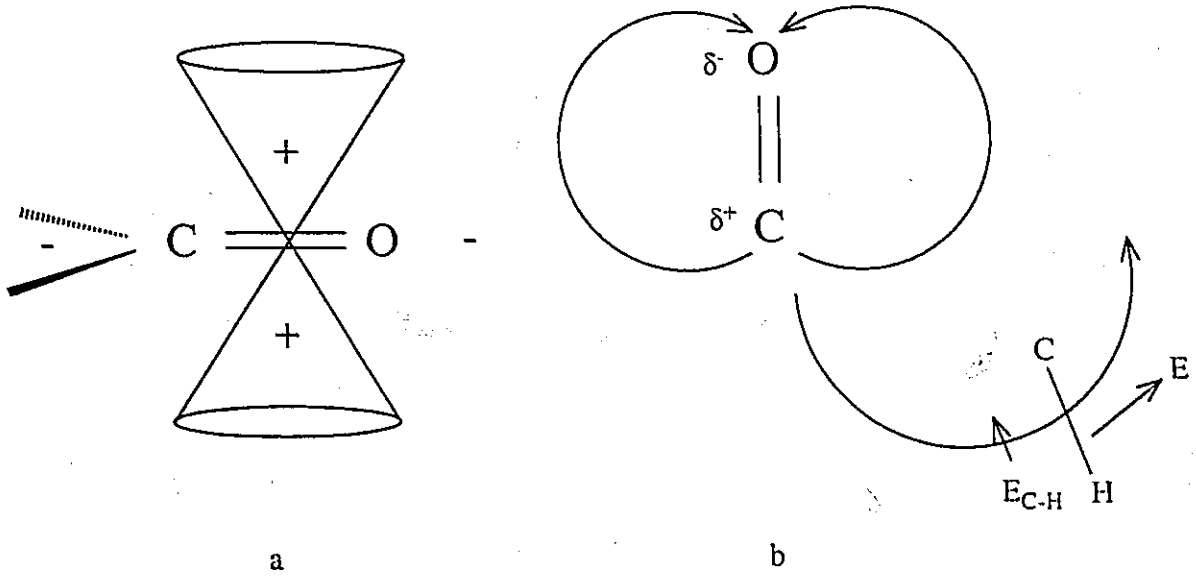

Figure 6.22: Models of magnetic anisotropy (a) and electric field (b) shielding mechanisms for the C=O bond. In a), the + and - signs refer to areas of nuclear shielding and deshielding, respectively. In b), the electric field vector along the C-H bond, E_{C-H}, determines nuclear shielding; in this case, the E_{C-H} vector is in the H⟶C bond direction and the proton is shielded.

CHAPTER 7

EXPERIMENTAL

7.1 Materials

N,N-dimethylformamide was heated at reflux and distilled from BaO prior to use. Acetonitrile was distilled from P_2O_5 and the distillate was redistilled from CaH_2 discarding the first 5 and the last 10%. Ethanol (EtOH) was dried and purified *via* distillation from magnesium turnings and stored over freshly-activated 4Å molecular sieves. Pyridine was distilled from CaH_2 just prior to use. Chloroform-*d* ($CDCl_3$) was stored over 4Å molecular sieves. All chemical were purchased from Aldrich Chemical Company (Milwaukee, WI, USA) unless otherwise noted.

Melting points (mp) were recorded on a Gallenkamp capillary tube melting point apparatus and are uncorrected.

7.2 Chromatography

Analytical thin layer chromatography (TLC) and column chromatography (according to the "flash" method of Still *et al.*[161]) were carried out on E. Merck silica gel 60 F_{254} coated Al plates of 0.2 mm thickness and 0.040-0.063 mm (230-400 mesh), respectively. TLC visualization was achieved using a combination of either a UV lamp (254 nm), I_2 vapour or a ninhydrin spray (0.2% ninhydrin in EtOH) followed by heating and treatment with a phosphomolybdic acid spray (20 g of phosphomolybdic acid and 15 g $CeSO_4$ dissolved in 1 L of 10% H_2SO_4). A spray solution of 9.2 mL of

m-anisaldehyde in 338 mL of 95% EtOH, 3.75 mL glacial HOAc and 12.5 mL of concentrated H_2SO_4 followed by heating at 100-150 °C was used to visualize the β-cyclodextrin derivatives.

AMBERLYST A-26 anion-exchange resin (Cl^-) was prewashed and converted to the OH^- form just prior to use. Approximately 150 mL of crude, commercial grade resin was purified in a 150 mL coarse sintered glass funnel according to the following wash protocol: 1 N HCl (3 X 100 mL), distilled water (2 X 100 mL), 1:1 v/v aqueous acetone (2 X 100 mL), EtOH (3 X 100 mL), 1 N NaOH (3 X 100 mL), distilled water (until eluate became neutral) and EtOH (3 X 100 mL). Washings were allowed to percolate through the resin under gravity. The washed resin was stored under EtOH until it was ready to be used.

7.3 Spectroscopy

Proton nuclear magnetic resonance (^1H NMR) spectra were recorded on Varian EM 390, Bruker MSL-100, AC-200, WM-250 or AM-500 spectrometers, with the majority of experiments acquired at 500.135 MHz on the latter instrument using a 5 mm dual frequency ^1H-^{13}C probe. Sample concentrations were approximately 1-2% w/v. Spectra were typically obtained in 8 scans in 16K data points over a 5.000 KHz spectral width (1.638 s acquisition time). The free induction decay (FID) was processed using exponential multiplication (line broading: 0.2 Hz) and was zero-filled to 32K before Fourier transformation. Sample temperature was maintained at 303 K by a Bruker BVT-1000 variable temperature unit. The abbreviations s=singlet, d=doublet, t=triplet, q=quartet and m=multiplet refer to the multiplicities of the signals observed.

Broad band decoupled, natural abundance carbon thirteen nuclear magnetic resonance (^{13}C NMR) spectra were recorded on a Bruker AM-500 spectrometer at

125.759 MHz using the 5 mm dual frequency ^{1}H-^{13}C probe, except in one experiment, which was acquired on a Bruker WP-80 instrument at 20.115 MHz. The spectra were acquired over a 30.0 KHz spectral width in 16K data points (0.279 s acquisition time) using a ^{1}H decoupler power level of 17H. The ^{13}C pulse width was 2.5 μs (35° flip angle). A 0.5 s relaxation delay was used. For spectral edited ^{13}C experiments, the standard *J*-modulated spin sort pulse sequence was used, incorporating a 7.3 μs ^{13}C 90° pulse width and a relaxation delay of 2.5 s. The FIDs were processed using exponential multiplication (line broading: 3.5 Hz) and zero-filled to 32K before Fourier transformation.

NOE difference spectra were obtained by subtraction of the off-resonance control FID from the on-resonance FID under non-spinning conditions and employing a sweep rate of 19 Hz. The signal of interest was selectively saturated for 5 s and the decoupler was gated off during acquisition. This saturation period also served as the relaxation delay. Normally 8 scans were acquired for each irradiation with the cycle of irradiation repeated 10 times. Free induction decays were processed using exponential multiplication with a line broadening of 4 Hz before Fourier transformation.

^{13}C dynamic nuclear magnetic resonance (DNMR) spectra were recorded over a 2.066 KHz spectral width in 8K data points (1.98 s acquisition time) incorporating a 5.5 μs pulse width and a 9.0 s relaxation delay to optimize sensitivity and digital resolution. The sample and probe were allowed a 10-minute equilibration period per 5 °C increment. An external digital thermocouple was used to measure the probe temperature to an accuracy of ± 0.5 °C. Rate constants were estimated by visual fitting of experimental to computer-simulated spectra measured for a given temperature. The calculated spectra were generated on an IBM PS/2 Model 30 (286) microcomputer equipped with a HP 7550A graphics plotter using the simulation

program EXCHANGE (available from R.E.D. McClung, Department of Chemistry, University of Alberta, Edmonton, Alberta, Canada, T6G 2G2). The intrinsic linewidth of 0.35 Hz was obtained from a measurement of the peak width at one-half peak height of the S-CH_2 resonance at 35.61 ppm at 25.0 °C. The $\Delta G^{\neq}$ for disulfide rotation was calculated from the slope of the regression line derived from an Arrhenius plot of ln$k$ versus $1/T$ in Quattro Pro (3.01). The data points corresponding to T=298.5, 317.6 and 329.7 K were omitted from the regression analysis. The error in $\Delta G^{\neq}$ was measured by the standard deviation of the regression coefficient.

Solid state ^{13}C spectra were obtained at 25.18 MHz on a Bruker MSL-100 spectrometer operating at 2.35 T. The cross polarization magic angle spinning (CP-MAS) spectrum was obtained by using a 1 ms contact time and a recycle time of 10 s. Crystals of **40** - obtained by slow evaporation of a THF solution of the compound - were pulverized and diluted with KBr prior to analysis.

The ^{13}C-^{1}H 2-D chemical shift correlation spectra were acquired using the standard pulse sequence incorporating the BIRD pulse during the evolution period for the ^{1}H - ^{1}H decoupling in F_1.[162-164] The spectra in F_2 were recorded over a spectral width of 3.76 KHz in 4K data points. The 256 FIDs in F_1 were obtained over a ^{1}H spectral width of 1.52 KHz. Each FID was acquired in 200 scans. The fixed delays in the pulse sequence were a 1.0 s relaxation delay, BIRD pulse and polarization transfer delays (1/2 $^{1}J_{CH}$) of 0.003571 s and a refocussing delay (1/4 $^{1}J_{CH}$) of 0.001786 s. The ^{13}C 90° pulse width was 6.4 μs, while the ^{1}H 90° pulse width through the decoupler channel was 18.6 μs. The data were processed using exponential multiplication (line broadening: 5.0 Hz) in F_2 and unshifted sine bell in F_1. Zero-filling in F_1 resulted in a 2048 X 1024 data matrix.

The compounds analyzed *via* NMR spectroscopy were dissolved in either

deuterated acetone, deuterated benzene, deuterochloroform or deuterated dimethyl sulfoxide or deuterated methanol (CD_3COCD_3, C_6D_6, $CDCl_3$, DMSO-d_6 or CD_3OD, respectively), or mixtures thereof, obtained from MSD Isotopes. ^1H and ^{13}C chemical shifts are reported in parts per million (ppm) using either TMS (0.0 ppm) as an internal reference or the residual signal of the following solvents: CD_3COCD_3 (2.04; 29.8 ppm), C_6D_6 (7.15; 128.0 ppm), $CDCl_3$ (7.26; 77.0 ppm) and DMSO-d_6 (2.49; 39.5 ppm).

Low resolution mass spectra (MS) and high resolution mass spectra (HRMS) were obtained on either a VG Micromass 7070F or a VG ZAB-E mass spectrometer with sample introduction *via* a direct inlet system. Infrared (IR) spectra were recorded on a Perkin-Elmer 283 spectrometer using either liquid cells with methylene chloride or chloroform as solvents or potassium bromide pellets. The abbreviations (s)=strong, (m)=medium and (w)=weak are used to to describe the intensity of particular bands in the IR spectra.

7.4 X-ray Diffraction of **40**

Crystals of **40** were grown by very slow recrystallization from freshly-distilled tetrahydrofuran at -15 °C. A colorless plate having approximate dimensions of 0.20 X 0.05 X 0.15 mm was mounted on a glass fiber. All measurements were made on a Rigaku AFC6R diffractometer with graphite monochromated CuKα radiation (λ = 1.54178 Å) and a rotating anode generator. The crystal data for **40** is presented in the Appendix (see Tables A.1 to A.6).

Cell constants and an orientation matrix for data collection were obtained from a least-squares refinement using the setting angles of 24 carefully centered reflections in the range $7.0 < 2\Theta < 45.0°$. Based on packing considerations, a statistical

analysis of intensity distribution and the successful solution and refinement of the structure, the space group was determined to be $P\bar{1}$ (#2).

The data were collected at a temperature of 23 ± 1 °C using the ω - 2Θ scan technique to a maximum 2Θ value of 110.1°. Scans of (1.21 + 0.30tanΘ)° were made at a speed of 32.0°/min (in omega). The weak reflections ($I < 10.0\sigma_I$) were rescanned (maximum of 9 rescans) and the counts were accumulated to assure good counting statistics. Stationary background counts were recorded on each side of the reflection. The ratio of peak counting time to background counting time was 2:1. The diameter of the incident beam collimator was 0.5 mm and the crystal to detector distance was 400.0 mm.

Of the 1479 reflections which were collected, 1362 were unique (R_{int} = 0.032). The intensities of three representative reflections - which were measured after every 150 reflections - remained constant throughout data collection indicating crystal and electronic stability (no decay correction was applied). The data were corrected for Lorentz and polarization effects.

The structure was solved by direct methods. All non-hydrogen atoms were refined with anisotropic thermal parameters. Hydrogen atoms were placed geometrically and not refined. A correction was made for extinction (χ = 0.005(3) where $F^* = F[1 + 0.002\chi F^2/\sin 2\Theta]^{-1/4}$) and an absorption correction was applied using the program DIFABS,[165] employing transmission factors ranging from 0.69 to 1.20. Atomic scattering factors for all atoms and corrections for anomalous dispersion for C, O, N and S were taken from the International Tables for Crystallography, Vol. C.[166] Refinement minimized the function $\Sigma\, \omega(|F_o| - |F_c|)^2$, with $\omega = (\sigma^2 F + 0.0008F^2)^{-1}$. The final solution, with R = 4.67 % and ωR = 6.80 % ($R = \Sigma\, (||F_o| - |F_c||)/ \Sigma\, F_o$) for 1006 reflections ($I > 2\sigma_I$), showed no significant peaks in the final difference map. The

goodness-of-fit was S = 1.51. The program SHELXTL PC was used for all calculations.[167]

7.5 Molecular Mechanics Studies on **40**

Steric energies and conformations were calculated and minimized in PCMODEL V4.0 (available from K. Gilbert, Serena Software, Box 3076, Bloomington, IN 47402-3076, USA) using the MMX force field derived from the MM2 force field of N.L. Allinger (available from Quantum Chemistry Program Exchange, Chemistry Department, Indiana University, Bloomington, IN 47405, USA). The calculations were performed on an IBM PS/2 Model 70 (486) microcomputer. The MMX force field includes the parameters necessary for the minimization calculations. Calculated steric energies were reported relative to the global minimum structure. Vicinal coupling constants measured from energy-minimized structures were calculated using the Altona modification of the Karplus equation which takes into account substituent electronegativity.[168]

To ensure a comprehensive search of conformational space, initial geometries were generated by either systematic or random methods.[169] Systematic geometry searches were typically conducted by merging all combinations of accepted ground state geometries of the disulfide, amide and ethyl functional groups of **40**; *ie.*, 90° torsional angle for the disulfide linkage, 180° (*trans*) and/or 0° (*cis*) torsional angles for the amide groups and a staggered configuration for the ethyl fragment. Random geometries were typically generated by either random or pseudorandom atomic variations on either minimized structures or two-dimentionally drawn images. After a crude starting geometry was produced, it was allowed to relax into an optimized geometry by the MMX force field. The search was terminated when new minima

within 5 kcal/mol of the global minimum ceased be to found. Starting geometries were preminimized without hydrogen atoms and then reminimized with added hydrogens. This procedure avoids forcing hydrogens and lone electron pairs into high energy configurations.[170] Minimized structures were finally reminimized to ensure full convergence.

Geometrical parameters (see Figure 6.21) were measured in PCMODEL *via* atomic distance and bond angle queries on reformatted structure files. To calculate R, a dummy atom was defined as the origin and positioned at the midpoint of the required C=O bond. Dummy atoms were further employed to locate the y and z magnetic susceptibility axes for Θ_y and Θ_z determinations by arbitrarily defining their cartesian coordinates to be (0,3,0) and (0,0,3) respectively. Angle γ was measured by adding the C-H difference vector of concern to the appropriate carbonyl carbon coordinates; this ensures a parallel C-H transformation from which γ can be directly measured. All parameters were substituted into the appropriate chemical shift expressions, which were formulated in the spreadsheet format of Quattro Pro (3.01). Since the Z,Z_1 and Z,Z_2 isomers of **40** possess C_2 symmetry, only the chemical shifts for each pair of symmetry-related protons were calculated.

7.6. Synthesis and Characterization

7.6.1 2-(Triphenylmethyl)thioethanoic acid (**1**)

This synthesis was performed according to the method of Brenner *et al.*[35] A solution of triphenylmethanol (48.0 g, 184.0 mmol), mercaptoacetic acid (12.2 mL, 184.0 mmol) and glacial acetic acid (160 mL) was heated to 70 °C. Boron trifluoride etherate (32.0 mL) was added and the resulting brown solution was

magnetically-stirred at room temperature for 50 minutes. The reaction mixture was poured into ice-cold distilled water, depositing a clear oil which solidified at 5 °C after 18 hours. The solid was broken and washed with distilled water, then a small amount of diethyl ether and dried *in vacuo* to give **1** as an opaque solid (40.0 g, 65%). A further crop of **1** (4.3 g, 7%) was recovered from the ether washings and purified by recrystallization from toluene. The compound showed:

mp:	155.0-157.0 °C (lit.[35] 158.5-160.0 °C)
TLC:	R_f 0.33 (90% CH_2Cl_2:10% MeOH)
IR (KBr pellet):	ν_{MAX} 3000(s)(OH), 1700(s)(C=O), 1600,1490,1445(m)(aromatic C=C), 735,695(s)(monosubstituted aromatic)
MS (FAB-):	*m/z*(RI%); 333(22)[M-1], 441(11)[M+TG-1], 243(73)[Tr-]
^{1}H NMR (CD_3COCD_3):	δ2.90(s,2H,S-CH_2), 7.25(m,15H,aryl), 10.20(s,1H,COOH) (90 MHz)
^{13}C NMR ($CDCl_3$):	δ34.67(S-CH_2), 67.44(C-Ph_3), 128.05, 144.09(aryl), 175.77(COOH) (20.1 MHz)

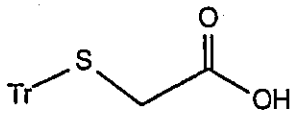

1

7.6.2 N-Succinimido 2-(triphenylmethyl)thioethanoate (2)

This synthesis was performed according to the method of Brenner *et al.*[35] To

an ice-cooled solution of **1** (5.01 g, 15.00 mmol) and *N*-hydroxysuccinimide (1.72 g, 15.00 mmol) in DME (38 mL) was added DCC (3.20 g, 15.50 mmol) such that the temperature remained at approximately 0 °C. The resulting mixture was then stored at 5 °C for 18 hours and then filtered and washed with ice-cold CH_2Cl_2. The filtered solid (DCU) was collected and discarded. The combined CH_2Cl_2 filtrate and washings were pooled and concentrated *in vacuo*, to afford **2** as a white solid. Residual amounts of DCU were removed *via* recrystallization from ethyl acetate to give large, opaque prisms (5.43 g, 84%). The compound showed:

mp:	178.5-180.0 °C (lit.[35] 178.5-179.5 °C)
TLC:	R_f 0.46 (98% CH_2Cl_2:2% MeOH)
IR (KBr pellet):	υ_{MAX} 3070(w)(aromatic C=C-H), 2940,2860(w)(aliphatic C-H), 1820,1790(s)(N-C=O), 1745(s)(C=O,ester), 1630(w),1580(w),1495(m),1445(m)(aromatic C=C), 735,690(s)(monosubstituted aromatic)
MS (+NH_3 DCI):	*m/z*(RI%); 449(7)[M+NH_4^+], 243(100)[Tr+]
^{1}H NMR ($CDCl_3$):	δ2.67[s,4H,(CH_2-C=O)$_2$], 3.08(s,2H,S-CH_2), 7.17(m,18H (overlapping residual $CHCl_3$),aryl) (500 MHz)
^{13}C NMR ($CDCl_3$):	δ25.71 [$\underline{C}H_2$-C=O)$_2$], 31.60(S-CH_2), 127.32-129.94,143.73 (aryl), 165.24(COON), 168.76(CH_2-$\underline{C}$=O) (126 MHz)

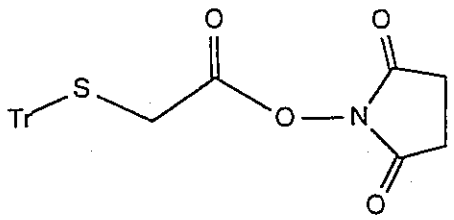

2

7.6.3 *N,N'*-Bis[2-(triphenylmethyl)thioethanoyl]-2,3- diaminopropanoic acid (3)

To a solution of activated ester **2** (6.00 g, 13.91 mmol) in dry THF (100 mL) was added a solution of 2,3-diaminopropanoic acid monohydrochloride (0.98 g, 6.95 mmol) and NEt_3 (12.00 mL) in dry MeOH (160 mL). The methanolic diamino acid solution was added in 1 mL aliquots over a thirty-minute period. The resulting turbid solution cleared after the addition of about three-quarters of the amino acid solution and the mixture was allowed to magnetically stir at room temperature for 60 minutes and then concentrated *in vacuo* to give an opaque oil. This oil was then extracted twice into CH_2Cl_2 (100 mL) from a 9:1 (v/v) of 1.0 N HCl and saturated NaCl solution (200 mL) and the combined organic solution was backwashed twice with 9:1 (v/v) 1.0 N HCl and saturated NaCl solution (200 mL). The washed CH_2Cl_2 solution was separated, dried over anhydrous $MgSO_4$, filtered and concentrated *in vacuo* to give an amorphous white solid (3.43 g, 67%). TLC and NMR spectra of this crude residue indicate approximately 30% contamination by the methanolysis product, methyl *S*-tritylthioacetate. Recrystallization from isopropanol gave **3** as a sharp-melting sample after three cycles. The compound showed:

mp: 206.0-207.5 °C

TLC: R_f 0.22 (90% CH_2Cl_2:10% MeOH)

IR (KBr pellet): ν_{MAX} 3000(s)(OH), 1725(s)(C=O,acid), 1665(s)(C=O,Amide I), 1600,1490,1440(m)(aromatic C=C), 735,690(s)(monosubstituted aromatic)

MS (FAB+): *m/z*(RI%); 737(19)[M+1], 493(31), 391(100)[M+1-$C_{22}H_{20}OSN$], 243(71)[Tr+]

^{1}H NMR (DMSO-d_6): δ2.75(s,2H,H-5), 2.79(AB q,*J*=-13.9 Hz,2H,H-7), 3.16[m,1H,H-3a(b)], 3.21[m,1H,H-3a(b)], 3.89(m,1H,H-2), 7.21-7.33(m,30H,aryl), 7.61(d,*J*=7.2 Hz,1H,C_6O-NH), 7.75(t,*J*=5.2 Hz,1H,C_6O-NH) (500 MHz)

^{13}C NMR ($CDCl_3$): δ35.66,35.84(C_5 and C_7), 41.59(C_3), 55.24(C_2), 67.72(C-Ph_3), 127.03-129.66,143.94,144.09(aryl), 169.28,170.24(br,C_4 and C_6), 177.05(br,C_1) (126 MHz)

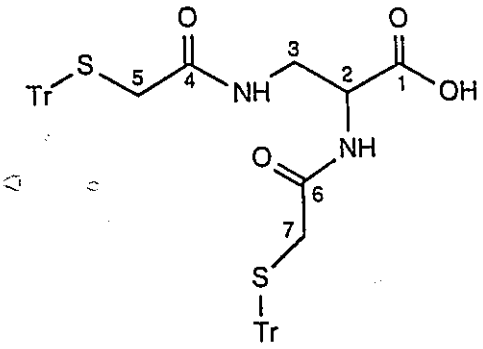

3

7.6.4 Alternative Synthesis of *N,N'*-Bis[2-(triphenylmethyl)thioethanoyl]-2,3-diaminopropanoic acid (3)

To a solution of ester **7** or **10** (1.61 mmol) in a 2:1 v/v EtOH/CH_2Cl_2 mixture (120 mL) was added EtOH-swollen, freshly-generated AMBERLYST A-26 (OH^-) anion-exchange resin (100 mL, 100 mmol), Aliquat 336 (5 drops) and ddH_2O (10 mL). After 48 hours at ambient temperature with occassional swirling, the pale-yellow suspension was filtered and the collected resin was washed with EtOH and acetone. The resin was then eluted with a mixture of 0.08 N HCl and acetone (1:1 v/v) until the eluate had a pH of less than 2, then the desorbed resin was washed with $CHCl_3$. The aqueous and organic eluants were combined and concentrated under reduced pressure at 30 °C to *ca.* one-third of its original volume, at which point a white precipitate was noted. The suspension was extracted with $CHCl_3$ and the organic layer was backwashed with 0.5 N HCl and dried over $MgSO_4$ for two hours. Filtration and rotary evaporation of the filtrate afforded a yellow oil. The oil was triturated with diethyl ether (100 mL) and the suspension was chilled at -15 °C for 18 hours, gravity filtered and the residue washed with cold ether and dried under high vacuum to give **3** as a taupe-colored solid. A further crop was isolated from the ethereal filtrate by dilution with hexanes and collection of the precipitate (total yield: 92%). Recrystallization from isopropanol gave **3** as a sharp-melting, white solid; mp 206.5-207.5 °C.

7.6.5 *N,N'*-Bis(2-mercaptoethanoyl)-2,3-diaminopropanoic acid (4)

This synthesis was a modification of the procedure of Brenner *et al.*[35] To an ice-cold, amber-yellow solution of *S*-protected acid **3** (100 mg, 0.14 mmol) in trifluoroacetic acid (1.3 mL) was added triethylsilane (45 µL, 2.1 eq., 0.29 mmol) with magnetic stirring. Immediate color discharge and the formation of a white precipitate (triphenylmethane) was observed. After 10 minutes, the suspension was diluted with

ddH_2O (10 mL), filtered, with ddH_2O washings (2 X 25 mL), and the filtrate was concentrated *in vacuo* to give **4** as a pungent-smelling, clear oil (31 mg, 87%). TLC of the product revealed a yellow spot at R_f 0.17 (40% $CHCl_3$:40% MeOH:20%(17% NH_4OH)) using a 1.98% methanolic-aqueous (9:1 v/v) solution of 5,5'-dithiobis-(2-nitrobenzoic acid) (DTNB) as a thiol detector. The compound showed:

^1H NMR (DMSO-d_6): δ3.15(s,4H,S-CH_2), 3.29,3.48(m,1H each,diastereotopic N-C<u>H</u>$_2$-CH), 4.30(m,1H,N-C<u>H</u>-COOH), 7.15(br t,~1H,SH), 8.12(t,J=5.8 Hz,1H,<u>H</u>-N-CO-CH_2), 8.27(d,J=7.9 Hz,1H,<u>H</u>-N-CO-CH), 9.45(br s,1H,SH) (500 MHz)

7.6.6 <u>*N,N'*-(2,2'-Dithioethanoyl)-2,3-diaminopropanoic acid (5)</u>

The dithiol **4** (76 mg, 0.3 mmol) was dissolved in 1 mM ammonium hydroxide (500 mL, [**4**] = 0.6 mM) with magnetic stirring and the resulting solution was adjusted to pH 10.0 with concentrated ammonium hydroxide. Filtered air was bubbled into the mixture *via* an air stone and the reaction mixture was left at room temperature for 17 hours. Filtration of the pale-yellow solution and concentration of the filtrate *in vacuo* gave a taupe-colored, amorphous material (75 mg, 94%). Recrystallization from ddH_2O afforded **5** as an off-white solid. The compound showed:

TLC: R_f 0.81 [40% $CHCl_3$:40% MeOH:20%(17% NH_4OH); bromocresol green positive; DTNB negative]

IR (KBr pellet): ν_{MAX} 3150(s)(N-H,OH bonded), 1665(s)(C=O,acid and Amide I), 1550(w)(C=O,Amide II), 1400(m), 1195(s)(C-O), 1120(m)

MS (FAB-):	*m/z*(RI%); 249(30)[M-1], 227(100)
^{1}H NMR (DMSO-d_6):	δ3.2-3.7[m,~10H(overlapping H_2O),H-5,H-7 and H-3], 3.82(m,0.4H,H-$2_{ISOMER\ 1}$), 4.41(m,0.1,H-$2_{ISOMER\ 2}$), 4.47(m,0.2H,H-$2_{ISOMER\ 3}$), 4.77(m,0.3H,H-$2_{ISOMER\ 4}$), 7.84-8.45(m,2H,amide) (500 MHz)
^{13}C NMR:	See Table 7.1

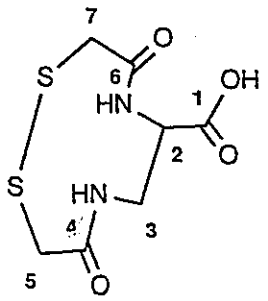

5

Table 7.1: ^{13}C NMR (126 MHz) assignments for **5** in DMSO-d_6 at 303 K.

CARBON	δ (ppm)	RI[a]
C_3	40.57	0.58
	41.25	4.60
	41.92	0.78
C_5, C_7	42.27	2.10
	42.47	0.74
	42.59	1.81
	43.50	5.04
	43.71	4.76
C_2	52.15	-0.83
	52.34	-0.85
	52.49	-0.86
	53.12	-4.21
C_1,C_4,C_6	168.17	0.30
	168.40	0.40
	168.77	0.56
	170.34	1.01
	170.48	1.06
	171.20	0.91
	171.31	0.93
	171.62	0.30

[a] Relative intensity

7.6.7 Ethyl 2,3-diaminopropanoate .2HCl (6)

This synthesis was performed according to the method of Fritzberg *et al.*[171] HCl gas was bubbled, for about 30 minutes, into a suspension of 2,3-diaminopropanoic acid .HCl (504 mg, 3.58 mmol) in absolute EtOH (84 mL) with magnetic stirring and cooling in an ice-bath. The suspension was allowed to reflux for four days. The resulting clear solution was filtered and concentrated *in vacuo* to afford **6** as an amorphous solid (704 mg, 98%). The compound showed:

mp: 164-166 °C

TLC:	R_f 0.27 (70% $CH_3CH_2CH_2OH$:28% H_2O:2% HCOOH; ninhydrin positive)
IR (KBr pellet):	ν_{MAX} 2900(s)(N-H stretch of salt), 1745(s)(C=O), 1580,1505(m)(N-H bend of salt), 1245(s)(O-C)
MS (FAB+):	*m/z*(RI%): 133(100)[(M-2HCl)+1], 265(10)[2(M-2HCl)+1]
^{1}H NMR (DMSO-d_6):	δ1.25(t,*J*=7.1 Hz,3H,O-CH_2-$C\underline{H}_3$), 3.31-3.34(m,2H,diastereotopic H-3), 4.22(m,2H,diastereotopic O-$C\underline{H}_2$-CH_3), 4.40(m,1H,H-2), 8.82(br s,6H,NH_3^+) (200 MHz)
^{13}C NMR (DMSO-d_6):	δ13.75(O-CH_2-$\underline{C}H_3$), 38.34(C_3), 50.10(C_2), 62.65(O-$\underline{C}H_2$-CH_3), 166.44(C_1) (126 MHz)

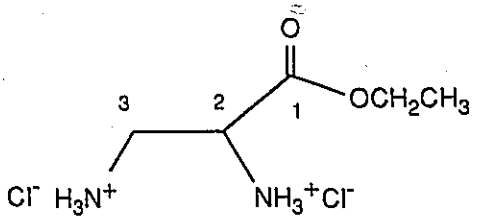

6

7.6.8 Ethyl *N,N'*-bis[2-(triphenylmethyl)thioethanoyl]-2,3- diaminopropanoate (7)

A solution of diamino ester **6** (0.91 mg, 4.41 mmol) in dry AN (40 mL) and NEt_3 (3 mL) was slowly added to a solution of the succinimido ester **2** (3.81 g, 8.82 mmol) in dry AN (160 mL) under a N_2 atmosphere with magnetic stirring. After 36 hours, the reaction mixture was concentrated *in vacuo* on a rotary evaporator and the

residual white paste was extracted into CH_2Cl_2 (2 X 100 mL) from 0.5 N HCl (100 mL). The combined CH_2Cl_2 layer was backwashed with 0.2 N $NaHCO_3$ (200 mL) and saturated brine (200 mL) and dried over $MgSO_4$ for an hour. Filtration and *in vacuo* concentration of the filtrate afforded **7** as an opaque solid (3.28g, 97%). The compound showed:

mp:	63-66 °C
TLC:	R_f 0.50 (98% CH_2Cl_2:2% MeOH)
IR (KBr pellet):	ν_{MAX} 3300(s)(N-H bonded), 3060(m)(aromatic C=C-H), 2980,2940(s)(aliphatic C-H), 1740(s)(C=O,ester), 1660(s)(C=O,Amide I), 1520(s)(N-H,Amide II), 1490,1450(s)(aromatic C=C), 1200(s)(C-O), 740,695(s)(monosubstituted aromatic C-H)
^{1}H NMR ($CDCl_3$):	δ1.27(t,*J*=6.7 Hz,3H,O-CH_2-$C\underline{H}_3$), 3.05(br s,4H,H-5 and H-7), 3.21(m,2H,H-3), 4.15(m,3H,overlapping H-2 and O-$C\underline{H}_2$-CH_3), 6.26(t,*J*=6.4 Hz,1H,C_4O-NH), 6.82(d,*J*=6.8 Hz,1H,C_6O-NH), 7.19-7.47[m,31H (overlapping residual $CHCl_3$),aryl] (200 MHz).
^{13}C NMR ($CDCl_3$):	δ13.93(O-CH_2-$\underline{C}H_3$), 35.70,35.88(C_5 and C_7), 41.27(C_3), 52.68(C_2), 61.84(O-$\underline{C}H_2$-CH_3), 67.57,67.62(C-Ph_3), 126.86-129.49, 143.74,143.79(aryl), 168.48,168.69(C_4 and C_6), 169.46(C_1) (126 MHz)

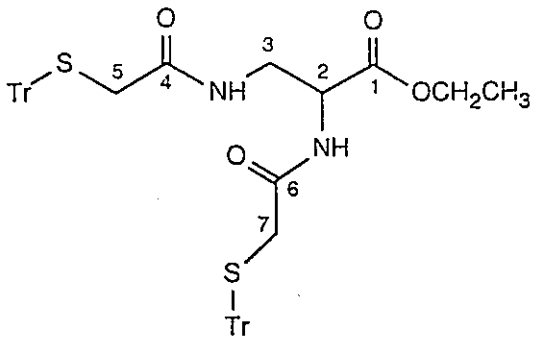

3

7.6.9 Alternative Synthesis of Ethyl *N,N'*-bis[2-(triphenylmethyl) thioethanoyl]-2,3- diaminopropanoate (7) *via* DCC Coupling of **1** and **6**

A suspension of diamino ethyl ester **6** (0.61 mg, 3.00 mmol), NEt_3 (4 drops) in AN (10 mL) was added dropwise to a magnetically-stirred solution of acid **1** (2.00 g, 6.00 mmol), DCC (1.36 g, 1.1 eq., 6.59 mmol) in AN (55 mL) after a 10-minute acid activation period under a N_2 atmosphere. After 12 hours, the pale-orange suspension was chilled at -15 °C for three hours, gravity filtered and the residue (DCU) washed with cold CH_2Cl_2 and discarded. The filtrate was concentrated to 10 mL on a rotary evaporator, diluted with CH_2Cl_2 (100 mL), washed with 0.5 N HCl (2 X 100 mL) and dried over $MgSO_4$ for two hours. Filtration and rotary evaporation of the filtrate afforded a light-amber oil (2.14 g, 107%) which solidified under high vacuum. This DCU-contaminated crude product was used without further purification for ion-exchange mediated, ester hydrolysis. For characterization purposes, a sample of this crude product was recrystallized from absolute EtOH and the recrystallized material was found to be identical to the ester **7**, which was synthesized *via* the modified procedure of Brenner *et al.*[35]

7.6.10 Ethyl *N,N'*-(2,2'-dithioethanoyl)-2,3-diaminopropanoate (**8**)

This synthesis was a modification of the method of Kamber.[37] A solution of the *S*-trityl ester **7** (400 mg, 0.52 mmol) and resublimed I_2 (145 mg, 1.1 eq., 0.57 mmol) was prepared in a degassed 2:1 v/v mixture (264 mL) of AN and absolute EtOH under an argon atmosphere. The amber-brown solution was further degassed for 30 minutes under aspirator vacuum (15 mm Hg), vented to dry argon gas and allowed to magnetically stir at room temperature. After nine hours, the reaction mixture was concentrated on a rotary evaporator to 20 mL, diluted to 250 mL with ddH_2O and washed with diethyl ether (2 X 200 mL) to remove trityl ethyl ether. After decolorization with $Na_2S_2O_3$ (2 mL, 0.1 N), the aqueous solution was concentrated on a rotary evaporator until turbidity was induced (30 mL mark). The turbid mixture was chilled at 5 °C for 10 hours, filtered and washed with ice-cold ddH_2O and dried under high vacuum to afford **8** as an opaque solid (80 mg, 55%). The compound showed:

mp:	209.0-211.0 °C
TLC:	R_f 0.78 (80% $CH_3CH_2CH_2OH$:18% H_2O:2% HCOOH)
IR (KBr pellet):	ν_{MAX} 1735(s)(C=O,ester), 1640(s)(C=O,Amide I), 1550(s)(N-H,Amide II), 450(w)(S-S)
MS (DEI):	*m/z*(RI%); 278(28)[M^+], 144(100), 102(80), 85(32), 72(58)
HRMS (DEI):	for $C_9H_{14}N_2O_4S_2$: calculated: 278.0395; observed: 278.0383
^1H and ^{13}C NMR:	See Table 7.2

Table 7.2: ^{1}H NMR (500 MHz) and ^{13}C NMR (126 MHz) assignments for **8** in DMSO-d_6 and $CDCl_3$ at 303 K.

NUCLEUS	SOLVENT	δ (ppm)	MULTIPLICITY	AREA	ASSIGNMENT
^{1}H	DMSO-d_6	1.19	t (J=6.8 Hz)	3H	O-CH_2-$\underline{C}H_3$ [b]
		3.1-3.6	m	11H[a]	H-5, H-7, H-3
		3.84	broad m	0.2H	H-2 of Isomer 1 [b]
		4.10	broad m	2H	O-$\underline{C}H_2$-CH_3 [b]
		4.43	m	0.3H	H-2 of Isomer 2 [b]
		4.52	m	0.3H	H-2 of Isomer 3 [b]
		4.85	broad m	0.2H	H-2 of Isomer 4 [b]
		8.1-8.6	m	2H	amide [b]
^{13}C		13.94	-	-	O-CH_2-$\underline{C}H_3$
		41.02-43.63	-	-	C_5 , C_7 , C_3
		52.13-53.00	-	-	C_2
		60.90	-	-	O-$\underline{C}H_2$-CH_3
		168.34-170.35	-	-	C_1 , C_4 , C_6
^{1}H	$CDCl_3$	1.18	broad s	3H	O-CH_2-$\underline{C}H_3$
		3.42	broad s	4H	H-5, H-7
		3.62	broad s	2H	H-3
		4.10	broad s	2H	O-$\underline{C}H_2$-CH_3
		4.58	broad s	1H	H-2
		7.87	broad m	1H	} amide
		8.01	broad s	1H	
^{13}C [c]		13.92	-		O-CH_2-$\underline{C}H_3$
		39.60	broad s	-	C_5, C_7
		42.33	broad s	-	C_3
		52.87	broad s	-	C_2
		61.66	broad s	-	O-$\underline{C}H_2$-CH_3
		169.22	-	-	} C_1 , C_4 , C_6
		169.70	-	-	

[a] overlapping H_2O

[b] COSY confirmed

[c] *J*-modulated confirmed

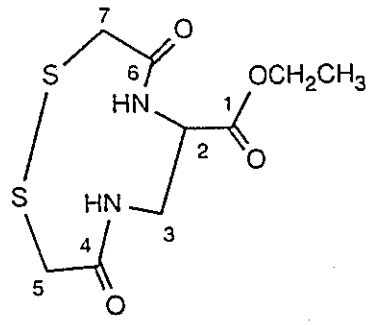

8

7.6.11 Methyl 2,3-diaminopropanoate .2HCl (9)

HCl gas was bubbled, for about 30 minutes, into a suspension of 2,3-diaminopropanoic acid .HCl (1.03 g, 7.35 mmol) in absolute EtOH (200 mL) with magnetic stirring and cooling in an ice-bath. The suspension was allowed to reflux for two days. The resulting clear solution was filtered and concentrated *in vacuo* to afford **9** as an amorphous solid (1.38 g, 98%). The compound showed:

mp:	152-155 °C
TLC:	R_f 0.20 (70% $CH_3CH_2CH_2OH$:28% H_2O:2% HCOOH; ninhydrin positive)
MS (FAB+):	*m/z*(RI%); 133(100)[(M-2HCl)+1], 265(10)[2(M-2HCl)+1]
^{1}H NMR (DMSO-d_6):	δ3.28,3.36(s,2H,diastereotopic H-3), 3.80(s,3H,OCH_3), 4.42(m,1H,H-2), 9.00(br s,6H,-NH_3^+) (90 MHz)
^{13}C NMR (DMSO-d_6):	δ38.42(C_3), 50.17,51.46(C_2 and OCH_3), 167.48(C_1) (126 MHz)

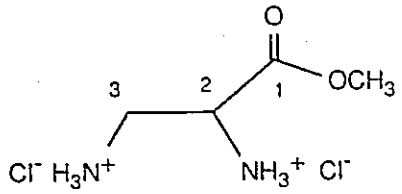

9

7.6.12 Methyl *N,N'*-bis[2-(triphenylmethyl)thioethanoyl]-2,3-diaminopropanoate (**10**)

A solution of the diamino methyl ester **9** (1.40 g, 7.34 mmol) in DME (30 mL) and NEt_3 (3 mL) was added to a solution of succinimido ester **3** (6.04 g, 14.01 mmol) in dry DME (40 mL) under a N_2 atmosphere with magnetic stirring. After 24 hours, the reaction mixture was concentrated *in vacuo* on a rotary evaporator and the residual white paste was extracted into CH_2Cl_2 (2 X 200 mL) from 0.5 N HCl (250 mL). The combined CH_2Cl_2 layer was backwashed with 0.3 N $NaHCO_3$ (200 mL) and saturated brine (200 mL) and dried with $MgSO_4$ for 18 hours. Filtration and *in vacuo* concentration of the filtrate afforded **10** as an opaque solid (5.17 g, 94%). The compound showed:

mp:	66.0-70.0 °C.
TLC:	R_f 0.44 (98% CH_2Cl_2:2% MeOH)
^{1}H NMR ($CDCl_3$):	δ3.06(s,2,H-5), 3.07(AB q,*J*=-15.0 Hz,2H,H-7), 3.23(m,2H,H-3), 3.72(s,3H,OCH_3), 4.21(m,1H,H-2), 6.22(t,*J*=5.9 Hz,1H,C_4O-NH), 6.84(d,*J*=6.7 Hz,1H,C_6O-NH), 7.23-7.44[m,35H(overlapping residual $CHCl_3$),aryl] (500 MHz).

^{13}C NMR ($CDCl_3$): δ35.39,35.59(C_5 and C_7), 40.87(C_3), 52.34,52.38(C_2 and OCH_3), 67.35,67.38(C-Ph_3), 126.58-129.22, 143.49,143.53(aryl), 168.22,168.58(C_4 and C_6), 169.71(C_1) (126 MHz)

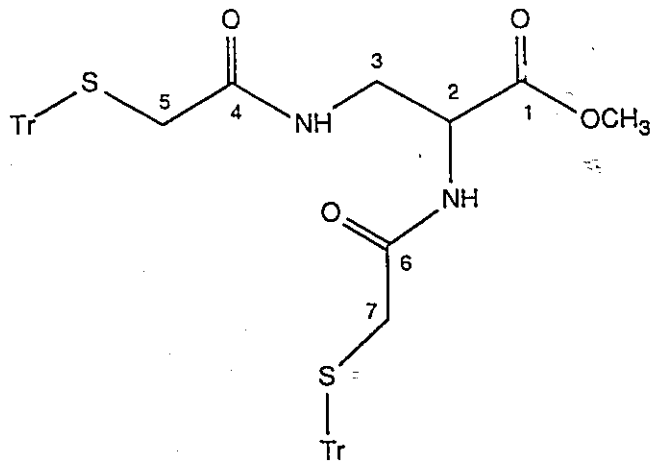

10

7.6.13 Attempted Synthesis of Cholesterol *N,N'*-bis[2-(triphenylmethyl) thioethanoyl]-2,3- diaminopropanoate (**11**) *via* CDI Coupling

To a solution of acid **3** (200 mg, 0.27 mmol) in dry THF (5 mL) under a N_2 atmosphere was added carbonyldiimidazole (57 mg, 1.3 eq., 0.35 mmol) and the solution was magnetically stirred for 10 minutes at room temperature. In the meantime, a 0.05 mole % solution of sodium imidazolide - generated *in situ* by dissolving an excess of sodium metal in a solution of imidazole (68 mg, 0.10 mmol) in dry THF (2 mL) - was added to cholesterol (100 mg, 0.26 mmol) and the resulting mixture was immediately added to the activated imidazolide with dry THF washings (2 X 0.5 mL). The light-amber solution was left at room temperature under a N_2 atmosphere for four hours, concentrated *in vacuo* and the oily residue was extracted twice into CH_2Cl_2 (200

mL) from a 0.1 M NaH_2PO_4/H_3PO_4 buffer (pH 2.1). The combined organic extracts were backwashed with more buffer (400 mL), brine (400 mL) and then dried for 18 hours over anhydrous $MgSO_4$. Filtration of the suspension and concentration of the filtrate *in vacuo* at 35 °C gave a pale-yellow oil which solidified under high vacuum. ^1H NMR spectroscopy and TLC of this solid indicated it to be primarily cholesterol.

7.6.14 Attempted Synthesis of Cholesterol *N,N'*-bis[2- (triphenylmethyl) thioethanoyl]-2,3-diaminopropanoate (**11**) *via* DCC/DMAP Coupling

To a slightly turbid suspension of acid **3** (100 mg, 0.14 mmol), cholesterol (52 mg, 0.14 mmol) and DCC (52 mg, 1.8 eq., 0.25 mmol) in CH_2Cl_2 (1.0 mL) was added a couple crystals of DMAP with stirring under a N_2 atmosphere. TLC of the reaction mixture after 12 hours showed primarily unreacted cholesterol, **3** and a new UV-active component at R_f 0.09 (CH_2Cl_2). Four cycles - each consisting of DCC addition (~50 mg), a 12-hour reaction period, followed by TLC of the reaction mixture - failed to change the initial TLC profile. Moreover, two cycles of freshly-activated, 4Å molecular sieve additions (~10 beads/cycle) and one cycle of additional DMAP (5 mg), also produced no detectable change. After one week, the reaction mixture was filtered with CH_2Cl_2 washings (4 X 10 mL) and the filtrate was washed with 0.5 N HCl (50 mL) and a saturated brine/water mixture (1:1 v/v, 2 X 50 mL) and dried with $MgSO_4$ for 18 hours. Filtering the suspension and concentrating the filtrate under reduced pressure afforded a gritty, yellow oil. Chromatographic purification of the oil on silica (20% CH_2Cl_2 in 35-60 °C petroleum ether) gave a yellow oil after solvent removal. TLC of the residue showed the major component eluted at R_f 0.09 (UV active) but with some contamination by DCC and DCU. However, ^1H NMR spectroscopy revealed the major component to be DCC. A second set of signals was detected and subsequently assigned to compound **14**.

7.6.15 Cyclohexyl *N,N'*-bis[2-(triphenylmethyl)thioethanoyl]-2,3-diaminopropanamide (**12**)

To a milky-white suspension of acid **3** (80 mg, 0.11 mmol) in CH_2Cl_2 (2.0 mL) under a N_2 atmosphere was added DCC (27 mg, 1.2 eq., 0.13 mmol) with magnetic stirring. After a 15-minute activation period, during which some clearing of the reaction mixture was noted, cyclohexylamine (28 μL, 0.22 mmol) was introduced. The reaction was diluted with CH_2Cl_2 (100 mL) after an hour and washed with 0.5 N HCl (100 mL), 0.5 N $NaHCO_3$ (100 mL) and then dried over $MgSO_4$ for an hour. Filtration and concentration of the filtrate *in vacuo* afforded a granular film. This residue was resuspended in $CDCl_3$ (1 mL), filtered through glass wool and the filtrate was used for TLC and NMR spectroscopy. The collected solid was determined to be DCU (NMR, TLC). The compound showed:

TLC:	R_f 0.32 (98% CH_2Cl_2:2% MeOH)
^{1}H NMR ($CDCl_3$):	δ1.0-1.9(m,10H,$(CH_2)_5$), 2.90-2.93(m,4H,H-5 and H-7), 3.56(br m,1H,H-1'), 3.88(m,1H,H-2), 6.49(t,*J*=5.8 Hz,1H,C_4O-NH), 6.69(d,*J*=6.9 Hz,1H,C_1O-NH), 7.06(d,*J*=6.2 Hz,1H,C_6O-NH), 7.15-7.48[m,32H (overlapping residual $CHCl_3$),aryl] (500 MHz)

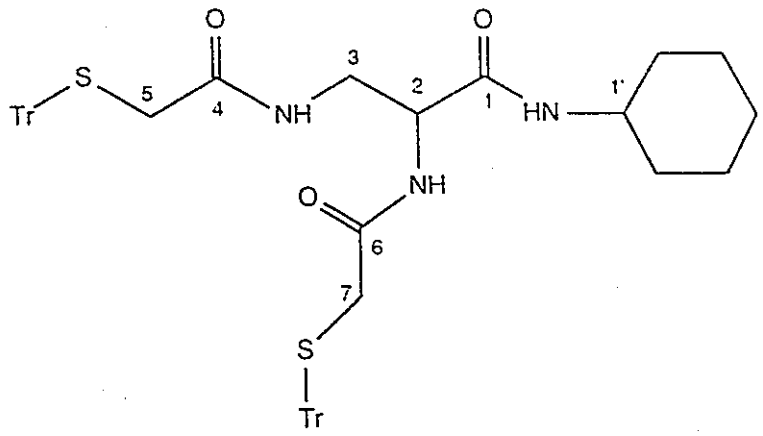

12

7.6.16 Cyclohexyl *N,N'*-bis[2-(triphenylmethyl)thioethanoyl]-2,3-diaminopropanoate (**13**)

To a milky-white suspension of acid **3** (80 mg, 0.11 mmol) in CH_2Cl_2 (2.0 mL) under a N_2 atmosphere was added DCC (25 mg, 1.3 eq., 0.12 mmol) with magnetic stirring. After a 15-minute activation period, during which some clearing of the reaction mixture was noted, cyclohexanol (18 μL, 0.18 mmol) and a couple small crystals of DMAP was introduced. The reaction was diluted with CH_2Cl_2 (100 mL) after 48 hours and washed with 0.5 N HCl (100 mL), distilled water (100 mL) and dried over $MgSO_4$ for an hour. Filtration and concentration of the filtrate *in vacuo* afforded a granular, oily film (98 mg). This residue was resuspended in CH_2Cl_2 (1 mL) and filtered through glass wool with CH_2Cl_2 washings (2 X 1 mL). The collected solid was determined to be DCU (NMR, TLC). Concentration of the filtrate *in vacuo* and flash chromatography of the yellow residue on silica (step-wise elution with 100% CH_2Cl_2 then 2% MeOH in CH_2Cl_2) gave a yellow, oily film (*ca.* 20 mg). TLC indicated contamination with DCU and a second, more intense, component at R_f 0.67 (**14**). The compound showed:

TLC: R_f 0.75 (98% CH_2Cl_2:2% MeOH)

^{1}H NMR ($CDCl_3$): δ0.88-1.97[m,38H,$(CH_2)_5$], 3.05-3.11(m,5H,H-5 and H-7), 3.22(m,2H,H-3), 4.33(m,1H,H-2), 4.78(br m,1H,H-1'), 6.14(t,*J*=6.5 Hz,1H,C_4O-NH), 6.85(d,*J*=6.6 Hz,1H,C_6O-NH), 7.1-7.5[m,39H (overlapping residual $CHCl_3$),aryl] (200 MHz)

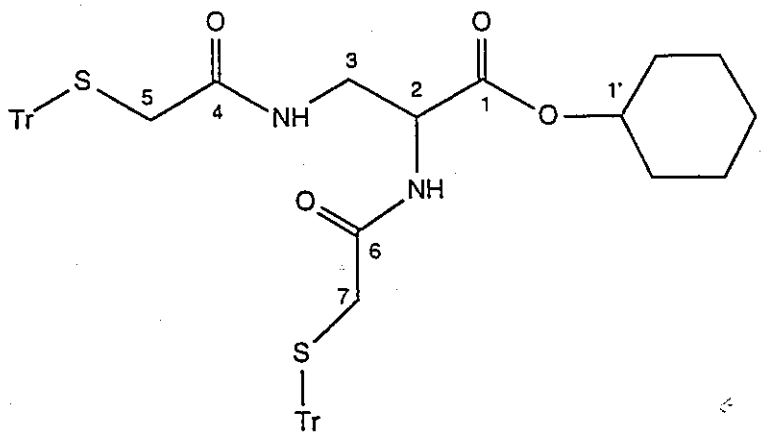

13

7.6.17 Dicyclohexylurea *N,N'*-bis[2-(triphenylmethyl)thioethanoyl]-2,3-diaminopropanamide (**14**)

To a milky-white suspension acid **3** (70 mg, 0.10 mmol) in CH_2Cl_2 (2 mL) under a N_2 atmosphere was added DCC (24 mg, 1.1 eq., 0.10 mmol) with magnetic stirring. After a 15-minute activation period, during which some clearing of the reaction mixture was noted, DMAP (1.2 mg, 10 mol%) was introduced. TLC of the slightly turbid, yellow reaction mixture after 12 hours revealed unreacted acid and DCC (16 mg) was further added. After four days, the reaction mixture was flash chromatographed on silica (step-wise elution with 100% CH_2Cl_2 then 2% MeOH in

CH_2Cl_2) to afford a yellow, gritty film after *in vacuo* removal of the solvent. The residue was suspended in $CDCl_3$ (1 mL), filtered through glass wool with $CDCl_3$ washings (2 X 0.5 mL) and concentrated *in vacuo* to give a yellow foam (56 mg). TLC indicated DCU contamination and a second major component at R_f 0.8. The compound showed:

TLC: R_f 0.67 (98% CH_2Cl_2:2% MeOH)

^{1}H NMR ($CDCl_3$): δ0.88-1.97[m,61H,$(CH_2)_5$], 3.05-3.11(m,6.5H,H-5 and H-7), 3.22(m,2H,H-3), 3.30-3.75(m,H-3' and residual methines of DCU), 3.95(m,1H,H-1'), 4.27(m,1H,H-2), 5.88(t,*J*=5.5 Hz,1H,C_2-O-NH), 6.10(t,*J*=7.2 Hz,1H,C_4O-NH), 7.00(d,*J*=5.8 Hz,1H,C_6O-NH), 7.1-7.5[m,109H (overlapping residual $CHCl_3$),aryl] (200 MHz)

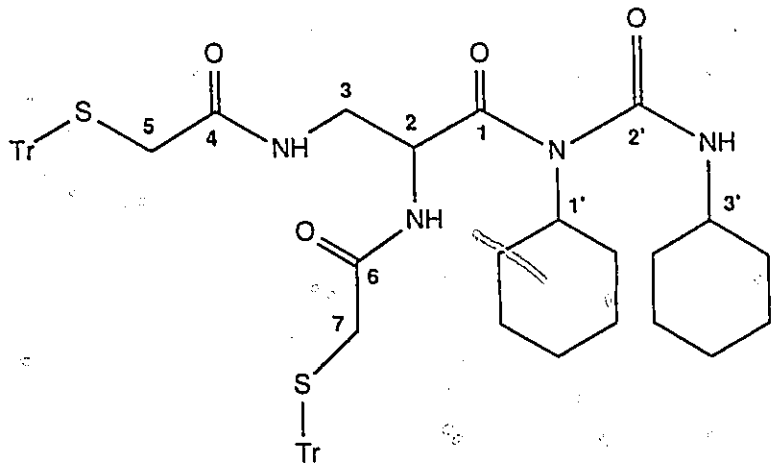

14

7.6.18 Cholesteryl diphenylethanoate (15)

To a magnetically-stirred solution of diphenylacetic acid (500 mg, 2.36 mmol), cholesterol (851 mg, 2.20 mmol) and DCC (535 mg, 1.1 eq., 2.59 mmol) in CH_2Cl_2 (7 mL) at room temperature was added DMAP (29 mg, 10 mol%). After four hours, the suspension was filtered (to remove precipitated DCU) and the filtrate diluted with CH_2Cl_2 (100 mL). The organic phase was washed with 0.5 N HCl (2 X 100 mL), distilled water (100 mL), 0.5 N $NaHCO_3$ (2 X 100 mL) and dried with $MgSO_4$ for 18 hours. Filtration and concentration of the filtrate *in vacuo* afforded **15** as an opaque solid (1.22 g, 89%). The compound showed:

mp:	150.0-155.0 °C
TLC:	R_f 0.93 (98% CH_2Cl_2:2% MeOH)
MS (+NH_3 DCI):	*m/z*(RI%); 598(23)[M+NH_4^+], 386(33)[M-($C_{14}H_{12}O_2$)+NH_4^+], 369(100)[M-($C_{14}H_{12}O_2$)+1], 230(38)[$C_{14}H_{11}O_2$+NH_4^+]
^{1}H NMR ($CDCl_3$):	δ0.70-2.36(m,47H,steroid), 4.69(m,1H,H-3), 5.01(s,1H,H-2'), 5.40(m,1H,H-6), 7.27-7.37[m,11H (overlapping residual $CHCl_3$),aryl] (200 MHz)

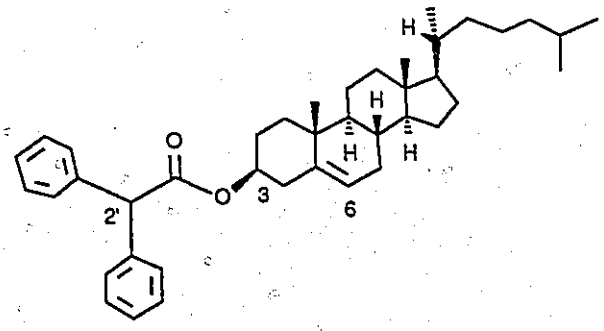

15

7.6.19 Methyl *N*-{*N'*,*N''*-bis[2-(triphenylmethyl)thioethanoyl]-2,3-diaminopropanoyl} glycinate (**16**)

A suspension of glycine methyl ester .HCl (195 mg, 1.55 mmol), NEt_3 (6 drops) in AN (10 mL) was added dropwise to a magnetically-stirred solution of acid **3** (1.14 g, 1.55 mmol) and DCC (352 mg, 1.1 eq., 1.70 mmol) in CH_2Cl_2 (20 mL) after a 10-minute activation period under a N_2 atmosphere. After 12 hours, the suspension was chilled at -15 °C for two hours and filtered (to remove DCU). The filtrate was diluted with $CHCl_3$ (150 mL) and washed with 0.5 N $NaHCO_3$ (300 mL) then 0.5 N HCl (2 X 300 mL) and dried over $MgSO_4$ for two hours. Filtration and rotary evaporation of the filtrate gave **16** as an off-white solid (1.19 g, 95%). The compound showed:

mp:	168.0-171.0 °C
TLC:	R_f 0.30 (98% CH_2Cl_2:2% MeOH)
MS (+NH_3 DCI):	*m/z*(RI%); 808(<1)[M+1], 322(10), 262(38), 243(100)[Tr+], 167(48)
IR (KBr pellet):	ν_{MAX} 3400,3250(s)(N-H bonded), 3060(w)(aromatic C=C-H), 2930,2850 (w)(aliphatic C-H), 1735(m)(C=O,ester), 1660(s)(C=O,Amide I), 1540(m)(N-H,Amide II), 1490,1440(m)(aromatic C=C), 735,690(s)(monosubstituted aromatic C-H)
^{1}H NMR ($CDCl_3$):	δ3.03[m,5H,H-5,H-7 and H-3a(b)], 3.27[m,1H,H-3a(b)], 3.70(s,3H, $COOCH_3$), 3.92(ABX,2H,H-8), 3.99(m,1H,H-2), 6.53(t,*J*=6.3 Hz,1H,C_4O-NH), 7.09(d,*J*=5.8 Hz,1H,C_6O-NH), 7.16-7.44[m,31H(overlapping residual $CHCl_3$),aryl and C_1O-NH] (500 MHz)

^{13}C NMR ($CDCl_3$): δ35.80,36.06(C_5 and C_7), 41.18(C_3), 52.31(C_2), 54.75(OCH_3), 67.72(C-Ph_3), 126.98-129.56, 143.93(aryl), 169.35,169.69,169.80,170.13(C_1,C_4,C_6 and C_9) (126 MHz)

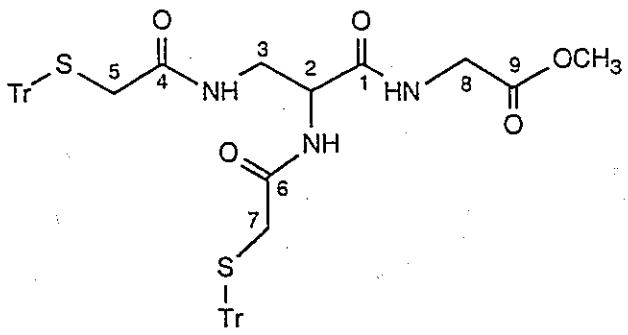

16

7.6.20 *N*-{*N'*,*N''*-Bis[2-(triphenylmethyl)thioethanoyl]-2,3- diaminopropanoyl} glycine (**17**)

To a magnetically-stirred suspension of ester **16** (1.19 g, 1.47 mmol) in absolute EtOH (25 mL) was added 1 NaOH (2.9 mL). After 12 hours, the suspension was rotary evaporated to 10 mL, diluted with 0.5 N $NaHCO_3$ (300 mL) and extracted with $CHCl_3$ (200 mL). The organic layer was washed with 0.5 N HCl (2 X 300 mL) and dried over $MgSO_4$ for two hours. Filtration and rotary evaporation of the filtrate gave a yellow solid. This crude product was dissolved in $CHCl_3$ (3 mL), diluted with diethyl ether (60 mL) and filtered to afford **17** as an off-white solid (1.06 g, 91%). The compound showed:

mp: 118.5-121.0 °C

TLC: R_f 0.13 (90% CH_2Cl_2:10% MeOH)

IR (KBr pellet): ν_{MAX} 3300(s)(N-H bonded), 3060(w)(aromatic

C=C-H), 2920(w)(aliphatic C-H), 1730(s)(C=O,acid), 1650,1635(s)(C=O,Amide I), 1530(s)(N-H,Amide II), 1490,1440(m)(aromatic C=C), 1200(m), 740,695(s)(monosubstituted aromatic C-H)

^{1}H NMR (CD_3COCD_3): δ2.89,2.92(s,4H,H-5 and H-7), 3.31[m,3H (absorbed H_2O),H-3], 3.89(m,2H,H-8), 4.25(m,1H,H-2), 7.17-7.38(m,29H,aryl) (500 MHz)

^{13}C NMR (CD_3COCD_3): δ35.11(C_5 and C_7), 39.55(C_3), 40.24(C_8), 52.70(C_2), 66(C-Ph_3), 125.83-128.51,143.31(aryl), 167.24, 167.87,168.78,169.26(C_1,C_4,C_6 , and C_9) (126 MHz)

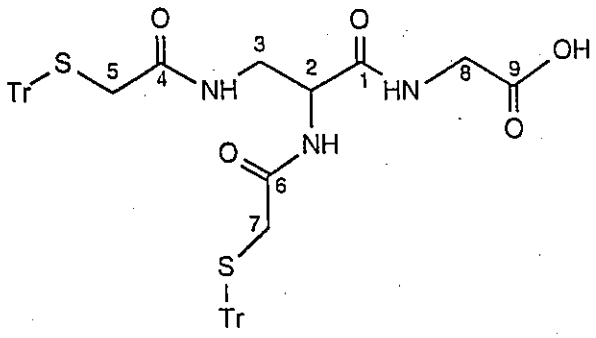

16

7.6.21 Cholesteryl *N*-{*N'*,*N''*-bis[2-(triphenylmethyl)thioethanoyl]-2,3-diaminopropanoyl} glycinate (**18**)

To an ice-bath cooled suspension of acid **17** (150 mg, 0.19 mmol), cholesterol (73 mg, 0.19 mmol), DMAP (2 mg, 10 mol%) in CH_2Cl_2 (2 mL) was added DCC (59 mg, 1.5 eq., 0.28 mmol) under a N_2 atmosphere. After five minutes, the opaque suspension was allowed to warm to ambient temperature and significant

clearing was noted after 10 minutes. After 48 hours, the reaction suspension was chilled for two hours at -15 °C, filtered and the residue (DCU) was washed with cold CH_2Cl_2 and discarded. The filtrate was diluted with 30-60 °C petroleum ether (50 mL) and stored at -15 °C for 18 hours. The suspension was filtered and the residue washed with cold petroleum ether and dried under high vacuum to afford cholesterol-free crude product as an opaque solid (205 mg). Chromatographic purification of this crude (stepwise elution: CH_2Cl_2 then 1% MeOH in CH_2Cl_2) gave **18** as a pure sample (119 mg, 54%). The compound showed:

mp:	92.5-96.0 °C
TLC:	R_f 0.81 (90% CH_2Cl_2:10% MeOH)
IR (KBr pellet):	ν_{MAX} 3320(s)(N-H bonded), 3050(m)(aromatic C=C-H), 2940(s)(aliphatic C-H), 1740(s)(C=O,ester), 1660(s)(C=O,Amide I), 1510(s)(N-H,Amide II), 1490,1440(s)(aromatic C=C), 1200(s)(C-O), 730,690(s)(monosubstituted aromatic C-H)
^{1}H NMR ($CDCl_3$):[172]	δ0.70-2.32(m,48H,steroid skeleton), 2.93-3.14[m,5H,H-5',H-7' and H-3'a(b)], 3.20-3.34[m,1H,H-3'a(b)], 3.88(ABX,2H,H-8'), 4.01(br s,1H,H-2'), 4.62(m,1H,H-3), 5.36(br s,1H,H-6), 6.55(br t,1H,C_4'O-NH), 7.09(d,J=5.9 Hz,1H,C_6'O-NH), 7.13(br s,1H,C_1'O-NH), 7.18-7.43[m,32H (overlapping residual $CHCl_3$),aryl] (500 MHz)
^{13}C NMR ($CDCl_3$):[173]	δ11.85(C_{18}), 18.71-39.72(C_5',C_7' and remaining steroid), 41.51(C_3'), 41.93(C_8'), 50.02(C_9),

54.66($C_{2'}$), 56.15(C_{17}), 56.70(C_{14}), 67.70(C-Ph_3), 75.37(C_3), 122.92(C_6), 129.55-126.96,143.95(aryl), 139.34(C_5), 168.67,169.25,169.71,170.05($C_{1'}$,$C_{4'}$,$C_{6'}$ and $C_{9'}$) (126 MHz)

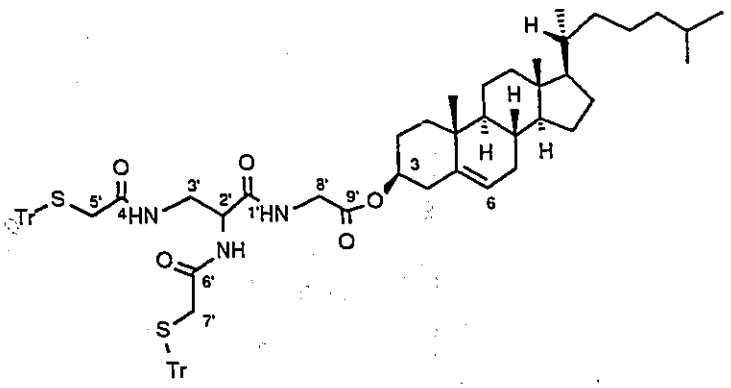

18

7.6.22 Cholesteryl *N*-[*N'*,*N''*-(2,2'-dithiobisethanoyl)-2,3- diaminopropanoyl] glycinate (**19**)

This synthesis was a modification of the method of Kamber.[37] Resublimed I_2 (120 mg, 1.1 eq., 0.47 mmol) was added to a solution of *S*-tritylated steroid conjugate **18** (500 mg, 0.43 mmol) in degassed absolute EtOH (100 mL) under a N_2 atmosphere. The amber-brown solution was further degassed for 30 minutes under aspirator vacuum (15 mm Hg), vented to dry N_2 gas and allowed to magnetically stir at room temperature. After 12 hours, the amber suspension was rotary evaporated to 1 mL, diluted with ddH_2O (70 mL), decolorized with 0.1 N $Na_2S_2O_3$ (5 drops) and the resultant suspension was extracted with $CHCl_3$ (100 mL). The organic layer was washed with a dilute solution of $Na_2S_2O_3$ and dried over Na_2SO_4 for two hours.

Filtration and concentration of the filtrate *in vacuo* to 10 mL followed by gradual dilution with cold hexanes afforded an amber solid (221 mg) after filtration. Chromatographic purification of the resultant crude product (stepwise elution: 100% CH_2Cl_2 followed by 5% MeOH in CH_2Cl_2) gave **19** as an off-white solid (94 mg, 32%). The compound showed:

mp:	165.0-167.5 °C
TLC:	R_f 0.51 (90% CH_2Cl_2:10% MeOH)
IR (KBr pellet):	ν_{MAX} 3300(s)(N-H bonded), 3060(w)(C=C-H) 2940,2869(s)(aliphatic C-H), 1740(s)(C=O,ester), 1655(s)(C=O,Amide I), 1530(s) (N-H,Amide II), 1200(s)(C-O)
MS (+NH_3 DCI):	*m/z*(RI%); 402(10), 383(12), 367(50), 262(100)
^{1}H NMR ($CDCl_3$):[172]	δ0.68-2.32(m,48H,steroid skeleton), 3.07[br s,1H,H-3'a(b)], 3.23-3.82[br overlapping s,5H,H-5',H-7' and H-3'a(b)], 3.82-4.33(br overlapping s,2H,H-8'), 4.62(br s,1H,H-3), 4.75(br s,1H,H-2'), 5.36(br s,1H,H-6), 6.80-8.40(br m,3H,amide) (500 MHz)
^{13}C NMR ($CDCl_3$):[173]	δ11.85(C_{18}),18.72-39.74($C_{5'}$,$C_{7'}$ and remaining steroid), 41.67(br,$C_{3'}$), 42.32($C_{8'}$), 50.01(C_9), 56.22(C_{17}), 56.71(C_{14}), 75.47(br,C_3), 122.99(C_6), 139.28(C_5), 169.69(br,$C_{1'}$,$C_{4'}$,$C_{6'}$ and $C_{9'}$) (126 MHz)

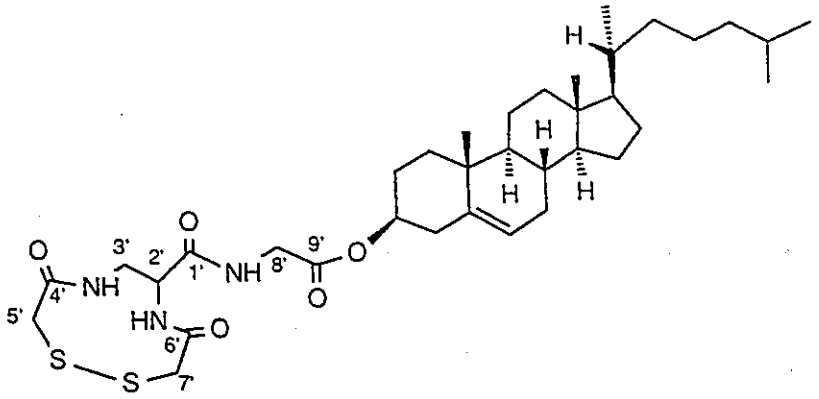

19

7.6.23 Digitoxigenin 3-[*N*-{*N'*,*N''*-bis[2-(triphenylmethyl)thioethanoyl]- 2,3-diaminopropanoyl} glycinate] (**20**)

To an ice bath-cooled suspension of acid **17** (318 mg, 0.40 mmol), digitoxigenin (Sigma Chemical Co.) (150 mg, 0.40 mmol), DMAP (4 mg, 10 mol%) in CH_2Cl_2 (6 mL) was added DCC (91 mg, 1.1 eq., 0.44 mmol) under a N_2 atmosphere. After five minutes, the opaque suspension was allowed to warm to ambient temperature and significant clearing was noted after 10 minutes. After 48 hours, the reaction suspension was chilled for two hours at -15 °C, filtered and the residue (DCU) was washed with cold CH_2Cl_2 and discarded. The filtrate was rotary evaporated to a pale-yellow solid and dissolved in MeOH (10 mL). Five drops of dH_2O was added and the resulting suspension was stored at -15 °C for two hours. The suspension was filtered and the residue washed with cold MeOH/H_2O (98:2 v/v) and dried under high vacuum to afford **20** as an off-white residue (257 mg). The turbid, aqueous-methanolic filtrate was concentrated to 3 mL, diluted with dH_2O (2 mL), filtered and the residue washed with cold MeOH/H_2O (98:2 v/v). After drying under high vacuum, 15 mg of digitoxigenin-free product (total yield = 272 mg, 59%) was recovered. The compound showed:

mp: 115.0-118.0 °C

TLC: R_f 0.71 (90% CH_2Cl_2:10% MeOH)

IR (KBr pellet): ν_{MAX} 3380(s)(N-H,O-H bonded), 3050(m)(aromatic C=C-H), 2930(s)(aliphatic C-H), 1740(s)(C=O,ester), 1660(s)(C=O,Amide I), 1510(s)(N-H,Amide II), 1485,1440(s)(aromatic C=C), 1200(m)(C-O), 735,690(s)(monosubstituted aromatic C-H)

^{1}H NMR ($CDCl_3$):[172] δ0.88(s,3H,H-18), 0.95(s,3H,H-19), 1.20-2.14(m,28H,steroid), 2.78(m,1H,H-17), 3.02[m,5H,H-5',H-7' and H-3'a(b)], 3.30[m,1H,H-3'a(b)], 3.92(ABX,2H,H-8'), 4.00(m,1H,H-2'), 4.89(AB q,*J*=-18.1 Hz,2H,H-21), 5.12(br s,1H,H-3), 5.88(s,1H,H-22), 6.55(t,*J*=6.3 Hz,1H,C_4'-O-NH), 7.10(d,*J*=5.8 Hz,1H,C_6'-O-NH), 7.18-7.44[m,31H,(overlapping residual $CHCl_3$),aryl] (500 MHz)

^{13}C NMR ($CDCl_3$):[173] δ15.73(C_{18}), 21.11,21.19(C_7 and C_{11}), 23.61(C_{19}), 24.96-35.10(remaining steroid), 35.66,36.69(C_5 and C_9), 35.66,35.81(C_5' and C_7'), 39.94(C_{12}), 41.56(C_3'), 41.77(C_8), 42.04(C_8'), 49.55(C_{13}), 50.85(C_{17}), 54.74(C_2'), 67.67(C-Ph_3), 71.90(C_3), 73.40(C_{20}), 85.43(C_{14}), 117.69(C_{22}), 126.95-129.53,143.91(aryl), 168.71,169.28,169.71,170.06(C_1',C_4' ,C_6' and C_9'), 174.43(C_{23}) (126 MHz)

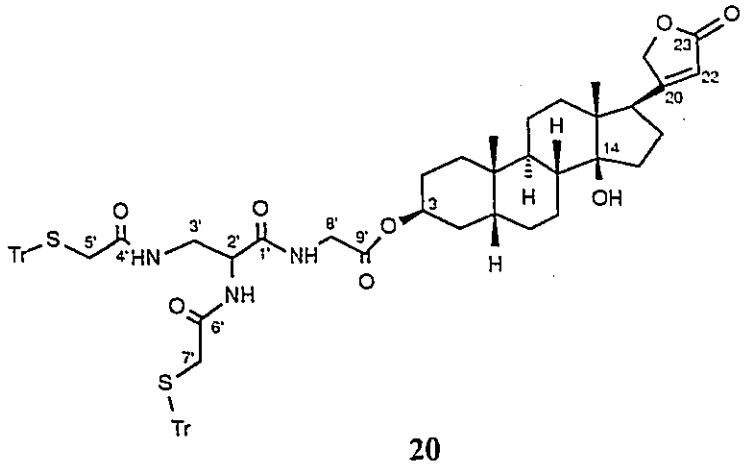

20

7.6.24 Digitoxigenin *N*-{*N'*,*N''*-(2,2'-dithiobisethanoyl)-2,3-diaminopropanoyl} glycinate (**21**)

This synthesis was a modification of the method of Kamber.[37] Resublimed I_2 (77 mg, 1.1 eq., 0.30 mmol) was added to a solution of *S*-tritylated steroid conjugate **20** (316 mg, 0.27 mmol) in degassed absolute EtOH (80 mL) under a N_2 atmosphere. The amber-brown solution was further degassed for 30 minutes under aspirator vacuum (15 mm Hg), vented to dry N_2 gas and allowed to magnetically stir at room temperature. After 12 hours, the amber-brown suspension was concentrated to 5 mL, diluted with CH_2Cl_2 (70 mL) and the resultant suspension filtered with CH_2Cl_2 washings. The tan-brown residue was dissolved in a 15% v/v MeOH in $CHCl_3$ mixture (60 mL) and decolorized by washing with dilute aqueous $Na_2S_2O_3$ solution (200 mL). A solid precipitated and was separated by decanting the liquid phases. The residue was redissolved in 15% v/v MeOH in $CHCl_3$ (30 mL), filtered and the filtrate was rotary evaporated to give **21** as an opaque solid (43 mg, 24%) which was homogenous *via* TLC. The compound showed:

mp:	180 °C (dec.)
TLC:	R_f 0.34 (90% CH_2Cl_2:10% MeOH)
IR (KBr pellet):	ν_{MAX} 3415(s)(O-H,N-H bonded), 2920,2850(s)(aliphatic C-H), 1735(s)(C=O,ester), 1655(s)(C=O,Amide I), 1530(s)(N-H,Amide II), 1200(s)(C-O)
MS (FAB+):	*m/z*(RI%); 664(5)[M+1], 339(12)
^{1}H NMR ($CDCl_3/CD_3OD$):[172]	δ0.81(s,3H,H-18), 0.90(s,3H,H-19), 1.11-2.12(m,28H,steroid), 2.73(m,1H,H-17), 3.20-3.80(br m,7H,H-5',H-7' and H-3'), 3.95(br m,2H,H-8'), 4.89(AB q,*J*=-18.3 Hz,2H,H-21), 5.08(br s,1H,H-3), 5.80(s,1H,H-22), 7.17(br m,0.5H,exchanging amide) (500 MHz)
^{13}C NMR ($CDCl_3/CD_3OD$):[173]	δ15.31(C_{18}), 20.79(C_7 and C_{11}), 23.14(C_{19}), 24.58-34.93(remaining steroid), 35.25,36.70(C_5 and C_9), 39.51(C_{12}), 40.94(br,$C_{3'}$), 41.02(C_8), 41.15(br,$C_{8'}$), 49.51(C_{13}), 50.66(C_{17}), 52.39(br)($C_{2'}$), 72.01,72.10(C_3), 73.63(C_{20}), 84.64(C_{14}), 116.74(C_{22}), 168.95,169.28,169.72,170.29 (br,$C_{1'}$, $C_{4'}$,$C_{6'}$ and $C_{9'}$), 175.50,176.03(C_{23}) (126 MHz)

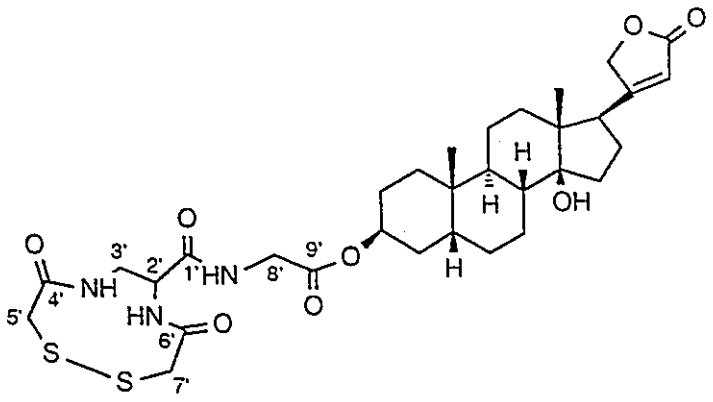

21

7.6.25 3-Cholamido-1-{*N,N'*-bis[2-(triphenylmethyl) thioethanoyl]-2,3-diaminopropanamido} propane (22)

To a magnetically-stirred solution of acid **3** (316 mg, 0.43 mmol) in DMF (2 mL) was added DCC (97 mg, 1.1 eq., 0.47 mmol) under a N_2 atmosphere. After 10 minutes, a solution of 3-cholamidopropylamine[102] (200 mg, 0.43 mmol), NEt_3 (2 drops) in DMF (2 mL) was added and the mixture was allowed to stir under a N_2 atmosphere. After five hours, the reaction mixture was added to 0.5 N HCl (500 mL) and extracted with CH_2Cl_2 (200 mL). The organic layer was backwashed with 0.5 N $NaHCO_3$ (500 mL) and dH_2O (500 mL) and dried over $MgSO_4$ for 48 hours. Filtration and rotary evaporation of the filtrate afforded a solid (497 mg, 98%). Chromatographic purification of this crude material (stepwise elution: CH_2Cl_2 then 10% MeOH in CH_2Cl_2) gave **22** as an opaque solid. The compound showed:

mp:	129.0-131.0 °C
TLC:	R_f 0.17 (90% CH_2Cl_2:10% MeOH)
IR (KBr Pellet):	ν_{MAX} 3380(s)(N-H,O-H bonded), 3060(m)(aromatic C=C-H), 2930,2860(s)(aliphatic C-H), 1655(s)(C=O,Amide I), 1525(m)(N-H,Amide II),

1490,1445(m)(aromatic C=C), 1380(w), 1075(m), 1030(m), 740,695(s)(monosubstituted aromatic C-H)

^{1}H NMR (DMSO-d_6):[172] δ0.57(s,3H,H-18), 0.80(s,3H,H-19), 0.83-2.15(m,42H,steroid), 2.72,2.78 (s,4H,H-5' and H-7'), 2.98[br m,5H,H-25,H-27 and H-3'a(b)], 3.17[br m,3H,H-3 and H-3'a(b)], 3.62(br s,1H,H-7), 3.79(br s,1H,H-12), 3.98,4.07,4.32(br s,3H total,-OH), 4.13(m,1H,H-2'), 7.20-7.32(m,36H,aryl), 7.73(br t,1H,C_{24}O-NH), 7.86(m,2H,C_1·O-NH and C_4·O-NH), 8.00(d,*J*=7.6 Hz,1H,C_6·O-NH) (500 MHz)

^{13}C NMR (DMSO-d_6):[173] δ12.31(C_{18}), 17.10(C_{21}), 22.60(C_{19}), 22.81(C_{15}), 26.21(C_9), 27.28(C_{16}), 28.54(C_{11}), 29.01(C_{26}), 30.40(C_2), 31.72(C_{22}), 32.57(C_{23}), 34.37(C_1), 34.89(C_6), 35.15(C_{10}), 35.32(C_{20}), 35.89,35.95(C_5· and C_7·), 36.04(C_{25}), 36.21(C_{27}), 40.67(C_3·), 41.35(C_5), 41.54(C_{14}), 45.73(C_{13}), 46.10(C_{17}), 54.83(C_2·), 65.90(C-Ph_3), 66.28(C_7), 70.48(C_3), 71.06(C_{12}), 126.57-129.43,144.05(aryl), 169.12,167.76,167.42 (C_1·, C_4· and C_6·), 172.78(C_{24}) (126 MHz)

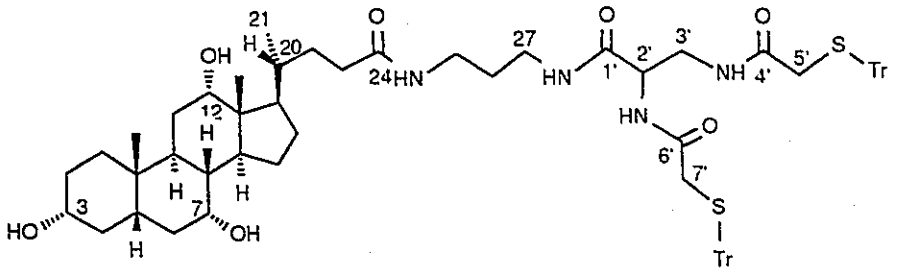

22

7.6.26 3-Cholamido-1-[*N,N'*-(2,2'-dithiobisethanoyl)-2,3- diaminopropanamido] propane (23)

This synthesis was a modification of the method of Kamber.[37] Resublimed I_2 (71 mg, 1.1 eq., 0.28 mmol) was added to a solution of *S*-tritylated steroid conjugate **22** (300 mg, 0.25 mmol) in degassed absolute EtOH (60 mL) under a N_2 atmosphere. The amber-brown solution was further degassed for 30 minutes under aspirator vacuum (15 mm Hg), vented to dry N_2 gas and allowed to magnetically stir at room temperature. After 12 hours, the amber solution was rotary evaporated to 1 mL, diluted with ddH_2O (30 mL), decolorized with 0.1 N $Na_2S_2O_3$ (5 drops) and the resultant light-brown precipitate was vacuum filtered and washed with ddH_2O and $CHCl_3$. The precipitate was dissolved in hot absolute EtOH (10 mL), decolorized with 0.1 N Na_2SO_3 (3 drops) and, after concentration to 1 mL, diluted with a 1:1 v/v mixture of ddH_2O and saturated brine. The precipitated solid was vacuumed filtered, washed with ddH_2O and $CHCl_3$, redissolved in hot EtOH (5 mL) and precipitated by the gradual addition of CH_2Cl_2 (50 mL). The suspension was stored at -15 °C for 18 hours and filtered with cold CH_2Cl_2 washings to afford **23** as an opaque solid (78 mg, 45%). The compound showed:

mp:	174.0 °C (dec.)
TLC:	R_f 0.79 (100% MeOH)
IR (KBr Pellet):	ν_{MAX} 3400(s)(N-H,O-H bonded), 2930,2860(m)(aliphatic C-H), 1655(s)(C=O,Amide I), 1540(m) (N-H,Amide II), 1075,1040(w)
MS (FAB+):	*m/z*(RI%); 698(70)[M+1], 466(100)[(M+1) - $C_7H_7N_2O_3S_2$]
^{1}H NMR (DMSO-d_6):[172]	δ 0.57(s,3H,H-18), 0.79(s,3H,H-19), 0.83-2.24(m,31H,steroid), 3.01-3.07 (br m,4H,H-25 and H-27), 3.17(m,2H,H-3β), 3.25-3.59[br m,8.4H (overlapping H_2O),H-3',H-5' and H-7'], 3.60(br m,1H,H-7β), 3.76(br m,1H,H-12β), 3.96,4.05,4.28(d,*J*=3.3 Hz,1H,,-OH), 4.30-4.42(br m,0.5H,H-2'$_{ISOMER\ 1}$), 4.68(br m,0.4H,H-2'$_{ISOMER\ 2}$), 7.95-8.43 (br m,4H,amide) (500 MHz)
^{13}C NMR (DMSO-d_6):[173]	δ12.29(C_{18}), 17.07(C_{21}), 22.57(C_{19}), 22.75(C_{15}), 26.17(C_9), 27.23(C_{16}), 28.51(C_{11}), 29.07(C_{26}), 30.35(C_2), 31.70(C_{22}), 32.53(C_{23}), 34.34(C_1), 34.84(C_6), 35.13(C_{10}), 35.28(C_{20}), 36.03,36.26, 36.39(br)($C_{5'}$,$C_{7'}$,C_{25},$C_{2\ 7}$), 40.76,42.00(br)($C_{3'}$), 41.32(C_8), 41.50(C_{14}), 45.70(C_5), 46.10(C_{13}), 47.48(C_{17}), 52.18,52.91(br)($C_{2'}$), 66.19(C_7), 70.38(C_3), 70.96(C_{12}), 167.96,168.21,168.33, 168.47,169.16, 169.61(br)($C_{1'}$,$C_{4'}$,$C_{6'}$), 172.12,172.37,172.51(C_{24}) (126 MHz)

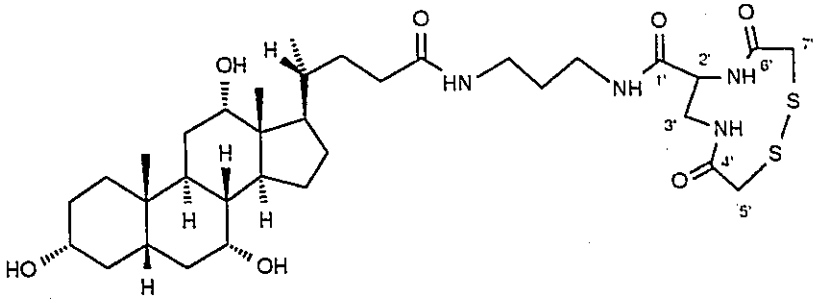

23

7.6.27 Methyl 11-aminoundecanoate .1HCl (24)

HCl gas was bubbled for about 30 minutes into a suspension of 11-aminoundecanoic acid .HCl (7.00 g, 34.8 mmol) in absolute MeOH (250 mL) with magnetic stirring. After refluxing for 12 hours and discarding the first 50 mL of distillate, the solution was rotary evaporated to a fluffy, opaque solid (8.59 g, 98%). Recrystallization from absolute MeOH gave **24** as opaque plates. The compound showed:

mp:	136.5-140.0 °C
TLC:	R_f 0.09 (90% CH_2Cl_2:10% MeOH; ninhydrin positive)
IR (KBr Pellet):	ν_{MAX} 3000(s)(N-H stretch of salt), 2920,2850(w) (aliphatic C-H), 1720(s)(C=O,H-bonded ester), 1555,1500(m)(N-H bend of salt), 1160(s)(O-C)
^{1}H NMR (DMSO-d_6):	δ1.22(s,12H,H-4 to H-9), 1.49(m,4H,H-3 and H-10), 2.26(t,J=7.4 Hz,2H,H-2), 2.68(m,2H,H-11), 3.55(s, 3H,$COOCH_3$), 8.14(br s,3H,-NH_3^+) (200 MHz)
^{13}C NMR (DMSO-d_6):	δ24.36,25.84,26.81,28.46-28.69 (C_3 to C_{10}),

33.20(C_2), 38.60(C_{11}), 51.06(OCH_3), 173.25(C_1)

(126 MHz)

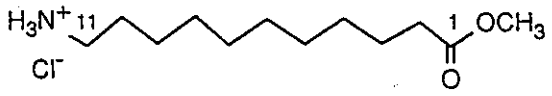

24

7.6.28 Methyl 11-{*N,N'*-bis[2-(triphenylmethyl)thioethanoyl]-2,3-diaminopropanamido} undecanoate (**25**)

To a magnetically-stirred solution of acid **3** (550 mg, 0.75 mmol) in AN/CH_2Cl_2 (2:1 v/v, 7 mL) was added DCC (170 mg, 1.1 eq., 0.82 mmol) under a N_2 atmosphere. After 10 minutes, a suspension of amine hydrochloride **24** (189 mg, 0.75 mmol), NEt_3 (2 drops) in AN (3 mL) was added and the mixture allowed to stir under a N_2 atmosphere. After 14 hours, the suspension was chilled for 30 minutes at -15 °C, gravity filtered and the residue (DCU) washed with cold CH_2Cl_2 and discarded. The filtrate was diluted to with CH_2Cl_2 (100 mL), washed with 0.5 N HCl (2 X 100 mL) and dried over $MgSO_4$ for two hours. Filtration and rotary evaporation of the filtrate afforded a pale-yellow solid (675 mg, 93%). Recrystallization from absolute MeOH gave **25** as opaque plates. The compound showed:

mp:	117.0-119.0 °C
TLC:	R_f 0.21 (98% CH_2Cl_2:2% MeOH)
IR (KBr Pellet):	ν_{MAX} 3300(s)(N-H bonded), 3050(m)(aromatic C=C-H), 2920,2850(aliphatic C-H), 1730(m)(C=O,ester), 1650(s)(C=O,Amide I),

1510(s)(N-H,Amide II), 1480,1440(m)(aromatic C=C), 740,690(s)(monosubstituted aromatic C-H)

^{1}H NMR ($CDCl_3$): δ1.17(s,12H,H-4 to H-9), 1.36(br m,2H,H-3), 1.54(m,4H,H-10 and overlapping H_2O), 2.22(t,*J*=7.5 Hz,2H,H-2), 2.93[m,5H,H-5',H-7' and H-3'a(b)], 3.08(m,2H,H-11), 3.17[m,1H,H-3'a(b)], 3.59(s,3H,$COOCH_3$),3.86(m.1H,H-2'), 6.44(t,*J*=6.2 Hz,1H,C_4·O-NH), 6.64(br t,1H,C_1·O-NH), 6.94(d,*J*=5.9 Hz,1H,C_6·O-NH), 7.12-7.33[m,32H (overlapping residual $CHCl_3$),aryl] (500 MHz)

^{13}C NMR ($CDCl_3$): δ24.94,26.85,29.12-29.42(C_3 to C_{10}), 34.11(C_2), 35.84,36.15(C_5· and C_7·), 39.66(C_{11}), 42.08(C_3·), 51.41(OCH_3), 54.69(C_2·), 67.79(C-Ph_3), 127.01-129.56,143.96(aryl), 169.03,169.29,169.94 (C_1·,C_4· and C_6·) (126 MHz)

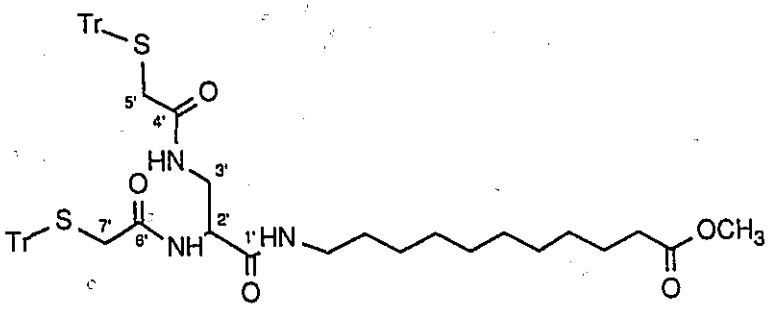

25

7.6.29 Methyl 11-[*N,N'*-(2,2'-dithiobisethanoyl)-2,3- diaminopropanamido] undecanoate (**26**)

This synthesis was similar to the general *S*-detritylation procedure described for compound **8** except that the resultant disulfide conjugate was extracted into $CHCl_3$ (along with trityl impurities) from a decolorized, NaCl-saturated, aqueous suspension. The crude sample was purified on silica gel (stepwise elution: 100% CH_2Cl_2, 1%, 2% and 4% MeOH in CH_2Cl_2) and **26** was isolated as an opaque solid (37%) from concentration of the 4% MeOH fractions. When purification and characterization were not necessary, the crude sample was used directly in the subsequent ion-exchange mediated hydrolysis so that the yield of the disulfide acid is maximized. The compound showed:

mp:	150.0-152.0 °C
TLC:	R_f 0.39 (90% CH_2Cl_2:10% MeOH)
IR (KBr Pellet):	ν_{MAX} 3290(s)(N-H bonded), 2920(s)(C-H), 1740(s)(C=O,ester), 1640(s)(C=O,Amide I), 1550(s)(N-H,Amide II), 430(w)(S-S)
^{1}H NMR ($CDCl_3$):	δ1.25(s,22H,H-4 to H-14), 1.62(br m,4H,H-3 and H-15), 2.30(t,*J*=6.4 Hz,2H,H-2), 2.72-3.32[br s,3H,H-16 and H-3'a(b)], 3.33-3.95[overlapping br s and m,~8H,$COOCH_3$,H-3'a(b), H-5' and H-6'], 4.36-5.20(br s,1H,H-2'), 7.61-8.71(br s,~2H,amide) (200 MHz)
^{13}C NMR ($CDCl_3$):	δ24.92-29.37(C_3 to C_{10}), 33.94,34.08(C_2), 39.84, 42.61(br), 49.19, 51.42(OCH_3), 169.33,169.47 (br,C_1',C_4' and C_7'), 174.31(C_1) (126 MHz)

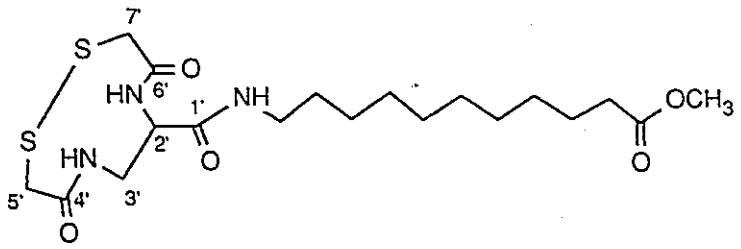

26

7.6.30 11-[*N,N'*-(2,2'-dithiobisethanoyl)-2,3- diaminopropanamido] undecanoic acid (27)

This synthesis was similar to the general hydrolytic procedure described for the esters **7** or **10** (Section 7.6.4). Compound **27** was isolated as a pale-yellow, pungent-smelling solid (56% minimum) from rotary evaporation of the aqueous-acetone eluate. The compound showed:

IR (KBr Pellet): ν_{MAX} 3404(s)(N-H bonded), 2926,2853(s)(C-H), 1700-1630(s)(C=O,acid and Amide I), 1547(m)(N-H,Amide II), 1261(m), 702(m)

^{1}H NMR (DMSO-d_6): δ1.22(s,22H,H-3 to H-14), 1.36(br s,2H,H-3), 1.45(br m,2H,H-15), 2.17(t,*J*=7.2 Hz,2H,H-2), 3.00(br m,2.6H,ligand), 3.30[br m,~12H (overlapping H_2O),ligand], 4.31(br m,0.5H,H-2'), 7.99,8.65,8.78(br m,~2H total,amide) (500 MHz)

^{13}C NMR (DMSO-d_6): δ24.44-28.99(C_3 to C_{15}), 32.23-33.14($C_{5'}$,$C_{7'}$), 33.62(C_2), 47.54,47.78$C_{2'}$), 169.37, 169.45,169.58,169.68,169.80 ($C_{1'}$,$C_{4'}$,$C_{6'}$), 174.40(C_1) (126 MHz)

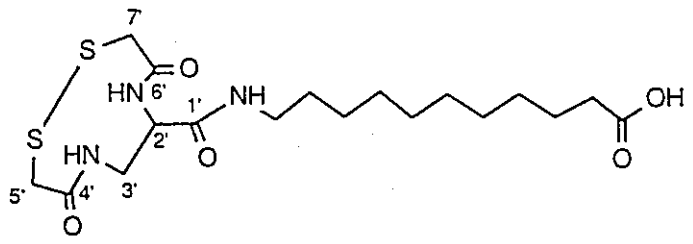

27

7.6.31 Methyl 16-hydroxyhexadecanoate (28)

HCl gas was bubbled for about 20 minutes into a solution of 16-hydroxyhexadecanoic acid (900 mg, 3.30 mmol) in absolute MeOH (1 L). After an hour, the solution was degassed *in vacuo* at 0 °C for 50 minutes on a rotary evaporator and concentrated to give **28** as a light-yellow, opalescent solid (904 mg, 96%). The compound showed:

mp:	52.5-53.5 °C
TLC:	R_f 0.64 (90% CH_2Cl_2:10% MeOH)
IR (KBr Pellet):	ν_{MAX} 3410(s)(O-H bonded), 2920,2850(w)(C-H), 1735(s)(C=O), 1160(m)(O-CH_3,ester), 1040(m)(O-CH_2,alcohol)
^{1}H NMR ($CDCl_3$):	δ1.34(m,22H,H-4 to H-14), 1.58(m,4H,H-3 and H-15), 2.30(t,*J*=7.5 Hz,2H,H-2), 3.60(t,*J*=6.6 Hz,2H,H-16), 3.66(s,3H,$COOCH_3$) (200 MHz)
^{13}C NMR ($CDCl_3$):	δ24.95,25.73,29.14-29.60(C_3 to C_{14}), 32.81(C_{15}), 34.11(C_2), 51.40(OCH_3), 63.06(C_{16}), 174.34(C_1) (126 MHz)

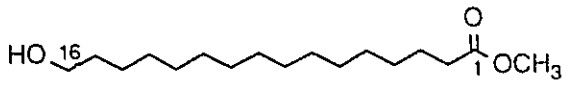

28

7.6.32 Methyl 16-tosylhexadecanoate (**29**)

Hydroxy ester **28** (900 mg, 3.14 mmol) was added in equal proportions over 20 minutes to a magnetically-stirred, yellow solution of freshly-recrystallized tosyl chloride (1.20 g, 2 eq., 6.28 mmol) in pyridine (3 mL) with 4Å molecular sieves under a N_2 atmosphere. After 12 hours, the light-brown mixture was pipetted into 0.5 N HCl (300 mL) and extracted into CH_2Cl_2 (200 mL). The aqueous layer was removed and re-extracted with CH_2Cl_2 (50 mL) and the pooled organic layers were backwashed with 0.5 N HCl (300 mL) and dried over $MgSO_4$ for an hour. Filtration, *in vacuo* concentration of the filtrate and chromatographic purification of the resultant light-yellow oil (stepwise elution: 40% CH_2Cl_2 then 80% CH_2Cl_2 in hexanes) gave **29** as a crystalline, opaque solid (551 mg, 40%) from the evaporation of the 80% CH_2Cl_2 fractions. The 40% CH_2Cl_2 fractions contained the 16-bis ether as the major component (^{1}H NMR spectroscopy). The compound showed:

TLC:	R_f 0.28 (85% hexanes:15% EtOAc)
IR (KBr Pellet):	ν_{MAX} 2920,2850(s)(aliphatic C-H), 1740(s)(C=O), 1450(m)(aromatic C=C), 1355(s)(antisymmetric SO_2), 1170(s)(symmetric SO_2), 950(s), 805,830,840(s)(disubstituted aromatic C-H), 660(s)
^{1}H NMR ($CDCl_3$):	δ1.23(m,22H,H-4 to H-14), 1.70(m,4H,H-3 and H-15), 2.27(t,*J*=7.5 Hz,2H,H-2), 2.42(s,3H,aryl-CH_3), 3.64(s,3H,$COOCH_3$),

3.99(t,*J*=6.5 Hz,2H,H-16), 7.32(d,*J*=8.1 Hz,2H,aryl), 7.75(d,*J*=8.3 Hz,2H,aryl) (200 MHz).

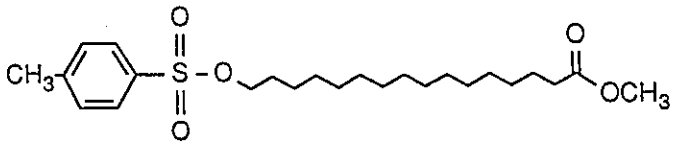

29

7.6.33 Methyl 16-azidohexadecanoate (**30**)

To a solution of tosylate **29** (550 mg, 1.25 mmol) in dry DMF (5 mL) under a N_2 atmosphere was added NaN_3 (406 mg, 5 eq., 6.24 mmol) with magnetic stirring. After 12 hours, the suspension was pipetted into 0.5 N $NaHCO_3$ (300 mL) and extracted with CH_2Cl_2 (150 mL). The aqueous layer was removed and re-extracted with CH_2Cl_2 (50 mL) and the pooled organic layers were backwashed with 0.5 N $NaHCO_3$ (300 mL) and dried over $MgSO_4$ for one hour. Filtration, *in vacuo* concentration of the filtrate afforded **30** as a clear, non-viscous oil that solidified on standing after three days at -15 °C (380 mg, 98%). The compound showed:

mp:	29.0-31.0 °C
TLC:	R_f 0.51 (85% hexanes:15% EtOAc)
IR (KBr Pellet):	ν_{MAX} 2920,2850(s)(C-H), 2090(s)(N=N), 1740(s)(C=O)
^{1}H NMR ($CDCl_3$):	δ1.24(m,22H,H-4 to H-14), 1.60(m,4H,H-3 and H-15), 2.28(t,*J*=7.6 Hz,2H,H-2), 3.24(t,*J*=7.0 Hz,2H,H-16), 3.65(s,3H,$COOCH_3$) (200 MHz)
^{13}C NMR ($CDCl_3$):	δ24.94-29.58(C_3 to C_{15}), 34.09(C_2),

51.48,51.40(OCH_3), 174.30(C_1) (126 MHz)

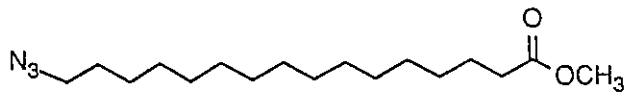

30

7.6.34 Methyl 16-aminohexadecanoate .1HCl *Via* Catalytic Hydrogenation (31)

A solution of azide **30** (85 mg, 0.27 mmol) in anhydrous MeOH (2 mL) was added to a suspension of H_2-presaturated 10% Pd/C (10 mg) in MeOH (5 mL). The suspension was allowed to magnetically stir under 1 atmosphere of H_2 gas. After 12 hours, 2 M HCl (5 drops) was added and the suspension was gravity filtered with MeOH washings. The filtrate was concentrated on a rotary evaporator to give an opaque solid (62 mg, 71%). Recrystallization from $CHCl_3$ gave **31** as opaque plates. The compound showed:

TLC:	R_f 0.30 (80% $CHCl_3$:20% MeOH; ninhydrin positive)
IR (KBr Pellet):	ν_{MAX} 3450(s)(N-H bonded), 2920,2850(s)(C-H), 1740(s)(C=O)
MS (FAB+):	*m/z*(RI%); 300(28), 286(100)[M+1-HCl]
^{1}H NMR (DMSO-d_6):	δ1.23(m,22H,H-4 to H-14), 1.49(m,4H,H-3 and H-15), 2.27(t,*J*=7.3 Hz,2H,H-2), 2.72(t,*J*=8.4 Hz,2H,H-16), 3.56(s,3H,$COOCH_3$), 7.96(br s,3H,-NH_3^+) (200 MHz)
^{13}C NMR ($CDCl_3$):	δ24.94-29.58(C_3 to C_{15}), 34.11(C_2), 40.03(C_{16}), 51.40(OCH_3), 174.33(C_1) (126 MHz)

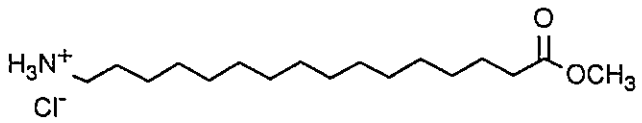

31

7.6.35 Alternative Synthesis of **31** *Via* Catalytic Transfer Hydrogenation

This synthesis was a modification of the method of Gartiser *et al.*[174] To a magnetically-stirred solution of azide **30** (60 mg, 0.21 mmol) and ammonium formate (53 mg, 4 eq., 0.84 mmol) in MeOH (2 mL) was added 10% Pd/C (6 mg, 10% by weight). After 12 hours, 2 N HCl (4 drops) was added and the suspension was allowed to stir at room temperature for two hours further. The mixture was gravity filtered with and the filtrate rotary evaporated to about 2 mL then diluted with AN (30 mL) and rotary evaporated to 20 mL. Chilling the solution for two hours at -15 °C induced precipitation of a solid (NH_4OOCH). The suspension was filtered and the filtrate concentrated to an opaque solid (19 mg, 28%) which was TLC and ^1H NMR characterized to be the required amine hydrochloride **31**.

7.6.36 Methyl 16-{*N,N'*-bis[2-(triphenylmethyl)thioethanoyl]-2,3-diaminopropanamido}hexadecanoate (32)

To a magnetically-stirred suspension of acid **3** (126 mg, 0.17 mmol) in CH_2Cl_2 (2 mL) was added DCC (54 mg, 1.5 eq., 0.26 mmol) of under a N_2 atmosphere. After 15 minutes, the suspension cleared and a solution of amine hydrochloride **31** (57 mg, 0.17 mmol), 2 drops of NEt_3 in CH_2Cl_2 (1 mL) was added and the mixture allowed to stir under a N_2 atmosphere. After 14 hours, the suspension was chilled for 30 minutes at -15 °C, gravity filtered and the residue (DCU) washed with cold CH_2Cl_2 and discarded. The filtrate was diluted to 100 mL with CH_2Cl_2, washed with 0.5 N

$NaHCO_3$ (150 mL), 0.5 N HCl (2 X 150 mL) and dried over $MgSO_4$ for two hours. Filtration and rotary evaporation of the filtrate afforded **32** as a pale-yellow solid (130 mg, 76%). The compound showed:

TLC:	R_f 0.75 (90% CH_2Cl_2:10% MeOH)
IR (KBr Pellet):	ν_{MAX} 3400(s)(N-H bonded), 3060(w)(aromatic C=C-H) 2920,2850(s)(aliphatic C-H), 1740(s)(C=O,ester), 1640(m)(C=O,Amide I), 740,695(s)(monosubstituted aromatic C-H)
MS (+NH_3 DCI):	*m/z*(RI%); 554(15), 532(40), 518(100)
^{1}H NMR ($CDCl_3$):	δ0.67-2.04(m,26H,H-3 to H-15), 2.26(t,*J*=7.4 Hz,2H,H-2), 3.00(s,4H,H-5' and H-7'), 3.16(m,4H,H-3' and H-16), 3.65(s,3H,$COOCH_3$), 3.97(m,1H,H-2'), 6.55(t,*J*=6.7 Hz,1H,C_4'-O-NH), 6.82(t,*J*=6.3 Hz,1H,C_1'-O-NH), 7.03(d,*J*=5.8 Hz,1H,C_6'-O-NH), 7.19-7.55[m,34H (overlapping residual $CHCl_3$),aryl] (200 MHz)
^{13}C NMR ($CDCl_3$):	δ24.96-29.63(C_3 to C_{15}), 34.12,33.96(C_2), 35.82,36.15(C_5' and C_7'), 39.67(C_{16}), 42.06(C_3'), 51.42(OCH_3), 54.75(C_2'), 67.78(C-Ph_3), 127.00-129.56,143.90 (aryl), 169.03,169.28,169.96 (C_1',C_4',C_6'), 174.32(C_1) (126 MHz)

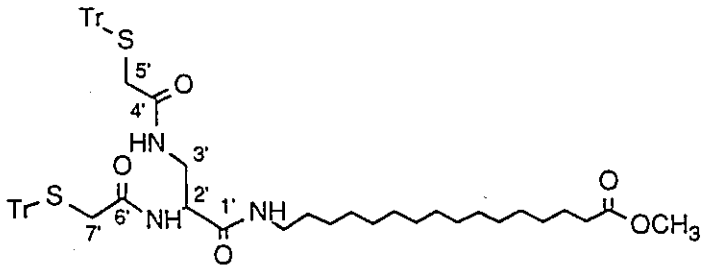

32

7.6.37 Methyl 16-[*N,N'*-(2,2'-dithiobisethanoyl)-2,3- diaminopropanamido] hexadecanoate (33)

This synthesis was similar to the general *S*-detritylation procedure described for compound **8**. Ten minutes after the addition of I_2, an opaque precipitate was noted and the suspension was stored at -15 °C for 18 hours. The suspension was filtered and the residue washed with cold absolute EtOH and dried under high vacuum. The pale-yellow solid was dissolved in $CHCl_3$ (100 mL) and washed with 0.1 N $Na_2S_2O_3$ (2 X 100 mL) and the organic layer dried over $MgSO_4$ for an hour. Filtration and rotary evaporation of the filtrate afforded **33** as a clear oil (43%). To optimize yields when characterization was not necessary, the disulfide conjugate and trityl impurities were co-isolated, *via* $CHCl_3$ extraction or the reaction suspension, and used directly used for the subsequent, ion-exchange mediated hydrolysis. The compound showed:

TLC :	R_f 0.67 (90% CH_2Cl_2:10% MeOH)
IR (KBr Pellet):	ν_{MAX} 3290(s)(N-H bonded), 2920(s)(C-H), 1740(s)(C=O,ester), 1640(s)(C=O,Amide I), 1550(s)(N-H,Amide II), 430(w)(S-S)
MS (+NH_3 DCI):	*m/z*(RI%); 518(22)[M+1], 488(10), 456(7), 286(100), 252(10)

^{1}H NMR ($CDCl_3$): δ1.25(s,22H,H-4 to H-14), 1.62(br m,4H,H-3 and H-15), 2.30(t,*J*=7.4 Hz,2H,H-2), 2.72-3.32[br s,3H,H-16 and H-3'a(b)], 3.33-3.95[overlapping br s and m,~8H,OCH_3,H-3'a(b), H-5' and H-7'], 4.36-5.20(br s,1H,H-2'), 7.61-8.71(br s,~2H,amide) (200 MHz)

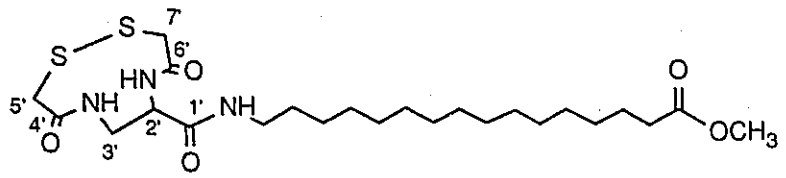

33

7.6.38 16-[*N,N'*-(2,2'-Dithioethanoyl)-2,3- diaminopropanamido] hexadecanoic acid (**34**)

To a solution of methyl ester crude **33** (~68 mg, ~0.13 mmol maximum) in EtOH (30 mL) was added EtOH-swollen AMBERLYST A-26 (OH^-) (20 mL, 20 mmol) ion-exchange resin, Aliquat 336 (1 drop) and ddH_2O (5 drops). After four days at ambient temperature with occasional swirling, the pale-yellow suspension was filtered and the collected resin was washed with EtOH and acetone. The resin then eluted with a mixture of 0.08 N HCl and acetone (1:1 v/v) until the eluate had a pH of less than 2. The clear filtrate was rotary evaporated to give **34** as a pale-amber, pungent-smelling solid (25 mg, 39% minimum). The compound showed:

IR (KBr Pellet): ν_{MAX} 3386(s)(N-H bonded), 2918,2851(s)(C-H),

	1730(s)(C=O,acid and Amide I),
	1557(m)(N-H,Amide II), 1218(m)
MS (+NH_3 DCI):	*m/z*(RI%); 397(28), 386(32), 369(100), 351(18),
	302(68), 272(82), 77(42)
^{1}H NMR (DMSO-d_6):	δ1.22(s,22H,H-3 to H-14), 1.36(br s,2H,H-3), 1.45(br
	m,2H,H-15), 2.17(t,*J*=7.3 Hz,2H,H-2), 3.00(broad
	m,2.6H,ligand and H-16), 3.30[br m,~12H
	(overlapping H_2O),ligand], 4.31(broad m,0.5H,H-2'),
	7.99,8.65,8.78(br m,~2H total,amide) (500 MHz)
^{13}C NMR (DMSO-d_6):	24.44-28.99(C_3 to C_{15}), 33.62(C_2), 174.40(C_1) (126
	MHz)

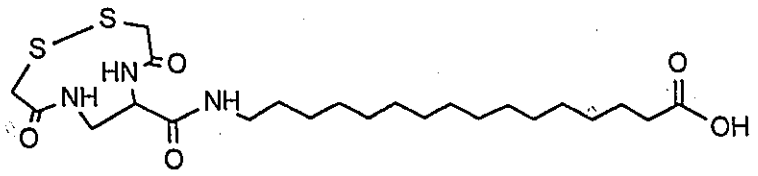

34

7.6.39 *N*-{*N'*,*N''*-Bis[2-(triphenylmethyl)thioethanoyl]-2,3 -diaminopropanoyl} taurine, sodium salt (**35**)

A saturated solution of taurine in 0.5 N $NaHCO_3$ (1 mL) was added dropwise over two minutes to a magnetically-stirred solution of acid **3** (150 mg, 0.20 mmol), EDC (46 mg, 1.2 eq., 0.24 mmol) in DMF (1 mL) after a 10-minute activation period under a N_2 atmosphere. After 12 hours, the suspension was concentrated under high

vacuum at 35 °C to a viscous semi-solid, suspended in hot EtOH (40 mL) and vacuumed filtered. The filtrate was concentrated on a rotary evaporator to about 5 mL and diluted with dH_2O (50 mL). To this clear, soapy solution was added NaCl (2 g) and 2 N HCl (5 drops) and the precipitation of an opaque solid was noted. The milky-white suspension was chilled at -15°C for an hour and vacuum filtered. The filtered residue was suspended in hot EtOH, filtered and the filtrate rotary evaporated to afford **35** as an off-white solid (167 mg, 96%). The compound showed:

TLC:	R_f 0.16 (90% CH_2Cl_2:10% MeOH)
IR (KBr Pellet):	ν_{MAX} 3420(s)(N-H bonded,sulfonate), 3060(w)(aromatic C=C-H), 2920,2850(w)(aliphatic C-H), 1660(s)(C=O,Amide I), 1520(m)(N-H,Amide II), 1490,1440(s)(aromatic C=C), 1040(m), 735,695(s)(monosubstituted aromatic C-H)
MS (FAB-):	*m/z*(RI%); 842(100)[M-23], 736(15)[M-23 - $C_2H_3O_2S$], 622(30), 600(100), 526(50)
^{1}H NMR (DMSO-d_6):	δ2.56(t,*J*=7.1 Hz,2H,H-1), 2.82(AB q,*J*=-13.9 Hz,2H,H-2), 3.24(m,2H,H-3'), 3.32[m,13H (overlapping H_2O),H-5' and H-7'], 4.07(m,1H,H-2'), 7.13-7.38 (m,30H,aryl), 7.85(t,*J*=5.8Hz,1H, C_4'O-NH), 7.90(t,*J*=5.5 Hz,1H,C_1'O-NH), 8.00(d,*J*=7.8 Hz,1H,C_6'O-NH) (500 MHz)
^{13}C NMR (DMSO-d_6):	δ35.57,35.90(C_5' and C_7'), 40.47(C_1), 50.09(C_2), 52.84(C_2'), 65.85(C-Ph_3), 126.71-129.03,144.04(aryl), 167.35,167.65,168.72(C_1',C_4' and C_6') (126 MHz)

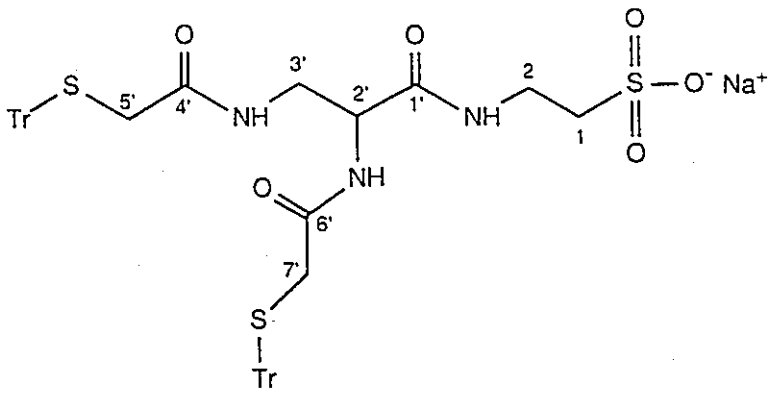

35

7.6.40 *N*-[*N'*,*N''*-(2,2'-Dithiobisethanoyl)-2,3- diaminopropamido] taurine, sodium salt (36)

This synthesis was a modification of the method of Kamber.[37] Resublimed I_2 (71 mg, 1.1 eq., 0.28 mmol) was added to a solution of *S*-tritylated taurine conjugate **35** (300 mg, 0.25 mmol) in degassed absolute EtOH (60 mL) under a N_2 atmosphere. The amber-brown solution was further degassed for 30 minutes under aspirator vacuum (15 mm Hg), vented to dry N_2 gas and allowed to magnetically stir at room temperature. An opaque precipitate was noted after 10 minutes and after four hours, the suspension was stored at -15 °C for 18 hours. The amber-brown solid was isolated by gravity filtration, washed with cold EtOH, dissolved in warm, ddH_2O (50 mL) and extracted with CH_2Cl_2 (2 X 70 mL) without vigorous mixing of the biphasic emulsion. The aqueous layer was carefully separated and rotary evaporated at 30 °C to an amber-brown, glassy solid. Recrystallization from a water-acetone mixture afforded **36** as an opaque solid (31 mg, 33%). The compound showed:

mp:	282-284 °C
IR (KBr Pellet):	ν_{MAX} 3420(s)(N-H bonded,sulfonate),
	2920(w)(C-H), 1655(s)(C=O,Amide I),

1530(m)(N-H,Amide II), 1210(m), 1040(m)

MS (FAB-): *m/z*(RI%); 251(10), 165(15), 143(30)

^{1}H NMR (DMSO-d_6): δ2.48(br t,2H,H-1), 2.57(br m,~3H), 3.78(br m,~3H), 2.83(AB q,*J*=-14.2 Hz,2H,H-2), 3.48[br m,~7H (overlapping H_2O)], 4.0-4.4(br m,~1H,H-2'), 7.8-8.3(br m,~3H,amide) (500 MHz)

^{13}C NMR (DMSO-d_6): δ35.59,35.93(C_5· and C_7·), 40.47(C_1), 42.39,41.78(br,C_3·), 50.04(C_2), 52.91(br,C_2·), 169.52,168.77,168.21(br,C_1·,C_4· and C_6·) (126 MHz)

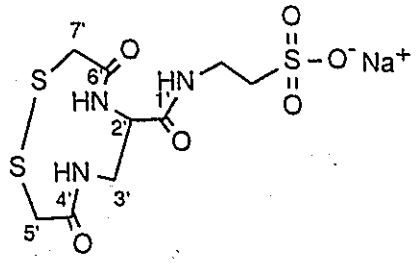

36

7.6.41 3-(Mono-6-amino-β-cyclodextrin)-1-{*N,N'*-bis[2-(triphenylmethyl)thioethanoyl]-2,3-diaminopropanamido} propane (37)

A solution of 3-(mono-6-amino-β-cyclodextrin)propylamine (20 mg, 0.02 mmol), NEt_3 (1 drop) in DMF (1 mL) was added dropwise to a magnetically-stirred solution of acid **3** (13 mg, 0.02 mmol), EDC (6 mg, 1.5 eq., 0.03 mmol) in DMF (1 mL) after a 10-minute activation period under a N_2 atmosphere. After 48 hours, the clear solution was concentrated under high vacuum to a viscous, clear oil, suspended in ddH_2O (10 mL) and filtered with ddH_2O and $CHCl_3$ washings. The collected solid was

dissolved in hot EtOH, hot-filtered and the ethanolic filtrate was rotary evaporated to give 37 as an amorphous solid (21 mg, 53%). The compound showed:

TLC : R_f 0.85 (43% *i*-PrOH:37% $H_2$0:20% EtOAc; ninhydrin positive)

IR (KBr Pellet): ν_{MAX} 3410(s)(N-H,O-H bonded), 3060(m)(aromatic C=C-H), 2930(s)(aliphatic C-H), 1655(s)(C=O,Amide I), 1520(m)(N-H,Amide II), 1490,1440(m)(aromatic C=C), 1150(w), 1075,1030(m)(C-O), 735.695(s)(monosubstituted aromatic C-H)

^{1}H NMR (DMSO-d_6): δ2.76,2.8(s,~4H,H-5' and H-7'), 3.00(m,~4H,H-8 and H-9), 3.16-3.62[br m,87H (overlapping H_2O),sugar methines and H-3'], 4.04(br m,1H H-2'), 4.35(br s,~4H,H-6 substituted sugar), 4.75(br s,~5H,H-6 unsubstituted sugars), 5.70(br m,~18H,-OH and -NH), 7.30(m,52H,aryl), 7.91(br m,3H,amide) (500 MHz)

^{13}C NMR (DMSO-d_6): δ26.28(C_8), 35.88,35.98(C_5· and C_7·), 36.67(C_9), 40.00(C_3·), 43.17(C_7), 52.83(C_6-NHR), 55.32(C_2·), 59.88(C_6 unsubstituted), 65.85(C-Ph_3), 72.00(C_2), 72.39(C_3), 73.00(C_4), 81.51(C_5), 101.89(C_1), 126.76-129.02,143.98(aryl), 167.33,167.43,167.71 (C_1·,C_4· and C_6·) (126 MHz)

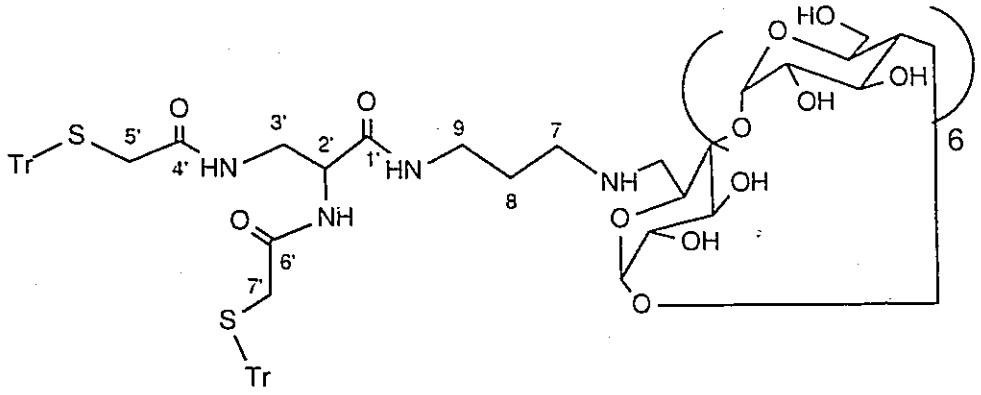

37

7.6.42 3-(Mono-6-amino-β-cyclodextrin)-1- {*N'*,*N''*-(2,2'-dithiobisethanoyl)-2,3- diaminopropanamido} propane .1HI (**38**)

This synthesis was a modification of the method of Kamber.[37] Resublimed I_2 (31 mg, 2.1 eq., 0.12 mmol) was added to a solution of *S*-tritylated cyclodextrin conjugate **37** (65 mg, 0.06 mmol) in a 4:1 v/v mixture of degassed absolute EtOH and CH_2Cl_2 (50 mL) under a N_2 atmosphere. The amber-brown solution was further degassed for 30 minutes under aspirator vacuum (15 mm Hg), vented to dry N_2 gas and allowed to magnetically stir at room temperature. After 12 hours, the amber-brown suspension chilled at -15° C for 18 hours and filtered with cold EtOH washings. The amber-colored residue was dissolved in luke-warm ddH_2O (100 mL) and was further washed with $CHCl_3$ (2 X 50 mL), filtered through glass wool and rotary evaporated at 30 °C to give **38** as a clear, pale-yellow solid (29 mg, 31%). The compound showed:

mp:	195-200 °C (dec.)
TLC:	R_f 0.0 (43% *i*-PrOH:37% H_2O:20% EtOAc; ninhydrin positive))
IR (KBr pellet):	ν_{MAX} 3444(s)(O-H,N-H bonded),

	2924,2853(s)(aliphatic C-H), 1652(s)(C=O,Amide I), 1558,1535(m)(N-H,Amide II), 1156,1079,1028(s)(C-O)
MS (FAB+):	*m/z*(RI%); 1423(20)[M-I^-], 1216(100)[(M-I^-)-$C_6H_{11}N_2O_2S_2$]
^{1}H NMR (D_2O):	δ3.47(br m), 3.75(br m), 4.59(br m), 4.88(br m,H-6 of unsubstituted sugars) (500 MHz)
^{13}C NMR ($CDCl_3$):	δ25.83(C_8), 36.66(br,C_5, and C_7,), 37.19,38.98(C_9), 41.47(br,C_3,), 42.57, 43.29, 46.18(C_7), 47.34, 48.58, 53.69(C_6-N^+H_2R), 54.55(br,C_2,), 60.72,61.09(C_6 unsubstituted), 67.94(C_4 substituded), 69.22, 72.21(C_4 unsubstituted), 72.47(C_2 unsubstituted), 73.53(C_3 unsubstituted), 80.85, 81.53(C_5 unsubstituted), 83.56, 101.59(C_1 substituted), 102.28(C_1 unsubstituted), 172.25(br,C_1,,C_4, and C_6,) (126 MHz)

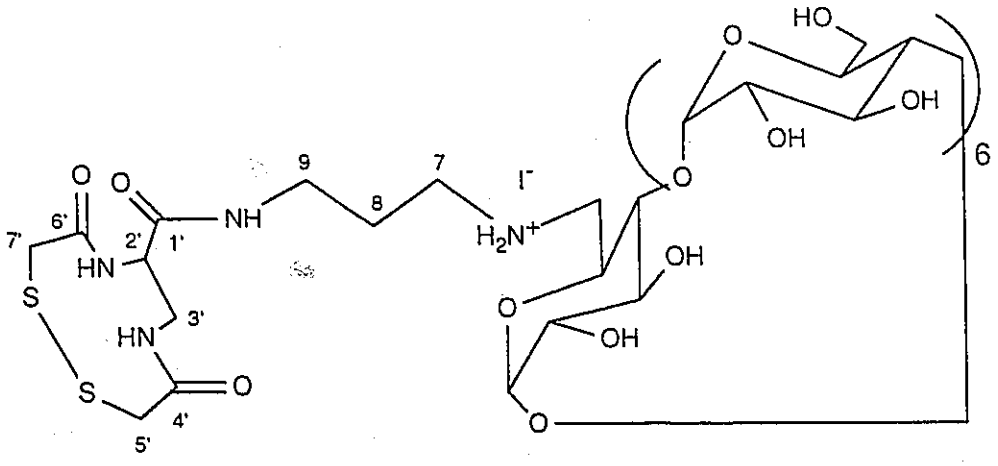

38

7.6.43 *N,N'*-{Dimethyl-bis[2-(triphenylmethyl)thioethanoyl]}ethylenediamine (39)

To a magnetically-stirred solution of succinimido ester **2** (1.00 g, 2.32 mmol) in AN (10 mL) was added a solution of *N,N'*-dimethylethylenediamine (120 μL, 1.13 mmol) in AN (1 mL) and NEt_3 (2 drops) under a N_2 atmosphere. After 12 hours, the milky-white suspension was concentrated to 2 mL, diluted with 0.5 N HCl (100 mL) and extracted with CH_2Cl_2 (200 mL). The organic layer was backwashed with 0.5 N HCl (200 mL), 0.5 N $NaHCO_3$ (200 mL) and dried over $MgSO_4$ for an hour. Filtration and concentration of the filtrate *in vacuo* afforded a solid (621 mg, 76%). Chromatographic purification of the resultant crude (stepwise elution: 100% CH_2Cl_2 followed by 2% MeOH in CH_2Cl_2) gave **39** as an opaque solid. The compound showed:

mp:	71.0-72.5 °C
TLC:	R_f 0.79 (90% CH_2Cl_2:10% MeOH)
IR (KBr Pellet):	ν_{MAX} 3055(w)(aromatic C=C-H), 2930,2850(w)(aliphatic C-H), 1645(s)(C=O,Amide

I), 1485(s), 1440(s)(aromatic C=C), 1400(m),

735,695(s)(monosubstituted aromatic C-H)

^{1}H NMR: See Table 7.3

Table 7.3:. ^{1}H NMR (500 MHz) assignments for **39** in $CDCl_3$ at 303 K.

CONFORMER	*Z,Z*	*Z,E*	*E,E*
SIGNAL	ppm (multiplicity, integral[a])		
N-CH_3	2.60(s,6H)	2.42(s,3H) 2.71(s,3H)	2.52(s,6H)
S-CH_2	2.79(s,4H)	2.77(s,2H) 2.84(s,2H)	2.72(s,4H)
(N-CH_2)$_2$	3.28(s,4H)	3.08(t,2H) 3.16(t,2H)	2.93(s,4H)
Aromatic	7.14-7.38(m,32H[b])		

[a] Integrals are relative within a geometrical isomer.

[b] Overlapping residual $CHCl_3$.

^{13}C NMR: See Table 7.4

Table 7.4: *J*-modulated ^{13}C NMR (126 MHz) assignments for **39** in $CDCl_3$ at 303 K.

CONFORMER	*Z,Z*	*Z,E*	*E,E*	*Z,Z*/*Z,E*	*Z,Z*/*E,E*	*Z,E*/*E,E*
	ppm(relative intensity)					
SIGNAL						
$N\text{-}CH_3$	35.98(-52)	34.02(-10) 36.67(-10)	------	2.6	------	------
$S\text{-}CH_2$	35.10(55)	34.64(11) 34.83(11)	33.88(5)	2.5	11.0	4.4
$(N\text{-}CH_2)_2$	44.76(52)	46.94(11) 47.53(11)	------	2.4	------	------
Aromatic	126.64 - 129.73, 143.80(4), 143.92(17), 144.00(18), 144.05(18)					
C-Tr	66.71(11)	66.81(3.03) 66.94(2.74)				
CO-NH	168.77(26)	168.24(6) 168.52(7)				

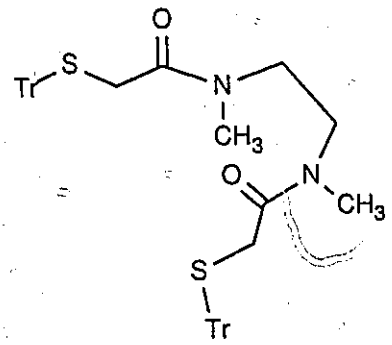

39

7.6.44 *N,N'*-[Dimethyl-(2,2'-dithiobisethanoyl)]ethylenediamine (**40**)

This synthesis was similar to the general *S*-detritylation procedure described for compound **8**, except isopropyl alcohol was used as the quench for trityl cation. After 12 hours, the amber solution was concentrated to 20 mL, diluted with ddH_2O, decolorized with 1.0 N $Na_2S_2O_3$ and extracted with diethyl ether. An opaque solid was seen at the interface. The organic phase was decanted and, after salting the aqueous layer, the precipitate extracted into $CHCl_3$ and dried over $MgSO_4$ for two hours. Filtration and rotary evaporation of the filtrate afforded an off-white, semi-solid (66%). The residue was suspended in isopropyl alcohol, chilled at -15 °C and filtered to separate most of the insoluble trityl carbinol impurity. Recrystallization from peroxide-free THF gave **40** as opaque, non-geometric plates. The compound showed:

mp:	139.0-140.0 °C
TLC:	R_f 0.49 (90% CH_2Cl_2:10% MeOH)
MS (+NH_3 DCI):	252(100)[M+NH_4^+], 235(48)[M+1], 205(10)
IR (KBr pellet):	ν_{MAX} 3445(m)(N-H bonded), 2930,2853(m)(C-H), 1629(s)(C=O,Amide I), 1458(m), 1396(m)
Raman:	645(m)(CH_2-S), 510(s)(S-S)
^{1}H NMR:	See Table 7.5
^{13}C NMR:	See Table 7.6

Table 7.5: ^{1}H NMR (500 MHz) assignments for **40** in $CDCl_3$ at 303 K.

CONFORMER	Z,Z_1	Z,E	Z,Z_2
SIGNAL	ppm (multiplicity, integral[a], amide stereochemistry[b])		
N-CH_3	3.13(s,~6H)	3.04(s,~3H,*E*) 3.24(s,~3H,*Z*)	3.15(s,~6H)
N-$(CH_2)_2$	2.64(dd,2H)[c] 4.68(dd,2H)[c] ^{2}J=-13.7 Hz[e] $^{3}J_{ax\text{-}ax}$=11.2 Hz[f] $^{3}J_{ax\text{-}eq}$=4.8 Hz $^{3}J_{eq\text{-}eq}$=1.4 Hz	3.01(m,~1H,*Z*)[c] 4.27(obs[d] m,~1H,*Z*)[c] ^{2}J=-14.41 Hz 3.09(obs m,~1H,*E*)[c] 4.27(obs m,~1H,*E*)[c] $^{3}J_{ax\text{-}ax}$=11.6 Hz $^{3}J_{eq\text{-}ax}$=3.6, 3.9 Hz $^{3}J_{eq\text{-}eq}$=2.4 Hz	2.71(dd,2H)[c] 4.88(dd,2H)[c] ^{2}J=-13.5 Hz $^{3}J_{ax\text{-}ax}$=11.1 Hz $^{3}J_{ax\text{-}eq}$=5.1 Hz $^{3}J_{eq\text{-}eq}$=1.3 Hz
S-CH_2	3.42(AB d,2H)[c] 3.45(AB d,2H)[c] ^{2}J= -12.7 Hz	3.55(AB d,1H,*E*)[c] 3.99(AB d,1H,*E*)[c] ^{2}J= -13.2 Hz 3.03(obs AB d,~1H,*Z*)[c] 4.16(AB d,1H,*Z*)[c] ^{2}J= -12.8 Hz	3.19(obs AB d,~2H)[c] 3.91(AB d,2H)[c] ^{2}J= -14.7 Hz

[a] Integrals are relative within a conformer series.

[b] Assignment of amide stereochemistry was based on NOE, MM2 and X-ray crystallographic data.

[c] Geminally coupled (determined from ^{1}H-^{13}C chemical shift correlated experiment).

[d] Obscured.

[e] All ^{2}J couplings were assumed to be negative.

[f] All ^{3}J couplings were measured from MMX-calculated structures.

Table 7.6:. *J*-modulated ^{13}C NMR (126 MHz) assignments for **40** in $CDCl_3$ at 303 K.

CONFORMER	ZZ_1	Z,E	ZZ_2
SIGNAL	ppm(relative intensity,amide stereochemistry[a])		
N-CH_3	36.58(-98)	33.59(-17,E) 41.17(-18,Z)	37.10[b]
S-CH_2	36.98(144)	37.49(31,Z) 42.17(20,E)	40.69(18)
N-$(CH_2)_2$	44.23(127)	48.20(26) 48.99(22)	46.17(16)
CO-NH	166.55(14)	168.84(6) 169.46(5)	---

[a] Stereochemical assignments are based on the analysis of NOE and ^{1}H-^{13}C shift correlated data.
[b] This resonance is absent from the *J*-modulated spectrum and was determined from the standard ^{13}C experiment.

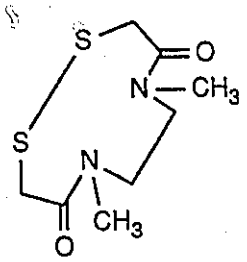

40

7.6.45 *N,N'*-Bis[2-(triphenylmethyl)thioethanoyl] ethylenediamine (**41**)

To a magnetically-stirred solution of succinimido ester **2** (1.00 g, 2.32 mmol) in AN (20 mL) was added a solution of ethylenediamine (Fisher Scientific) (78 μL, 1.1 mmol) of in AN (1 mL) and NEt_3 (2 drops) under a N_2 atmosphere. After two hours, the milky-white suspension was filtered with cold AN washings and dried under high vacuum to afford **41** as an opaque solid (625 mg, 82%). The compound showed:

mp:	166-168 °C
TLC:	R_f 0.79 (90% CH_2Cl_2:10% MeOH)
IR (KBr Pellet):	ν_{MAX} 3400,3280(s)(N-H bonded), 3050(m)(aromatic C=C-H), 2920(w)(aliphatic C-H), 1640(s)(C=O,Amide I), 1550(s)(N-H,Amide II), 1490(m), 1440(s)(aromatic C=C), 735,695(s)(monosubstituted aromatic C-H)
^{1}H NMR (DMSO-d_6):	δ2.65(s,4H,CH_2-S), 2.84(pseudo t,4H,CH_2-N), 7.10-7.20(m,30H,aryl), 7.72(s,2H,amide) (500 MHz)
^{13}C NMR ($CDCl_3$):	δ35.83(CH_2-S), 39.47(CH_2-N), 65.92(C-Ph_3), 126.03-129.43,143.95(aryl), 168.78(CO-NH) (126 MHz)

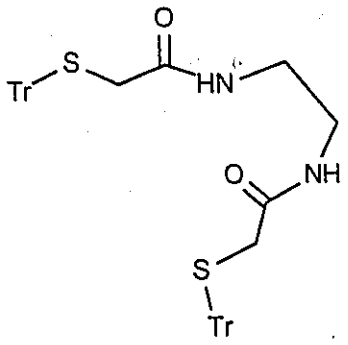

41

7.6.46 N,N'-(2,2'-Dithiobisethanoyl)ethylenediamine (42)

This synthesis was similar to the general *S*-detritylation procedure described

for compound **8**. In the work-up, the decolorized, turbid, aqueous suspension was washed with diethyl ether, concentrated to 200 mL, saturated with NaCl and extracted with $CHCl_3$. The organic phase was dried over $MgSO_4$ for two hours, filtered and the filtrate concentrated *in vacuo* to afford **42** as an off-white solid (39%). The compound showed:

mp:	185.0-187.0 °C
MS (+NH_3 DCI):	m/z(RI%); 296(20), 224(100)[M+NH_4^+], 207(20)[M+1], 162(16), 145(40)
^{1}H NMR (DMSO-d_6):	δ3.27-3.75[m,15H,(CH_2-N,CH_2-S and overlapping H_2O)], 4.05-4.22(br m,0.5H,CH_2-N of minor isomer), 7.82(br s,1H,amide), 8.17(br s,1H,amide) (500 MHz)

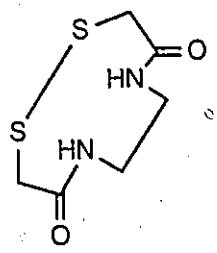

42

Appendix

X-ray Crystal Data for **40**

Table A.1: Crystal Data for **40**.

Empirical Formula	$C_8H_{14}N_2O_2S_2$
Formula Weight	234.33
Space Group	$P\bar{1}$ (#2)
Crystal System	triclinic
Crystal Color, Habit	colorless, plate
Crystal Dimensions	0.20 X 0.05 X 0.15 mm
a	7.0570(10) Å
b	8.071(2) Å
c	11.012(2) Å
α	106.05(2)°
β	93.41(1)°
γ	114.93(1)°
V	535.3(3) Å^3
Z	2
D_{calc}	1.454 g cm^{-3}
μ(Cu K_α)	4.342 mm^{-1}
F_{000}	248
Final R (obs. data)[a]	R=4.67%[b], ωR=6.82%[c]
Weighting scheme	$(\sigma^2 F + 0.0008F^2)^{-1}$
Largest Difference Peak	0.31eÅ^{-3}
Largest Difference Hole	-0.28 eÅ^{-3}

[a] for 1006 reflections with $I > 2\sigma_I$

[b] $R = \Sigma (||F_o| - |F_c||) / \Sigma F_o$

[c] $\omega R = [\ \Sigma(\text{weight, del})^2 / \Sigma(\text{weight}, F_o)^2\ ]^{1/2}$ where del = $||F_o| - |F_c||$

Table A.2: Atomic coordinates ($X10^4$) and equivalent isotropic displacement coefficients ($Å^2 X 10^3$).

Atom	*x*	*y*	*z*	U_{eq}[a]
S(1)	2354(2)	581(2)	1211(1)	57(1)
S(2)	1815(2)	2637(2)	2470(1)	56(1)
C(3)	2612(7)	4613(7)	1793(5)	40(2)
C(4)	3905(7)	6481(7)	2911(4)	37(2)
O(4)	3040(6)	6847(6)	3814(3)	55(2)
N(5)	5926(6)	7663(5)	2905(4)	38(2)
C(5)	7114(9)	9380(8)	4057(5)	60(3)
C(6)	7089(7)	7342(7)	1883(4)	37(2)
C(7)	8656(7)	6622(7)	2219(5)	39(2)
N(8)	7584(6)	4821(5)	2511(3)	35(2)
C(8)	7751(9)	4980(8)	3888(5)	55(3)
C(9)	6531(7)	3148(7)	1506(5)	39(2)
O(9)	6581(6)	3115(5)	382(3)	50(2)
C(10)	51177(9)	1295(8)	1766(5)	49(3)

[a] Equivalent isotropic U defined as one third of the trace of the orthogonalized U_{ij} tensor.

Table A.3: Bond lengths (Å) with estimated standard deviations in parentheses.

Bond	Length	Bond	Length
S(1)-S(2)	2.035(2)	S(1)-C(10)	1.835(6)
S(2)-C(3)	1.836(6)	C(3)-C(4)	1.517(6)
C(4)-O(4)	1.229(7)	C(4)-N(5)	1.342(6)
N(5)-C(5)	1.468(6)	N(5)-C(6)	1.461(7)
C(6)-C(7)	1.520(9)	C(7)-N(8)	1.466(7)
N(8)-C(8)	1.479(7)	N(8)-C(9)	1.353(5)
C(9)-O(9)	1.234(7)	C(9)-C(10)	1.515(8)

Table A.4: Bond angles (deg) with estimated standard deviations in parentheses.

Bond	Angle	Bond	Angle
S(2)-S(1)-C(10)	104.0(2)	S(1)-S(2)-C(3)	104.4(2)
S(2)-C(3)-C(4)	106.6(4)	C(3)-C(4)-O(4)	117.6(4)
C(3)-C(4)-N(5)	120.5(4)	O(4)-C(4)-N(5)	122.0(4)
C(4)-N(5)-C(5)	117.2(4)	C(4)-N(5)-C(6)	125.8(3)
C(5)-N(5)-C(6)	116.9(4)	N(5)-C(6)-C(7)	112.9(4)
C(6)-C(7)-N(8)	111.4(4)	C(7)-N(8)-C(8)	117.1(3)
C(7)-N(8)-C(9)	117.7(4)	C(8)-N(8)-C(9)	125.1(5)
N(8)-C(9)-O(9)	121.3(5)	N(8)-C(9)-C(10)	119.2(5)
O(9)-C(9)-C(10)	119.4(4)	S(1)-C(10)-C(9)	108.8(5)

Table A.5: Hydrogen atom coordinates (X 10^4) and equivalent isotropic displacement coefficients (Å^2 X 10^3).

Atom	*x*	*y*	*z*	U
H(3A)	1310	4855	1499	80
H(3B)	3234	4124	1042	80
H(5A)	6271	10070	4465	80
H(5B)	7334	8860	4893	80
H(5C)	8323	10241	4063	80
H(6A)	7774	8433	1645	80
H(6B)	5952	6293	960	80
H(7A)	9204	6338	1359	80
H(7B)	9867	7622	2946	80
H(8A)	8451	4127	3840	80
H(8B)	6348	4137	3992	80
H(8C)	8162	6271	4375	80
H(10A)	5285	1229	2691	80
H(10B)	5578	231	904	80

Table A.6: Torsional angles with estimated error in parentheses (deg).

Bond	Angle	Bond	Angle
C(10)-S(1)-S(2)-C(3)	85.9(0.3)	S(2)-S(1)-C(10)-C(9)	-69.2(0.4)
S(2)-S(1)-C(10)-H(10A)	61.7(0.4)	S(2)-S(1)-C(10)-H(10B)	-170.5(0.3)
S(1)-S(2)-C(3)-C(4)	-135.8(0.3)	S(1)-S(2)-C(3)-H(3A)	115.4(0.3)
S(1)-S(2)-C(3)-H(3B)	-5.9(0.3)	C(8)-N(8)-C(9)-O(9)	-175.1(0.6)
C(8)-N(8)-C(8)-H(8B)	-43.3(0.9)	C(7)-N(8)-C(9)-O(9)	4.5(0.8)
C(7)-N(8)-C(9)-C(10)	-172.4(0.5)	C(9)-N(8)-C(8)-H(8B)	-43.2(0.9)
C(9)-N(8)-C(8)-H(8C)	-162.3(0.5)	C(9)-N(8)-C(8)-H(8A)	59.1(0.6)
C(7)-N(8)-C(8)-H(8B)	137.2(0.6)	C(7)-N(8)-C(8)-H(8C)	18.1(0.8)
C(7)-N(8)-C(8)-H(8A)	-120.5(0.5)	C(9)-N(8)-C(7)-C(6)	79.8(0.6)
C(9)-N(8)-C(7)-H(7A)	-32.4(0.7)	C(9)-N(8)-C(7)-H(7B)	-154.5(0.5)
C(8)-N(8)-C(7)-C(6)	-100.5(0.5)	C(8)-N(8)-C(7)-H(7A)	147.2(0.5)
C(8)-N(8)-C(7)-H(7B)	25.1(0.7)	C(4)-N(5)-C(6)-C(7)	-102.5(0.6)
C(4)-N(5)-C(6)-H(6A)	131.9(0.6)	C(4)-N(5)-C(6)-H(6B)	20.4(0.8)
C(5)-N(5)-C(6)-C(7)	74.1(0.6)	C(5)-N(5)-C(6)-H(6A)	-51.5(0.7)
C(5)-N(5)-C(6)-H(6B)	-163.0(0.5)	C(6)-N(5)-C(4)-O(4)	179.5(0.6)
C(6)-N(5)-C(4)-C(3)	0.3(0.9)	C(5)-N(5)-C(4)-O(4)	2.9(0.9)
C(5)-N(5)-C(4)-C(3)	-176.3(0.6)	C(6)-N(5)-C(5)-H(5A)	143.4(0.6)
C(6)-N(5)-C(5)-H(5B)	-111.0(0.6)	C(6)-N(5)-C(5)-H(5C)	11.4(1.1)
C(4)-N(5)-C(5)-H(5A)	-39.7(0.9)	C(4)-N(5)-C(5)-H(5B)	65.9(0.7)
C(4)-N(5)-C(5)-H(5C)	-171.8(0.8)	N(5)-C(6)-C(7)-N(8)	57.5(0.4)
N(5)-C(6)-C(7)-H(7A)	174.3(0.3)	N(5)-C(6)-C(7)-H(7B)	-67.1(0.5)
H(6A)-C(6)-C(7)-N(8)	-176.0(0.4)	H(6A)-C(6)-C(7)-H(7A)	-59.2(0.5)
H(6A)-C(6)-C(7)-H(7B)	59.4(0.6)	H(6B)-C(6)-C(7)-N(8)	-66.0(0.5)
H(6B)-C(6)-C(7)-H(7A)	50.8(0.5)	H(6B)-C(6)-C(7)-H(7B)	169.4(0.4)
N(8)-C(9)-C(10)-S(1)	109.0(0.5)	N(8)-C(9)-C(10)-H(10A)	-12.6(1.0)
N(8)-C(9)C(10)-H(10B)	-144.2(0.5)	O(9)-C(9)-C(10)-S(1)	-68.1(0.7)
O(9)-C(9)-C(10)-H(10A)	170.4(0.6)	O(9)-C(9)-C(10)-H(10B)	38.8(0.7)
O(4)-C(4)-(C3)-S(2)	-58.2(0.7)	O(4)-C(4)-C(3)-H(3A)	59.5(0.7)
O(4)-C(4)-C(3)-H(3B)	-174.1(0.6)	N(5)-C(4)-C(3)-S(2)	121.0(0.5)
N(5)-C(4)-C(3)-H(3A)	-121.3(0.6)	N(5)-C(4)-C(3)-H(3B)	5.2(1.0)

Glossary

aglycone: the alcohol (*e.g.*, steroid) with which a sugar is combined with in a glycoside.

antiarrhythmic: capable of supressing or preventing an arrhythmia (any variation from normal, regular (cardiac) rhythm).

atrial fibrillation: an arrhythmia characterized by total disorganization of atrial electrical activity, in which multiple wavelets course in a chaotic fashion across the atrium.

cardioactive: of or pertaining to a drug or other substance affecting the function of the heart.

cardiotonic: having a tonic or stimulatory effect on the heart.

Caroli's disease: a congential condition characterized by cyctic dilatation of the intrahepatic bile ducts.

carrier-free: free from cold isotopes of the same element. With respect to ^{99m}Tc, carrier-free preparations would be relatively devoid of the daughter nuclide, ^{99}Tc)

cholecystitis: inflammation of the gallbladder.

cholescintigraphy: scintigraphy of the gallbladder.

conjugate: joined in pairs; coupled. In bifunctional radiopharmaceutical chemistry, a combination of a biologically active molecule (*e.g.*, a steroid) with a bifunctional ligand or chelate. In this research, the conjugative bond was either an amide or ester linkage.

Crohn's disease: a chronic inflammatory bowel disease involving the small intestine, the colon, or both, and characterized pathologically by transmural inflammation, deep linear ulceration, and often granulomas.

enterohepatic: pertaining to the intestines and liver.

gastric affecting, originating in, or relating to the stomach.

gastroenterological: of or pertaining to the function and disorders of the stomach, small and large intestine, esophagus, pancreas, liver and biliary tract.

gastrointestinal: relating to the stomach and the intestines.

glycoside: any substance consisting of an alcohol (*e.g.*, a steroid) with the hydrogen of its hydroxyl group replaced by a glycosyl group.

hepatobiliary: pertaining to the liver and biliary system.

hypoglycemic agent: a chemical substance acting to lower the level of glucose in the blood.

infarct: an area of coagulation necrosis in a tissue (as of the heart) resulting from obstruction of the local circulation by a thrombus or embolus.

inotropic: affecting the force or speed of muscular contraction.

ischemia: inadequate blood flow to a part or organ.

macroreticular ion-exchange resin: a macroporous, crosslinked polymer containing ionized or ionizable groups such as $-SO_3H$, $-SO_3Na$, -COOH, $-NH_2$, $-NH_3Cl$ or NMe_3Cl.

metastable radionuclide: a radionuclide that remains in an excited state for an appreciable time before decaying by isomeric transition.

myocardium: the intermediate, contractile muscular layer of the heart wall, constituting cardiac muscle, and comprising atrial and ventricular fibers separated by fibrous rings.

myocytes: muscle cells

Na^+,K^+-ATPase: an enzyme responsible for the active transport of Na^+ and K^+ ions across a cell membrane.

ouabain: 3-[(6-Deoxy-α-L-mannopyranosyl)oxy]-1,5,11α,14,19- pentahydroxy card-20(22)-enolide. A cardiac glycoside obtained from the seed of *Strophanthus gratus* or the wood or root of *Acocanthera schimperi*. The pharmacological action of ouabain is similar to that of digitalis but it acts more rapidly and has a shorter duration.

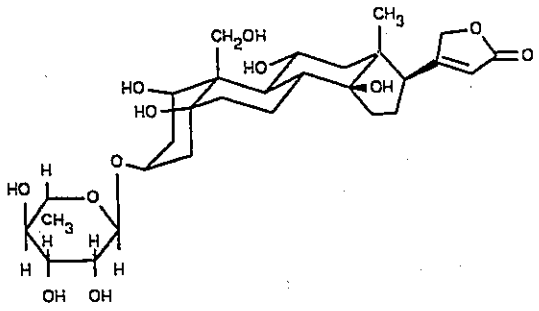

perfusion: the passage of blood or other fluid through the blood or lymph vessels of the body or in part of it.

radionuclide: a nuclide that spontaneously exhibits radioactive decay; a radioactive nuclear species.

radiopharmaceutical: a drug or other administrable agent that is tagged with a radionuclide so that its course can be traced, measured, or imaged.

^{131}I-sodium rose bengal: a hepatic function, diagnostic agent.

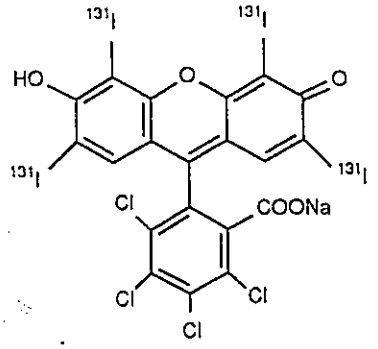

scintigraphy: a clinical diagnostic procedure consisting of the injection, usually intravenously, of a solution containing a radioactive agent with a specific affinity for an organ or tissue of interest, followed by the determination, with the aid of a special external detector (*e.g.*, gamma camera).

References

1 E. Doo, G.T. Krishramurthy, M.J. Eklem, S. Gilbert and P.H. Brown J. Nucl. Med. **32**, 48 (1991).

2 M.K. Dewanjee Semin. Nucl. Med. **20**, 5 (1990).

3 P. Richards Comitata Nazionale Ricerche Nucleari **2**, 233 (1960).

4 K.J. Franklin, Ph.D. Thesis, McMaster University, p. 8.

5 G. Mariani, C. Rosa, M. Raciti, M. Giganti, L. Fatigante, C. Giraldi, E. Consoli and G. Parenti, in Technetium in Chemistry and Nuclear Medicine, Vol. II, *edited by* M. Nicolini, G. Bandoli and U. Mazzi. Raven Press, New York, 1986. p. 305.

6 J.G. McAfee, in Radiopharmaceuticals, *edited by* G. Subramanian, B.A. Rhodes, J.F. Cooper and V.J. Sodd. The Society of Nuclear Medicine Inc., New York, 1975. pp. 3-14.

7 L.G. Marzilli, A.V. Kramer, H.D. Burns and L.A. Epps, in Technetium in Chemistry and Nuclear Medicine, Vol. I, *edited by* E. Deutch, M. Nicolini and H.N. Wagner. Cortina International, Verona, 1983. pp. 63-72.

8 S.M. Larson. Univ. Washington Med. **8**, 22 (1981).

9 D. Parker. Chemistry in Britain. October, 942 (1990).

10 D.A. Goodwin and C.F. Meares, in Radiopharmaceuticals: Structure-Activity Relationships, *edited by* R.P. Spencer. Grune and Stratton, New York, 1980. pp. 281-306.

11 E. Deutsch and K. Libson, in Technetium in Chemistry and Nuclear Medicine, Vol. I, *edited by* E. Deutch, M. Nicolini and H.N. Wagner. Cortina International,

Verona, 1983. pp. 29-36.

12 W.C. Eckelman, R.C. Reba, R.E. Gibson, W.J. Rzeszotarski, F. Vieras, J.K. Mazaitis and B. Francis. J. Nucl. Med. **20**, 350 (1979).

13 N.D. Heindel, H.D. Burns, R. Schneider and N.I. Foster, in Radiopharmaceuticals: Structure-Activity Relationships, *edited by* R.P. Spencer. Grune and Stratton, New York, 1980. pp. 101-127.

14 R.E. Counsell and R.D. Ice, in Drug Design, Vol. 6, *edited by* E.J. Ariens. Academic Press, New York, 1975. pp. 172-259.

15 N.D. Heindel, H.D. Burns and T. Honda, in The Chemistry of Radiopharmaceuticals, *edited by* N.D. Heindel. Mason Press, New York, 1978. pp. 11-33.

16 L.F. Larinov, S.A. Degteva and N.A. Lesnaia. Vop. Onkol. **8**, 12 (1962).

17 S.A. Degteva. Vop. Onkol. **10**, 52 (1964).

18 M.E. Wall, G.S. Abernethy and F.I. Carroll. J. Med. Chem. **12**, 180 (1969).

19 A. Liu, J.A. Katzenellenbogen, H.F. VanBrocklin, C.J. Mathias and M.J. Welch. J. Nucl. Med. **32**, 81 (1991).

20 A. Yokayama, A. Yamada, Y. Arano, K. Horiuchi, K. Yamamoto and K. Torizuka, in Technetium in Chemistry and Nuclear Medicine, Vol. I, *edited by* E. Deutch, M. Nicolini and H.N. Wagner. Cortina International, Verona, 1983. pp. 109-111.

21 A. Yokoyama, T. Hosotani, Y. Arano, K. Horiuchi, K. Yamamoto, N. Tamaki and K. Torizuka, in Technetium in Chemistry and Nuclear Medicine, Vol. I, *edited by* E. Deutch, M. Nicolini and H.N. Wagner. Cortina International, Verona, 1983. pp. 125-127.

22 J.G. McAfee, in Radiopharmaceuticals, *edited by* G. Subramanian, B.A. Rhodes,

J.F. Cooper and V.J. Sodd. The Society of Nuclear Medicine Inc., New York, 1975. pp. 3-14.

23 S. Kasina, T. Rao, A. Srinivasan, J.A. Sanderson, J.N. Fitzner, J.M. Reno, P.L. Beaumier and A.R. Fritzberg. J. Nucl. Med. **32**, 1445 (1991).

24 A.R. Fritzberg, P.G. Abrams, P.L. Beaumier, S. Kasina, A.C. Morgan, T. Rao, J.M. Reno, J.A. Sanderson, A. Srinivasan, D.S. Wilbur and J.-L. Vanderheyden. Proc. Natl. Acad. Sci. USA. **85**, 4025 (1988).

25 A. Davison, M. Sohn, C. Orvig. J. Nucl. Med. **20**, 641 (1979) abst.

26 S. Kasina, A.R. Fritzburg, D.L. Johnson *et al.* J. Med. Chem. **29**, 1933 (1986).

27 A.R. Fritzburg, S. Kasina, D. Eshima *et al.* J. Nucl. Med. **25**, 16 (1984).

28 R.F. Schneider, G. Subramaniam, T.A. Feld *et al.* J. Nucl. Med. **25**, 223 (1984).

29 A. Fritzberg and A. Nun, in Analytical and Chromatographic Techniques in Radiopharmaceutical Chemistry, *edited by* D.M. Wieland, M.C. Tobes and T.J. Manger. Springer, New York, 1985. pp. 193-195.

30 D. Eshima, A.R. Fritzberg and A.Taylor. Semin. Nucl. Med. **20**, 28 (1990).

31 L.G. Marzilli, A.V. Kramer, H.D. Burns and L. A. Epps, in Technetium in Chemistry and Nuclear Medicine, Vol. I, *edited by* E. Deutch, M. Nicolini and H.N. Wagner. Cortina International, Verona, 1983. pp. 63-72.

32 R.H. Mach, H.F. Kung, P. Jungwiwattanaporn and Y.-Z. Guo. Tetrahedron Lett. **30**, 4069 (1989).

33 T. W. Greene. Protecting Groups in Organic Chemistry, J. Wiley, New York, 1981. p. 320.

34 J. Xan, E.A. Wilson, L.D. Roberts and N.H. Horton. J. Am. Chem. Soc. **63**, 1139 (1941).

35 D. Brenner, A. Davison, J. Lister-James and A.G. Jones. Inorg. Chem. **23**, 3793

(1984).

36 S.Z. Lever, K.E. Baidoo, A.V. Kramer and H.D. Burns. Tetrahedron Lett. **29**, 3219 (1988).

37 B. Kamber. Helv. Chim. Acta. **54**, 417 (1971).

38 F. Zetzsche and A. Fredrich. Ber. Dtsch. Chem. Ges. **72**, 1735 (1939).

39 J.K.M. Saunders and B. Hunter. Modern NMR Spectroscopy: a Guide for Chemists, Oxford University Press, Oxford, 1987. pp. 299-301.

40 E.D. Hughes, C.K. Ingold and C.S. Patel. J. Chem. Soc. 526 (1933).

41 R. Paul and G.W. Anderson. J. Am. Chem. Soc. **82**, 4596 (1960).

42 R.C. Morton, D. Mangroo and G.E. Gerber. Can. J. Chem. **66**, 1701 (1988).

43 T.H. Lowry and K.S. Richardson. Mechanism and Theory in Organic Chemistry, Third Ed., Harper and Row, New York, 1987. p. 369.

44 J.C. Sheenan, P.A. Cruickshank and G.L. Boshart. J. Org. CHem. **26**, 2525 (1961).

45 J.C. Sheehan, J. Preston and P.A. Cruickshank. J. Am. Chem. Soc. **87**, 2492 (1965).

46 H. Fraenkel-Conrat. J. Biol. Chem. **217**, 373 (1955).

47 L. Field, J.L. Vanhorne, and L.W. Cunningham. J. Org. Chem. **35**, 3267 (1970).

48 N.W. Tideswell and J.D. McCullough. J. Am. Chem. Soc. **79**, 1031 (1957).

49 H. Tsubomura and R.P. Lang. J. Am. Chem. Soc. **83**, 2085 (1961).

50 J.P. Danehy, C.P. Egan and J. Switalski. J. Org. Chem. **36**; 2530 (1971).

51 E. Ciuffarin and G. Guaraldi. J. Org. Chem. **35**, 2006 (1970).

52 J. Xan, E.A. Wilson, L.D. Roberts and N.H. Horton. J. Am. Chem. Soc. **63**, 1139 (1941).

53 L. Holman, V. Sporn, A.G. Jones, S.T.B. Sia, N. Perez-Balino, A. Davison, J.

Lister-James, J.F. Kronauge, A.E.A. Mitta, L.L. Camin, S. Campbell, S.J. Williams and A.T. Carpenter. J. Nucl. Med. **28**, 13 (1987).

54 H.W. Strauss and B. Pitt. Semin. Nucl. Med. 7, 7 (1977).

55 E. Deutsch, K.A. Glavan, V.J. Sodd, H. Nishiyama, D.L. Ferguson and S.J. Lukes. J. Nucl. Med. **22**, 897 (1981).

56 A.G. Jones, M.J. Abrams, A. Davison *et al.* Int J. Nucl. Med. Biol. **11**, 225 (1984).

57 B.L. Holman, C.A. Campbell, J. Lister-James *et al.* J. Nucl. Med. **27**, 1172 (1986).

58 B.L. Holman, V. Sporn, A.G. Jones *et al.* J. Nucl. Med. **28**, 13 (1987).

59 K. McKusick, B.L. Holman, A.G. Jones. *et al.* J. Nucl. Med. 27, 878 (1986) abst.

60 S.T.B. Sia and B.L. Holman. Am. J. Cardiac Imaging. **1**, 125 (1987).

61 A.D. Nunn, E.N. Treher and T. Feld. J. Nucl. Med. **27**, 893 (1986) abst.

62 R.E. Coleman, M. Maturi, A.D. Nunn *et al.* J. Nucl. Med. **27**, 894 (1986) abst.

63 D.W. Webster, D.L. Nosco, J.R. Coveney *et al.* J. Nucl. Med. **27**, 894 (1986) abst.

64 B.L. Liu, H.K. Kung, Y.T. Jin *et al.* J. Nucl. Med. **30**, 367 (1989).

65 A.D. Nunn. Semin. Nucl. Med. **20**, 111 (1990).

66 E. Deutsch, K.A. Glavan, V.J. Sodd, H. Nishiyama, D.L. Ferguson and S.J. Lukes. J. Nucl. Med. **22**, 897 (1981).

67 E. Livini, M.A. Davis and V.D. Warner. J. Med. Chem. **22**, 580 (1979).

68 J.R. Evans, R.W. Gunton and D.S. Beanlands. Circulation. **26**, 714 (1962).

69 E. Livini, M.A. Davis and V.D. Warner, in Radiopharmaceuticals II: Proceedings 2nd International Symposium on Radiopharmaceuticals, The Society of Nuclear Medicine Inc., 1979. pp. 487-495.

70 R.W. Gunton, J.R. Evans, R.G. Baker, J.C. Spears and D.S. Beanlands. Am. J. Cardiol. **16**, 482 (1965).

71 J.R. Evans, R.W. Gunton, R.G. Baker, D.S. Beanlands and J.C. Spears. Circ. Res. **16**, 1 (1965)

72 F.J. Bonte, K.D. Graham and J.G. Moore. Radiology. **108**, 195 (1973).

73 N.D. Poe, G.D. Robinson Jr., L.S. Graham and N.S. MacDonald. J. Nucl. Med. **17**, 1077 (1976).

74 H.H. Coenen, M.-F. Harmand, G. Kloster and G. Stöcklin. J. Nucl. Med. **22**, 891 (1981).

75 E.S. Weiss, E.J. Hoffman, M.E. Phelps, M.J. Welch, P.P. Henry, M.M. Ter-Pogossian and B.E. Sobel. Circ. Res. **39**, 24 (1976).

76 C. Freundlieb, A. Höck, K. Vyska, L.E. Feinendegen, H.-J. Manchulla and G. Stöcklin. J. Nucl. Med. **21**, 1043 (1980).

77 K. Vyska, A. Höck, C. Freundlieb *et al.* J. Nucl Med. **20**, 650 (1979).

78 M.D. Loberg, E.H. Corder, A.T. Fields and P.S. Callery. J. Nucl. Med. **20**, 1181 (1979).

79 C.J. Pouchert. The Aldrich Library of NMR Spectra, Ed. II, Vol. 2. Aldrich Chemical Company, Inc., Milwaukee, 1983. p. 611.

80 S. Ram and R.E. Ehrenkaufer. Synthesis. 133 (1986).

81 H.N. Hunter, Ph.D. Thesis, McMaster University, p. 26.

82 The Merck Index, Eleventh Ed., edited by S. Budavari. Merck and Co., Rahway, New Jersey, 1989. p. 3143.

83 W.W. Zorbach and K.V. Bhat. Advan. Carbohydrate Chem. **21**, 273 (1966).

84 K. Repke and H.J. Portius, in Scientiae Pharmaceuticae, Vol. 1. *edited by* O. Hanč and J. Hubík. Butterworths, London and Czechoslovak Medical Press,

Prague, 1966. p. 39.

85 R. Thomas, John Boutagy and A. Gelbart. J. Pharm. Sci. **63**, 1649 (1974).

86 B.F. Hoffman and J.T. Bigger, Jr., in The Pharmacological Basis of Therapeutics, Seventh Ed. *edited by* L.S. Goodman and A. Gilman. Macmillan, New York, 1985. pp. 716-46.

87 K.K. Chen, E.B. Robbins and H. Worth. J. Am. Pharm. A. **27**, 189 (1938).

88 D.C. Humber, P.S. Jones, G.H. Phillipps, M.G. Dodds and P.G. Dolamore. Steroids. **42**, 171 (1983).

89 D.C. Humber, G.H. Phillipps, M.G. Dodds and P.G. Dolamore and I. Machin. Steroids. **42**, 189 (1983).

90 B. Neises and W. Steglich. Angew. Chem. Int. Ed. Engl. **17**, 522 (1978).

91 G. Höfle, W. Steglich and H. Vorbrüggen. Angew. Chem. Int. Ed. Engl. **17**, 569 (1978).

92 M.B. Robin, F.A. Bovey and H. Basch, in The Chemistry of Amides, *edited by* S. Patai and J. Zabicky. Interscience Publishers, London, 1970. pp. 1-72.

93 C.J. Pouchert. The Aldrich Library of NMR Spectra, Ed. II, Vol. 1. Aldrich Chemical Company, Inc., Milwaukee, 1983. p. 566.

94 G. Galli and C.L. Maini, in Technetium in Chemistry and Nuclear Medicine, Vol. II, *edited by* M. Nicolini, G. Bandoli and U. Mazzi. Raven Press, New York, 1986. pp. 309-15.

95 E. Heftman, in The Encyclopedia of Chemistry, Third Ed., *edited by* C.A. Hampel and G.G. Hawley. Van Nostrand Reinhold Co., New York, 1973. p. 138.

96 G.S. Boyd, M.V. Merrick, R. Monks and I.L. Thomas. J. Nucl. Med. **22**, 720 (1981).

97 A.F. Hofmann. Gastroenterology. **77**, 955 (1979).

98 S. Alpert *et al.* J. Gen. Physiol. **53**, 288 (1969).

99 A.R. Fritzberg, in Cholescintigraphy, *edited by* P.H. Cox. Martinus Nijhoff Publishers, 1981. p. 54.

100 A.R. Fritzberg and J. Reichen. J. Nucl Med. **24**, 126 (1983).

101 N.B. Javitt. Med. Clin. North Am. **59**, 817 (1975).

102 D.C. Boag, M.Sc. Thesis, McMaster University, 1987. p. 88.

103 F. Scopinaro, G. Linari, M. Baldieri, E. Corti, C. Signori and M. Liberatore, in Technetium in Chemistry and Nuclear Medicine, Vol II, *edited by* M. Nicolini, G. Bandoli and U. Mazzi. Raven Press, New York, 1986. pp. 281-83.

104 S.C. Harvey, in The Pharmacological Basis of Therapeutics, Seventh Ed., *edited by* A.G. Gilman, L.S. Goodman, T.W. Rall and F. Murad. Macmillan Publishing Co., New York, 1985. p. 988.

105 K. Steiner, K.U. Bühring, H.-P. Faro, A. Garbe and H. Nowak. Arzneim.-Forsch./Drug Res. **32**, 512 (1982).

106 N. Terao, N. Yoshida and R. Nagashima. Arzneim.-Forsch./Drug Res. **30**, 73 (1980).

107 R.J. Jenkins, R.L. Goodacre, P.J. Rooney, J. Bienenstock, T. Sivakumaran, W.H.C. Walker. Clin. Biochem. **19**, 298 (1986).

108 W.A. Walker. Immunology Today. **2**, 30 (1981).

109 W. Saenger. Angew. Chem. Int. Ed. Engl. **19**, 344 (1980).

110 J.S. Pagington. Chemistry in Britain, May, 455 (1987).

111 W.J. James and D. French. Proc. Iowa Acad. Sci. **59**, 197 (1952).

112 J.F. Foster, in Starch: Chemistry and Technology, Vol. 1, *edited by* R.L. Whistler and E.F. Paschall. Academic Press, New York, 1965. p. 385.

113 D. Parker, R.J. Taylor, G. Ferguson and A. Tonge. Tetrahedron. **42**, 617 (1986).

114 S. Gronowitz and Z. Lidert. Chemica Scripta. **16**, 97 (1980).

115 D.W. Hughes and C.M. Deber. Biopolymers. **21**, 169 (1982).

116 R.J. Abraham and P. Loftus. Proton and Carbon-13 NMR Spectroscopy - an Integrated Approach, Heyden, London, 1979. p. 169.

117 T.H. Siddhall and W.E. Stewart. J. Chem. Phys. **48**, 2928 (1968).

118 C.A. Hunter and J.K.M. Sanders. J. Am. Chem. Soc. **112**, 5525 (1990).

119 J.V. Hatton and R.E. Richards. Mol Phys. **5**, 139 (1962).

120 G. Claeson, G. Androes and M. Calvin. J. Am. Chem. Soc. **83**, 9357 (1961).

121 C.H. Bushweller and M.H. Gianni, in The Chemistry of Ethers, Crown Ethers, Hydroxyl Groups and Their Sulphur Analogues, Part 1, *edited by* S. Patai. Interscience, Chichester. 1980. pp. 221-22.

122. M.B. Robin, F.A. Bovey and H. Basch, in The Chemistry of Amides, *edited by* S. Patai and J. Zabicky. Interscience, New York. 1970. p. 21.

123 F. Bohlmann and D. Schumann. Tetrahedron. Lett. **28**, 2435 (1965).

124 J. Dale and K. Titlestad. J. Chem. Soc. Chem. Commun. 656 (1969).

125 Z. Lidert. Tetrahedron, **27**, 967 (1981).

126 L.M. Jackman and S. Sternhell. Applications of Nuclear Magnetic Resonance Spectroscopy in Organic Chemistry, 2nd ed. Pergamon Press, Oxford. 1969. p. 91.

127 D. Neuhaus and M. Williamson. The Nuclear Overhauser Effect in Structural and Conformational Analysis. VCH Publishers, New York. 1989. pp. 143-148.

128 S. Gronowitz and Z. Lidert. Chemica Scripta, **16**, 97 (1980) and references therein.

129 W.E. Stewart and T.H. Siddall III. Chem. Rev. **70**, 517 (1970).

130 M. Frucht, A.H. Lewin and F.A. Bovey. Tetrahedron Lett. **42**, 3707 (1970).

131 J.V. Hatton and R.E. Richards. Mol. Phys. **5**, 139 (1963).

132 L.A. LaPlanche and M.T. Rogers. J. Am. Chem. Soc. **85**, 3728 (1963).

133 L.L. Graham and M.R. Miller. Org. Mag. Reson. **4**, 327 (1972).

134 R.C. Weast (*Editor*). CRC Handbook of Chemistry and Physics, 68th ed. CRC Press, Boca Raton, Florida. 1987. p. D-188.

135 B. Staskun. J. Org. Chem. **46**, 1643 (1981).

136 T.H. Siddall, III, W.E. Stewart and A.L. Marston. J. Phys. Chem. **72**, 2135 (1968).

137 M.A. Cremonini, L. Lunazzi, G. Placucci, R. Okazaki and G. Yamamoto. J. Am. Chem. Soc. **112**, 2915 (1990).

138 F.A.L. Anet and R. Anet, in Dynamic Nuclear Magnetic Resonance Spectroscopy. *edited by* L.M. Jackman and F.A. Cotton. Academic Press, New York. 1975. p. 575.

139 J. Sandrström. Dynamic NMR Spectroscopy. Academic Press, London. 1982. pp. 77, 86-91.

140 G. Claeson, G. Androes and M. Calvin. J. Am. Chem Soc. **83**, 4357 (1961).

141 C.H. Bushweller, J. Golini, G. Rao and J.W. O'Neil. J. Am. Chem. Soc. **92**, 3055 (1970).

142 A. Komornicki and J.W. McIver. J. Am. Chem. Soc. **95**, 4512 (1973).

143 O. Foss, in Organic Sulfur Compounds, Vol I. *edited by* N. Kharash. Pergamon Press, New York. 1961. p. 77.

144 R. Rahman, S. Safe and A. Taylor. Quart. Rev. **24**, 208 (1970).

145 A. Lidén, C. Roussel, T. Liljefors, M. Chanon, R.E. Metzger and J. Sandström. J. Am. Chem. Soc. **98**, 2853 (1976).

146 M. Barfield, A.M. Dean, C.J. Fallick, R.J. Spear, S. Sternhell and P.W.

Westerman. J. Am. Chem. Soc. **97**, 1482 (1975).

147 R.F. Zürcher. Progress in N.M.R. Spectroscopy. Vol II. *edited by* J.W. Emsley, J. Feeney and L.H. Sutcliffe. Pergamon Press, Oxford. 1967. p. 205.

148 N.J. Clayden and R.J.P. Williams. J. Mag. Reson. **49**, 383 (1982).

149 S. Winstein, P. Carter, F.A.L. Anet and A.J.R. Bourn. J. Am. Chem. Soc. **87**, 5247 (1965).

150 S. Li and N.L. Allinger. Tetrahedron. **44**, 1339 (1988).

151 D.B. Chestnut and W.P. Johnson. J. Mag. Reson. **65**, 110 (1985).

152 J.P. Idoux, J.M. Scandrett and J.A. Sikorski. J. Am. Chem. Soc. **99**, 4577 (1977).

153 J.W. ApSimon and H. Beierbeck. Can. J. Chem. **49**, 1328 (1971).

154 H.M. McConnell. J. Chem. Phys. **27**, 226 (1957).

155 A.D. Buckingham. Can. J. Chem. **38**, 300 (1960).

156 G. Montaudo, P. Maravigna and P. Finocchiaro. J. Mol. Structure. **13**, 309 (1972).

157 S.F. Nelson, P.J. Hintz and R.T. Landis. J. Am. Chem. Soc. **94**, 7105 (1972).

158 J.-R. Didry and J. Guy. Compt. Rend. **253**, 422 (1961).

159 R.M. Lynden-Bell and R.K. Harris. Nuclear Magnetic Resonance Spectroscopy. The University Press, Belfast. 1969. pp. 89-93.

160 J.A. Pople. J. Chem. Phys. **37**, 60 (1962).

161 W.C. Still, M. Kahn and A.J. Mitra. J. Org. Chem. **43**, 2923 (1978).

162 A. Bax. J. Mag. Reson. **53**, 517 (1983).

163 V. Rutar. J. Mag. Reson. **58**, 306 (1984).

164 J.A. Wilde and P.H. Bolton. J. Mag. Reson. **59**, 343 (1984).

165 N. Walker and D. Stuart. Acta Cryst. **A39**, 158 (1983).

166 A.J.C. Wilson (*Editor*). International Tables for Cystallography. Vol. C. Kluwer

Academic Publishers, Dordrecht. 1992. pp. 477-87.

167 SHELXTL PC. Version 4.1. Siemens Analytical X-Ray Instruments, Inc., Madison, WI. May, 1990.

168 C.A.G. Haasnoot, F.A.A.M. de Leeuw and C. Altona. Tetrahedron, **36**, 2783 (1980).

169 M. Saunders, K.N. Houk, Y.-D. Wu, C. Still, M. Lipton, G. Chang and W.C. Guida. J. Am. Chem. Soc. **112**, 1419 (1990).

170 PCMODEL User's Guide. Version 4.0. Serena Software, Bloomington, IN. p. 32.

171 A.R. Fritzberg, C.C. Kuni, W.C. Klingensmith III, J. Stevens, W.P. Whitnet. J. Nucl. Med. **23**, 593 (1982).

172 Assignments were deduced by correlation with those of the parent steroid in: K.E. Smith, H.C. Toms, C. Douglas, K.A. White, D.N. Kirk, S. Latif and R.W.P. Hubbard. J. Chem. Soc. Perkin Trans. **2**, 1567 (1990).

173 Assignments were deduced by correlation with those of the parent steroid in: J.W. Blunt and J.B. Stothers. Org. Mag. Res. **9**, 439 (1977).

174 T. Gartiser, C. Selve and J.-J. Delpuech. Tetrahedron Lett. **24**, 1609 (1983).